

BYG·DTU

DANMARKS
TEKNISKE
UNIVERSITET



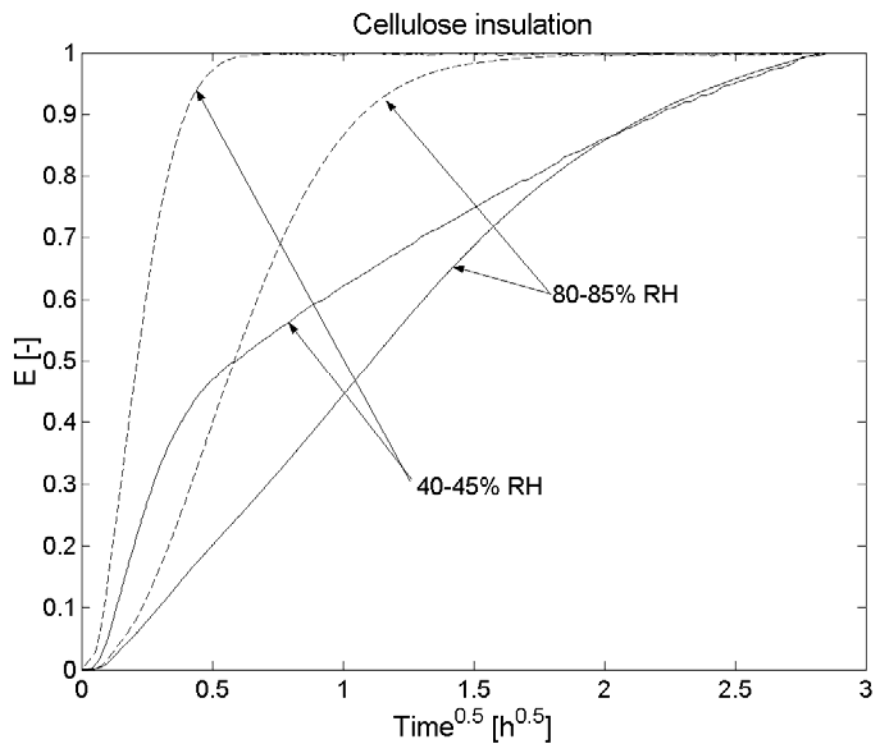
Moisture Dynamics in Building Envelopes

Ruut Peuhkuri

Ph.D. Thesis
Report R-071
Department of Civil Engineering
Technical University of Denmark
2003

Moisture Dynamics in Building Envelopes

Ruut Peuhkuri



Department of Civil Engineering
DTU-building 118
2800 Kgs. Lyngby
<http://www.byg.dtu.dk>

2003

ISSN 1601-2917
ISBN 87-7877-133-1

Illustration on the previous page:

Calculations with the Fickian model (- - -) are compared with the measurements (—) to illustrate the non-Fickian behaviour of most of the investigated materials. As an example, a couple of absorption steps for cellulose fiber insulation are used.

Preface

This Thesis is a part of the requirements for a Ph.D. degree at the Technical University of Denmark. The research work presented was financed by a grant from the *Technical University of Denmark* and has taken place at the *Department of Civil Engineering*, formerly the Department of Buildings and Energy, with Associate Professors Carsten Rode and Kurt Kielsgaard Hansen as supervisors. A great thank to both of you for many discussions and also practical help with the experiments. You have made an excellent supervisor team. I would also thank the laboratory and technical staff at the Department, as so many of you have assisted in my experimental work. It has been an easy task for me to ask for advice and help, and I always got it!

During spring 2002, I carried out two months research at the Glasgow Caledonian University under Professor Graham Galbraith. This stay was made possible by a grant from a private fund *Larsen & Nielsen Fonden* and from Professor Galbraith himself. Most of the sorption experiments were carried out during that stay. Grateful thanks go to Professor Galbraith and his staff, especially to Dr. David Kelly, who introduced me to Scottish building physics research in general, and to the actual measurement methods we were to use. Also thanks to David Bailly, who completed the sorption measurements after the end of my stay.

These last three years at the Department have been in many ways a good time, mostly due to great colleagues, particularly my fellow Ph.D. students. My special thoughts go to Charlotte, Toke and Peter. They shared my interest in Simulink modelling and were a part of the team which started the work on International Building Physics Toolbox in Simulink, together with Professor Carl-Eric Hagentoft and his team from Chalmers Technical University. The most delightful part of the final hard year has been, however, my office-mates and fellow Ph.D. students, Eva and Lennart. Without our daily laughs I couldn't have made this!

The most important condition for accomplishing this huge task, however, has been my wonderful husband Søren, who never complained about the long hours I spent at the University. Somehow we still managed to find time for each other, and for our great shared passion of bicycling and meeting friends. I also want to send my gratitude to my family. To my supportive parents, a unique sister, great Brothers, and lovely in-laws. My academic achievements will not be superior to the high standards of the family, but I know everyone will appreciate them. Finally, I would like to thank my brother-in-law Kevin for upgrading my English in this Thesis.

Lyngby, April 30, 2003 (edited August 29, 2003)

Ruut Peuhkuri

Summary

The overall scope of this Thesis "*Moisture dynamics in building envelopes*" has been to characterise how the various porous insulation materials investigated performed hygrothermally under conditions similar to those in a typical building envelope. As a result of the changing temperature and moisture conditions in the exterior weather and indoor climate the materials dynamically absorb and release moisture. The complexity of the impact of these conditions on the resulting moisture transport and content of the materials has been studied in this Thesis with controlled laboratory tests.

The first part of the Thesis consists of a theory and literature review on the moisture storage and transport processes (Chapter 2), on the non-Fickian moisture transport (Chapter 3) and on the methods for determining the moisture properties (Chapter 4). In the second part, the conducted experimental work, results, and analysis are presented (Chapters 5-7). The major findings are discussed (Chapter 8), before the final conclusion (Chapter 9). The Appendices include the material parameters used, some additional results and the description of the simulation models.

Chapter 2: Moisture transport theory The focus of this study concerns the dynamics of moisture transfer and storage in the hygroscopic range, and on the effects of temperature gradients on such transfer. An overview of the theory and literature of these mechanisms is given in this chapter.

Chapter 3: Non-Fickian moisture transport The literature review presents a number of authors that have studied non-Fickian moisture transport. The assumption of immediate local equilibrium has been generally rejected and moisture transport and storage were divided into a pore air phase and absorbed moisture phase. The link between the air and absorbed phase was modelled by a sorption equation, where the moisture flux was determined by a proportional coefficient and moisture potential. The focus in these studies has been on the development of transport equations.

Chapter 4: Determination of moisture properties Some experimental methods for determination of two of the most important moisture properties are described: the moisture capacity and the transport coefficients. The determination of diffusivity is also treated. These methods refer only to the hygroscopic range, i.e. $\varphi < 0.98$.

Chapter 5: Isothermal, dynamic moisture transfer This chapter describes experimental and numerical approaches to quantify the time-dependence of sorption mechanisms for some insulation materials. The experimental part included measurements with two different set-ups, where small samples were exposed to ab- and desorption steps in a controlled relative humidity and temperature environment. Changes in the bulk moisture content were continuously followed as the sample was attached directly to a balance.

The experimental results showed retarded sorption, most clearly for organic insulation materials. An exception was cellular concrete, whose sorption behaviour showed almost

only Fickian characteristics. The results were analysed theoretically to quantify some characteristic parameters, e.g. moisture diffusivity, penetration depth and moisture buffer capacity. The sensitivity of the results due to the used method was shown, e.g. the moisture buffer capacity was over-estimated when using steady state properties. The results were also analysed numerically and a model for non-Fickian moisture transport was developed. The traditional assumption of immediate local moisture equilibrium was rejected when modelling dynamic moisture transport. Instead, separate nodes for air moisture in the pores of porous materials and the absorbed moisture were modelled. The link between these nodes, which retard sorption, is described by a sorption equation. This is in accordance with approaches of other researches presented in Chapter 3. An approach for determining the sorption coefficient in this sorption equation *experimentally* was also shown. This preliminary approach for determining a sorption coefficient, which can model retarded sorption, was encouraging.

Chapter 6: Non-isothermal, steady state moisture transfer An experimental investigation was conducted in order to draw some conclusions on the magnitude of moisture transport due to temperature gradient on a range of porous light-weight building materials. A special constructed non-isothermal set-up allowed the creation of a temperature gradient of $10K$ and given humidity gradient over the sample. The resulting moisture flux as well as the hygrothermal states around and within the material was monitored.

The results showed that there exists some kind of 'other' transport in addition to Δp -driven one in all the materials analysed. Rather surprisingly, all the materials, including the almost non-hygroscopic materials (e.g. rock wool) and very hygroscopic materials (e.g. cellulose insulation) showed the same characteristics. The hypothesis of relative humidity being a driving force for non-isothermal moisture transport already in the hygroscopic could not be confirmed. On the contrary, indications exists that the temperature gradient itself is driving the moisture from the warm side towards the cold side. An attempt to identify and quantify the single contributions of the different transport forms involved was also presented.

Chapter 7: Non-isothermal, dynamic moisture transfer The set-up (the same one as in Chapter 6) was now used to create a dynamic climate with sinusoidal oscillations of relative humidity on the cold side over a period of 24 hours. The aim of these measurements was to identify the dynamic moisture response of a material exposed to a temperature gradient. The experimental results were compared with dynamic simulations partly with a 'conventional' model, and with a non-Fickian model.

Materials like cellulose and flax insulation and cellular concrete were able to moderate the oscillations. The difference in peak values of RH between the materials, however, was not significantly unambiguous. There existed a fairly good agreement between the measurements and the conventional Fickian model used. A minor phase delay on simulated results indicated that the true moisture capacity of the materials was lower than the mathematical one, i.e. the slope of the sorption isotherm. Implementing a hysteresis model increased the agreement between measurements and simulations but was not able to remove all the deviation. Implementing the non-Fickian model for this non-isothermal set-up did not give any good agreement with the measurements as it overly underestimated the moisture capacity. The moisture buffer capacity of the materials was also assessed. It was shown that the 'measured' buffer capacity was higher than the theoretical buffer capacity for the materials with *good buffer capacity*: flax and cellulose insulation and cellular concrete. There was no difference for materials with *poor buffer capacity*: glass wool, rock wool and perlite.

Sammenfatning

Dynamisk fugttransport i bygningers klimaskærme

Det overordnede formål med denne ph.d.-afhandling, "Dynamisk fugttransport i bygningers klimaskærme", er at karakterisere hvordan de forskellige undersøgte porøse isoleringsmaterialer opfører sig, under forhold svarende til dem der findes i en typisk klimaskærm. Disse forholds komplekse indflydelse på fugttransport og -indhold i materialerne er i nærværende studium undersøgt vha. kontrollerede laboratorieforsøg.

Første del af afhandlingen gennemgår teori og litteratur om fugtlagring og -transportprocesser (kapitel 2), om ikke-Fickske fugttransport (kapitel 3) og om metoder til at bestemme materialeparametre med relation til fugtlagring og -transport (kapitel 4). Anden del omfatter beskrivelse af de udførte forsøg, resultaterne af disse samt analyse (kapitel 5-7). De vigtigste resultater diskuteres (kapitel 8) inden den endelige konklusion præsenteres (kapitel 9). Appendices indeholder de anvendte materialeparametre, visse yderligere resultater samt beskrivelse af simuleringsmodellerne.

Kapitel 2: Fugttransportteori I dette kapitel gives et overblik over teori og litteratur for stationær og dynamisk, isotherm og ikke-isotherm fugttransport og -lagring.

Kapitel 3: Ikke-Fickske fugttransport Litteraturstudiet i dette kapitel gennemgår en række arbejder angående ikke-Fickske fugttransport. Antagelsen om øjeblikkelig lokal ligevægt forkastes i disse arbejder generelt og fugttransport og -lagring opdeles i en poreluftfase og en fase af fugt absorberet i selve materialet. Koblingen mellem fugt i poreluft og absorberet fugt bestemmes ved en transportkoefficient og et fugtdrivende potentiale. Fokus i de pågældende arbejder har i øvrigt generelt været på at udvikle transportligninger.

Kapitel 4: Bestemmelse af fugtegenskaber I dette kapitel introduceres nogle eksperimentelle metoder til bestemmelse af de vigtigste materialeparametre i relation til fugt: fugtkapacitet og transportkoefficienter. Ligeledes beskrives bestemmelsen af fugtdiffusivitet. De pågældende metoder refererer alene til det hygroskopiske område.

Kapitel 5: Isothermisk, dynamisk fugttransport Kapitlet beskriver eksperimentelle og numeriske tilgange til at kvantificere sorptionsmekanismernes tidsafhængighed. Den eksperimentelle del omfattede målinger med to forskellige opstillinger hvor små materialeprøver blev udsat for trinvis ab- og desorption ved kontrolleret relativ fugtighed og temperatur. Ændringer i det samlede fugtindhold målt løbende idet prøvene var ophængt i en vægt.

De eksperimentelle resultater viste forsinket sorption, tydeligst for de organiske isoleringsmaterialer. En undtagelse var porebeton hvis opførsel næsten svarede til den Fickske teori. Resultaterne blev analyseret teoretisk for at kvantificere nogle karakteristiske parametre,

herunder fugtdiffusiviteten, indtrængningsdybden og fugtbufferen. Resultaternes følsomhed overfor den anvendte beregningsmetode blev desuden undersøgt. Fx viste det at fugtbufferen overvurderes, hvis man bruger materialeparametre målt under stationære forhold. Resultaterne analyseres også numerisk, og der opbygges en model for ikke-Fickske fugttransport uden den traditionelle antagelse om øjeblikkelig lokal fugtligevægt. I stedet modelleres separate knuder for fugt i poreluft henholdsvis fugt absorberet i selve materialet. Forbindelsen mellem disse to knuder (den som forsinker sorptionen) beskrives med en sorptionsligning, svarende til andre forskeres fremgangsmåde som beskrevet i kapitel 3. Desuden demonstreres en eksperimentel metode til bestemmelse af sorptionskoefficienten i sorptionsligningen. Den ikke-Fickske model viser væsentligt bedre overensstemmelse med måleresultaterne end den Fickske.

Kapitel 6: Ikke-isotermisk, stationær fugttransport For at kunne vurdere størrelsesordenen af den fugttransport der skyldes en temperaturgradient, er der lavet en eksperimentel undersøgelse af en række lette, porøse bygningsmaterialer. Ved hjælp af en specialkonstrueret forsøgsopstilling er det muligt at påtrykke den enkelte prøve en temperaturforskel på 10 K og en given fugtighedsgradient. Den resulterende fugttransport såvel som temperatur- og fugtforhold omkring og i materialet er blevet registreret.

Resultaterne viser at der i alle de analyserede materialer eksisterer en slags 'anden' fugttransport, udover den der drives af forskelle i damptrykket. Overraskende nok udviser alle materialer, både de næsten uden hygroskopiske egenskaber (fx stenuld) og de meget hygroskopiske (fx papirisolering), samme karakteristika. Hypotesen om at relativ fugtighed allerede i det hygroskopiske område skulle være et drivende potentiale for ikke-isotermisk fugttransport kan ikke bekræftes. Derimod giver resultaterne indikationer af at temperaturgradienten i sig selv driver fugt fra den varme til den kolde side af materialerne. Afslutningsvis forsøges de forskellige involverede transportformer identificeret og kvantificeret.

Kapitel 7: Ikke-isotermisk, dynamisk fugttransport Forsøgene beskrevet i kapitel 6 er i dette kapitel modificeret ved, med samme opstilling, at skabe et skiftende klima hvor den kolde side påtrykkes en harmonisk svingende, relativ fugtighed med en periode på 24 timer.

Materialer som fx papir- og hørisolering og porebeton viser sig her i stand til at dæmpe udsvingene. Forskellen i spidsværdier for relativ fugtighed de enkelte materialer imellem er dog ikke særligt tydelig. De eksperimentelle resultater sammenlignes også med dynamiske simuleringer, dels med en 'konventionel' model og dels med en ikke-Fickske model.

Der viser sig for de fleste materialer en rimelig overensstemmelse mellem måleresultater og den 'konventionelle' Fickske model. En mindre faseforskydning (en forsinkelse) i den simulerede relative fugtighed indikerer dog at materialernes reelle fugtkapacitet er mindre end den teoretiske, sorptionsisotermens hældning. Implementeringen af en hysteresemodel forbedrer overensstemmelsen mellem målinger og simuleringer, men giver ikke en endelig forklaring på afvigelsen. Implementering af den ikke-Fickske model for denne ikke-isoterm situation giver ikke nogen god overensstemmelse med målingerne, da fugtkapaciteten i denne model nu undervurderes. En forklaring på dette vil kræve yderligere undersøgelser. Endelig vurderes materialernes fugtbufferen. Det vises at den ud fra målinger bestemte bufferevne for materialer med stor bufferevne, hør- og papirisolering og porebeton, er større end den teoretiske, mens der er ikke nogen forskel for materialer med lille bufferevne: glasuld, stenuld og perlite.

Contents

Preface	1
Summary	3
Sammenfatning	5
Nomenclature	11
1 Introduction	13
1.1 Background	13
1.2 Hypothesis and Scope	14
1.3 Scientific method	14
1.4 The Thesis	15
2 Moisture transport theory	17
2.1 Moisture retention	17
2.1.1 Sorption process	17
2.1.2 Moisture storage capacity	19
2.2 Moisture transport	19
2.2.1 Transport of water vapour	20
2.2.2 Transport of liquid water	23
2.2.3 Combined transport forms	25
2.3 Dynamic moisture transport	28
2.3.1 Moisture diffusivity	29
2.3.2 Moisture uptake	29
2.3.3 Moisture buffer capacity	31

3	Non-Fickian moisture transport	33
3.1	Christensen	34
3.2	Wadsö	35
3.3	Cunningham	36
3.4	Salin	37
3.5	Håkansson	38
3.6	Koponen & Liu	41
3.7	Scarpa & Milano	42
3.8	Krabbenhøft & Damkilde	42
3.9	Concluding remarks	44
4	Determination of moisture properties	45
4.1	Determination of moisture storage capacity ξ	45
4.2	Determination of transport coefficients	46
4.2.1	Determination of water vapour permeability δ_p	47
4.2.2	Determination of thermal moisture diffusion coefficient D_T	51
4.3	Determination of moisture diffusivity D_w	54
5	Isothermal, dynamic moisture transfer	57
5.1	Background	57
5.2	Experiments	58
5.2.1	Materials	58
5.2.2	Experimental set-up	62
5.2.3	Results	64
5.3	Analysing moisture response	68
5.3.1	Moisture diffusivity	68
5.3.2	Moisture buffer capacity	74
5.3.3	Conclusion on analysis of the moisture response	78
5.4	Modelling dynamic moisture transfer	79
5.4.1	Measurements vs. calculations with Fickian model	79
5.4.2	The non-Fickian model	81
5.4.3	Determination of the sorption coefficient	82
5.4.4	Calculations with the new model	84
5.5	Discussion	85
5.6	Conclusion	86

6	Non-Isothermal, steady state moisture transfer	87
6.1	Background	87
6.2	Experimental set-up	88
6.2.1	Measurement strategy	88
6.2.2	The Megacup equipment	91
6.2.3	Materials	92
6.3	Measurement results	93
6.4	Discussion	96
6.4.1	Assessment of the results	99
6.4.2	Relevant observations in literature	105
6.4.3	Sources for uncertainties	108
6.5	Conclusion	112
7	Non-Isothermal, dynamic moisture transfer	113
7.1	Background	113
7.2	Experimental set-up	114
7.2.1	Measurement strategy	115
7.3	Measurement results	116
7.3.1	Measured distribution of RH	116
7.3.2	Penetration depth	119
7.3.3	Measured moisture flux	121
7.4	Simulation results	121
7.4.1	Conventional model	122
7.4.2	Non-Fickian model	127
7.5	Discussion	127
7.5.1	Buffer capacity	128
7.5.2	Phase delay	131
7.5.3	The modelling	131
7.6	Conclusion	132

8 Discussion on the major findings	135
8.1 Retarded sorption and non-Fickian transport	135
8.2 Driving potentials for non-isothermal transport	136
8.3 Buffer capacity of materials	137
8.4 Significance of uncertainties	137
8.4.1 Uncertainty of measurements	137
8.4.2 Uncertainty of modelling	138
8.5 Recommendations for future works	139
8.5.1 Additional measurements	139
8.5.2 Additional modelling	140
9 Conclusion	141
References	143
APPENDIX	147
A Material parameters	149
B Additional results	165
B.1 Isothermal, dynamic moisture transport	166
B.1.1 Measurements with IGAsorp and Climate Chambers	166
B.1.2 Non-dimensional absorption steps	176
B.2 Non-Isothermal steady-state moisture transport	177
B.2.1 Relative humidity and vapour pressure profiles	177
B.2.2 Determination of transport coefficients	183
B.2.3 Identifying driving potentials	190
B.2.4 Calibration of RH sensors	195
B.3 Non-Isothermal dynamic moisture transport	198
B.3.1 Measurements of moisture flux	198
B.3.2 Measurements vs. Simulations	200
C SIMULINK model	205
D New SIMULINK models	233
D.1 Non-Fickian model	234
D.2 Model for determination of sorption coefficient	238

Nomenclature

Latin letters

b	thermal effusivity	$J/(m^2K \cdot s^{0.5})$
b_m	moisture accumulation capacity	$kg/(m^2Pa \cdot s^{0.5})$
c_p	heat capacity	$J/(kg \cdot K)$
D_a	molecular diffusivity of water vapour in air	m^2/s
D_T	non-isothermal moisture diffusion coefficient	$kg/(K \cdot m \cdot s)$
D_w	moisture diffusivity	m^2/s
$D_{s,l}$	surface diffusion coefficient	m^2/s
$D_{T,l}$	non-isothermal liquid transport coefficient	$kg/(K \cdot m \cdot s)$
$D_{T,v}$	non-isothermal vapour transport coefficient	$kg/(K \cdot m \cdot s)$
$D_{w,l}$	moisture content-driven liquid diffusion coefficient	m^2/s
$D_{w,v}$	moisture content-driven vapour diffusion coefficient	m^2/s
D_φ	liquid conduction coefficient	$kg/(m \cdot s)$
d	thickness	m
d_p	penetration depth	m
E	non-dimensional moisture content	-
G	moisture flux	kg/s
g	total moisture flux density	$kg/(m^2s)$
g_a	vapour flux density in air	$kg/(m^2s)$
g_c	suction pressure-driven moisture flux density	$kg/(m^2s)$
g_l	liquid moisture flux density	$kg/(m^2s)$
g_p	vapour pressure-driven moisture flux density	$kg/(m^2s)$
g_T	temperature-driven moisture flux density	$kg/(m^2s)$
g_v	vapour flux density	$kg/(m^2s)$
g_w	moisture content-driven moisture flux density	$kg/(m^2s)$
g_φ	relative humidity-driven moisture flux density	$kg/(m^2s)$
$g_{s,l}$	surface diffusion flux density	$kg/(m^2s)$
$g_{T,l}$	non-isothermal liquid moisture flux density	$kg/(m^2s)$
$g_{T,v}$	non-isothermal vapour flux density	$kg/(m^2s)$
h_c	convective heat transfer coefficient	$W/(m^2K)$
Δh	enthalpy of liquid-vapour phase change	J/kg
K	hydraulic conductivity	$kg/(Pa \cdot m \cdot s)$
k	sorption coefficient	$kg/(Pa \cdot m^2s)$
l	half length	m
M_w	molecular weight of water	kg/mol
m	mass	kg
m_0	mass of the dry material	kg
Δm_w	available water	kg/m^2

P	total pressure	Pa
P_0	standard atmospherical pressure 101325 Pa	Pa
P_c	suction pressure	Pa
P_l	liquid pressure	Pa
p	partial water vapour pressure	Pa
p_{sat}	partial water vapour pressure at saturation	Pa
R	general gas constant	$J/(mol \cdot K)$
RH	relative humidity	%
R_v	gas constant of water vapour 461.5 $J/(kg \cdot K)$	$J/(kg \cdot K)$
r	radius	m
r_K	Kelvin radius	m
S_M	generation or absorption of moisture	$kg/(s \cdot m^3)$
t	time	s
$t_{0.5}$	half time of the sorption	s
t_c	isothermal time constant	s
t_p	period	s
T	absolute temperature	K
u	moisture content by weight	kg/kg
V	volume	m^3
w	moisture content by volume	kg/m^3
w_{cr}	critical moisture content by volume	kg/m^3
x, y, z	spatial coordinates	m
Z_p	convective moisture surface resistance	$Pa \cdot m^2 \cdot s/kg$

Greek letters

α	thermal diffusivity	m^2/s
B	overall moisture transfer coefficient	$kg/(Pa \cdot s)$
β	surface moisture transfer coefficient	$kg/(Pa \cdot m^2 \cdot s)$
δ_p	water vapour permeability (vapour pressure gradient)	$kg/(Pa \cdot m \cdot s)$
δ_v	water vapour permeability (concentration gradient)	m^2/s
λ	thermal conductivity	$W/(m \cdot K)$
μ	vapour diffusion resistance	-
ξ	moisture capacity	-
ρ_0	density of solid material (dry density)	kg/m^3
ρ_w	density of water	kg/m^3
ρ_v	concentration of water vapour	kg/m^3
$\rho_{v,sat}$	concentration of water vapour at saturation	kg/m^3
σ	surface tension of the water	N/m
φ	relative humidity	-
ψ	porosity of the material	m^3/m^3

Chapter 1

Introduction

The complexity of combined heat and moisture transfer has been described in recent years using various simulation tools. The overall motivation for the most accurate description of combined transient heat and moisture transport involves dimensioning of building envelopes. The continuous introduction of new constructions and materials has raised demands for simulation models of long-term heat and moisture performance of such envelopes, especially where long-term practical experience is lacking.

Moreover, some questions on moisture dynamics around the non-isothermal behaviour and available moisture capacity, especially for some "new" materials, remain unanswered.

This Thesis systematically studies these questions and aims to contribute towards filling just some of the gaps in our knowledge on moisture dynamics in building envelopes.

1.1 Background

The transport of heat and moisture is driven by potentials. When a temperature or water vapour pressure gradient through a specimen exists, transport takes place from the higher to the lower potential. Throughout the history of heat and moisture studies, a range of different driving potentials has been introduced, together with corresponding theoretical models. While most studies on heat transport processes largely agree, no consensus in the choice of driving potentials and necessary parameters for describing moisture transport phenomenon exists at this time.

Furthermore, a problem stated by many researchers – e.g. (Galbraith et al., 1998), involves the use of material properties determined under isothermal conditions to calculate combined heat and moisture transfer under non-isothermal conditions. Water vapour permeability measured by standard cup set-up is an example of one such property.

In dynamic cases, moreover, a gradient is naturally transient and the direction of local heat and moisture transport can alternate globally and/or locally. At the same time, the material is locally exposed to alternating processes of ab- and desorption. The connection between the relative humidity and the equilibrium moisture content, described by ab- and desorption isotherms, is hardly ever reached in the dynamic case. However, the modelling of hysteresis effects takes into account some of the reduced moisture capacity.

This work is inspired by some deviations between measurements and the calculated results when a porous building material – wood – is exposed to a dynamic change in the

boundary conditions (Wadsö, 1993; Håkansson, 1998; Koponen and Liu, 1999). The existence of so-called non-Fickian transport mechanisms could be an explanation for this divergence between measurements and the numerical calculations based on the classical assumption of Fickian transport and immediate local equilibrium. Non-Fickian behaviour is mostly seen for high relative humidities, relatively small changes of relative humidity and low temperatures, and thin samples. All these conditions, except the one with thin samples, are present in exterior building envelopes in Nordic climates during the heating season, where the outdoor climate is particularly variable on both daily and annual time scales. Therefore, it is relevant to study non-Fickian phenomena when modelling dynamic moisture mechanisms in building envelopes. As most of the studies on non-Fickian phenomena have been made on wood, there also exists a need to identify possible non-Fickian phenomena in other common porous building materials.

The moisture transport process under dynamic conditions in porous materials is a result of combined sorption and transport mechanisms, also known as dynamic diffusion (Padfield, 1999). Transport properties are usually determined under stationary conditions, e.g. with cup measurements. Beside the transport properties, the moisture capacity of a material is used to describe the dynamics of moisture retention. Exposing the material to different relative humidities and determining the moisture content at equilibrium usually determines its moisture capacity. For some materials it takes a very long time to reach equilibrium, because the sorption process is very slow. Nevertheless, these time-dependent material characteristics are not usually considered as a parameter in classical calculation models. As a consequence, the moisture capacity of the materials in the analysed construction might be overestimated and the true moisture not be predicted.

1.2 Hypothesis and Scope

It is hypothesised in this work that the assumption of the local equilibrium, when defining the moisture capacity of any porous material, leads to overestimation of the real moisture capacity. The sorption is in other words time-dependent. It is further hypothesised that it is possible to quantify this time-dependence of the sorption mechanisms by using the experimental and analytical approaches introduced in this thesis.

Another part of the hypothesis refers to the problem of definition of the driving forces for moisture transport, especially for non-isothermal cases. It is hypothesised that temperature and relative humidity also are driving potentials for moisture transfer when there is a temperature gradient. The aim of the experimental work represented in this Thesis is to verify this phenomenon.

The results of this study should make it possible to create and modify existing models in a way that takes into account the nature of dynamic and non-isothermal boundary conditions.

1.3 Scientific method

The research method described in this Thesis is a combination of experimental and theoretical study, where these two elements are united in a modelling approach. A set-up of a calculation model is a simplified mathematical description of the real physical phenomena

with a number of assumptions, e.g. the continuum approach which allows modelling of mathematical field variables (Roels et al., 1999).

The experimental verification of theoretical models is often restricted by the lack of good quality experimental data. The stated variables and driving forces may be difficult or impossible to measure directly, and the theoretical variables are often based on other measured variables that have been converted. These conversions are a great source of uncertainty and a key part of the numerous assumptions. One of these assumptions concerns local moisture equilibrium, which leads to one of the main experimental uncertainties in this type of studies, i.e. measurement of moisture content. Moreover, the destructive character of the most reliable measurement methods and the fact that the most non-destructive methods are indirect, further increases the possibilities for error.

The gravimetric method is well-known and reliable – but also destructive – when studying equilibrium moisture content in a test specimen. However, when studying dynamic and non-isothermal conditions in a building envelope or a test sample, some important information will be lacking, i.e. dynamic moisture distribution, if only destructive means are employed.

Therefore, new knowledge of local moisture mechanisms in building materials is needed under dynamic, and also under non-isothermal conditions. The original scope of this work was to develop a measurement method by using X-ray attenuation, where moisture content *and* relative humidity at the same location could be measured simultaneously. Unfortunately, and despite of great effort, the preliminary measurements produced no usable results, and the idea was rejected. This Thesis describes instead some other approaches to measure transient moisture transport and sorption processes in the hygroscopic range. Dynamic moisture transfer was investigated partly under isothermal and partly under non-isothermal conditions. The identification of involved driving forces under non-isothermal conditions was made by steady-state measurements. For non-isothermal measurements, a novel set-up was employed where the local distribution of relative humidity and total moisture flux were measured in parallel.

1.4 The Thesis

The research work documented in this Thesis has a following structure:

The first part of the Thesis consists of a theory and literature review on the moisture storage and transport processes (Chapter 2), on the non-Fickian moisture transport (Chapter 3) and on the methods for determining the moisture properties (Chapter 4).

In the second part, the conducted experimental work, results, and analysis are presented (Chapters 5-7). These three chapters present each a different investigation: Isothermal dynamic moisture transfer, Non-isothermal steady-state moisture transfer and Non-isothermal dynamic moisture transfer. For every investigation, the experimental set-up used and the results together with the analysis of the results are presented as independent tasks.

The major findings of these different investigations are discussed relative to each others (Chapter 8), before the final conclusion (Chapter 9). The Appendices include the material parameters used, some additional results and the description of the simulation models.

Chapter 2

Moisture transport theory

Moisture transfer in porous media involves a complex interaction of different transport mechanisms, their driving forces, and the effects of available capacity and possible temperature gradients. This Chapter points out those parts of the accepted theory that are both essential and interesting for this actual study. This description can partly be seen as a short definition of the essential terms used in the other parts of this study.

The focus in this study, as mentioned in Chapter 1, concerns the dynamics of moisture transfer in the hygroscopic range and on the effects of temperature gradients on such transfer. The following is therefore *not* an all-encompassing description of moisture transport theory, but possesses more the character of definitions of the concepts and terms used. In addition, moisture transfer is understood as being a part of combined heat and moisture transfer, as also non-isothermal effects on transport are studied. However, the effects of moisture on heat transfer processes are not discussed here.

The description is mainly seen from the modelling point of view, which equates with the simplified mathematical description of the transport phenomena. Physical descriptions are included, where they help to understand these phenomena.

2.1 Moisture retention

A material's ability to store moisture is experimentally determined by sorption and suction isotherms and mathematically described as the equation(s) of state. These isotherms together are called the retention curve. In order to better understand the moisture storage concept, the sorption process and the moisture capacity of a material are partially described in the following Section.

2.1.1 Sorption process

Moisture in the pores of a porous material can exist either adsorbed to the surface, or physically fixed in pores, or as free water. Some water can also be chemically bound with the material itself. The amount of hygroscopic moisture depends on relative humidity of the pore air φ [-] or RH [%]:

$$\varphi = \frac{p}{p_{sat}} = \frac{\rho_v}{\rho_{v,sat}} \quad (2.1)$$

where p [Pa] is water vapour pressure, p_{sat} [Pa] water vapour pressure at saturation, ρ_v [kg/m³] the water vapour concentration and $\rho_{v,sat}$ [kg/m³] the water vapour concentration at saturation. The temperature dependence of p_{sat} is illustrated with this empirical expression, valid for $0 < T < 80^\circ\text{C}$ with an accuracy of $\pm 0.15\%$:

$$p_{sat} = \exp^{23.5771 - \frac{4042.9}{T - 37.58}} \quad (2.2)$$

where T [K] is the absolute temperature. Moisture content can be given by weight u [kg/kg] or by volume w [kg/m³]

$$u = \frac{m - m_0}{m_0} \quad (2.3)$$

$$w = \frac{m - m_0}{V} = \rho_0 \cdot u \quad (2.4)$$

where m [kg] is the mass of the moist sample, m_0 [kg] is the mass of the dry sample, V [m³] volume of the sample and ρ_0 [kg/m³] dry density of the sample. For very low relative humidities, there exists just a single layer of water molecules on the inner surfaces of the material. The fixation of these molecules by hydrogen binding (based on "dipole moment" of water molecules) is very strong. When the relative humidity reaches 10-20 %, additional layers of molecules are created on the surface with increasing RH and their binding force decreases, until water molecule layers in very small pores coalesce and capillary condensation starts. Capillary condensation depends on the suction pressure P_c [Pa], which is the difference between the total pressure P [Pa] and the pressure in the liquid under a meniscus P_l [Pa] given by

$$P_c = P - P_l = \frac{2\sigma}{r_K} \quad (2.5)$$

where σ [N/m] is the surface tension of water and r_K [m] is the Kelvin radius. There is a connection between the relative humidity of the air in the pores and the suction pressure in the pores that are subject to capillary condensation, given by Kelvin equation:

$$\ln(\varphi) = -\frac{P_c \cdot M_w}{\rho_w \cdot R \cdot T} \quad (2.6)$$

where M_w [kg/mol] is the molecular weight of water, ρ_w [kg/m³] is the density of water and R [J/(mol · K)] the general gas constant. The equilibrium moisture content (EMC), i.e. where the moisture content of a porous material is in equilibrium with the relative

humidity in surrounding air, is a function of relative humidity. *EMC* and the point where the capillary condensation starts are very material specific, depending on the size of the inner surfaces available for adsorption and the pore volume suitable for capillary condensation. (Philip and De Vries, 1957) referred to $\varphi = 0.6$ as an arbitrary transition point for physical adsorption and capillary condensation.

In the hygroscopic range, $\varphi < 0.98$, the retention curve is given by the sorption isotherm, while in the over-hygroscopic range, $\varphi > 0.98$, *EMC* is expressed as a function of suction pressure P_c . At one relative humidity level, the liquid phase just becomes continuous. Critical moisture content w_{cr} [kg/m^3] is defined as the moisture content where this level is reached (Pedersen, 1990).

A very important distinction exists between moisture uptake and moisture release, described by absorption and desorption isotherms. The deviation between these curves is the hysteresis effect, where the desorption isotherm always gives a higher *EMC* than absorption for a given relative humidity. The hysteresis effect is not totally understood, but it is generally assumed that the higher *EMC* for desorption is due to a 'ink-bottle-effect', where moisture gets trapped inside the small pores.

Temperature also has influence on sorption isotherms, i.e. for increasing temperatures, the relative humidity also increases when the moisture content is given. This is also called *Le Chatelier* principle, i.e. moisture adsorption is an exothermal process and therefore moisture release is an endothermal process, and uses energy (Pedersen, 1990).

2.1.2 Moisture storage capacity

A porous material's ability to store moisture is described by the retention curve. A material's moisture capacity is its ability for moisture uptake and release, when the environmental moisture conditions are changed. Mathematically, the moisture capacity ξ [-] is defined by the slope of the retention curve, e.g. sorption isotherm:

$$\xi = \frac{\partial u}{\partial \varphi} \tag{2.7}$$

As it will be later discussed, this definition is valid under equilibrium conditions. The existence of hysteresis also influences moisture capacity, i.e. ξ will differ, depending on whether the material is drying or wetting.

The moisture storage capacity of a material is also a function of temperature, as stated in the previous section.

2.2 Moisture transport

In this section, different mechanisms for moisture transport are introduced and the relevant driving forces for different forms of transport are discussed together with the effects of temperature gradients. The important subject of anomalous moisture transport, e.g. non-Fickian transport, is introduced and discussed in Chapter 3 on the basis of literature findings.

Table 2.1: Transport forms of moisture in porous media. Physical potentials are given as driving forces and derived ones in parentheses.

Phase	Transport form	Driving force
Vapour	water vapour diffusion	concentration of water vapour ρ_v or vapour pressure p
	thermal diffusion	temperature T
	effusion (Knudsen diffusion)	p and T
Liquid	capillary suction	suction pressure P_c
	Soret effect	temperature T
	surface diffusion	moisture content w (relative humidity φ)

The moisture within a porous material can be transported in the pores by several different mechanisms. The solid matrix is not thought to be active in the transport process in conventional moisture transport theory. An exception to this assumption is the reported retarded sorption in wood cell-walls, see Chapter 3.

Moisture transport can either be diffusive or convective. Diffusive transport is proportional to the gradient of the driving force(s), a proportionality coefficient being a material parameter which is determined experimentally. The determination of these proportionality coefficients is described in Chapter 4. The convective flux is a product of the vehicle flux, e.g. air, and the transported density of moisture (Hens, 1996).

Moisture in a porous material can be transported either as water vapour or as liquid water, or as a combination of these two phases. The solid phase of moisture, ice, is not regarded as movable (Pedersen, 1990). Forms of moisture transport commonly mentioned in the literature are shown in Table 2.1, and depend on the pore structure of the material as well as environmental conditions. However, in reality, the allocation of the driving forces is not quite as straightforward and this will be discussed later. Convective moisture transfer is not regarded here, because all the experiments and analysis in this study are performed with no air pressure difference within the material such that the possibilities for natural convection are minimised. Gravitational forces are also ignored.

Figure 2.1 illustrates these different moisture transport processes in the microscopic pore size level for different moisture contents of the material. Inspiration to the Figure comes from (Kelly, 2002) and (Krus, 1995).

2.2.1 Transport of water vapour

In building physics, the transport of water vapour is a transport of gas (water vapour), in the pores of any porous material.

Isothermal vapour transport

Theory on moisture transport in porous materials is originally based on Fick's law of diffusion of ions in water (Fick, 1855). Fick's law is generally given for the concentration

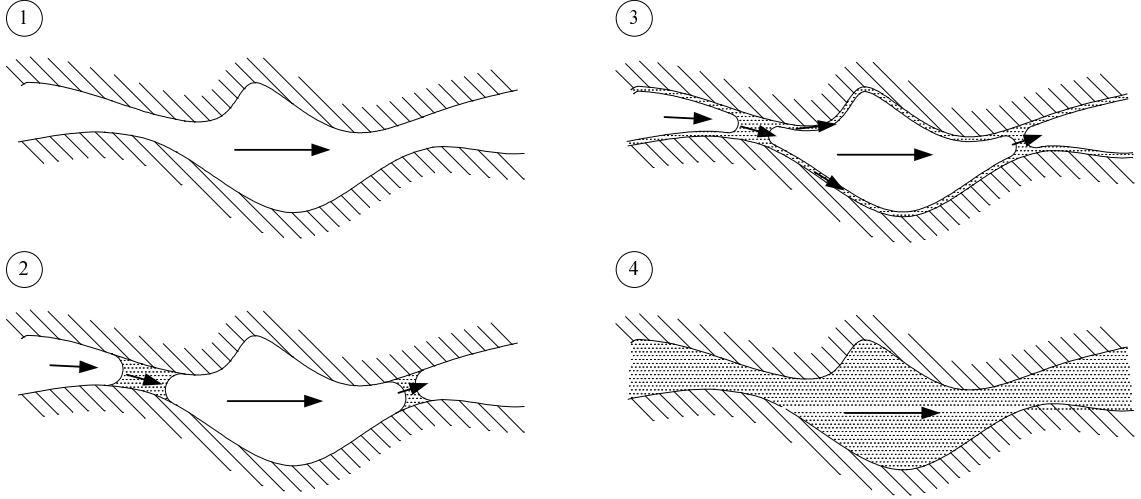


Figure 2.1: Different moisture transport processes, depending on the moisture content in pores. Stage 1 refers to low humidity, where there exits pure vapour diffusion. Stage 2 refers to series transport of vapour and liquid. Stage 3 refers partly to the series transport and partly to surface diffusion, also called vapour-liquid parallel transport. Stage 4 represents hydraulic flow for saturated media.

of the water vapour ρ_v as

$$g_a = -D_a \frac{\partial \rho_v}{\partial x} \quad (2.8)$$

where g_a [$kg/(m^2s)$] is the density of vapour transport in air and D_a [m^2/s] the diffusivity of water vapour in stagnant air. This simple law is adopted in building physics to describe the diffusion of water vapour in porous materials.

The driving potential for pure water vapour diffusion according to Equation 2.8 is ρ_v . The total pressure P [Pa], and especially temperature T also play roles in transport, see Equation 2.9 (Kumaran, 1996):

$$D_a = \frac{2.306 \cdot 10^{-5} \cdot P_0}{R_v \cdot T \cdot P} \left(\frac{T}{273.15} \right)^{1.81} \quad (2.9)$$

where P_0 [Pa] is standard atmospheric pressure and R_v [$J/(kg \cdot K)$] the gas constant of water vapour.

When regarding water vapour diffusion through a porous material, the water vapour flux density g_v [$kg/(m^2s)$] can be given by

$$g_v = -\frac{D_a}{\mu} \frac{\partial \rho_v}{\partial x} \quad (2.10)$$

where the vapour diffusion resistance μ [-] is defined as

$$\mu = \frac{D_a}{\delta_v} \quad (2.11)$$

where δ_v [m^2/s] is the water vapour permeability of the porous material.

The diffusion of water vapour in a porous material will therefore be regarded as diffusion in air, but with reductions because of the pore system, and is a function of parameters like porosity and tortuosity. Water vapour diffusion through some fibrous insulation materials with very low density is practically equal to diffusion in still air. The concentration of water vapour ρ_v and water vapour pressure p have the following relationship by applying the ideal gas law:

$$\rho_v = \frac{p}{R_v \cdot T} \quad (2.12)$$

Equation 2.8 becomes, under isothermal conditions

$$g_v = -\delta_p \frac{\partial p}{\partial x} \quad (2.13)$$

where the water vapour permeability δ_p [$kg/(Pa \cdot m \cdot s)$] is determined as

$$\delta_p = \frac{\delta_v}{R_v \cdot T} \quad (2.14)$$

Knudsen diffusion, also called effusion, is water vapour diffusion that takes place in very narrow capillaries, where the mean free path of the water vapour molecules is greater than the pore dimensions, $\sim 10^{-8}m$ according to (Krus, 1995).

Non-Isothermal vapour transport

When a temperature gradient is applied, there are (according to Table 2.1), two forms of transport which make vapour migrate, i.e. Knudsen diffusion, and thermal diffusion. Thermal diffusion is based on the density difference between dry air and vapour molecules, which makes the lighter vapour move from cold to warm, and results therefore in transport against the temperature gradient (Pedersen, 1990). The thermal diffusion can be expressed as the non-isothermal vapour flux density $g_{T,v}$ [$kg/(m^2s)$]

$$g_{T,v} = -D_{T,v} \frac{\partial T}{\partial x} \quad (2.15)$$

where $D_{T,v}$ [$kg/(K \cdot m \cdot s)$] is the non-isothermal vapour diffusion coefficient. The non-isothermal transport equation (Equation 2.16) given by (Philip and De Vries, 1957) is

in general regarded as the governing equation for water vapour transport under a temperature gradient, where the first part represents vapour diffusion driven by a moisture content gradient and the second part thermal diffusion driven by the thermal gradient:

$$g_v = -D_{w,v} \frac{\partial w}{\partial x} - D_{T,v} \frac{\partial T}{\partial x} \quad (2.16)$$

where $D_{w,v}$ is the coefficient for moisture content-driven vapour diffusion.

Usually, in building physics applications, thermal diffusion is neglected as being insignificant compared to other transport forms. (Krus, 1995) mentions that only about 0.05% of the total moisture transport can be allocated to thermal diffusion due to the relatively small temperature gradients across the materials. The strongly non-linear temperature dependence of saturation vapour pressure p_{sat} is therefore regarded as the main non-isothermal effect in most moisture models.

By increasing the temperature gradient in a moist material, the permeability will also increase, according to (Pedersen, 1990) thus:

- temperature affects the vapour pressure
- temperature gradients in vapour phase (between the well conducting liquid islands) are locally larger and therefore give an increased permeability

For increasing temperature alone, without a gradient, the water vapour permeability will also increase in some respects and this is particularly true for high relative humidities. This subject is further treated in Chapter 4.

2.2.2 Transport of liquid water

It is generally assumed that liquid transfer begins at the critical moisture content w_{cr} , which is determined by the existence of a continuous liquid phase. Pure water vapour transfer decreases from this point with increasing moisture content until vapour transfer becomes zero at saturation. The vapour - liquid - vapour series transport, where liquid islands act as short-circuits for transfer of vapour, is normally treated as vapour transport (Pedersen, 1990).

One reason to distinguish between vapour and liquid transport is that the transfer of soluble salts under thermal gradients takes place in the liquid phase. (Philip and De Vries, 1957) called such a transfer *liquid transfer* when there was only liquid transport in saturated pores (Figure 2.1 state 4). Everything else was regarded as *vapour transfer* (Figure 2.1 states 1-3). Vapour and liquid transport are often distinguished with respect to the critical moisture content w_{cr}

$$\begin{array}{ll} w < w_{cr} & \text{vapour transfer} \\ w > w_{cr} & \text{continuous liquid phase} \rightarrow \text{liquid transfer} \end{array}$$

Isothermal liquid transport

Using Darcy's law, the liquid moisture transport can be expressed as the liquid moisture flux density g_l [$kg/(m^2s)$] with the suction pressure P_c as driving force:

$$g_l = -K \frac{\partial P_c}{\partial x} \quad (2.17)$$

where K [$kg/(Pa \cdot m \cdot s)$] is the hydraulic conductivity. However, the hydraulic conductivity is practically impossible to determine experimentally. Therefore, the isothermal liquid transfer can be determined as according to 2.18, where it is driven by the moisture content w :

$$g_l = -D_{w,l} \frac{\partial w}{\partial x} \quad (2.18)$$

where $D_{w,l}$ [m^2/s] is the coefficient for moisture-content driven liquid diffusion.

For $w < w_{cr}$ most of the moisture transport can be regarded as water vapour diffusion. Above this level, liquid transport exists as capillary suction. However, as discussed earlier, some liquid transport will already exist locally at quite low moisture contents. Furthermore, the limit where the liquid transport starts, is difficult to determine and it is obviously dependent on the pore structure of the different materials. (Philip and De Vries, 1957) explained how liquid transfer already exists at very low humidity levels by vapour - liquid - vapour transport in series. Total moisture transport increases with increasing moisture content, because hydraulic conductivity in small pores is larger than water vapour permeability (Pedersen, 1990).

Surface diffusion involves the transport of a sorbate, e.g. liquid water. When the moisture content exceeds a certain value, i.e. where there exists more moisture on the inner pore surfaces than just multi-molecular layers, the moisture becomes mobile. The binding forces of these outer molecules are not as strong as those bound to the pore wall. This transport takes place when the moisture content is less than that for capillary saturation, where capillary pores (radius $r < 10^{-7}m$) start to be filled and actual liquid transport takes over. According to (Künzel, 1995), the surface diffusion for paper products starts at $\varphi = 0.3$ and for sandstone at $\varphi = 0.6$.

In (Krus, 1995), moisture content w is used as the driving force for surface diffusion flux density $g_{s,l}$ [$kg/(m^2s)$]:

$$g_{s,l} = -D_{s,l} \frac{\partial w}{\partial x} \quad (2.19)$$

where $D_{s,l}$ [m^2/s] is the surface diffusion coefficient. If a continuous potential, e.g. relative humidity, is used instead, the equation for surface diffusion can also be given by the relative humidity as driving potential φ :

$$g_{s,l} = -D_{\varphi} \frac{\partial \varphi}{\partial x} \quad (2.20)$$

where D_φ [$kg/(m \cdot s)$] is the liquid conduction coefficient which for $\varphi > 0.95$ can be given as (Künzel, 1995):

$$D_\varphi = D_{s,l} \cdot \rho_0 \cdot \xi \quad (2.21)$$

Non-Isothermal liquid transport

When introducing a temperature gradient, the following mechanisms affect liquid transport:

1. The viscosity of a liquid decreases for increasing temperatures (Pedersen, 1990) The result is increasing liquid transport for increasing temperatures. However, this effect is minimal compared to the effect of increasing moisture content (Kelly, 2002).
2. The Soret effect involves the transfer of liquid water along a temperature gradient (from warm to cold).
3. There is a possibility for surface diffusion driven by the relative humidity and/or moisture content gradient, which is often against the temperature gradient.

Liquid flow due to a temperature gradient, the so-called Soret effect, can be expressed as $g_{T,l}$ [$kg/(m^2s)$]:

$$g_{T,l} = -D_{T,l} \frac{\partial T}{\partial x} \quad (2.22)$$

where $D_{T,l}$ [$kg/(K \cdot m \cdot s)$] is the non-isothermal liquid transport coefficient. (Luikov, 1966) operated with a Soret coefficient, i.e. the ratio of thermal diffusivity D_T and moisture diffusivity D_w . Surface diffusion can also be regarded as non-isothermal transport, as the relative humidity is a function of temperature. The well-known equation for liquid flow under non-isothermal conditions according to (Philip and De Vries, 1957) is:

$$g_l = -D_{w,l} \frac{\partial w}{\partial x} - D_{T,l} \frac{\partial T}{\partial x} \quad (2.23)$$

2.2.3 Combined transport forms

The transport of pure water vapour at very low relative humidities, or liquid transport in a saturated medium, exists only for a very limited set of conditions. In most cases, different combinations of these transport forms exist. In this work, such transport is called total moisture transport. In this Section, the focus is on total transport phenomena under non-isothermal conditions.

Number of driving forces

The total moisture flux g is not necessarily driven by just one potential, but is a linear combination of them and can be defined as:

$$g = \sum -coefficient \cdot \nabla(DrivingForce) \quad (2.24)$$

The moisture permeability coefficient is different for every driving force. Due to thermodynamics, the number of driving forces is equal to the involved fluxes. Therefore, for coupled heat and moisture transport, only 2 forces are regarded as necessary for a model, when the air flux is neglected, and there is no distinction between vapour and liquid moisture transport. As mentioned earlier, the convective moisture transfer and transport due to gravitational forces are also ignored.

Although various driving forces exist, as reviewed in (Hens, 1996), debate remains open as to which potentials to use in modelling combined heat and moisture transfer. Here, it was proposed that the only "legal" driving forces are those potentials continuous on the material boundaries, i.e. temperature (T), relative humidity (φ) and various pressures (p, P_c) and concentration of water vapour ρ_v .

Vapour-liquid-series transport

The existence of liquid islands and how they act as short-cuts for vapour transport in a fairly dry medium has already been mentioned.

When looking at moisture transport in porous materials on a microscopic scale, a temperature gradient across a pore with a liquid island (see Figure 2.1) makes the vapour condensate on the warm side of the liquid island (= cold side of the air filled pore) and to evaporate from the cold side of the liquid island (= warm side of the next air filled pore). In this way, the temperature gradient induces moisture transport in the direction of the temperature gradient (also in the direction of vapour pressure gradient), until there is an equilibrium in the liquid capillary flow due to the different curvature (Philip and De Vries, 1957).

Vapour-liquid-parallel transport

For moisture contents, where a sorbate layer of water exists on the pore walls, but not enough water to allow capillary condensation, a parallel transport of water vapour diffusion and liquid transport as surface diffusion can take place (Figure 2.1 state 3).

Theoretically, for migration of this adsorbed moisture to occur, the driving force is the relative humidity gradient, but this transport is unlikely to affect the total transport (Philip and De Vries, 1957). Instead, for increasing moisture content, the temperature-induced capillary potential gradient will dominate. However, (Krus, 1995) refers to a range of works, which show that transport induced by the surface diffusion is remarkable for $\varphi > 0.5$.

For isothermal cases, these two mechanisms will work in the same direction, i.e. higher water vapour pressure on one side will result in a higher relative humidity, which again

gives a higher moisture content and a thicker sorbate layer. When introducing a temperature gradient, these potentials usually become opposite. In Winter, in cold climates, there is usually an inward relative humidity gradient in the building envelopes, while the vapour pressure gradient is outwards. When considering only moisture transport driven by the water vapour pressure difference, therefore, the moisture flux is usually outwards in cold climates (Padfield, 1999; Künzle, 1995).

Some measurements and observations support the existence of a relative humidity/moisture content-driven surface diffusion parallel (used synonymously to *in the same direction* in this context in this Thesis) or opposite to water vapour diffusion:

Measurements in exterior massive walls by (Padfield, 1999) and following analyses gave an indication that there was a capillary water reservoir due to rain, fog and dew on the colder side of the construction. Water was moving inwards until at some point, the vapour transport took over. Here, vapour pressure was locally higher than on the warm side, which gave a movement parallel to the relative humidity gradient.

Measurements by (Krus, 1995) on gypsum plasterboard support this, i.e. parallel relative humidity and pressure gradients gave a higher diffusion coefficient than gradients that were contradictory. Relative humidity is therefore possibly also a driving force for the absorbed water in capillaries, when there is no air pressure gradient.

Combined non-isothermal moisture transport

The combined moisture transport becomes even more complex, when a temperature gradient is introduced, as already discussed in previous Sections. However, there exist some simplified ways of presenting this combined moisture transport mathematically, apart from non-isothermal transport equations (Equation 2.16 and 2.23) given by (Philip and De Vries, 1957):

The total moisture flux density g [$kg/(m^2s)$] through a porous material in the hygroscopic range can be expressed in terms of a water vapour pressure-driven component g_p and a temperature-driven component g_T as in Equation 2.25

$$g = g_p + g_T = -\delta_p \frac{\partial p}{\partial x} - D_T \frac{\partial T}{\partial x} \quad (2.25)$$

where D_T is the thermal moisture diffusion coefficient [$kg/(K \cdot m \cdot s)$]. This equation has been used, among others, by (Kumaran, 1988), (Galbraith et al., 1997) and (Galbraith et al., 1998). δ_p is here assumed to include some liquid transfer for high relative humidities.

Not only the temperature gradient itself but the subsequent moisture content gradient under non-isothermal conditions may also induce moisture transport in the same or opposite direction to the vapour pressure gradient. The total moisture flux g can therefore also be given as a water vapour pressure-driven component g_p and a moisture content-driven component g_w :

$$g = g_p + g_w = -\delta_p \frac{\partial p}{\partial x} - D_{w,l} \frac{\partial w}{\partial x} \quad (2.26)$$

where $D_{w,l}$ [m^2/s] is the liquid diffusion coefficient. This type of equation was used, e.g. by (Krus, 1995). If a continuous potential over the material boundaries is preferred, e.g. in (Künzel, 1995), a relative humidity gradient can be used instead of the moisture content gradient. In Equation 2.27 g_φ is a relative humidity-driven component.

$$g = g_p + g_\varphi = -\delta_p \frac{\partial p}{\partial x} - D_\varphi \frac{\partial \varphi}{\partial x} \quad (2.27)$$

Here δ_p is assumed to include pure vapour transfer while D_φ stands for the liquid transport, i.e. both capillary transport and surface diffusion.

Finally, the total moisture flux g can also be given as a sum of a water vapour pressure-driven component g_p and a suction pressure-driven component g_c as in Equation 2.28, as in (Pedersen, 1990):

$$g = g_p + g_c = -\delta_p \frac{\partial p}{\partial x} - K \cdot P_c \frac{\partial \ln P_c}{\partial x} \quad (2.28)$$

In (Pedersen, 1990), δ_p is a function of RH and therefore may not only stand for pure vapour diffusion. The capillary pressure-driven component g_c gives the liquid transfer. The use of logarithmic P_c is due to numerical reasons in (Pedersen, 1990) and is not discussed further here. The product $K \cdot P_c$ is used due to this mathematical manipulation.

All these equations are able to deal with at least some of the involved transport processes, but it is obvious that it depends on the pore structure of the material, which transport processes are active under the temperature gradient. As a result of this, some models will be more suited for some materials than others. However, from the modelling point of view, there should exist one model suitable for any material.

2.3 Dynamic moisture transport

When setting up the theoretical model to be able to analyse the dynamic moisture transport, the governing equation for conservation of mass in a volume unit can be expressed as in Equation 2.29:

$$\nabla g \pm S_M = -\frac{\partial w}{\partial t} \quad (2.29)$$

where ∇g is the divergence of moisture flux, S_M the moisture source term and t time.

Dynamic water vapour transport can be described by Fick's second law, Equation 2.30 (when combining Equations 2.29 and 2.13, neglecting moisture source term S_M and regarding only one dimensional transport):

$$\frac{\partial w}{\partial t} = \frac{\partial}{\partial x} \left(\delta_p \frac{\partial p}{\partial x} \right) \quad (2.30)$$

The connection between the state variable w and the driving force $\frac{\partial p}{\partial x}$ in Equation 2.30 is defined by the moisture capacity of the material ξ given by Equation 2.7.

2.3.1 Moisture diffusivity

Under the assumption of isothermal conditions, the driving force in Equation 2.30 can be expressed as moisture content w :

$$\frac{\partial w}{\partial t} = \frac{\partial}{\partial x} \left(\frac{\delta_p \cdot p_{sat}}{\rho_0 \cdot \xi} \frac{\partial w}{\partial x} \right) = \frac{\partial}{\partial x} \left(D_w \frac{\partial w}{\partial x} \right) \quad (2.31)$$

where D_w [m^2/s] is moisture diffusivity. The diffusivity includes information about the moisture transport and retention at any one time, and gives a measure for how quickly or slowly the moisture conditions in a material change under alternating ambient conditions. Not only the transport properties but also the moisture capacity of the material plays a very important role.

As given above, the diffusivity D_w can be calculated from the permeability δ_p by

$$D_w = \frac{\delta_p \cdot p_{sat}}{\rho_0 \cdot \xi} \quad (2.32)$$

or determined from dynamic sorption experiments as described in Section 4.3.

2.3.2 Moisture uptake

The dynamics of moisture transport is an important part of this present work. In this Section, the characteristics that define sorption, i.e. moisture uptake, according to purely Fickian behaviour, are discussed to give the right perspective to the discussion of non-Fickian phenomenon in the next Chapter.

When analysing the mechanisms for moisture uptake, the following characteristics appear, which might lead us to consider retarded sorption. Moisture uptake $\partial w/\partial t$ is slower for (see Equation 2.35):

- decreasing temperature due to decreasing $p_{sat}(T)$
- increasing relative humidity (RH , φ) and subsequently increasing moisture capacity $\left(\frac{dw}{d\varphi}\right)$

These characteristics are derived from a lumped analysis (as shown in (Håkansson, 1998)), of a small body of volume V exposed to an isothermal moisture uptake ($\partial w/\partial t$). B [$kg/(Pa \cdot s)$] is the overall moisture transfer coefficient and p_{inlet} is the water vapour pressure the body is exposed to, while p is the initial water vapour pressure in equilibrium with the moisture content of the body. This can be expressed as

$$V \cdot \frac{\partial w}{\partial t} = B(p_{inlet} - p) \quad (2.33)$$

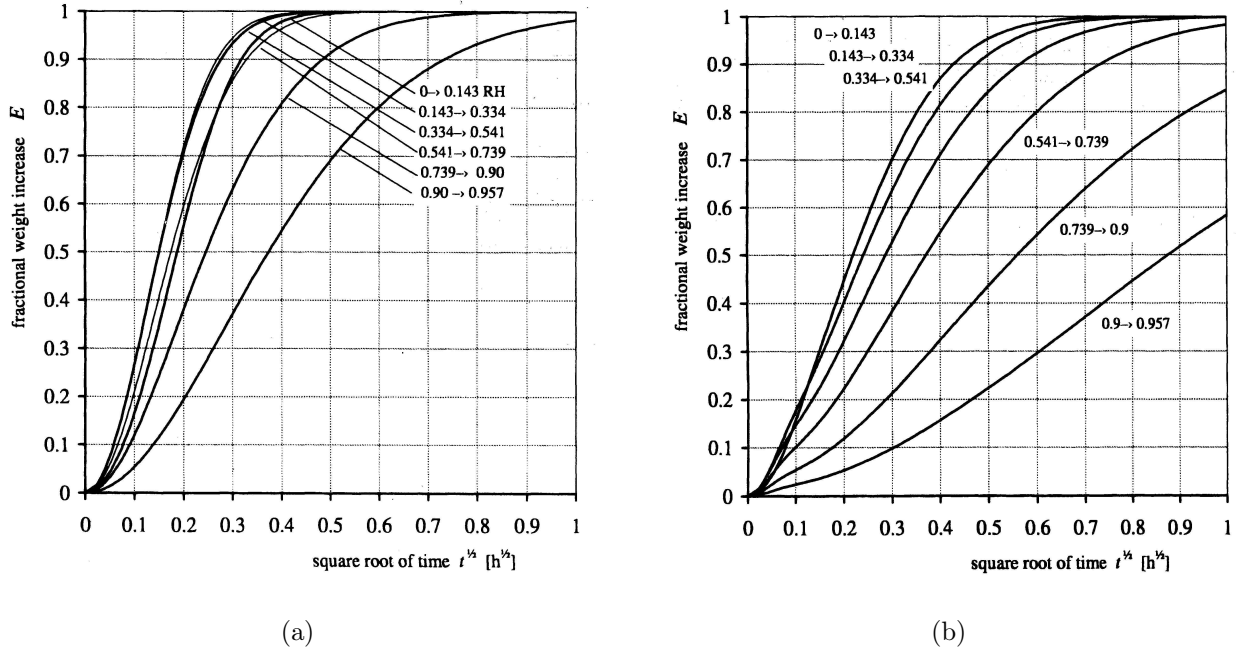


Figure 2.2: Calculated Fickian response (a) without and (b) with latent heat. From (Håkansson, 1998). Curves show non-dimensional moisture uptake of small wooden samples as a response to different step changes in the relative humidity of the boundary conditions.

When using the definition of the relative humidity and by linearising the sorption isotherm, Equation 2.33 becomes

$$w_{inlet} - w = t_c \cdot \frac{\partial w}{\partial t} \quad (2.34)$$

where t_c [s] is the isothermal time constant given by

$$t_c = \frac{\partial w}{\partial \varphi} \cdot \frac{V}{B \cdot p_{sat}} \quad (2.35)$$

The time constant t_c [s] defines the time t , when the ratio between the moisture uptake after this time t and the total possible moisture uptake (EMC) is ~ 0.63 . The higher t_c , the slower the moisture uptake.

Figure 2.2 from (Håkansson, 1998) illustrates the calculated Fickian behaviour for small wooden samples exposed to a stepwise change in relative humidity. The resulting non-dimensional moisture uptake E is shown as a function of the square root of time \sqrt{t} . It is clear that sorption slows for increasing φ . The effect of latent heat on the sorption process, i.e. which slows the sorption, is also illustrated. That sorption gets slower for increasing relative humidity is therefore not necessarily an indication of non-Fickian behaviour. In addition, (Crank, 1975) mentioned the role of latent heat on the sorption process, where increased temperature (moisture absorption releases energy) gives retarded sorption. In other words, sorption slows down due to decreasing RH for a given moisture content u , because saturation vapour pressure p_{sat} is a function of temperature T . The study by

Christensen (1965), also supports this role of latent heat. The calculations in Figure 2.2 correspond to these measurements. According to (Håkansson, 1998) the influence of latent heat on the sorption process increases for increasing T and φ , low convection, and thin samples.

2.3.3 Moisture buffer capacity

A material's ability to absorb or release moisture is sometimes called the moisture buffer capacity of the materials, and is a function of permeability and the absorptive power of the material. This ability is interesting for example when designing (partly) passive indoor climate regulation strategies or when studying the robustness of a construction against interstitial condensation. In the following, there are presented two different ways of characterising the moisture buffer capacity of the materials.

Moisture accumulation capacity

A material's ability to absorb and release heat is given by thermal effusivity b [$J/(m^2K \cdot s^{0.5})$], Equation 2.36:

$$b = \sqrt{\lambda \cdot \rho_0 \cdot c_p} = \frac{\lambda}{\sqrt{\alpha}} \quad (2.36)$$

where λ [$W/(m \cdot K)$] is thermal conductivity and α [m^2/s] thermal diffusivity, which shows how fast temperature changes propagate in a material (Hagentoft, 2001).

Analogous to thermal effusivity, also understood as the heat accumulation capacity of the material, is the moisture accumulation capacity of a material b_m [$kg/(m^2Pa \cdot s^{0.5})$] given by Equation 2.37. This is not given directly, but can be derived from the analysis in (Hagentoft, 2001):

$$b_m = \sqrt{\frac{\delta_p \cdot \rho_0 \cdot \xi}{p_{sat}}} = \frac{\delta_p}{\sqrt{D_w}} \quad (2.37)$$

When assessing the moisture accumulation capacity of porous materials, diffusivity plays a major role in quantifying this capacity because it is of great importance how much of the material's moisture capacity is activated under typical dynamic moisture conditions. The penetration depth d_p for a periodic (= sinusoidal) relative humidity change on the material surface of a semi-infinite body is a part of characterising the active mass:

$$d_p = \sqrt{\frac{D_w t_p}{\pi}} \quad (2.38)$$

d_p [m] defines the distance from the material surface where the amplitude is $\frac{1}{e} \sim 36.7\%$ of the amplitude on the material surface with a period of t_p [s]. This fraction is an arbitrary but analytically elegant choice.

Available water

As a part of determination of the other way of defining the moisture buffer capacity – the available water Δm_w [kg/m^2] – it is important to know how much of the material is activated in the moisture buffering. This can be expressed as the penetration depth d_p , Equation 2.38.

Now, the penetration depth alone is not capable to describe the buffer capacity; it also depends on the volumetric moisture capacity of the material $\rho_0\xi$ - and the size of the ambient relative humidity change $\Delta\varphi$, which is not a material parameter! The resulting moisture buffer capacity can be given as the amount of available water Δm_w the material is able to release or uptake during a given time period for a given change in relative humidity of the air, see Equation 2.39. Inspired from (Padfield, 1999).

$$\Delta m_w = \rho_0 \cdot \xi \cdot \Delta\varphi \cdot d_p \tag{2.39}$$

Chapter 3

Non-Fickian moisture transport

Measurements on wood by (Håkansson, 1998) among others have showed that moisture uptake is not instantaneous in all parts of a cell wall in wood, but is *retarded*. It has different time scales and depends on moisture history and the size of the step change in relative humidity. Mechanisms for this *retarded* moisture capacity are an important part of this study and are discussed in this Chapter together with recent theoretical and experimental approaches documented in the literature.

The slope of the retention curve gives the moisture capacity of a material. In Equation 2.29 it is assumed that all the absorbed moisture is immediately available locally for moisture transfer. A number of investigations have shown that, for wood at least, this general assumption is not quite correct. This phenomenon is called retarded sorption or non-Fickian transport, which also illustrates the duality of the problem: Either the transport equations, or the description of moisture capacity are incorrect, or neither of them are. This distinction between transport and sorption is always ambiguous, as it is a question of definition whether a process involves sorption or transport.

In building physics and material science, moisture transport is regarded as Fickian, if the dynamic transport can be described by Fick's second law (see Equation 2.30). There are normally two further conditions for Fick's law to be valid:

- The moisture capacity (the slope of the sorption isotherm ξ) is instantaneous, i.e. all the moisture capacity is immediately available.
- The transport coefficient is either determined under steady-state conditions or via the assumption of immediate equilibrium is valid, when determining the transport coefficient from the transient sorption experiments.

Strictly speaking, only water vapour diffusion is normally regarded as Fickian moisture transport. Other moisture transport forms, such as surface diffusion and capillary transport, may exist within the material and are also usually described by a gradient law like Fick's. Non-Fickian behaviour may be equally relevant for these other transport forms, because immediate local equilibrium is also assumed.

When analysing non-Fickian transport, Fick's second law (Equation 2.30) is supposed to be valid *sensu stricto*, as the problem resides in the determination of a material's properties. In calculation models, the handling of the material data, especially moisture capacity, often neglects the presence of time-dependent processes.

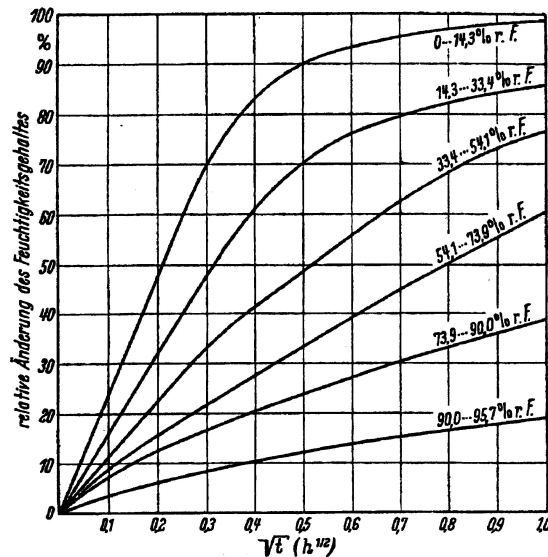


Figure 3.1: Moisture absorption as a response to different steps in relative humidity. The response is given as relative change in moisture content of the sample. This equates to the non-dimensional moisture content E in Section 4.3. From (Christensen and Kelsey, 1959). These measurements are comparable with Fickian calculations in Figure 2.2

A number of authors have investigated non-Fickian moisture transport and the problem of modelling it. In the following sections, some of the most interesting approaches are briefly described in chronological order. The nomenclature is not the original one used in the references, and the present nomenclature is also applied here.

3.1 Christensen

One of the first studies that showed clear non-Fickian behaviour was the work by (Christensen and Kelsey, 1959), where non-Fickian effects on thin samples of wood in pure water vapour were analysed under conditions of rapidly changing relative humidity. An example of the results is given in Figure 3.1, which can be compared with Fickian calculations in Figure 2.2. The study included mostly absorption processes and found;

- Fickian transport occurred only when $u_{start} = 0$ weight-%
- Retarded sorption was found for all type of wood or wood derivate
- Significant:
 - step size
 - fraction of sorption: different sorption before and after a "breaking point"
 - moisture history, both the level and the exposure time of the previous step: Both half-time of sorption $t_{0.5}$ and moisture content u are changed.
- Non-significant:
 - cell wall thickness

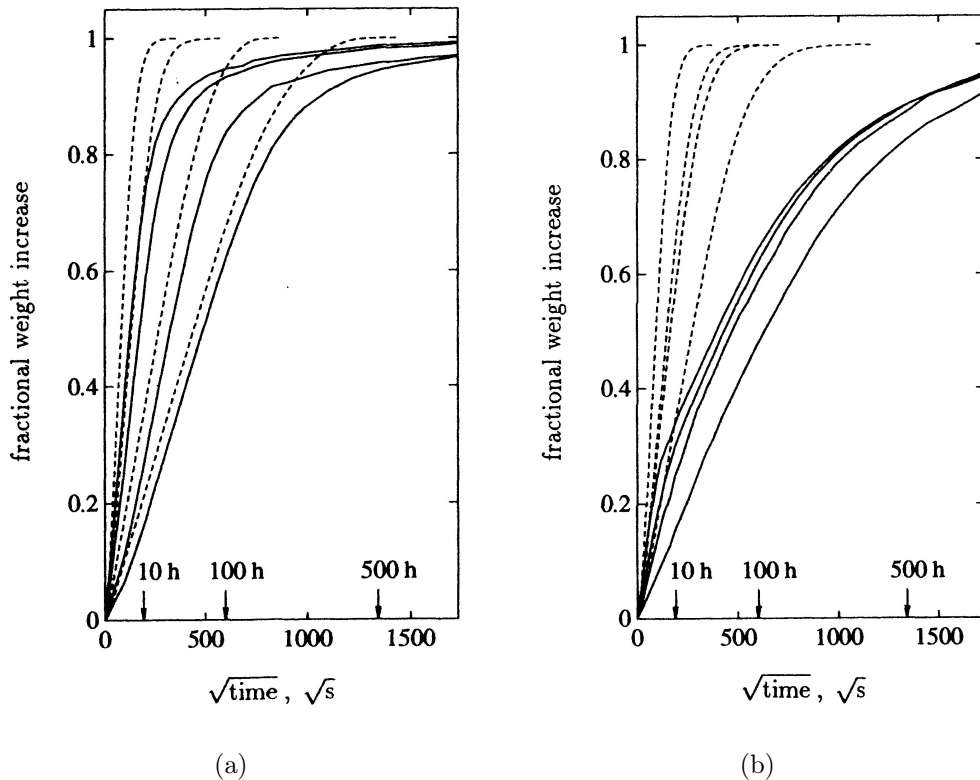


Figure 3.2: Measurements (—) on small samples of wood are compared with Fickian simulations (- - -). (a) Absorption step 54–75%RH. (b) Absorption step 75–84%RH. From (Wadsö, 1993)

3.2 Wadsö

A fundamental study on non-Fickian behaviour on wood is reported in (Wadsö, 1993). He measured absorption on small thin wood samples and found that the sorption was not Fickian, especially at the end of the sorption process, see Figure 3.2, where measurements are compared with Fickian simulation. Transport was defined to be Fickian if the fractional moisture uptake as a function of \sqrt{t} was linear up to $\varphi \sim 0.6$, there was no thickness effect and the permeability measured with steady-state methods (cup method) was equal with the one determined from these transient sorption measurements. The steady state permeability was assumed to be the true permeability, which was not influenced by non-Fickian effects.

From Figure 3.2, it was evident that for particularly high relative humidities, (step 75 – 84 %RH), a two-stage sorption process was observed, i.e. a rapid, almost linear initial sorption, followed by a slower process. In addition, the sorption curves showed a slight delay, with an initial sigmoid phase, indicating that the surface mass transfer may have been limited. Evaluation of the mass flux through a boundary layer could be described as

$$g = \beta(p_w - p) \quad (3.1)$$

where p_w is the vapour pressure on the moist surface and β is a mass transfer coefficient. This expression originates from the early 1800's. In general, (Wadsö, 1993) included a

comprehensive literature review up to 1993 on non-Fickian phenomena. He also discussed common methods of evaluating diffusivities from the sorption measurements. One of the main assumptions for the validity of the methods (discussed in more detail in Chapter 4), is that the process can be described with Fick's second law (Equation 2.30). For large k -values, i.e. high air velocities, the different methods gave similar results, but small k -values using Equation 4.11 gave a large error. It was found that k values did not vary remarkably for different materials and was basically a function of air velocity.

(Wadsö, 1993) did not find any existing, suitable model for non-Fickian transport nor did he propose a final model. He did, however, thoroughly discuss the essential nature of such a model, summarised in the following points;

- 1) The model should consist of 2 parts, i.e. flow through the material and sorption in the cell walls.
- 2) The model should be able to handle both rapid and slow changes in ambient humidity.
- 3) The model should be a physical model, not 'just' a numerical model.

3.3 Cunningham

(Cunningham, 1995) divided the transport in wood in two processes, i.e. Fickian diffusion in the cavity (Equation 3.2), and non-Fickian sorption processes in the cell wall (Equation 3.3). Under the assumption of a large surface mass transfer coefficient, a constant sorption coefficient k for the studied interval, isothermal conditions and by neglecting the moisture transfer inside the cell wall, the equations for the moisture transfer became;

$$\frac{\partial \rho_v}{\partial t} = D_{w,v} \frac{\partial^2 \rho_v}{\partial x^2} - k (\xi_1 \cdot \rho_v - \xi_2 \cdot w) \quad (3.2)$$

$$\frac{\partial w}{\partial t} = k (\xi_1 \cdot \rho_v - \xi_2 \cdot w) \quad (3.3)$$

where $D_{w,v}$ is the water vapour diffusion coefficient, ρ_v concentration of water vapour, w moisture content and ξ_1 and ξ_2 are the slopes of the linearised sorption isotherms for humid air and wood. A time constant for Fickian transport t_1 (cavity diffusion) is given by Equation 3.4 and for the non-Fickian transport t_2 (cell wall sorption) by Equation 3.5, where l is half the length of the analysed slab.

$$t_1 = \frac{4 \cdot l^2}{\pi^2 \cdot D_{w,v}} \quad (3.4)$$

$$t_2 = \frac{\xi_1}{k \cdot \xi_2} \quad (3.5)$$

When this model and the measurements from (Wadsö, 1993) were compared, a rather good agreement was found, see Figure 3.3. It was also pointed out that determination of diffusion coefficients from dynamic sorption measurements – as presented in Section 4.3 – gives correct values only if the cell wall absorption is negligible.

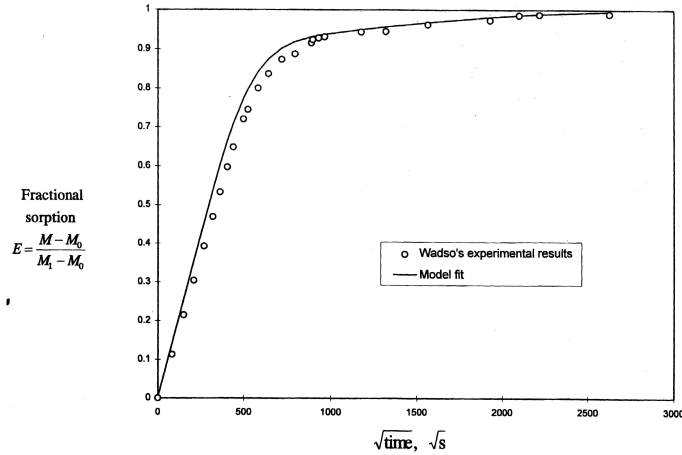


Figure 3.3: Comparison of the measured – from (Wadsö, 1993) – and calculated moisture response. From (Cunningham, 1995).

3.4 Salin

(Salin, 1996a) and (Salin, 1996b) studied the drying of wood and divided moisture transport into transport in the gas phase (Equation 3.6), and as bound water (Equation 3.7). In this way, the assumption of the local equilibrium is replaced with a mass transfer coefficient k between the water vapour and bound water.

$$\frac{\partial \rho_v}{\partial t} = D_{w,v} \frac{\partial^2 \rho_v}{\partial x^2} - k (w_{surf} - w_{eq}) \quad (3.6)$$

$$\frac{\partial w}{\partial t} = D_{w,l} \frac{\partial^2 w}{\partial x^2} + k (w_{surf} - w_{eq}) \quad (3.7)$$

Numerical results with this model showed, however, that there was no increased deviation between the Fickian and this model for increased time. According to experimental results by others, non-Fickian behaviour was precisely characterised by this deviation. Therefore, the model in Equations 3.6 and 3.7 with a constant k was not sufficient for modelling non-Fickian phenomena. A model with a lower sorption coefficient k towards equilibrium was suggested as a next step in the development.

A more recent approach in (Salin, 2002) and (Salin, 2003) discusses another explanation of the slower drying rates than the ones modelled with Fickian models. There exists a 'dry shell' on the material surface, where moisture content is lower than deeper within the material. As a result, the driving potential ($w_{surf} - w_{eq}$) will be smaller than expected, resulting in a lower moisture transfer rate. This was especially valid for moisture content greater than the fibre saturation point ($u \sim 0.3$). For those cases below the fibre saturation point (more relevant to this actual work in the hygroscopic range), the explanation for slower drying rates was found to be largely due to the lack of hysteresis in the model. It was shown for some cases the anomalous drying behaviour could be fully modelled including sorption hysteresis. Overall, careful modelling, including modelling of heat transfer and the interaction between air and material surfaces, could remove any 'non-Fickian behaviour' seen on wood drying.

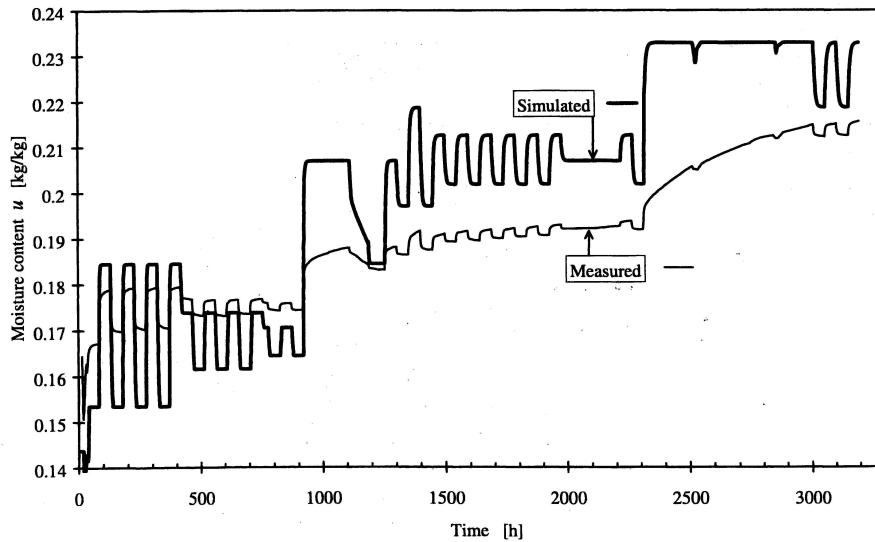


Figure 3.4: A measurement sequence compared with Fickian calculation. From (Håkansson, 1998).

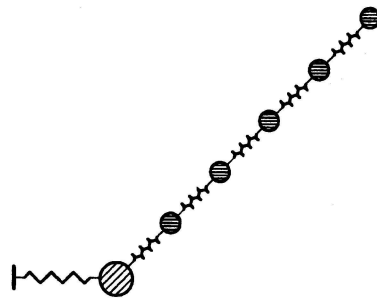


Figure 3.5: Calculation node with 5 internal levels according to (Håkansson, 1998)

3.5 Håkansson

An important and a slightly different approach to understand non-Fickian behaviour in wood is documented in (Håkansson, 1998). Håkansson measured different ab- and desorption and periodic sorption sequences on small samples of wood in order to investigate effects of temperature level, relative humidity level, step size, sample thickness and hysteresis. The results showed non-Fickian behaviour in the form of retarded sorption when compared with Fickian simulation (Figure 3.4).

Some main observations were:

- Sorption was slower for lower temperatures
- Some kind of blocking was observed, i.e. sorption became progressively smaller for consequent steps
- Diverging results when superimposing steps gave evidence for non-linearity

Based on these experimental results, a non-linear retarded sorption model was developed. (Håkansson, 1998) implemented the retarded behaviour both in the description of the moisture capacity and the diffusion coefficient, which had to be non-linear and a function of step size. Furthermore, the model of a calculation node was extended with several

internal layers to enhance the retarded effect (see Figure 3.5). The response from two small steps superimposed to one larger step, with divergent results, showed non-linearity of sorption, and led to some kind of conclusion, where Fickian transport equates to linear transport, and non-Fickian transport equal with non-linear transport. The non-linearity was modelled using non-linear conductances K_n , (also a function of the gradient of the driving force $K(\rho_v, \nabla\rho_v)$), with n internal levels (Equation 3.8).

$$K_n = k_n |\Delta\rho_v|^\gamma \quad (3.8)$$

where k_n is a coefficient that decreases inwards to give more retarded effect for small gradients and close to equilibrium, and γ is an indication for how strong a non-linear diffusion coefficient is needed and gets numerical values of 1 or 2. The model of (Håkansson, 1998) is therefore able to meet these phenomena given by the experimental results:

- small RH -step \rightarrow small gradient \rightarrow small flux
- low T \rightarrow small gradient \rightarrow small flux

The outer node which is supposedly Fickian, has a conductance K_0 :

$$K_0 = \frac{1}{Z_{inlet} + Z_{surface} + Z_{material}} \quad (3.9)$$

where moisture resistances Z refer to the inlet resistance of the set-up, surface resistance and Fickian diffusion in the material respectively.

Moisture capacity was subdivided in two factors, i.e. immediate capacity and retarded capacity. Capacities were determined as "usual", as a slope of the sorption isotherm ξ . Then the sorption isotherm was divided in two parts: $u = u_{im} + u_{ret}$, as shown in Figure 3.6(a).

The immediate moisture capacity ξ_{im} was determined by fitting initial (=Fickian) sorption from one RH -level to another, $\Delta\varphi$ (see Figure 3.6 for definition of u_0 and u_1) with following equations:

$$u(t) = u_1 - a \cdot e^{-\frac{t}{t_0}} \quad (3.10)$$

$$\xi_{im} = \frac{u_1 - u_0}{\Delta\varphi} \quad (3.11)$$

where $u(t)$ is the moisture content at time t , and u_1 , a and t_0 are constants.

Håkansson (1998) found that the immediate capacity was nearly constant and that there was no difference either for ab- and desorption or for step size. A more retarded sorption for high RH was observed, which corresponded with the fact that ξ_{im} was a smaller fraction of the total ξ for high RH . The retarded part of the moisture capacity was divided further into sublevels to corresponding to the internal levels.

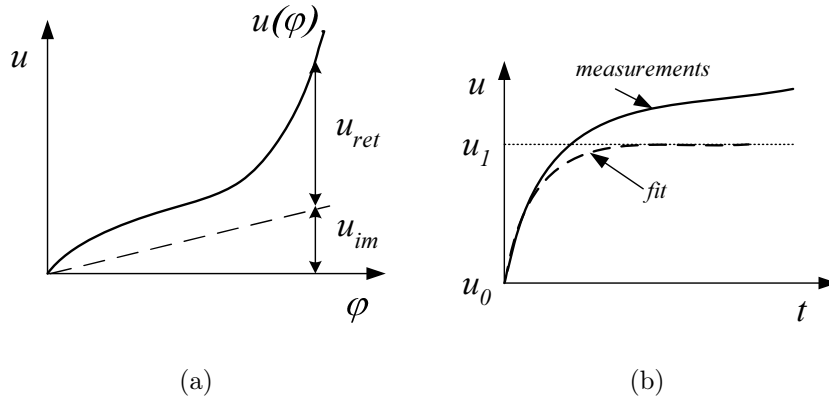


Figure 3.6: Analysis according to (Håkansson, 1998): (a) Sorption isotherm divided in immediate capacity u_{im} and retarded capacity u_{ret} . (b) Determination of immediate moisture capacity ξ_{im} from the initial sorption. u_0 is the moisture content at the start RH -level and u_1 is the fitted "end" moisture content, while the measured u increases beyond u_1 . (Diagrams are reproduced)

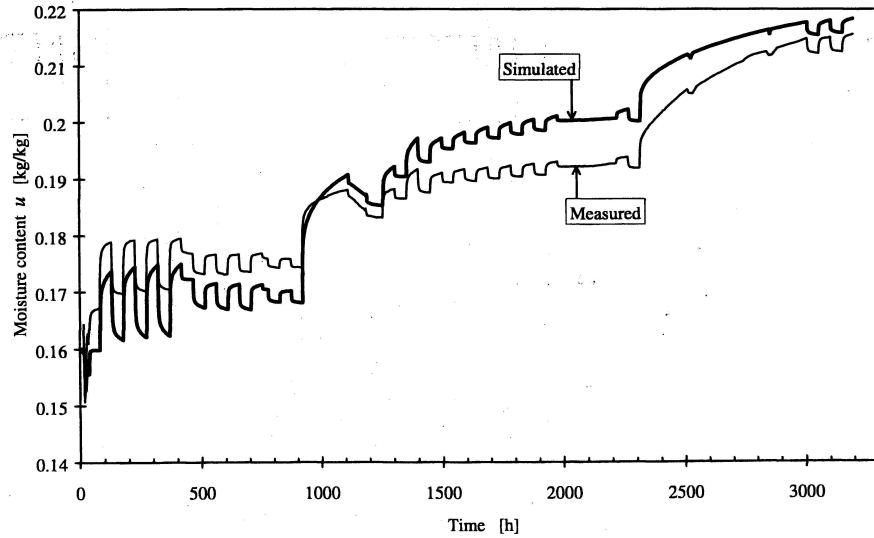


Figure 3.7: A measurement sequence compared with non-Fickian calculation with 5 internal nodes and hysteresis in the innermost node. From (Håkansson, 1998).

The resulting equations for moisture content in outer (0) and inner nodes (1...N) are (see Figure 3.5)

$$u = u_{im} + u_{ret} = u_0 + (u_1 + \dots + u_n) \quad (3.12)$$

$$u_0 = \xi_{im} \cdot \varphi \quad (3.13)$$

$$u_n = \alpha_n (u - u_0) \quad (3.14)$$

where α_n is a coefficient which increases inwards in the inner nodes. Calculations with this model with 5 internal levels, resulted in relatively good agreement with the actual measurements. See Figure 3.7 for comparison of measurements and calculations. The model ignores latent heat, because it was assumed to be non-significant in the actual case.

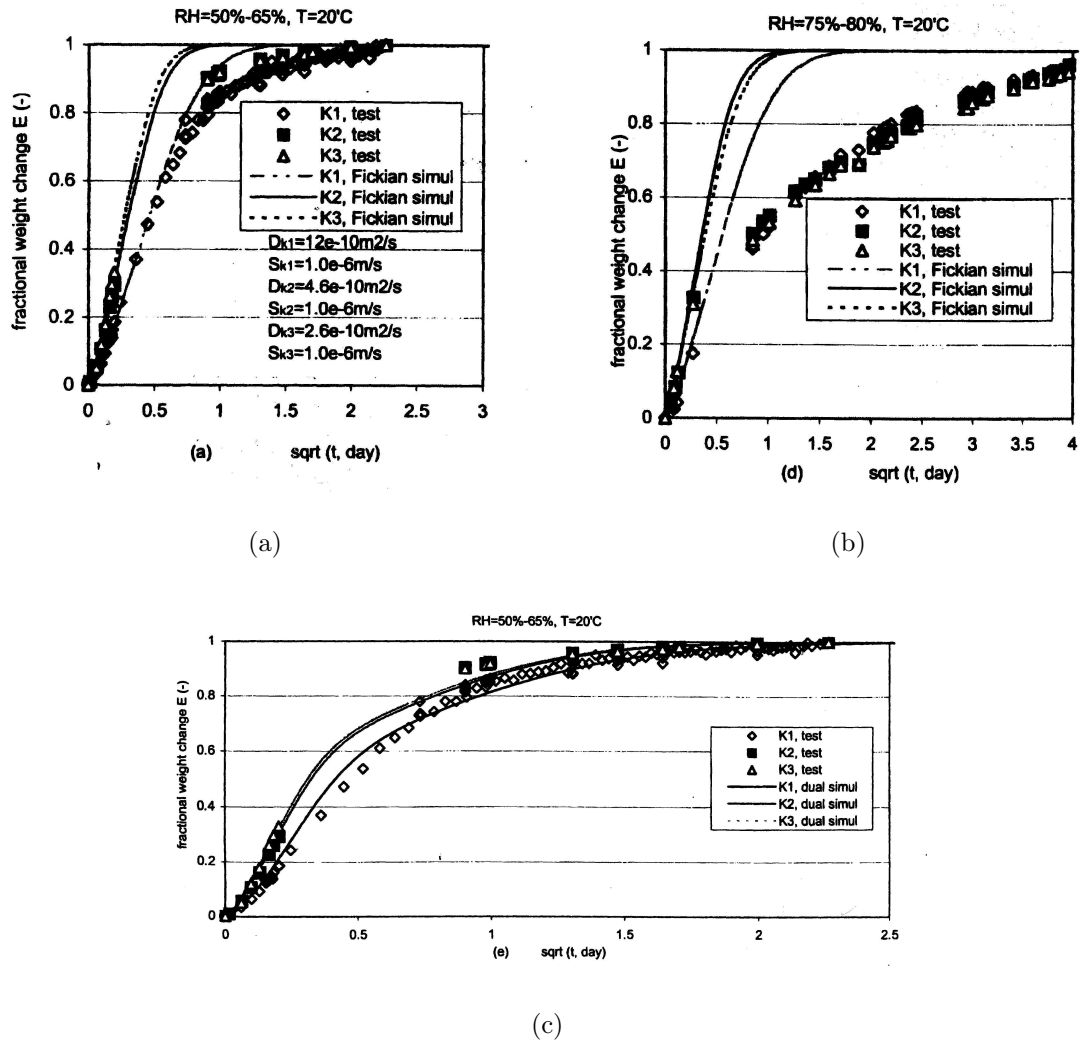


Figure 3.8: Moisture response measurements compared with the Fickian model (a) for low RH , (b) for high RH and (c) with the dual-diffusivity model for low RH . From (Koponen and Liu, 1999).

3.6 Koponen & Liu

The three explanations mentioned in (Koponen and Liu, 1999) for non-Fickian behaviour in wood are commonly cited in the literature. They include surface resistance, stress relaxation inside the wood, and slow sorption in the cell walls. (Koponen and Liu, 1999) included tests on spruce (longitudinal direction) as well as modelling. The experiments, involving transient sorption tests, showed non-Fickian behaviour in all cases and especially near equilibrium and/or in high relative humidity levels, when compared with Fickian simulations (see Figure 3.8(a)-(b)). Fickian sorption was observed until the fractional moisture uptake range of 0.3 - 0.8. As a result, the transient moisture sorption in the single cell wall (in wood) should be accounted for. A dual diffusivity model was suggested, which takes into account the early/late wood effects (Equations 3.15 and 3.16), and slow cell wall sorption (Equation 3.17). The model is isothermal and no latent heat is considered.

$$c_{m,1} \frac{\partial p_1}{\partial t} = \delta_{p,1} \frac{\partial^2 p_1}{\partial x^2} - k_1 (p_1 - p_2) \quad (3.15)$$

$$c_{m,2} \frac{\partial p_2}{\partial t} = \delta_{p,2} \frac{\partial^2 p_2}{\partial x^2} + k_1 (p_1 - p_2) - k_2 (p_2 - p_a) \quad (3.16)$$

$$c_{m,a} \frac{\partial p_a}{\partial t} = \delta_{p,a} \frac{\partial^2 p_a}{\partial x^2} + k_2 (p_2 - p_a) \quad (3.17)$$

where c_m is the moisture capacity, and indexes 1 and 2 refer to early- and late wood, and index a to air cavity. The resulting response, compared with the measurements is given in Figure 3.8(c).

3.7 Scarpa & Milano

(Scarpa and Milano, 2002) studied the absorption characteristics of expanded perlite board. Transient experiments were supplied with modelling, where an evaporation source was introduced instead of the assumption of equilibrium. For small volumes of liquid moisture, it was argued that the most realistic and simple models for coupled heat and moisture transfer have temperature T and water vapour concentration ρ_v as independent variables. In the model, ρ_v is not in equilibrium with the moisture content of the material w according to sorption isotherm.

The model, described by Equations 3.18 and 3.19, included also latent heat (heat transfer equation is not shown here) and was used for studying the influence of absorption on the temperature distribution and moisture flow direction. τ in the evaporation source is a time delay coefficient, and is equal to the time constants mentioned earlier in this Thesis. The form of the evaporation source was chosen due its simplicity and was therefore understood as one possible way of modelling it.

$$\frac{\partial \rho_v}{\partial t} = \frac{\partial}{\partial x} \left(D_{w,v} \frac{\partial \rho_v}{\partial x} \right) + (1 - \rho_v) \frac{1}{\tau} (\rho_{v,sat} \cdot \varphi - \rho_v) \quad (3.18)$$

$$\frac{\partial w}{\partial t} = -\frac{1}{\tau} (\rho_{v,sat} \cdot \varphi - \rho_v) \quad (3.19)$$

where time delay coefficient τ was determined for the experiments on perlite board by fitting, until a good agreement between the model and the experimental data was achieved. The resulting $\tau = 0.3s$ was very small and means that the assumption of equilibrium (for perlite board), was not erratic at all.

3.8 Krabbenhøft & Damkilde

The diffusivities determined from transient measurements (Wadsö, 1993), was shown to be much lower for wood than the diffusivities determined from steady-state cup measurements, and indicated therefore the existence of non-Fickian transport. The work in

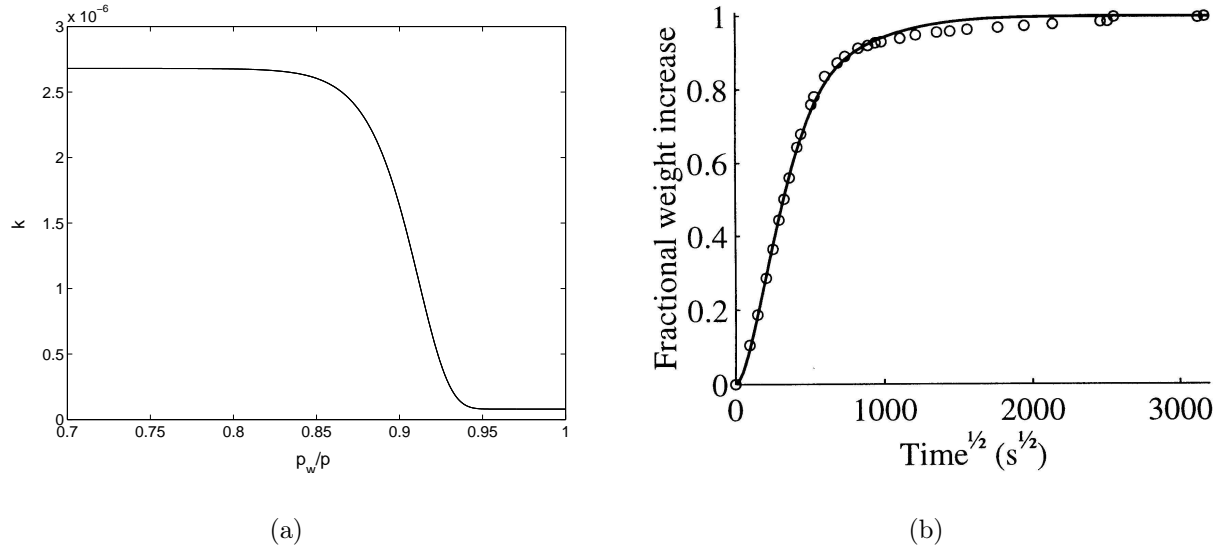


Figure 3.9: (a) The nature of coefficient k as a function of proximity to equilibrium p_w/p (Diagram is reproduced). (b) Comparison of calculated moisture absorption with measurements by (Wadsö, 1993). From (Krabbenhøft and Damkilde, 2002).

(Krabbenhøft and Damkilde, 2002) introduces a way to model non-Fickian transport in wood. Diffusion of water vapour in the cavities and bound water in the cell walls (Equation 3.20 and Equation 3.21 respectively), are treated separately and the interaction is given with a sorption term.

$$\psi \frac{\partial p}{\partial t} = \nabla (K \nabla p_g) - \frac{RT}{M_a} \cdot k (p - p_w) \quad (3.20)$$

$$\frac{\partial w}{\partial t} = \nabla (D_{w,l} \nabla w) + k (p - p_w) \quad (3.21)$$

where ψ is the porosity, K bulk transport coefficient of gas (defined in this way in this presentation for the sake of simplicity), and M_a is the molecular weight of air. The sorption coefficient k was proposed to be a function of the moisture content w and the proximity to equilibrium p_w/p , where p_w is the vapour pressure at the saturated pore surface. This type of function for sorption interaction made it possible to model the situation starting with a dry sample, which gave Fickian sorption according to (Christensen and Kelsey, 1959), because the result was independent of the the final moisture content and also of the step size. An analytical expression for k was given, which allowed rapid sorption in the beginning and slow sorption nearer to equilibrium (see Figure 3.9(a)). Numerical values for k were determined by fitting the model with experimental data from (Wadsö, 1993). The resulting simulation with the model given by Equations 3.20 and 3.21 showed good agreement with the measurements (see Figure 3.9(b)).

3.9 Concluding remarks

The literature review in this Chapter presented a number of authors that have studied non-Fickian moisture transport. The assumption of immediate local equilibrium has been generally rejected and moisture transport and storage were divided in pore air phase and absorbed moisture phase. The link between the air and the absorbed phase was modelled by a sorption equation, where the moisture flux was determined by a proportional coefficient and a moisture potential. The focus in these studies has been on the development of transport equations. Only (Håkansson, 1998) attempted to model the retarded moisture capacity, also. Some discussion on the nature of this sorption coefficient exists, e.g. (Krabbenhøft and Damkilde, 2002; Salin, 1996b), but it was not shown based on the experimental data. The sorption coefficient mentioned by the referred authors (Cunningham, 1995; Salin, 1996b; Koponen and Liu, 1999; Scarpa and Milano, 2002) was constant in the studied interval, while the model in (Krabbenhøft and Damkilde, 2002) operated with a differential coefficient.

It must be stressed that, while Salin studied moisture transport on the *material surface*, the other authors studied a *material node*, where non-Fickian behaviour was modelled as a part of a moisture transport model in a porous material. However, an analogy between the macroscopic surface and the microscopic interaction between the absorbed moisture and water vapour in the pores of a material can be assumed to exist.

Due to retarded sorption, the available moisture capacity of a material is not equal to the slope of the sorption isotherm, as under the common assumption of instantaneous local moisture equilibrium. By implementing hysteresis, as already mentioned, a less steep slope of the intermediate curve is also one way of describing the reduced moisture capacity. Also, according to (Time, 1998), including hysteresis gives better results when compared with the measurements on wood. However, implementing hysteresis alone is not thought to take any time-dependent sorption processes into account.

Finally, the role of the latent heat on the sorption process must not be forgotten: Moisture absorption releases heat and makes temperature to raise, which again makes the sorption slower, i.e. retarded. This was already discussed in Section 2.3. The literature review in this Chapter has given an opposite conclusion on the importance of including latent heat in the moisture transport models. Nevertheless, including latent heat in a model is not supposed to be a disadvantage.

Chapter 4

Determination of moisture properties

In this Chapter, some of the experimental methods for the determination of two of the most important moisture properties are introduced, i.e. determination of the moisture capacity, and the transport coefficients. In addition, determination of diffusivity is also treated. This Chapter describes some standard methods and is therefore not necessarily a description of the experimental methods used in this work. However, most of the standard methods described here are used also in the actual experimental work, besides the used non-standard methods, and therefore included here. The methods here refer only to the hygroscopic range, i.e. $\varphi < 0.98$.

4.1 Determination of moisture storage capacity ξ

Moisture storage capacity in the hygroscopic range is conventionally determined as a slope of the sorption isotherm (see Equation 2.7). The sorption isotherm is in turn determined experimentally by placing material samples in different relative humidities created by, e.g. saturated salt solutions (see Figure 4.1(a)), and weighing the samples until an equilibrium is reached, and the equilibrium moisture content (*EMC*) can be determined. Climate chambers of varying sophistication can also be used, where *RH* is controlled by dry and moist air streams, e.g. in an advanced micro-scale climate chamber, e.g. IGAsorp¹. There exists an European standard for determination of the sorption isotherms (EN-ISO, 1999).

The *EMC* should be determined for both absorption and desorption processes to reveal the hysteresis effect. The true absorption isotherm is attained by starting with a totally dry sample, which is then placed in monotonically increasing relative humidities until equilibrium is achieved for every point. The desorption isotherm is achieved in the same way, but with the starting point near 100%*RH*, and endpoint at 0%*RH*. The great difficulty here is normally the definition of the wet sample as the starting point for the desorption isotherm. One can stay in the hygroscopic range (*RH* < 98%) or start with a totally saturated sample. The following desorption isotherm will be greatly dependent on the start point chosen. Practically speaking, it might be difficult to even achieve *RH* = 98% due to condensation problems around the sample. For example, in the present work, the 'turning point' of ab- and desorption isotherms has been *RH* = 93 – 94%.

¹The IGAsorp apparatus is described in a data sheet from Hiden Isochema Ltd, 420 Europa Boulevard, Warrington, WA5 7UN, UK. E-mail: info@HidenIsochema.com



(a)



(b)

Figure 4.1: (a) An illustration of the desiccator-method for determination of sorption isotherms. 4 desiccators are seen in the picture, all including different saturated salt solutions. (b) A photo of an advanced micro scale climate chamber: IGA sorp.

In the same way, the definition of the dry sample can vary. The dry mass m_0 can be reached at 0%RH or by drying the sample in an oven. A dry sample is normally defined as one dried at 105°C, because all the physically bound water is then removed. However, some materials will decompose at this or already at lower temperature levels. Nevertheless, the grade of 'dryness' of a sample can have a great influence on the sorption isotherm.

The temperature dependence of retention curves is determined by running the experiments at different temperature levels. Standard isotherms are measured at 20°C.

4.2 Determination of transport coefficients

Discussion of the existing driving forces is closely bound with the experimental methods to determine them, including their corresponding flux coefficients. A transport coefficient is usually determined experimentally when all the driving forces except the one corresponding to the desired coefficient are constant. An example is the isothermal cup measurements determining water vapour permeability for a gradient of water vapour pressure. The transport coefficients are seldom constant but a function of the driving force, moisture content and/or temperature.

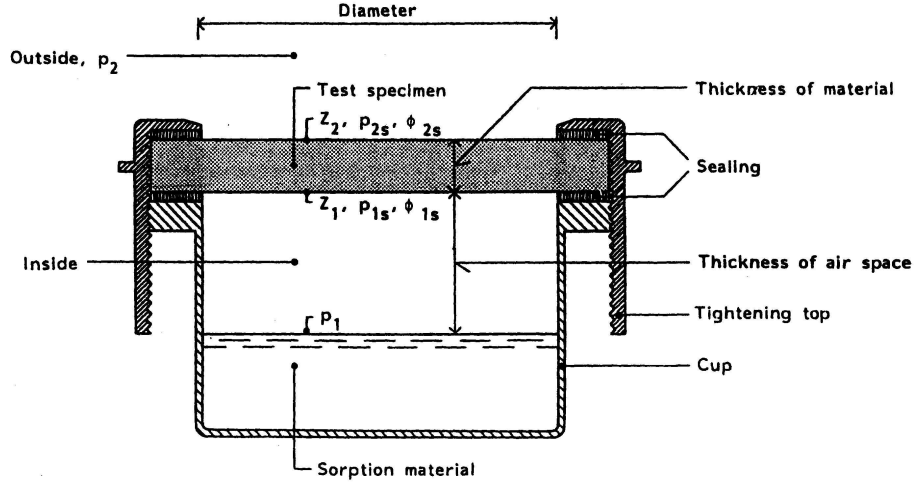


Figure 4.2: Standard cup for determination of water vapour permeability. In the figure, boundary layer resistances $Z_1=Z_{p,in}$ and $Z_2=Z_{p,out}$ are also shown. The sorption material is usually a saturated salt solution. From (Hansen and Lund, 1990).

4.2.1 Determination of water vapour permeability δ_p

The moisture transport properties for isothermal water vapour transport are usually determined with steady-state cup measurements: A sample with a given thickness d is exposed to a water vapour pressure gradient Δp , see Figure 4.2. This gradient is often provided by a saturated salt solution in the cup with a known relative humidity and a humidity controlled climate chamber outside the cup. The standard method is described in the international standard (EN-ISO, 2001). The weight change of the cups g [$kg/(m^2s)$] is measured until there exists a steady state. The water vapour permeability δ_p [$kg/(Pa \cdot m \cdot s)$] is given by

$$\delta_p = g \cdot \frac{d}{\Delta p} \quad (4.1)$$

This equation is valid only, if there is ideal mixing of the humid air on both sides of the sample. In reality this is difficult to reach, at least inside the cup. Therefore, taking into account the resistance of the boundary layers $Z_{p,in}$ and $Z_{p,out}$, and the air layer in the cup $Z_{p,air}$, the expression given by Equation 4.2 should therefore be preferred.

$$\delta_p = \frac{d}{\frac{\Delta p}{g} - (Z_{p,in} + Z_{p,out} + Z_{p,air})} \quad (4.2)$$

where the resistance of the boundary layers $Z_{p,in}$ and $Z_{p,out}$ is given as – here for $Z_{p,out}$

$$Z_{p,out} = \frac{1}{\beta_{out}} \quad (4.3)$$

β_{out} can be estimated from the measured air velocity v and by using Lewis relation, Equation 4.4. The same method can be used for β_{in} , just with an air velocity $v \sim 0m/s$.

$$\beta_{out} = \frac{h_{c,out}}{R_v \cdot T \cdot (\rho c_p)_{air}} \quad (4.4)$$

where $h_{c,out} = 5.82 + 3.96 \cdot v$ is the convective heat transfer coefficient (Pedersen, 1990) and $(\rho c_p)_{air}$ the volumetric heat capacity of air.

For dry cup measurements ($0 < \varphi < 0.5$) a value for stagnant air with the actual thickness can be used as $Z_{p,air}$, but not for wet cup ($0.5 < \varphi < 0.98$): there might exist natural convection due to the density difference of humid air (Krus, 1995). The resulting δ_p will thus be overestimated when using $Z_{p,air}$ for stagnant air. According to (Hansen and Lund, 1990), taking the boundary effects into account is especially important for materials with high permeability.

Several forms for so-called modified cup methods also exist, an example is described in (Bomberg et al., 2002).

Differential permeability $\delta_p(\varphi, T)$

This permeability measured with the cup method includes both water vapour diffusion and effusion because most materials have a broad pore size distribution (Krus, 1995). Also, according to Section 2.2.3, liquid transfer in the form of capillary suction or surface diffusion may take place, at least for high relative humidity. According to (Roels et al., 1999) δ_p includes pure diffusion, Knudsen diffusion, and for high relative humidities also reduction of the pore cross section area and the movement of the adsorbed moisture (see also Figure 2.1 Stages 1-3). Water vapour permeability, including the above mentioned transport forms, is not generally considered to be constant but a function of temperature and relative humidity or moisture content, increasing usually for increasing T and RH . The increase due to relative humidity is generally attributed to the increased liquid transfer for higher RH . Therefore, when strictly regarding *water vapour* permeability, the dependence on RH is often neglected and δ_p is assumed constant. Experiments with low pressure equipment in (Kelly, 2002) showed, however, that pure water vapour permeability decreased slightly for increasing RH . This observation agrees with the general assumption that the effective transfer area for water vapour decreases for increasing moisture content due to the amount of absorbed moisture.

The standard method for determining the differential permeability $\delta_p(\varphi)$ is to measure at least the permeability for 'dry cup' ($0 < \varphi < 0.5$) and 'wet cup' ($0.5 < \varphi < 0.98$). The whole relative humidity range can be investigated in more detail, if more exact knowledge on the permeability is needed. By treating the measured permeabilities as mean values for the respective RH -ranges, an analytical expression for δ_p can be integrated. A range of expressions has been suggested (collected in (Kelly, 2002)) and the majority are exponential or power law functions, where permeability increases strongly for high humidities.

The influence of temperature on permeability is primarily explained by the relationship in Equation 2.9, where the diffusivity in air D_a increases for increasing T . Experiments in (Galbraith et al., 2000) showed a significant increase in δ_p for MDF-board (30%) and for plywood (50%) for high relative humidities, when temperature was changed from 10°C to 30°C. However, according to (Galbraith et al., 2000), the increase could mostly be

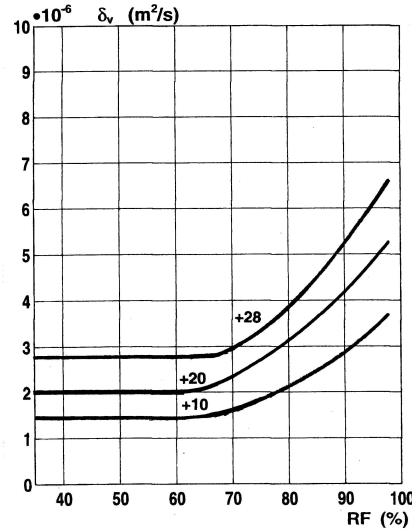


Figure 4.3: Illustration of the temperature dependence of the water vapour permeability for cellular concrete ($\rho_0 = 500 \text{ kg/m}^3$): δ_v increases with temperature and especially for high RH . From (Hedenblad, 1996).

allocated to the increased liquid transfer for increasing T . As stated above, the measured δ_p represents both vapour and liquid transport for $\varphi > 0.6$, approximately. Experiments by (Hedenblad, 1996) confirmed the temperature-dependence of permeability (see Figure 4.3).

Conversely, (Krus, 1995), concluded the opposite about temperature-dependence, i.e. that it was more significant for materials with low (e.g. sandstone), rather than high moisture content (gypsum and wood). His analysis is here referred to briefly. When setting up the equation for combined vapour and liquid transport,

$$g = g_v + g_l = -\delta_p \frac{dp}{dx} - D_{w,l} \frac{dw}{dx} \quad (4.5)$$

a fictive water vapour permeability of a material δ^* can be determined as

$$\delta^* = -\delta_p + \frac{g_l}{\frac{dp}{dx}} \quad (4.6)$$

g_l should not change with temperature. The viscosity of water decreases for increasing temperature (more transport) but the slope of the sorption isotherm decreases for increasing temperature (less transport). For increasing temperatures, the second part of Equation 4.6 decreases and thereby also δ^* . Measurements on paper membrane (Schascheck, 1956) also confirmed this. However, if one looks at moisture transport with respect to the moisture content of the material ($g_{moist} = g - g_{dry}$), transport increases for increasing temperature.

Finally, in (Mukhopadhyaya et al., 2001) the temperature dependency of water vapour permeability was tested on a natural fibreboard and gypsum board. Samples were tested at four different temperature levels between 7 and 43°C. No significant increase in permeability was found as a result of these tests.

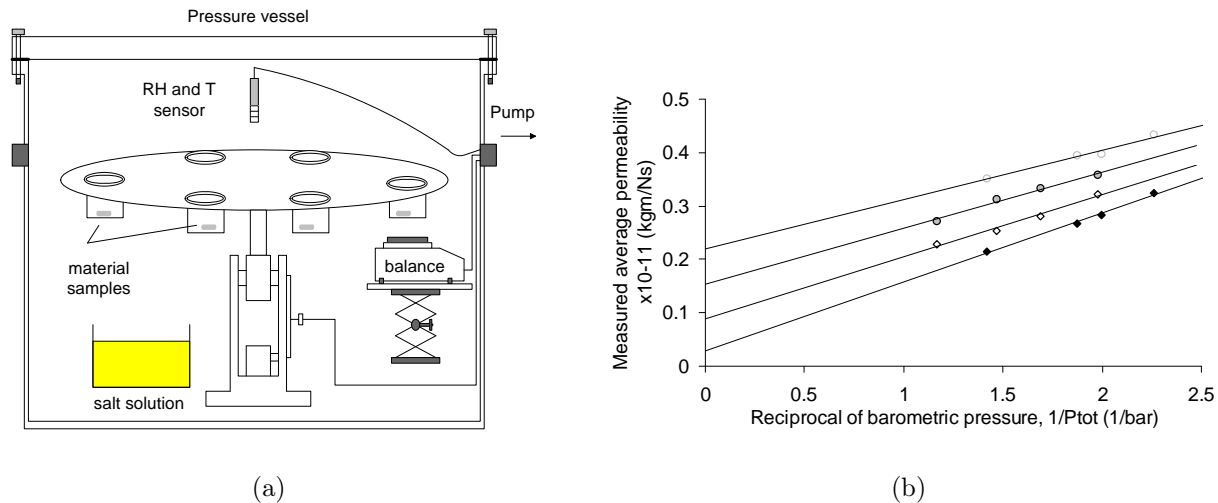


Figure 4.4: (a) The low pressure set-up with the pressure vessel and the measurement cups. (b) An example on the resulting permeability as a function of reciprocal barometric P_{tot} for plywood. The intersection with the y-axis denotes the liquid part and the slope the vapour part. There exists a clear tendency for the liquid part to increase with the RH -level, while the vapour part (slope) decreases. All from (Kelly, 2002).

Separation of driving forces for vapour g_v and liquid transfer g_l

A problem with the presented methods and definitions for determining water vapour transport coefficients is that there will always exist both vapour and liquid in the pores of the material, at least for high relative humidities. This co-existence depends on the pore structure of the material and the relative humidity level, as mentioned earlier. To be able to describe both processes, they have to be treated simultaneously (Kelly, 2002).

(Kelly, 2002) showed how it was possible to separate vapour and liquid transport coefficients by using low pressure measurements. Two experimental approaches for separating these transport forms were investigated using standard cup measurements and low pressure experiments (see Figure 4.4). As the theoretical basis for low pressure experiments, the technique of expressing the total moisture transport in terms of ∇p and ∇T was used, instead of ∇p and ∇P_l , by employing the Kelvin relation (Equation 2.6) and Clausius-Clapeyron equation. For the isothermal case, permeability can be expressed as a function of the reciprocal barometric pressure P_{tot} alone.

Another attempt to identify the driving forces and separate the transport forms was reported in (Krus, 1992) and (Krus, 1995) (see Figure 4.5). He carried out some non-isothermal permeability measurements on gypsum board and sandstone, which supported the hypothesis that the vapour diffusion coefficient is constant and co-exists with liquid transport, driven by a relative humidity gradient, and increases for increasing RH .

(Krus, 1995) also showed, among others e.g. (Künzel, 1995) and (Hagentoft, 2001), how the liquid transport coefficient $D_{w,l}$ can be determined from the dry and wet cup measurements under the assumption that the difference between these results gives the liquid part.

The liquid flow given as surface diffusion can be determined in terms of the liquid conductivity coefficient D_φ from a relative humidity gradient $\partial\varphi/\partial x$ for constant water vapour pressure p

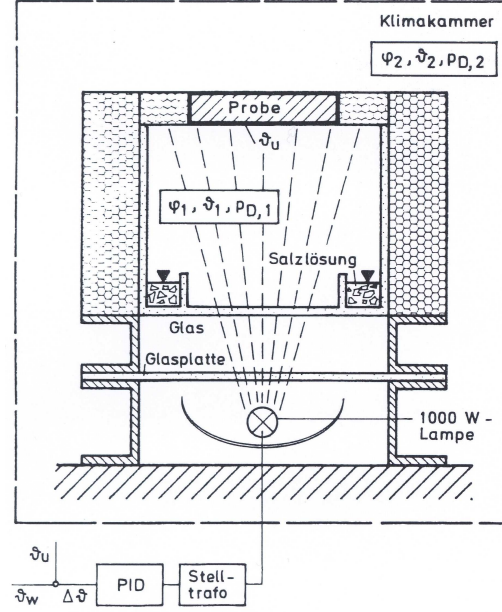


Figure 4.5: The non-isothermal set-up in (Krus, 1995) to reveal liquid transport driven by RH -gradient. A material sample (Probe) is exposed to a RH - (φ), T - (ϑ) and p -gradients (p_D), given by saturated salt solutions (Salzlösung) and a lamp (Lampe) inside the cup, and a climate chamber (Klimakammer) outside the cup. From (Krus, 1995).

$$D_\varphi = -\frac{g}{\frac{\partial \varphi}{\partial x}}|_p \quad (4.7)$$

On the other hand, (Hens, 1992) discussed and determined the coefficients used in the model suggested in (Krus, 1992), and concluded that the use of both water vapour pressure and relative humidity as driving potentials for the apparent vapour transport was less correct than using water vapour permeability, which is a function of relative humidity. (Hens et al., 1993) also made isothermal and non-isothermal permeability measurements on lightweight concrete and expanded polystyrene, and found no confirmation of the hypothesis that both vapour pressure and relative humidity are driving forces in the hygroscopic range.

4.2.2 Determination of thermal moisture diffusion coefficient D_T

Thermal moisture diffusion coefficient D_T [$kg/(K \cdot m \cdot s)$] is defined by

$$D_T = -\frac{g}{\nabla T}|_w \quad (4.8)$$

where D_T represents both water vapour and liquid transport driven by the thermal gradient ∇T (Kumaran, 1996). The assumption of constant moisture content in Equation 4.8 means also constant relative humidity, if there is no change in the sorption as a function of temperature. If the sorption is a function of temperature, the relative humidity for the

higher temperature will be slightly higher, (see also (Kumaran, 1996)). The definition above will therefore only be valid for uniform moisture content.

A study in (Philip and De Vries, 1957), showed that taking account of temperature-driven moisture transport gave moisture transport ratios that were 1.3-3 times larger than pure concentration-driven transport alone. However, the determination of the thermal diffusion coefficients has not been the major interest of the research society, although some investigations do exist.

(Nicolajsen, 1973) presented several ways of presenting total moisture transport as a combination of two driving forces at a time and the connected coefficients, including D_T . Non-isothermal measurements on cellular concrete in the hygroscopic range showed, however, that it was not possible to completely separate the driving forces. Nevertheless, three different phenomenological transport equations were given as a combination of two potentials each, even though transport forms could not be separated. The coefficients were determined by solving the treated equation for every measurement and by calculating the average and the standard deviation value.

Work in (Galbraith et al., 1998) and (Peuhkuri et al., 2003) reported different methods to determine temperature induced moisture transport described by Equation 4.8. An extensive experimental programme was undertaken, which consisted of both small- and large-scale moisture flow measurements under non-isothermal conditions carried out over a range of test temperatures (10-30°C). D_T was determined by

$$D_T = -\frac{g + \delta_p \frac{\partial p}{\partial x}}{\frac{\partial T}{\partial x}} \quad (4.9)$$

Small scale tests consisted of more or less standard cups, which were exposed to a temperature gradient either with a water bath or by a radiative heating mat (see Figure 4.6(a)). The cups were weighed the same way as in the standard cup method. Some of the measurements showed no thermal diffusion while others did. An example of the results for the latter is given in Figure 4.6(b).

The large-scale apparatus consisted of twin-climate chambers. Between these chambers, a measurement template was positioned, capable of holding four 800 x 800mm samples. Each sample had its own 500 x 500mm 'guard box' to minimise edge effects and to ensure one-dimensional moisture and temperature flow. The twin-chamber is shown in Figure 4.6(c). This set-up allowed gradients of both humidity and temperature to be imposed across each material test sample. The moisture flux through each of the four samples, was determined from the weight change against time of the tray of salt solution contained within each guard box.

The moisture flux over a temperature gradient, but in the deliberate absence of a vapour pressure gradient was measured at different RH -levels. The moisture flux was plotted against the vapour pressure gradient (which was not always equal to zero), for each sample, and a linear relationship was fitted to the data to estimate the moisture flux at zero vapour pressure difference (see Figure 4.6(d)). No thermal diffusive effect, independent of the temperature generated vapour pressure gradients, was measurable in this system for the materials tested.

As the non-isothermal coefficients are difficult to determine, the isothermal set of equations could be used with fairly good approximation to the non-isothermal water vapour

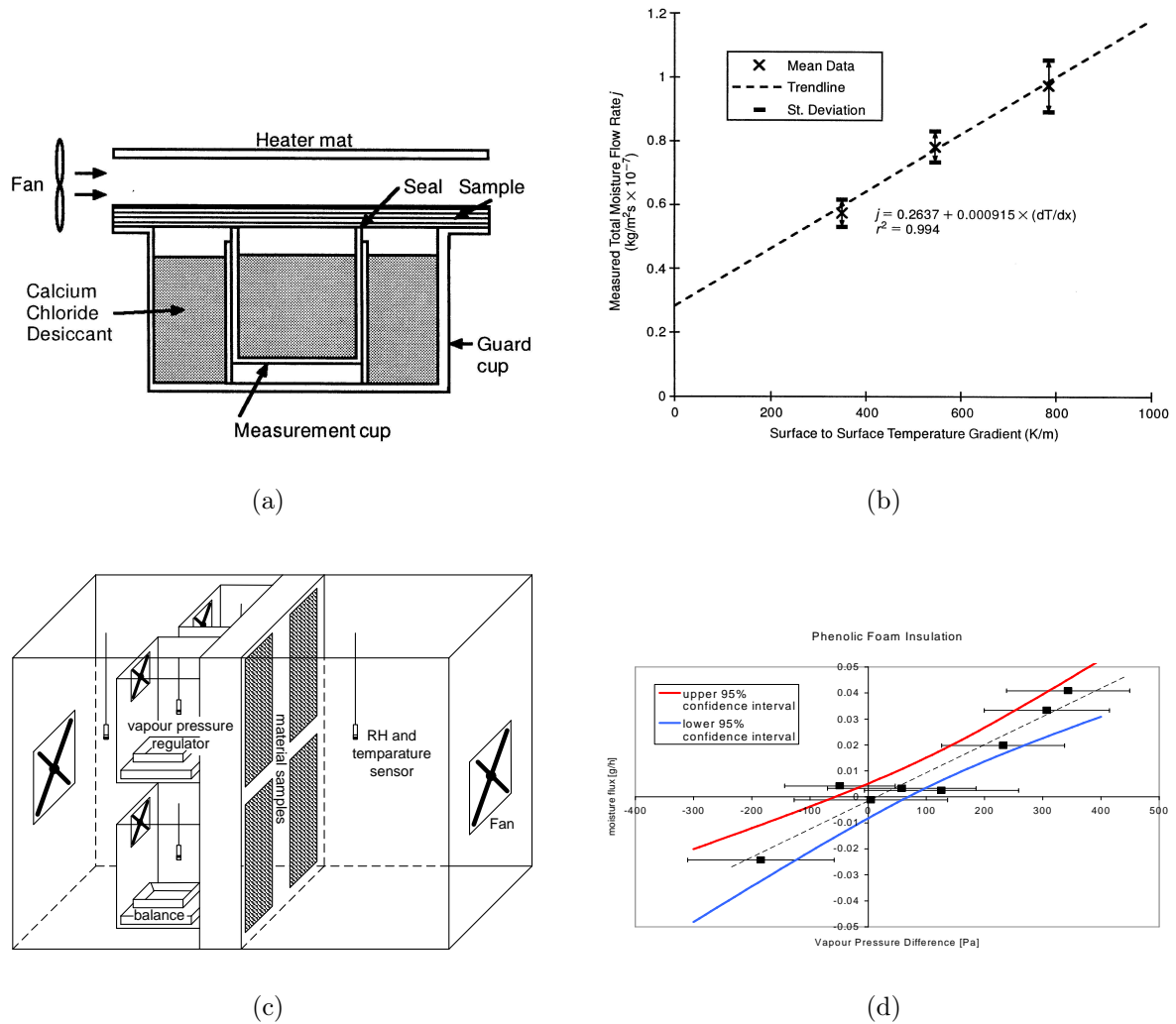


Figure 4.6: (a) The small scale non-isothermal set-up. (b) Results for polystyrene insulation for the small scale non-isothermal set-up. The intersection with y-axis stands for the isothermal moisture flux and the slope for D_T . From (Galbraith et al., 1998). (c) The large scale non-isothermal set-up at Glasgow Caledonian University. (d) Results for phenolic foam insulation for the large scale tests. From (Peuhkuri et al., 2003).

transport. The temperature dependence is mainly given by the saturation vapour pressure $p_s(T)$.

4.3 Determination of moisture diffusivity D_w

Under the assumption of immediate local equilibrium and Fick's law, a dynamic sorption approach can be used to directly determine moisture diffusivity D_w . This moisture diffusivity is related to the water vapour permeability coefficient δ_p , determined by the steady-state cup measurements given by Equation 2.32, which reorganised gives:

$$\delta_p = \frac{D_w \cdot \frac{\partial w}{\partial \varphi}}{p_{sat}} \quad (4.10)$$

Determination of the diffusivity from the dynamic sorption experiments is based on the assumption of sorption rates for a slab with a half thickness of l (Crank, 1975). The following expressions are widely used in several studies, e.g. (Künzel and Kiessl, 1990; Wadsö, 1993; Time, 1998). When studying the initial sorption rates, Equation 4.11 can be used, while for the final part of the sorption, Equation 4.12 is valid.

$$D_w = \frac{\pi}{4} \cdot l^2 \left(\frac{dE}{d\sqrt{t}} \right)^2 \quad \text{for} \quad E < 0.5 \quad (4.11)$$

$$D_w = \frac{4 \cdot l^2}{\pi^2 \cdot t} \ln \left(\frac{8}{\pi(1-E)} \right) \quad \text{for} \quad 0.4 < E < 1 \quad (4.12)$$

where the non-dimensional moisture content E – as an average over the thickness of the sample – is defined as, see also Figure 4.7,

$$E = \frac{u(t) - u(0)}{u(\varphi) - u(0)} \quad (4.13)$$

where $u(t)$ is moisture content at time t , $u(0)$ is moisture content at $t = 0$ and $u(\varphi)$ is the equilibrium moisture content by the target relative humidity φ .

Additional conditions for the validity of these expression for D_w are, partly referred to, as cited in (Time, 1998). They include;

- uniform initial concentration distribution in the sample
- for $t > 0$, the surface of the sample reaches the concentration equal to the ambient humidity level immediately

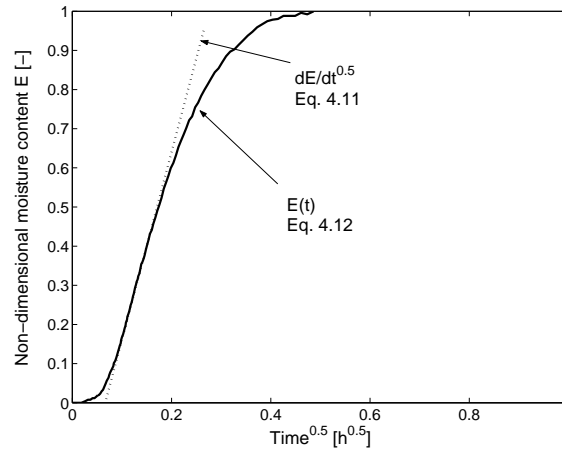


Figure 4.7: Definition of the non-dimensional moisture content E and the slope $\frac{dE}{d\sqrt{t}}$ from an ab- or desorption step.

- the concentration in the center of the sample does not change remarkably
- diffusion coefficient is constant in the measured interval

One of the indications for non-Fickian diffusion (treated separately in Chapter 3), is the deviation between the diffusion coefficients measured with steady state cup-method δ_p , and dynamic sorption measurements from D_w for $RH > 70\%$ (Wadsö, 1993). When determining D_w , it is assumed that Fick's law is valid and that all the local sorption (at least in the initial phase) is immediate. According to (Wadsö, 1993), one should not use Equation 4.12, if non-Fickian effects are expected, and concludes that it might be a good idea to first use several methods and then judge the results.

According to investigations by (Time, 1998), this divergence could also exist due to uncertainties in the parameters involved in Equation 2.32 alone, and not to non-Fickian behaviour.

If it is possible to determine the moisture content profile during moisture uptake, e.g. with NMR or X-ray measurements, the diffusivity D_w can be determined directly via the Boltzmann transformation. However, this method is usually employed for capillary moisture uptake experiments, which fall outside the hygroscopic range $\varphi < 0.98$, and therefore, is not treated further here.

Chapter 5

Isothermal, dynamic moisture transfer

This Chapter describes experimental and numerical approaches to quantify the time-dependence of sorption mechanisms for some hygroscopic building materials, e.g. mainly insulation materials. Previous investigations of retarded sorption and non-Fickian phenomena, mostly on wood, have inspired the present analyses on other materials, see Chapter 3. The slope of the sorption isotherm alone cannot describe the true moisture capacity of a material when that material is exposed to dynamic changes in moisture conditions. Nevertheless, the assumption of an immediate local equilibrium is well accepted in simulation models.

The experimental part includes measurements with two different set-ups, where small samples are exposed to ab- and desorption steps in a controlled relative humidity and temperature environment. The change in the bulk moisture content is followed continuously as the sample is attached directly to a balance.

The experimental results are not only analysed theoretically, but also used in a numerical analysis, which is based on a "conventional Fickian" model. The aim of the analysis is to quantify some characteristic parameters, e.g. moisture diffusivity, active depth and dynamic moisture storage model, by developing the simulation model also to include some dynamic parameters.

5.1 Background

As already mentioned in Chapter 3, isothermal step-response experiments have been used previously, e.g. by (Wadsö, 1993; Håkansson, 1998; Time, 1998; Koponen and Liu, 1999) when investigating dynamic moisture mechanisms (non-Fickian phenomena), in wood. (Künzel and Kiessl, 1990) analysed step-response in sandstone, cellular concrete and mortar. In these experiments, small and thin specimens (some millimetres in thickness) were subjected to rapid changes in relative humidity (RH). These RH -variations of the ambient air were of differing magnitude and at different levels. The response was measured as a gravimetric weight change for these geometrically well-defined specimens, which was translated to moisture content in the specimen.

For wood, these experiments have showed indications for non-Fickian behaviour, i.e. the measured moisture uptake is much slower than the calculated one, and the diffusion coefficients determined by the cup method (steady state) and by the sorption method

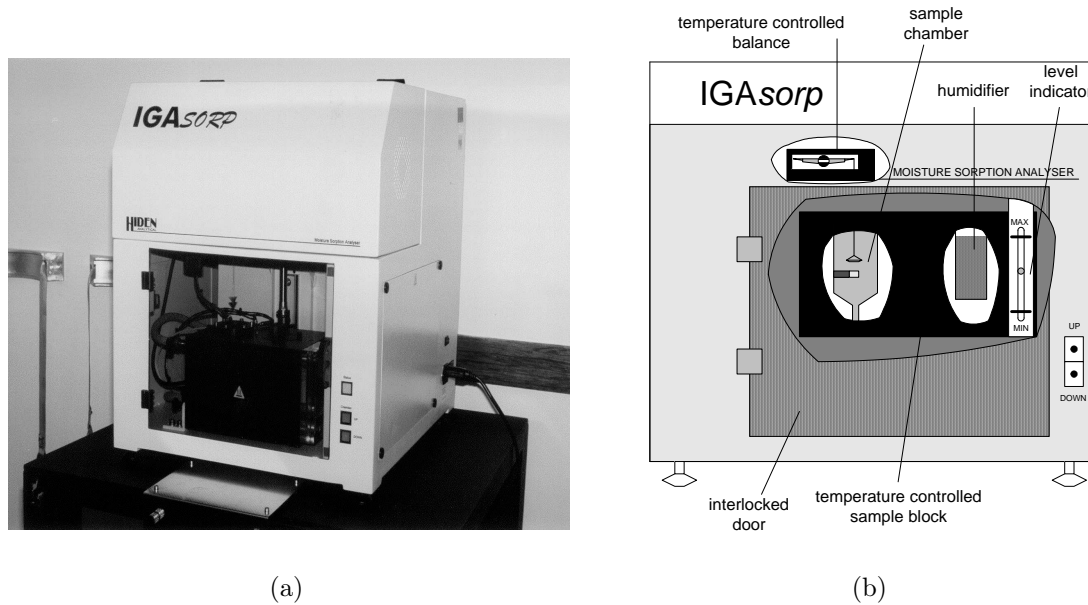


Figure 5.1: The IGAsorp equipment at GCU. (a) Overall photo. (b) Drawing with some main components. From (Kelly, 2002).

(transient) are not always comparable. By contrast, experiments in (Künzel and Kiessl, 1990) showed that sorption in sandstone is fully Fickian.

The characteristics of Fickian as well as non-Fickian behaviour were discussed in Chapters 2 and 3 in order to understand the complexity and significance of the parameters involved in dynamic moisture transfer, and to set the current work in the right context.

5.2 Experiments

The experimental part of the work was based on two different types of investigations on sorption behaviour, 1) using a micro-scale sorption apparatus and 2) following the weight change of a larger scale specimen in a climate chamber. The aim of the experiments was to study the sorption behaviour of a material when the sample was subjected to a step change in the ambient relative humidity. This type of investigation is also called a "step-response" analysis. The results from the first investigation were also used for the numerical investigation of the sorption behaviour, and to set-up a non-Fickian moisture transport model, while the results from the second experiment were used for validation of the model.

5.2.1 Materials

The materials used, together with some material parameters and sample dimensions are given in Tables 5.1 and 5.2.

Although very different, the materials used were all highly porous and relatively lightweight. They were chosen with the anticipation that their response to a dynamic change in moisture content of air would be very variable: some materials would absorb large amounts

of moisture, while others would not. The differences in sorption properties can be illustrated by sorption isotherms, given in Figures 5.2 (more absorbent materials) and 5.3 (less absorbent materials). It was also expected that some materials would possibly show retarded sorption.

Some of these materials are rather common in building envelopes, e.g. glass wool and aerated cellular concrete, but more 'exotic' insulation materials were also included in the experiments; i.e. cellulose, wool and flax insulation and expanded perlite. A more detailed description of the investigated materials is found in Appendix A.

Table 5.1: Some material parameters and test sample dimensions of the materials used in micro scale sorption experiments (IGAsorp measurements). Sample shape was close to spherical with the given radius. Only one sample used per material. Isothermal permeabilities originate from (Hansen et al., 1999) (6 samples for each condition), except for glass wool (3 samples) and cellular concrete (4 samples) that have been determined as a part of this work with the same experimental set-up and conditions as in (Hansen et al., 1999). Cellular concrete is the quality sent to several laboratories in Europe, North America and Japan in 1999 as a part of the CIB W40 TG on Material characterization and model bench-marking.

Material	Nominal dry density [kg/m^3]	Isothermal permeability		Sample dry weight [mg]	Sample size radius [mm]
		Dry cup [$10^{-9} \cdot kg / (Pa \cdot m \cdot s)$]	Wet cup		
Glass wool insulation	70	0.18 ± 0.01	0.17 ± 0.006	54.47	6
Aerated cellular concrete	450	0.02 ± 0.001	0.024 ± 0.0004	113.35	4
Cellulose insulation	65	0.13 ± 0.003	0.11 ± 0.002	62.48	6
Flax insulation	30	0.16 ± 0.02	0.15 ± 0.06	45.42	7
Wool insulation	25	0.19 ± 0.02	0.19 ± 0.05	12.39	5
Perlite insulation	100	0.13 ± 0.06	0.10 ± 0.02	50.08	5

Table 5.2: Materials and dimensions used in larger scale sorption experiments (DTU Climate Chambers). Only one sample used per material. Note: $d = 2l$ in Figure 5.4.

Material	Sample dry weight [g]	Sample size [mm]($d \times L \times W$)	Measured density [kg/m^3]
Glass wool insulation	76.69	20x300x300	43
Aerated cellular concrete	96.14	20x100x100	481
Cellulose insulation	64.14	20x300x300	36
Flax insulation	61.65	20x300x300	34

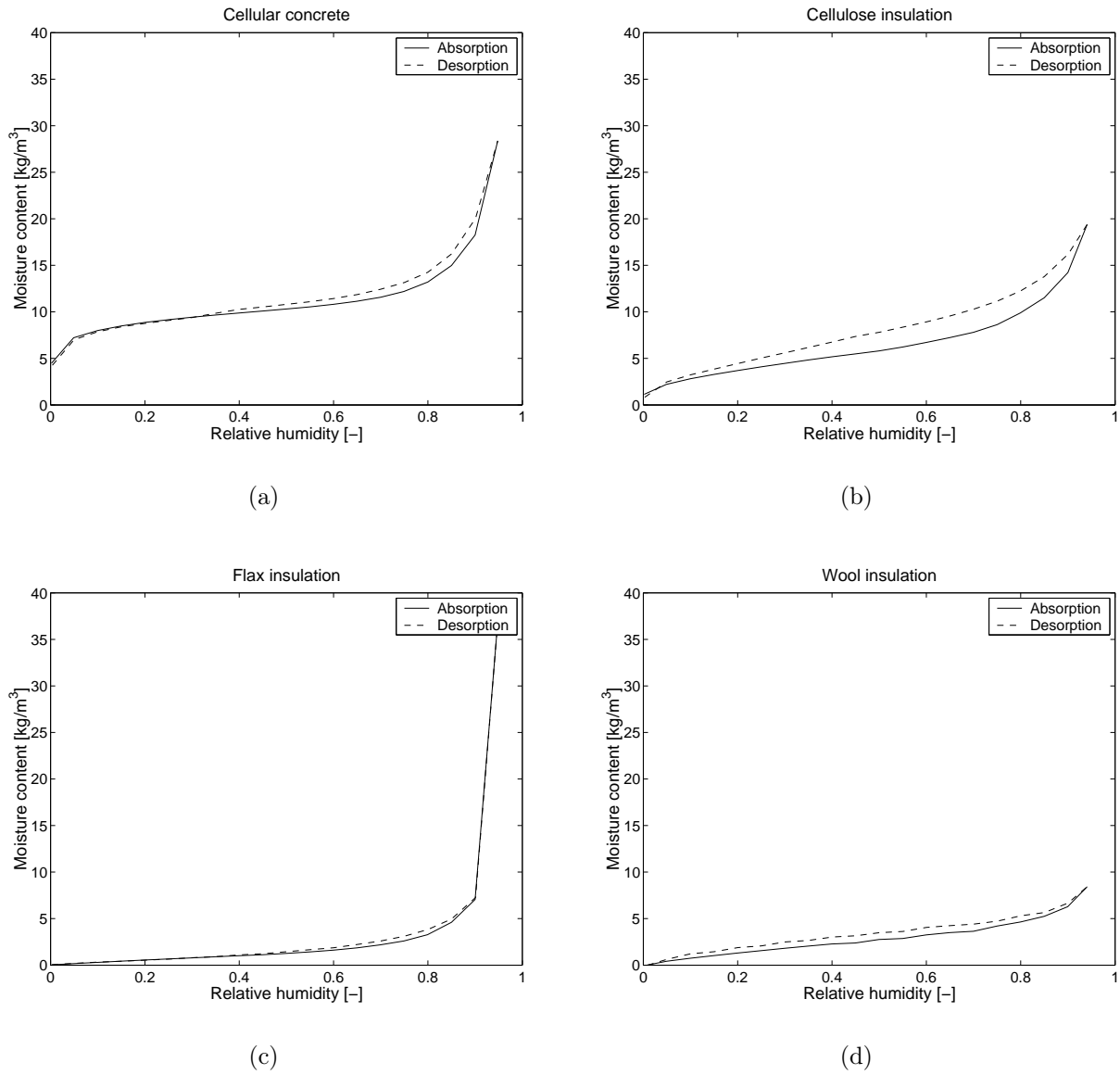


Figure 5.2: Sorption isotherms for absorbent materials: (a) Cellular concrete, (b) cellulose insulation, (c) flax insulation and (d) wool insulation. Moisture content w is given by volume [kg/m^3]. Note the same scale for all the materials, but different from that in Figure 5.3.

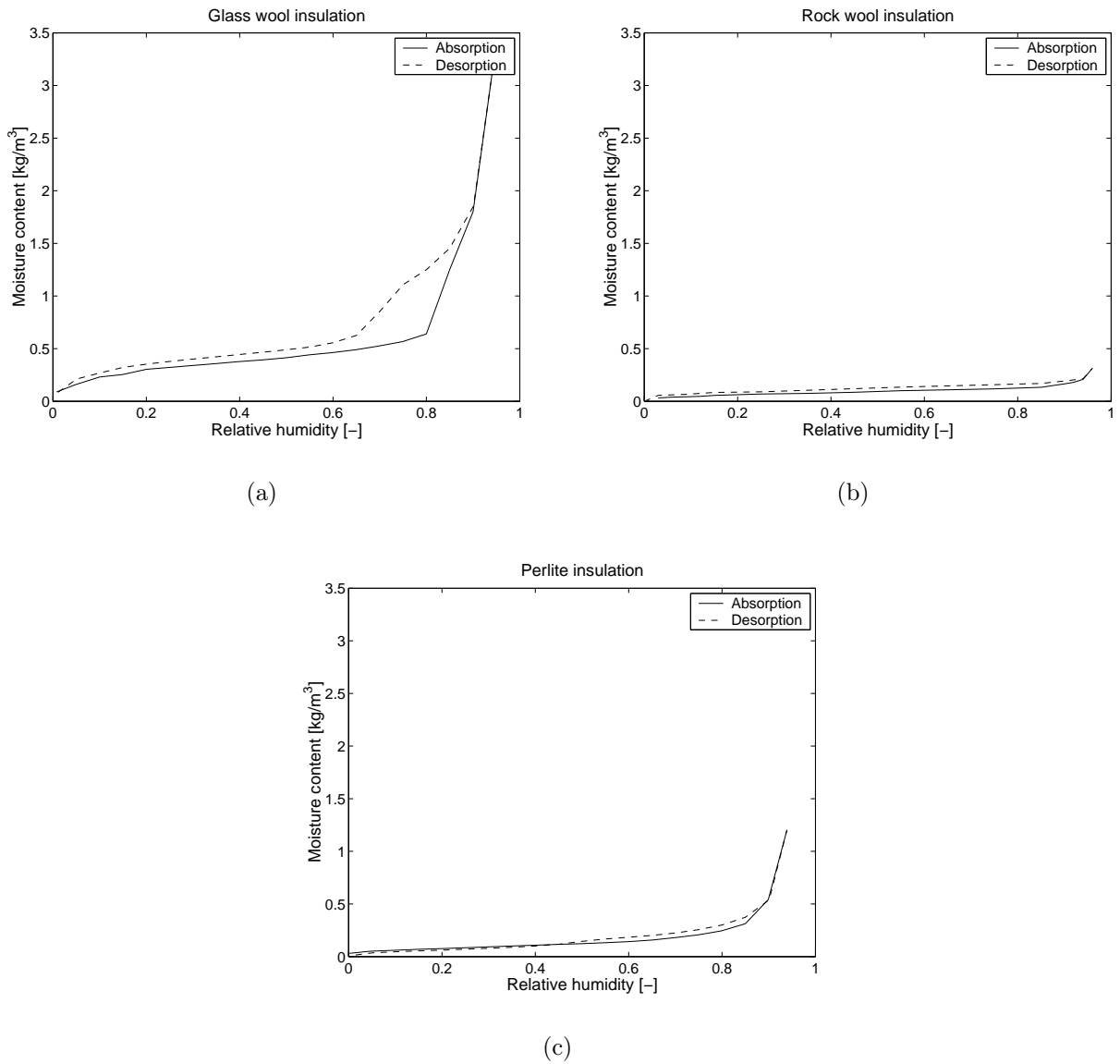


Figure 5.3: Sorption isotherms for non-absorbent materials: (a) Glass wool, (b) rock wool and (c) perlite insulation. Moisture content w is given by volume [kg/m^3]. Note the same scale for all the materials, but different from that in Figure 5.2.

Table 5.3: Accuracy of the IGAsorp equipment and the climate chambers at DTU

Component	IGAsorp	DTU Climate Chambers
Humidity control	$\pm 1\% RH$ (0-90% <i>RH</i>) $\pm 2\% RH$ (90-95% <i>RH</i>)	$\pm 0.2\% RH$ (low <i>RH</i>) $\pm 2\% RH$ (high <i>RH</i>)
Temperature control	$\pm 0.05^\circ\text{C}$	$\pm 0.4^\circ\text{C}$
Balance	1 μg	1 mg

5.2.2 Experimental set-up

IGAsorp equipment at GCU

The micro scale sorption experiments were carried out with standard sorption equipment IGAsorp (see Figure 5.1) at Glasgow Caledonian University, School of Engineering, Science and Design (GCU).

The IGAsorp has a sensitive microbalance (capacity 200mg) which continuously registers (on average every 15s, with a time span from 0.1 seconds to 10 minutes), the weight of the sample together with the temperature and relative humidity around the sample. The temperature can be varied from 5°C to 80°C and the relative humidity from 0% *RH* to 95% *RH*.

Wet and dry air streams controlled relative humidity while the temperature was regulated by water circulation in a kind of heat exchanger, around the sample. The sample was placed within a weighing basket and positioned on the microbalance. The chamber was then closed and the sample sealed in position. Sample drying before sorption measurements was carried out at 20°C in nitrogen until the sample weight reached equilibrium, in about 12 hours. After drying, the sorption measurements began. The climate around the sample was held constant until equilibrium or until a given time was exceeded, before changing the *RH* to the next level. The end drying could be made at different temperature levels. In the actual analysis, no elevated temperatures were used, but investigations on the effect of drying temperature on sorption will be dealt with in a future study. The significance of different step sizes in *RH* on the sorption behaviour was also analysed. Steps at 5%*RH*, 10%*RH* and 20%*RH* were used. The maximal time step used in these measurements was 8 hours to equilibrium at one *RH* increment.

In addition to the standard sorption isotherm, all the continuous registrations of *RH*, weight and *T* determined by the equipment (the kinetic data), could also be exported. This kinetic data was used in the following analysis of the dynamic moisture uptake and release in a small body. The accuracy of the equipment is given in Table 5.3.

The convective moisture resistance $Z_{p,c}$ was estimated to $0.03 \text{ m}^2\text{s} \cdot \text{GPa}/\text{kg}$ according to (Janz, 2000), where air flow around the sample in a similar equipment was $\sim 1 \text{ mm}/\text{s}$.

Climate chambers at DTU

The illustration of the set-up at the Technical University of Denmark (DTU) can be viewed in Figure 5.4.

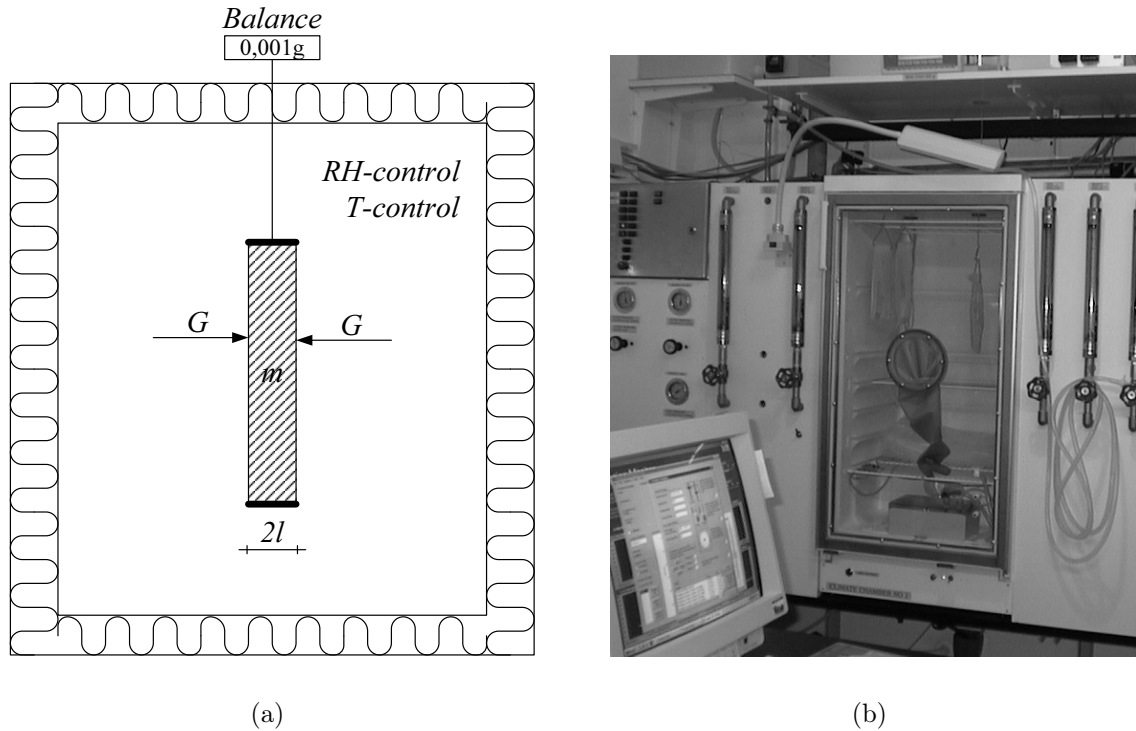


Figure 5.4: (a) The sorption set-up in the climate chambers at DTU. $2l$ = thickness of the sample, m = mass of the sample and G = moisture flux one-dimensionally to the sample. (b) Photo of a climate chamber.

A number of geometrically well defined, relatively thin specimens, were exposed to a one-dimensional combined moisture transport and sorption process in the climate chamber. The sample was continuously attached to a balance and positioned in a climate chamber, whose climate was automatically controlled and which maintained the desired temperature and relative humidity with an accuracy given in Table 5.3 (Strømdahl, 2000). The experimental procedure involved a series of rapid changes in the chamber's relative humidity, which was periodically altered in ab- and desorption steps for some weeks or months. The entire relative humidity range was not measured, only the area of practical interest, i.e. 50-95% *RH*.

The weight of the sample was measured by a balance that registers the measurements together with the temperature and the relative humidity of the chamber every 30 minutes. The sample was placed in a net bag, made of a practically moisture inert polyester to ensure no loss of material during the measurements. To make the sorption one dimensional, the soft samples had a stainless steel frame around their periphery, while cellular concrete was sealed with aluminium tape. To determine the moisture content, samples were dried afterwards at 50°C (for cellulose and flax insulation) or 103°C (for cellular concrete and glass wool) until all the physically bound water was removed.

The convective moisture surface resistance $Z_{p,c}$ was reduced by an air flow around the sample, which was measured to 0.2 m/s, corresponding to $Z_{p,c} = 0.02 (m^2 s \cdot GPa) / kg$. The accuracy of the set-up is given in Table 5.3.

5.2.3 Results

The step response measurement results were partly given as gravimetric moisture content u (Equation 2.3) and partly as non-dimensional moisture content of the sample $0 < E < 1$, which is determined by Equation 4.13

$$E = \frac{u(t) - u(0)}{u(\varphi) - u(0)} \quad (4.13)$$

where $u(t)$ is moisture content at time t , $u(0)$ is moisture content at $t = 0$ and $u(\varphi)$ is the equilibrium moisture content by the target relative humidity φ . Non-dimensional moisture content E has been used by several authors referred in Chapter 3 to illustrate deviations from Fickian behaviour. Therefore, this method of presenting the results is also adapted here. The reader must keep in mind that the results given as E are *relative* to the total amount of absorbed moisture and do not give the moisture uptake as a *function of time*.

Consecutive ab- and desorption steps

At first glance, the nature of ab- and desorption steps for the different materials used were very similar, apart from the amount of moisture. Figure 5.5(a) and (b) shows a typical absorption sequence for cellular concrete and flax insulation, see Appendix B.1.1 for all materials. Generally, the middle part (where the sorption isotherm is traditionally almost linear), was characterised by relatively rapid steps for all the materials, at least compared to high relative humidities. In this way, an overview of the results already showed the nature of retarded sorption, i.e. that sorption was slower at high relative humidities. The moisture content was given as in Equation 2.3.

The non-dimensional moisture content determined with Equation 4.13 was used in the following to illustrate the effect of moisture level on the sorption response.

Figure 5.6(a) shows how the sorption for flax becomes slower for decreasing relative humidity level, i.e. for $RH < 45\%$. This was not expected according to either Fickian, or non-Fickian behaviour, as referred to in Chapter 3, where sorption was found to decelerate for increasing RH for all relative humidity levels. For relative humidities higher than $RH > 40-45\%$, the picture was as expected, i.e. sorption was increasingly delayed for increasing RH (see Figure 5.6(b)). The same pattern was seen for all the materials. One obvious explanation could be the shape of the sorption isotherm, i.e. in the 'middle-range' of the relative humidities, the slope of the sorption isotherm ξ (the moisture capacity), is smallest. Here, the sorption according to Figure 5.6(a) and (b) became slower towards both low and high relative humidities, i.e. with higher ξ . For high ξ more moisture needed to be ab- or desorbed, and took more time, than less moisture for low ξ .

The difference between the investigated materials is illustrated also. When comparing the response of these very different materials (see Figure 5.6(c) and (d)), it was obvious that moisture sorption in, e.g. glass wool was much more rapid than in flax insulation. Again, an obvious explanation could simply be the different moisture capacity of the materials. In other words, a larger moisture capacity involved more moisture and the sorption took a longer time per RH -step, e.g. sorption in flax ($\xi = 0.28$ for $RH = 70 - 75\%$) was slower than in cellular concrete ($\xi = 0.027$) or glass wool ($\xi = 0.012$)

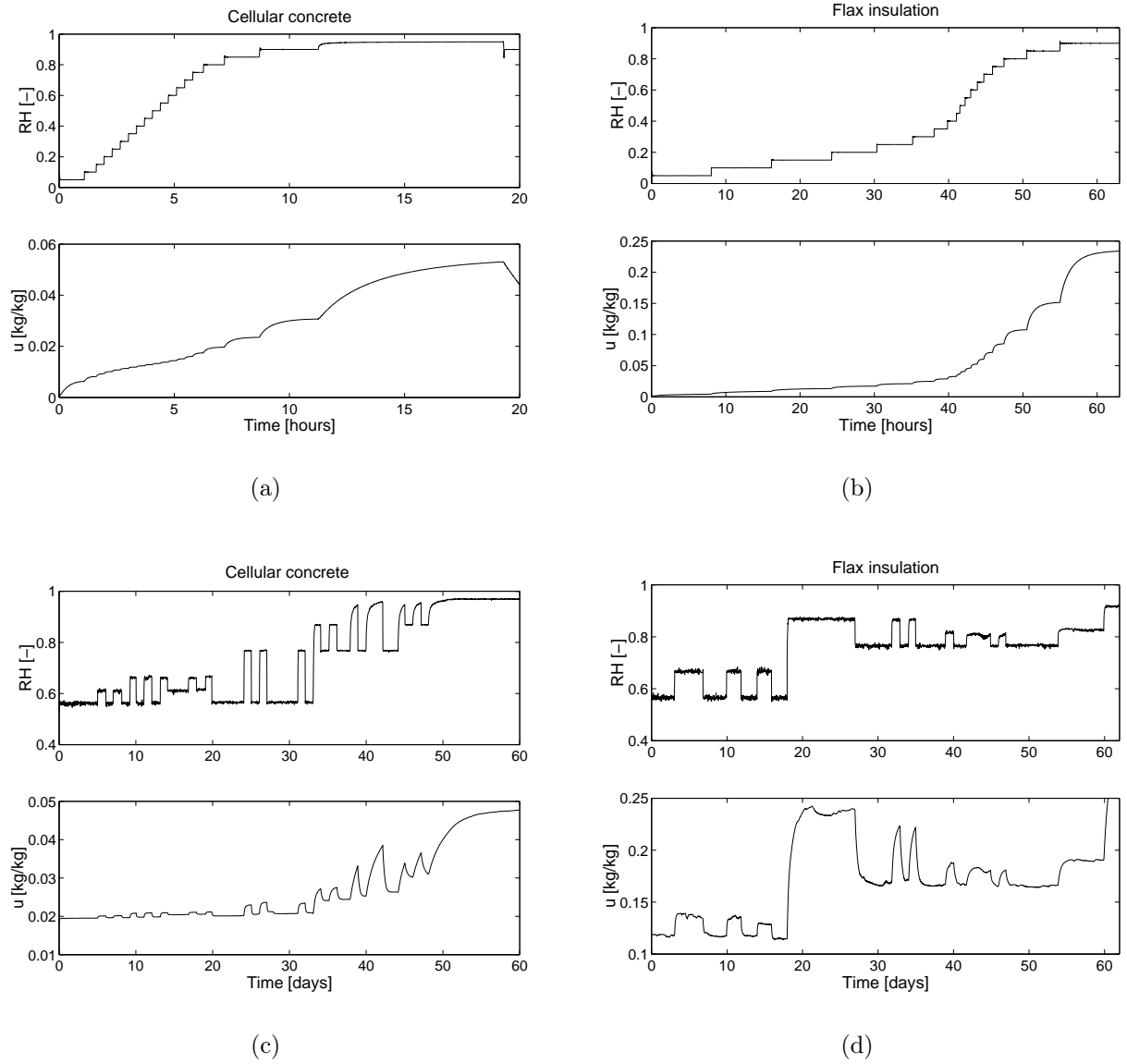


Figure 5.5: (a) Consecutive absorption steps for cellular concrete and (b) flax insulation. Measurements from IGAsorp. (c) Periodic steps for cellular concrete and (d) flax insulation. Measurements from Climate Chambers.

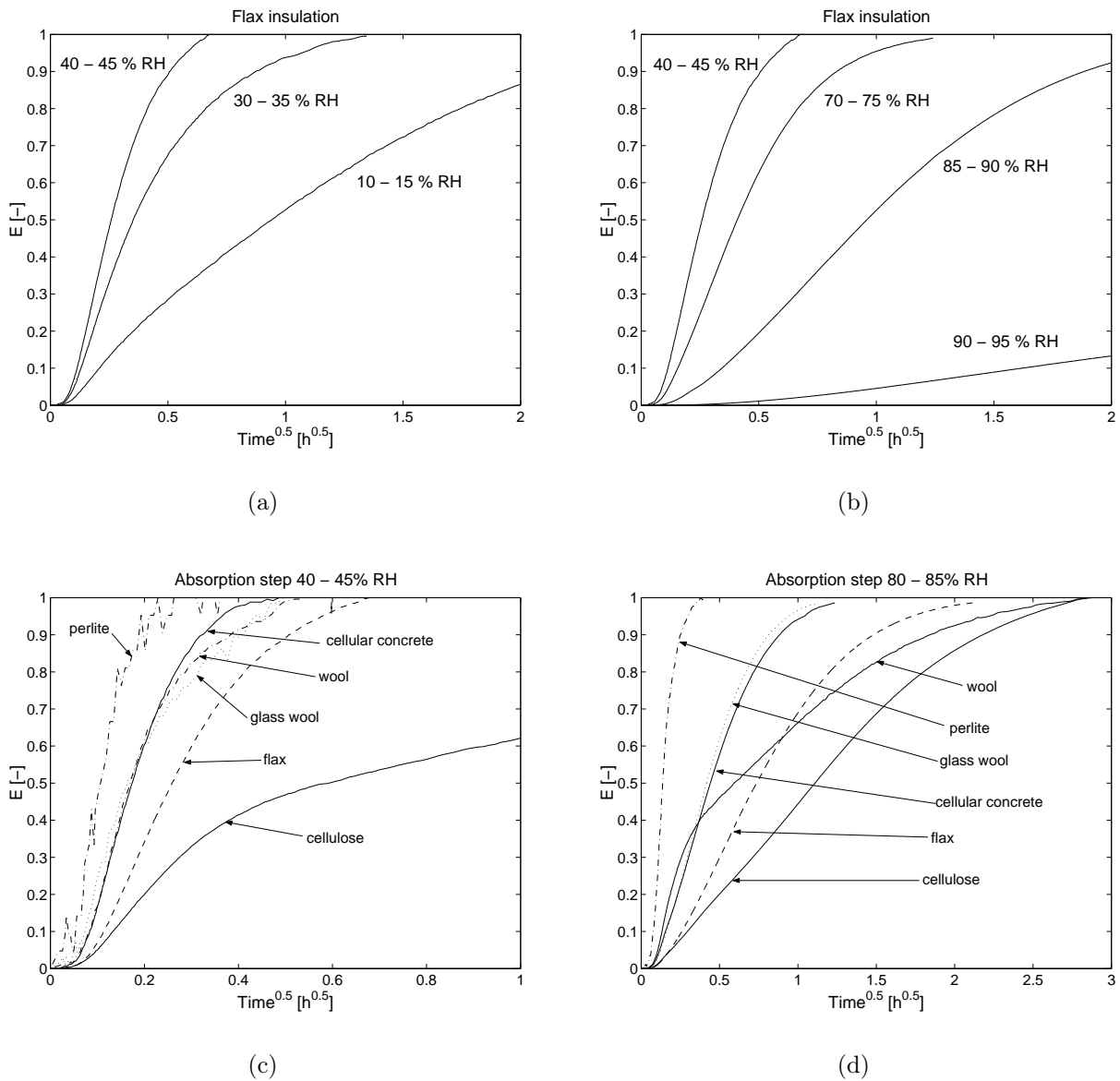


Figure 5.6: (a) Dimensionless absorption steps for flax insulation: low RH and (b) high RH . (c) Non-dimensional absorption steps 40–45% RH and (d) 80–85% RH for glass wool, cellular concrete, cellulose insulation, flax insulation, wool insulation and perlite insulation. Measurements from IGAsorp.

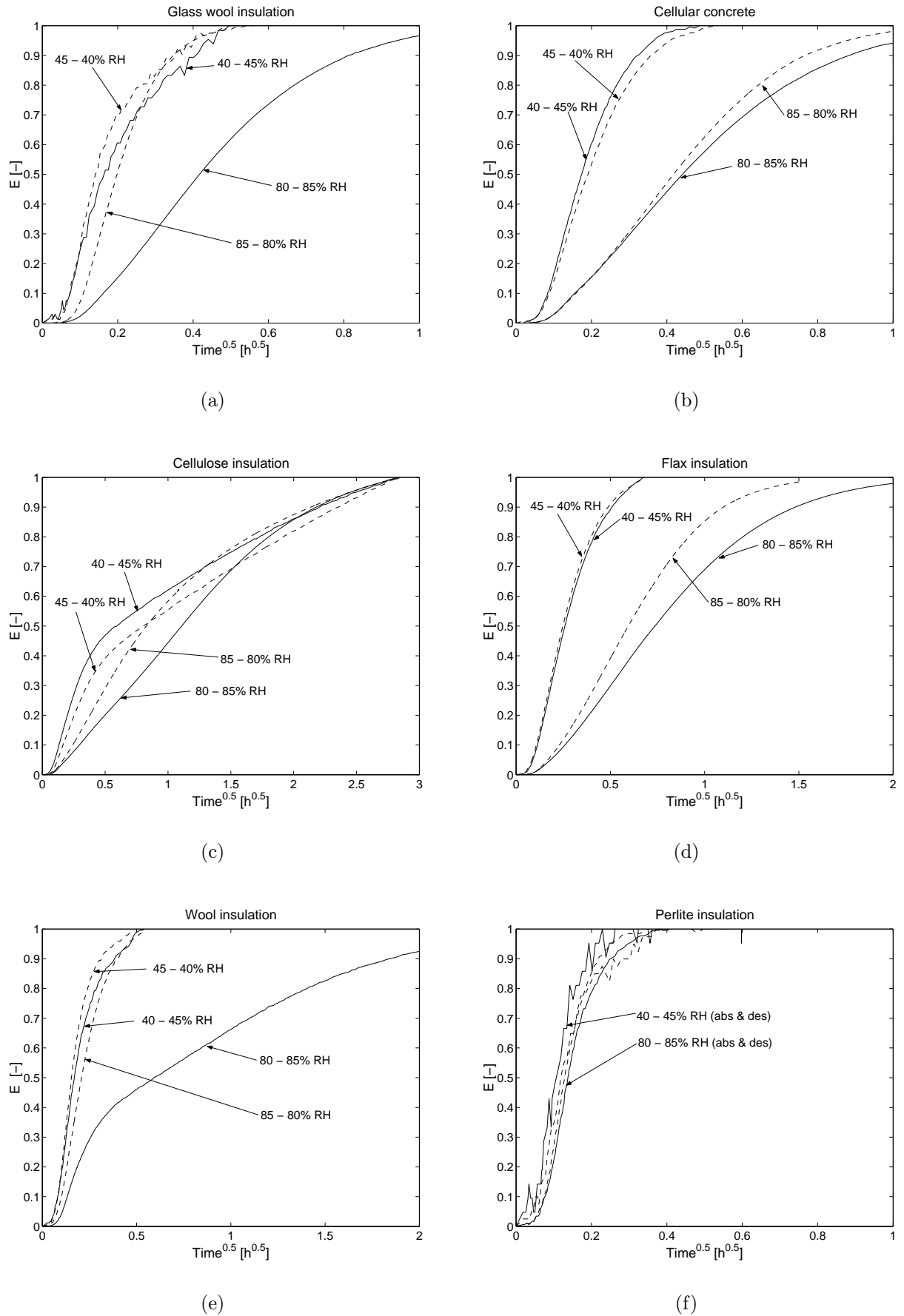


Figure 5.7: Non-dimensional ab- and desorption step for (a) glass wool insulation, (b) cellular concrete, (c) cellulose insulation (d) flax insulation, (e) wool insulation and (f) perlite. Measurements from IGAsorp. Absorption (—), desorption (- -).

The difference in moisture response depending on whether an ab- or desorption step was taken, was significant for some materials (e.g. glass wool, flax and wool insulation, see Figure 5.7(a), (d) and (e)), while for others it was almost non-existent. In general, the largest difference occurred at high RH -levels, i.e. absorption at these high levels was remarkably slower than desorption (e.g. glass wool and wool, see Figure 5.7(a) and (e)). Furthermore, the response of cellulose insulation with a two-stage sorption process has a similar character as the measurements of (Wadsö, 1993) and (Koponen and Liu, 1999) on wood as shown in Chapter 3.

Periodic steps (Climate chambers)

Selected measurement sequences for two of the materials (cellular concrete and flax insulation) in the Climate Chambers are given in Figure 5.5(c) and (d). All the measurements are given in Appendix B.1.1. The moisture content was given as in Equation 2.3. Some of these measurement results were used for 'validation' of the new simulation model in Section 5.4.

5.3 Analysing moisture response

In this section, some of the measurement results were treated analytically to obtain the characteristic time-dependent parameters. The analysis was based on the conventional Fickian theory introduced in Chapter 2.

5.3.1 Moisture diffusivity

A method for the determination of the moisture diffusivity from the dynamic sorption experiments was introduced in Section 4.3. The following equations (Equation 4.11 and 4.12) were used to calculate the moisture diffusivity D_w :

$$D_w = \frac{\pi}{4} \cdot l^2 \left(\frac{dE}{d\sqrt{t}} \right)^2 \quad \text{for} \quad E < 0.5 \quad (4.11)$$

$$D_w = \frac{4 \cdot l^2}{\pi^2 \cdot t} \ln \left(\frac{8}{\pi(1-E)} \right) \quad \text{for} \quad 0.4 < E < 1 \quad (4.12)$$

The necessary conditions for the validity of the Equations 4.11 and 4.12 were introduced in Section 4.3. When evaluating the actual experimental set-up, these conditions were generally fulfilled. The following list summaries the actual conditions;

- The initial concentration distribution was uniform, as the sample was in equilibrium before the start of a new step.

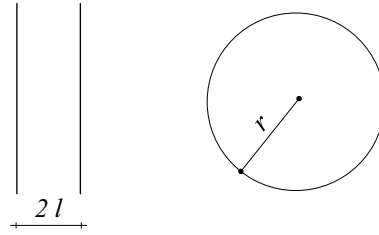


Figure 5.8: Illustration of the characteristic lengths, l for a slab and $r/3$ for a sphere.

- For $t > 0$, the moist air with a changed moisture content reached the sample surface almost immediately after a step change due to the mechanism of the equipment used. An open question remained whether there was an immediate equilibrium in the surface moisture content, but this condition was assumed to be met.
- The condition of almost unchanged concentration in the middle of the sample was also expected to have been fulfilled, at least in the beginning of each sorption step, where most of the moisture uptake is supposed to happen near the sample surface.
- The RH -steps were so small (at least for 5% RH -steps) that diffusivity could have been regarded as constant within the steps

The half-thickness of the slab l as a characteristic length was obvious, as the slab was supposed to be exposed one-dimensionally from both sides with a total area of $2A$. If the ratio between the volume of the sample V and the exposed area $2A$ is calculated, the result is exactly the characteristic length l . This definition was used here to define the characteristic length for a sphere with a radius of r as the micro-scale samples are close to that shape:

$$l = \frac{V}{A} = \frac{\frac{4}{3}\pi r^3}{4\pi r^2} = \frac{r}{3} \quad (5.1)$$

These characteristic lengths are illustrated in Figure 5.8.

In the first place only Equation 4.11 and 5% RH -steps were used for determining D_w . The slope $\frac{dE}{d\sqrt{t}}$ was determined for $0.15 < E < 0.3$. Figure 5.9 (a) and (b) shows D_w for all the materials as a function of RH . Only absorption data was used here. The lowest diffusivity was found for cellulose insulation, while it was highest for perlite and glass wool. A high D_w means that the moisture content of the material changes rapid after changes in ambient air relative humidity. The difference between the nature of ab- and desorption dynamics can be illustrated by comparing D_w for a couple of materials. Figure 5.9 (c) and (d) shows the diffusivity for cellular concrete and flax insulation. There was no significant difference between D_w for ab- and desorption steps. It was quite interesting, how two very different materials, e.g. flax and cellular concrete, had almost identical diffusivities.

Significance of analysis method and step size used

Until now, the diffusivities have been determined based on the initial slope of the sorption curve $\frac{dE}{d\sqrt{t}}$ (Equation 4.11). To investigate the effect of using Equation 4.12 instead, D_w

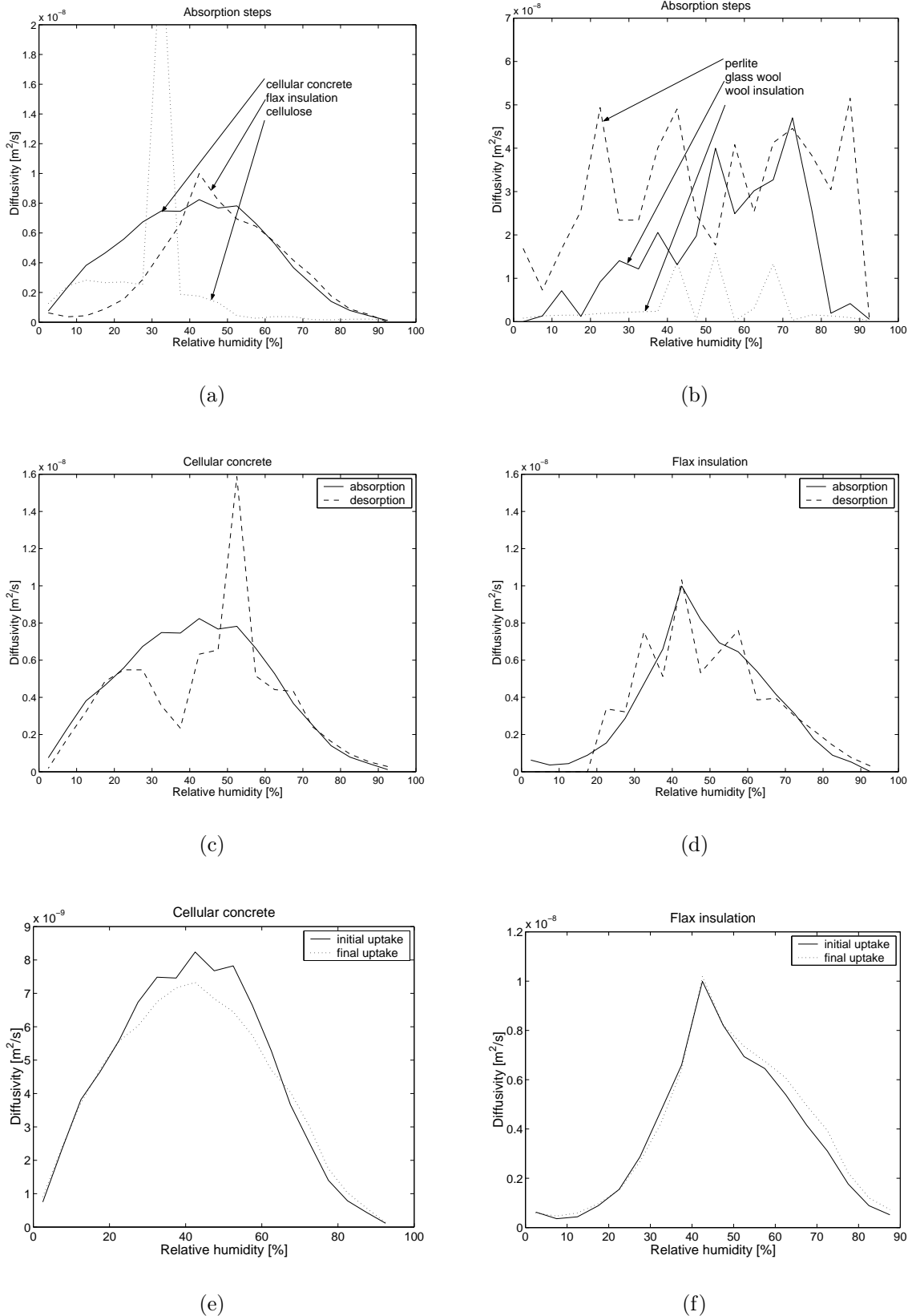


Figure 5.9: Moisture diffusivity as a function of RH for (a) cellular concrete, flax and cellulose insulation, and for (b) perlite insulation, glass wool and wool insulation. Note that there are different scales on y-axis. (c) Moisture diffusivity as a function of RH for cellular concrete and (d) flax insulation. Values for both ab- and desorption steps are shown. (e) Comparison of D_w determined on the basis of initial uptake (Equation 4.11 $0.15 < E < 0.3$) and final uptake (Equation 4.12 $E = 0.75$) for cellular concrete and (f) flax insulation.

(Figure 5.9(e) and (f)) determined with both equations were compared for cellular concrete and flax insulation. For calculations with Equation 4.12, values for $E = 0.75$ have been used.

Yet another parameter to be investigated was the effect of step size under measurements for the resulting D_w . Most of the actual measurements have been performed with steps in $\Delta RH = 5\%$. The dynamic sorption for some materials was also measured with $\Delta RH = 10\%$ and $\Delta RH = 20\%$. In the following, cellulose insulation was used as an example for the characteristic behaviour:

The influence of the chosen measurement and analysis method for the resulting diffusivity is illustrated in Figure 5.10 for cellulose. The differences between D_w determined with initial moisture uptake (Equation 4.11) and final moisture uptake (Equation 4.12) were quite similar for all step sizes although this deviation was quite large. However, for the humidity range of practical interest, i.e. $50\% < RH < 90\%$ equal with $w > 5 \text{ kg/m}^3$, the determined diffusivities were rather constant and the differences due to step size and ab- and desorption were relatively small. Finally, in Figure 5.10(d) – D_w is given as a function of moisture content, where all the 3 different absorption steps were compared for cellulose.

Resulting permeability $\delta_p(\varphi)$

Under the assumption of immediate equilibrium and Fick's law this dynamically determined moisture diffusivity D_w can be compared with the water vapour permeability determined by the steady state cup measurements δ_p . Conversion of the coefficients was done with the following relation, which is Equation 4.10:

$$\delta_p = \frac{D_w \cdot \xi \cdot \rho}{p_{sat}} \quad (4.10)$$

Equation 4.10 enhances the variation of D_w as a function of RH : D_w was smaller for the relative humidities where ξ was largest. The D_w determined directly from the measurement results with Equation 4.11 showed this characteristic also.

Figure 5.11(a) compares δ_p converted from the above calculated D_w based on dynamic sorption measurements ($RH=50-95\%$), and the measured permeability from the steady state wet cup measurements for the analysed materials. The resulting permeabilities showed that δ_p from cup measurements was much higher than δ_p from the dynamic measurements, from $\delta_{p,cup}/\delta_{p,dynamic}=1.8$ for cellular concrete to $\delta_{p,cup}/\delta_{p,dynamic}=41$ for cellulose insulation for absorption steps.

(Time, 1998) referred to measurements of (Wadsö, 1993) on wood, where diffusivities determined by both cup method and dynamic sorption method were compared. The deviation for lower RH -levels was not pronounced ($D_{cup}/D_{dynamic} = 1 - 2.3$ for $RH = 50 - 75\%$), while it increased for increasing RH ($D_{cup}/D_{dynamic} = 1.7 - 10.8$ for $RH = 75 - 85\%$).

Figure 5.11(b) shows the variation of the converted δ_p as a function of relative humidity for some materials. The permeability did not show the well known characteristic of increasing for increasing moisture content and relative humidity.

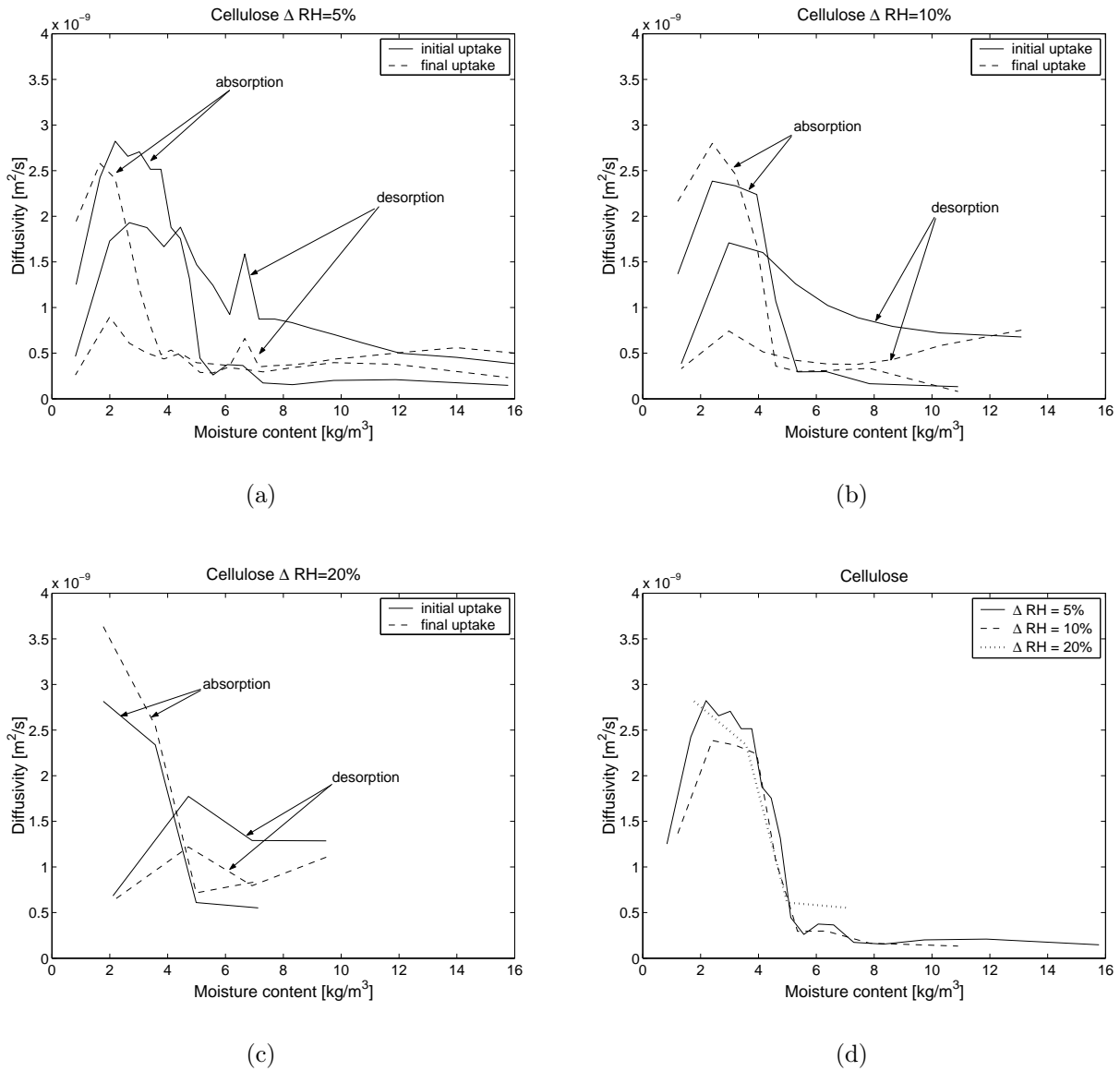


Figure 5.10: Moisture diffusivity D_w for cellulose insulation as a function of w for different step sizes. Also the effect of using Equation 4.11 or 4.12 is illustrated. (a) $\Delta RH = 5\%$, (b) $\Delta RH = 10\%$, (c) $\Delta RH = 20\%$ and (d) D_w as a function of moisture content w and step size for cellulose insulation (initial uptake for absorption steps).

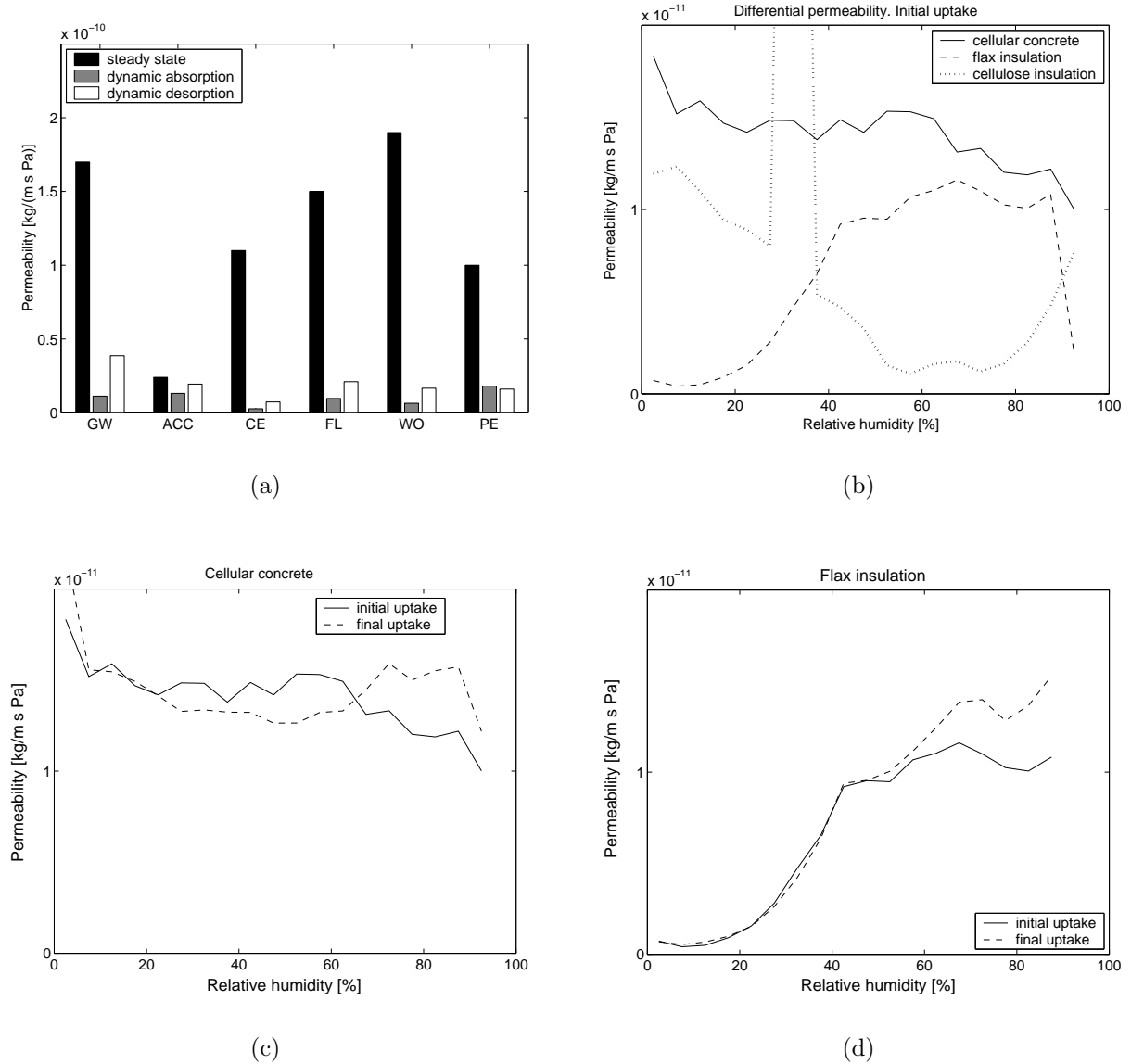


Figure 5.11: Water vapour permeability: (a) Permeability determined from dynamic measurements (both ab- and desorption steps) compared with the steady state wet cup-measurements. Mean values for $RH=50-95\%$. Steady state permeabilities from (Hansen et al., 1999), except cellular concrete (ACC) and glass wool (GW) that have been determined as a part of this work. CE = cellulose insulation, FL = flax insulation, WO = wool insulation and PE = perlite. (b) Variation of the permeability (dynamic measurements) as a function of RH for cellular concrete, flax and cellulose insulation, initial uptake. $\delta_p(\varphi)$ for other materials lies within the same range, but the values are rather scattered. (c) Comparison of δ_p determined on the basis of initial uptake (Equation 4.11 $0.15 < E < 0.3$) and final uptake (Equation 4.12 $E = 0.75$) for cellular concrete and (d) flax insulation.

The reason for dynamically measured permeability being lower than the steady state permeability could be the retarded sorption, i.e. the measured slope $\partial E/\partial\sqrt{t}$ was smaller than the one expected according to Fickian behaviour. The 'true' δ_p might be even smaller, because converting from the diffusivity D_w makes use of the moisture capacity ξ , which is still defined under the assumption of immediate equilibrium. However, for cellular concrete, the deviation between steady state and dynamically determined permeabilities was almost non-existent, which could be taken as an indication that the cellular concrete follows Fickian behaviour.

To investigate the effect of using Equation 4.12 instead of 4.11 (Figure 5.11(c) and (d)), δ_p determined with both equations were compared for cellular concrete and flax insulation. For determination with Equation 4.12, values for $E = 0.75$ have been used.

(Künzel and Kiessl, 1990) determined δ_p for sandstone, cellular concrete and mortar with cup measurements and with the dynamic sorption measurements and got practically equivalent results. Therefore, the sorption for these materials could be assumed to be Fickian.

5.3.2 Moisture buffer capacity

In Chapter 2, the moisture accumulation capacity was defined. In practical contexts, this capacity is often called the buffer capacity of a material, because it expresses the ability of a porous material to buffer the changes in ambient RH . The current approach could be seen as a preliminary part in developing a method for determining the moisture buffer capacity using data from dynamic sorption measurements.

Moisture accumulation capacity

The moisture buffer capacity of the materials can be expressed as the moisture accumulation capacity (analogous to the heat accumulation capacity, or thermal effusivity), and theoretically given by Equation 2.37

$$b_m = \sqrt{\frac{\delta_p \cdot \rho_0 \cdot \xi}{p_{sat}}} \quad (2.37)$$

Among the involved parameters are two of the most important moisture properties of porous materials, e.g. water vapour permeability δ_p and moisture capacity ξ . The validity of use of these steady state parameters to define a dynamic property like moisture accumulation capacity b_m , will be tested in the following by comparing this theoretical b_m with a dynamically measured b_m , the dynamic one given by Equation 5.2, which is reorganised from Equations 2.37 and 4.10.

$$b_m = \frac{D_w \cdot \rho_0 \cdot \xi}{p_{sat} \sqrt{D_w}} \quad (5.2)$$

where D_w was determined in the previous Section.

Figure 5.12(a) shows the buffer capacity as moisture accumulation capacity b_m according to Equation 2.37 and Figure 5.12(b) according to Equation 5.2. The trend of b_m was very

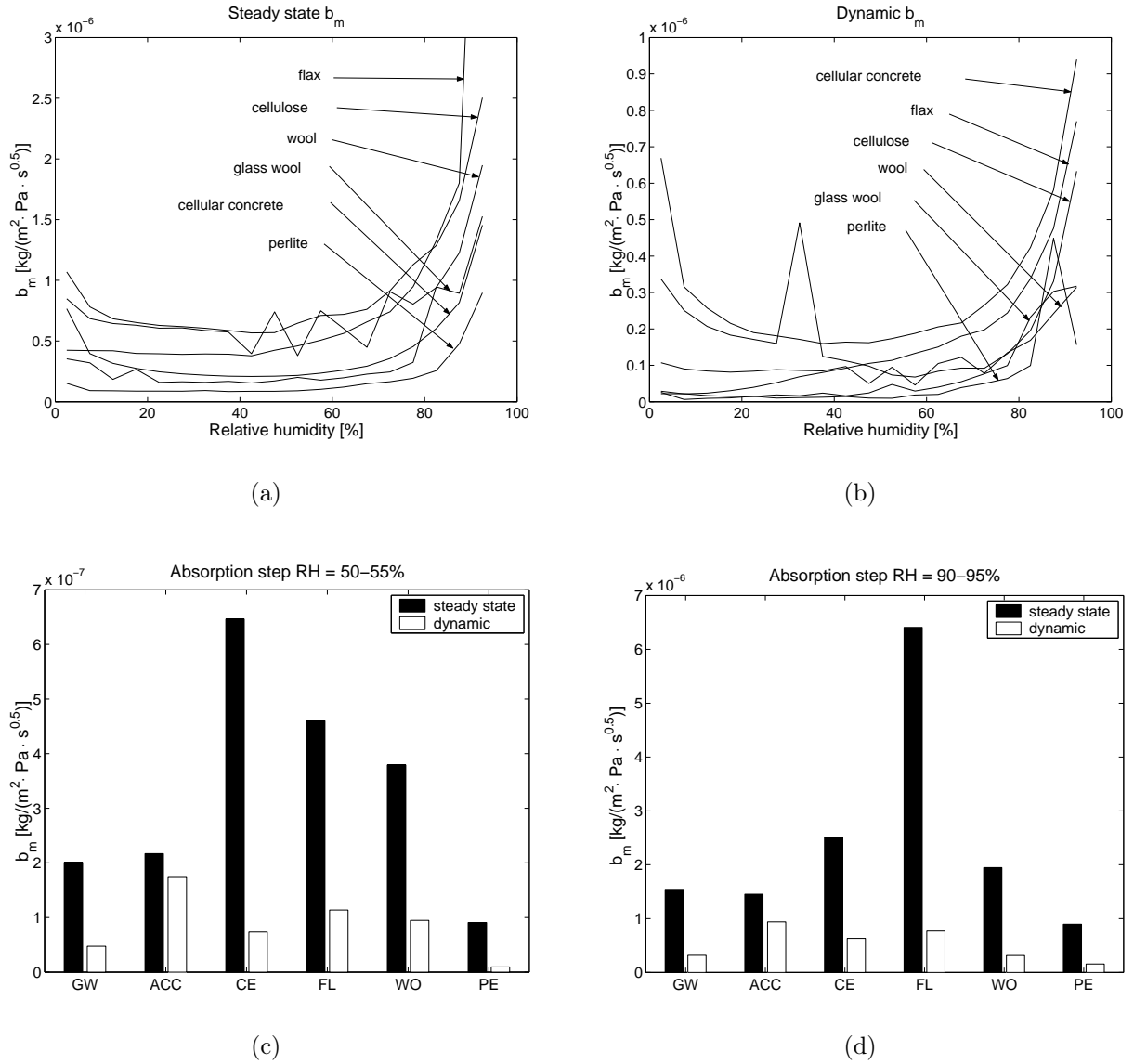


Figure 5.12: Moisture buffer capacity as moisture accumulation capacity b_m [$\text{kg}/\text{Pa} \cdot \text{m}^2 \cdot \text{s}^{0.5}$] and the significance of the analysis method. Comparison of b_m with steady state and dynamic approach. (a) Steady state parameters (Equation 2.37) and (b) dynamically determined D_w (Equation 5.2). (c) Absorption step $RH = 50 - 55\%$ and (d) absorption step $RH = 90 - 95\%$. Note the different scales. GW = glass wool insulation, ACC = cellular concrete, CE = cellulose insulation, FL = flax insulation, WO = wool insulation and PE = perlite.

similar for all materials, i.e. b_m was lowest for moderate RH 's, where the slope of the sorption isotherm was also smallest, and increases for increasing (and decreasing) RH . It was not indifferent which equation to use for the 'ranking' of the assessed materials. In the following list, the materials are ranked, the material with the largest moisture accumulation capacity b_m as the number 1:

Steady state parameters (Equation 2.37):

1. cellulose and flax insulation
2. wool insulation
3. cellular concrete and glass wool insulation
4. perlite

Dynamically determined D_w (Equation 5.2):

1. cellular concrete
2. flax insulation
3. cellulose
4. glass wool insulation, wool insulation and perlite

Figure 5.12(c) and (d) illustrates the big difference in magnitudes between the two methods analysed. b_m was in general much smaller when the dynamic method was applied, than using the steady state parameters. An exception was the cellular concrete, i.e. the two determined b_m were practically equal.

Available water

Another way of presenting the buffer capacity is to determine the amount of available water for given changes in ambient RH . This method was also presented in Chapter 2. The available water Δm_w is given with Equation 2.39:

$$\Delta m_w = \rho_0 \cdot \xi \cdot \Delta\varphi \cdot d_p \quad (2.39)$$

where penetration depth d_p is given with Equation 2.38

$$d_p = \sqrt{\frac{D_w t_p}{\pi}} \quad (2.38)$$

It is believed to be important as to how the moisture diffusivity for determining d_p and the moisture capacity ξ of the materials are determined. If diffusivity is determined from steady state permeability (Equation 2.32), d_p will be overestimated, see Figure 5.11(a). The dynamically measured diffusivity from the previous section turned out to be smaller than the one determined with Equation 2.32, due to the small slope of the measured non-dimensional moisture content versus the square root of time.

Therefore, a distinction was made between steady state and dynamically determined d_p . The latter was derived with Equation 2.38, where D_w was derived from dynamic sorption measurements. The 'steady state' d_p was determined from Equation 5.3. These resulting penetration depths are shown in Figure 5.13 (c) for a step $RH = 50 - 55\%$.

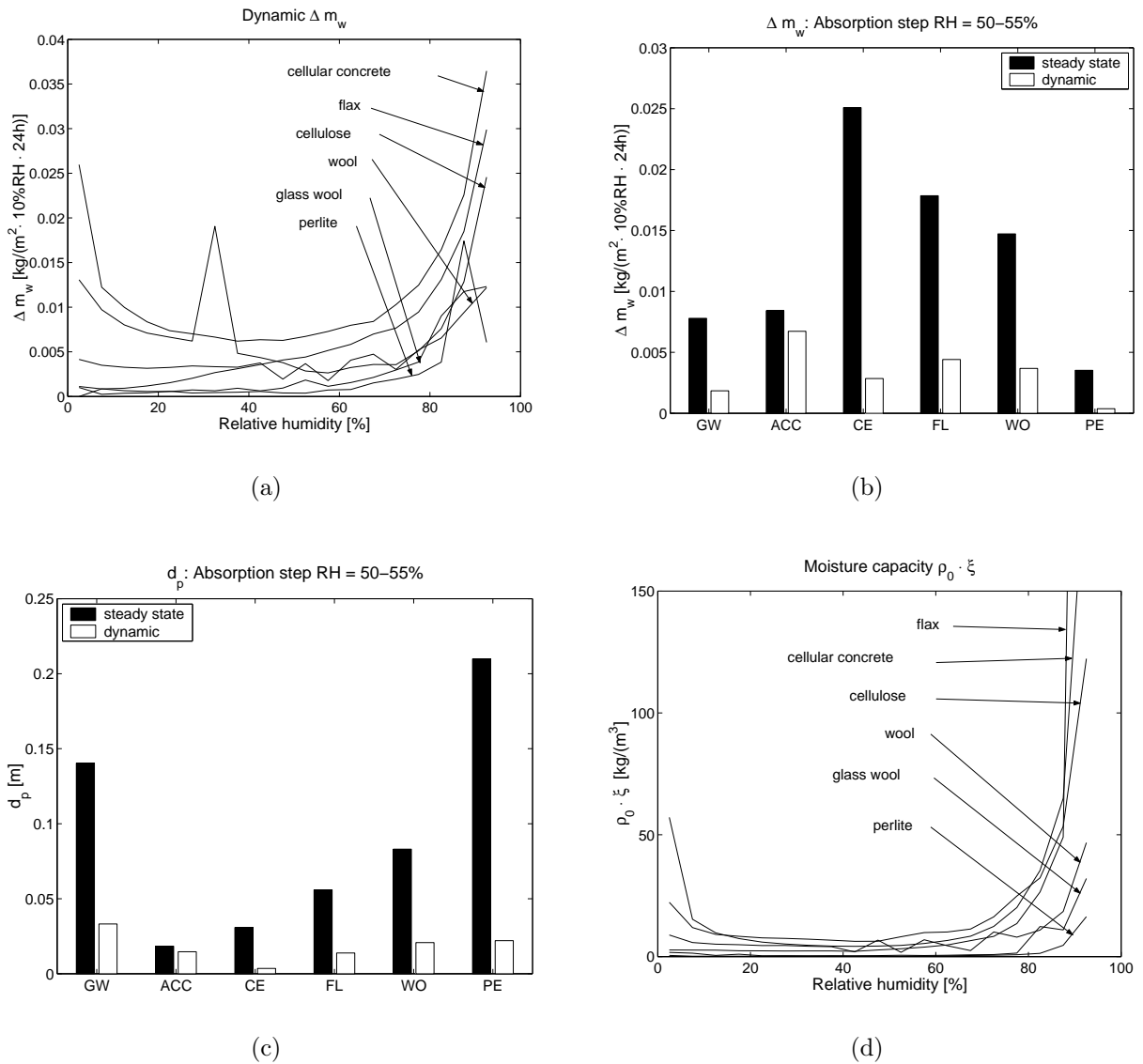


Figure 5.13: (a) Available water Δm_w [kg/m² per $\Delta\varphi = 0.1$ and $t_p = 24$ hours] as a function of relative humidity for the analysed materials, based on d_p determined from Equation 2.38. (b) Comparison of available water Δm_w for the absorption step $RH = 50 - 55\%$ between steady state and dynamically determined d_p . (c) Penetration depth d_p determined from steady state and dynamic measurements. (d) Volumetric moisture capacity $\rho_0 \cdot \xi$ as a function of RH . GW = glass wool insulation, ACC = cellular concrete, CE = cellulose insulation, FL = flax insulation, WO = wool insulation and PE = perlite.

$$d_p = \sqrt{\frac{\delta_p \cdot p_{sat} \cdot t_p}{\rho_0 \cdot \xi \cdot \pi}} \quad (5.3)$$

Overall, the picture was identical for Δm_w as for b_m , when assessing the analysed materials, see Figure 5.13 (a) and (b). This was not a surprise as these values were proportional, see Equation 5.4. Δm_w just gave a more realistic idea of the amounts of moisture involved during a typical period, here 24 hours, for a given change in RH , here $\Delta RH = 10\%$ ($\Delta\varphi = 0.1$).

$$\Delta m_w = b_m \cdot p_{sat} \cdot \Delta\varphi \sqrt{\frac{t_p}{\pi}} \quad (5.4)$$

The 'simple' moisture capacity

Finally, after it was clear that the moisture buffer capacity, at least to some extent, followed the well-known characteristics of the slope of the sorption isotherm, also called moisture capacity ξ , it was interesting to assess, if this definition of moisture capacity could be used for the sake of simplicity. Moisture capacity is given here as the volumetric moisture capacity in Equation 5.5 and shown in Figure 5.13(d) as a function of RH .

$$\frac{\partial w}{\partial \varphi} = \rho_0 \cdot \xi \quad (5.5)$$

The characteristics here approximate the two earlier definitions. Also the 'order' of the materials becomes more or less the same. Therefore, this traditional definition of moisture capacity was fully valid, with quite similar permeabilities and conditions for the materials analysed. Nevertheless, the moisture capacity $\frac{\partial w}{\partial \varphi}$ of flax was extremely high for $RH = 90 - 95\%$, but lower than for cellulose over the rest of RH 's. The reason for this deviation between b_m and Δm_w was that it takes a relatively long time for flax to reach this high equilibrium value, and therefore not all the capacity becomes activated in the dynamic case.

5.3.3 Conclusion on analysis of the moisture response

In the above analysis, the moisture diffusivity of several porous materials has been determined with a dynamic sorption approach, where the effect of the step size in RH and the analysis method used has been evaluated. It seems that the step size does not play any significant role, nor does the analysis method.

When assessing the characteristics for non-Fickian behaviour, it was clear that the only material analysed showing Fickian moisture transport was cellular concrete. The deviation between permeability determined from steady state cup measurements and from this dynamic sorption approach was almost non-existent for cellular concrete, while it was highly significant for all the other materials.

The ability of the materials to smooth changes in ambient air relative humidity, i.e. the buffer capacity, was assessed using several methods. The most significant observation was the great difference between using steady state and dynamically determined material parameters for all the materials, except for cellular concrete. In general, it can be concluded that the 'true' buffer capacity was overestimated using steady state parameters compared with the dynamic sorption approach. However, this conclusion is only valid, if it is assumed that the necessary conditions are present for the analysis methods used.

In (Padfield, 1999) a range of different porous building materials were investigated to find their buffer capacity. A specially constructed climate chamber was used to measure the *RH*-buffering ability of different materials, when there is a periodically varying vapour flux. The resulting relative humidity in the chamber was a function of both porosity and the adsorptive power of the material. The moisture buffering capacity was measured for wood, brick, cellular concrete and unfired clay. The set-up imitated the typical combination of material area, air volume, and water production in a room. Wood end grain panels showed the best buffering capacity due to rapid diffusion and high moisture capacity of wood. On the other hand, cellular concrete covered by a thin gypsum plaster turned out to be the best buffering commercial construction.

The observations in the present analysis support the findings in (Padfield, 1999).

5.4 Modelling dynamic moisture transfer

The modelling approach in this work was based on the literature study referred to in Chapter 3 and the results of the experimental investigations of step response behaviour of different materials in Section 5.2.3. This new modelling approach was also compared to the traditional Fickian model which is based on coupled heat and moisture transfer equations (given in Equations 5.6 and 5.7), including latent heat and capillary transport.

$$\rho_0 c_p \frac{\partial T}{\partial t} = \frac{\partial}{\partial x} \left(\lambda \frac{\partial T}{\partial x} \right) + \Delta h \frac{\partial}{\partial x} \left(\delta_p \frac{\partial p}{\partial x} \right) \quad (5.6)$$

$$\rho_0 \frac{\partial u}{\partial t} = \frac{\partial}{\partial x} \left(\delta_p \frac{\partial p}{\partial x} \right) + \frac{\partial}{\partial x} \left(K \frac{\partial P_c}{\partial x} \right) \quad (5.7)$$

where ρ_0 is the dry density of the material, c_p specific heat capacity of the material, T temperature, λ heat conductivity, Δh heat of phase change (vapour - liquid), δ_p water vapour permeability, p water vapour pressure, K capillary transport coefficient and P_c capillary suction pressure. The model was very similar to one described in (Rode, 1991) and is more fully described in (Peuhkuri, 2002), also found in Appendix C. All the modelling here was carried out in a Simulink environment in Matlab. The material parameters used in the simulations are found in Appendix A. In this one-dimensional calculation model, samples were given a thickness equal to $2l$ and $\frac{2r}{3}$ according to Equation 5.1. The model consisted of 3 nodes: one each on the upper and lower surfaces and one in the middle of the sample.

5.4.1 Measurements vs. calculations with Fickian model

Calculations with the Fickian model described by the Equations 5.6 and 5.7 are compared in the following with the measurements to illustrate the non-Fickian behaviour. As an

example, a couple of absorption steps for cellular concrete and flax are used. The steps in Figure 5.14(a) and (b) are measured with the IGAsorp equipment and the step in Figure 5.14(c) and (d) with the Climate Chambers.

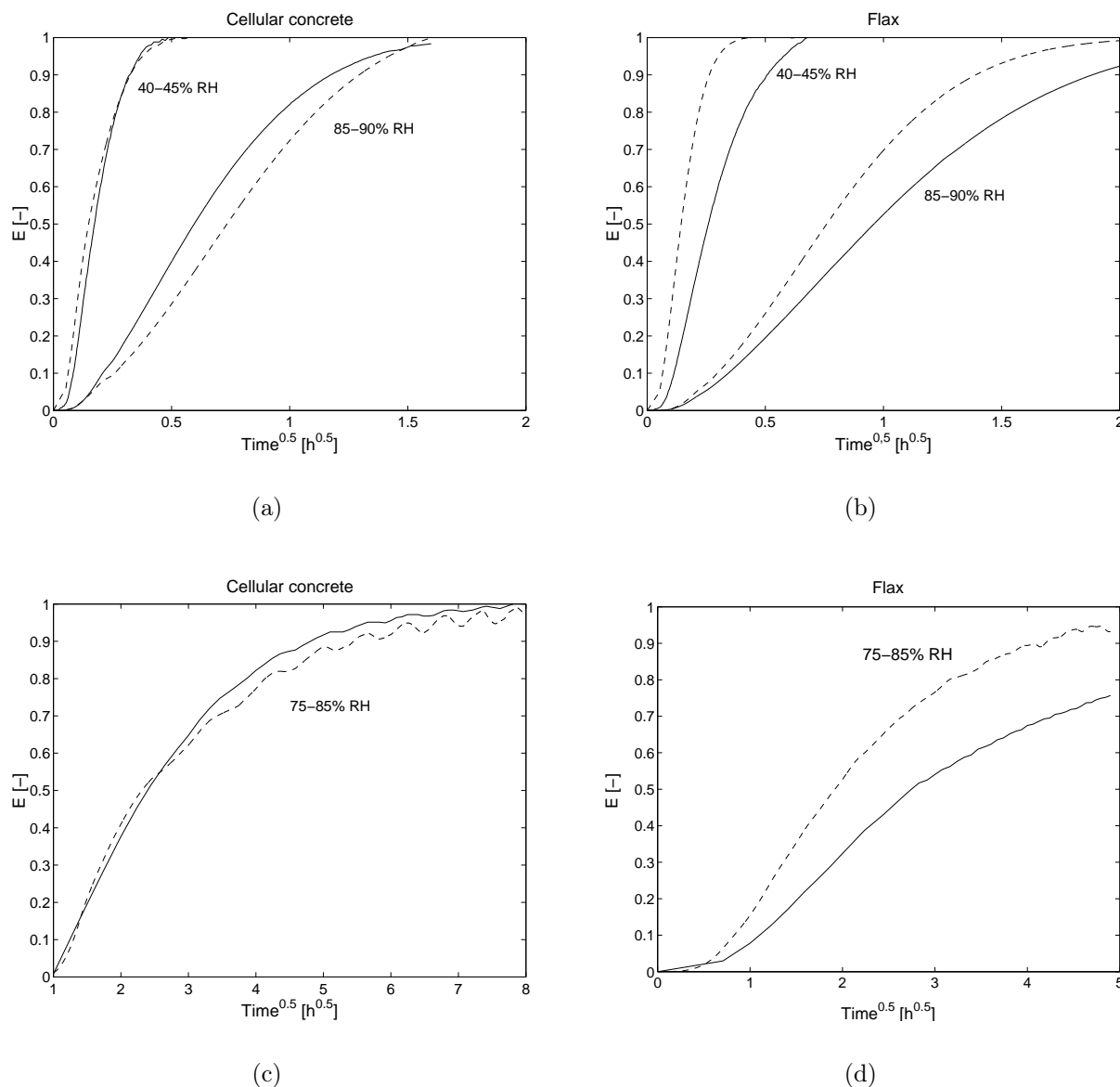


Figure 5.14: Measurements with the IGAsorp equipment (—) compared with calculations with the Fickian model (- - -). Absorption steps 40-45% RH and 85-90% RH . (a) Cellular concrete and (b) flax insulation. Measurements with the Climate Chambers (—) compared with calculations with the Fickian model (- - -). The step shown is an absorption step 75-85% RH (between 31.8 and 32.8 days in Figure 5.5 for flax). (c) Cellular concrete and (d) flax insulation.

The presence of non-Fickian behaviour was quite clear for flax, at both low and high moisture levels. By comparison, cellular concrete seemed to follow the Fickian behaviour very closely. Results for other materials are found in Appendix B.1.2, where non-Fickian behaviour was seen for cellulose and wool insulation, while the behaviour was mostly Fickian for glass wool and perlite insulation.

5.4.2 The non-Fickian model

With traditional Fickian models it is assumed that there is an instantaneous local equilibrium between the vapour pressure p in the air in the pores of the material and the moisture content of the material u , and that this equilibrium is determined by the sorption isotherm. In this way, the moist air phase and the moist material phase are understood as one node. In many applications, only the first part (water vapour diffusion) of Equation 5.7 is considered, which in itself might lead to deviations between measurements and calculations for capillary active materials.

According to the experimental results presented, numerical analyses, and the referred literature, there are strong indications that the traditional model has to be modified by introducing:

1. a delay between p and u , which could be a differential resistance, and/or
2. a moisture capacity that is divided into an instantaneous part and a retarded part.

To make item 1 possible, an additional node is needed. If the node according to Equation 5.7 represents the air phase, then a material node is introduced with corresponding water vapour pressure p^* and moisture content u^* in equilibrium with p^* . The connection between these inner air and material nodes could be given by a simple relation, as suggested by several authors referred to in Chapter 3:

$$g_{sorption} = k(p - p^*) \quad (5.8)$$

where k [$kg/(Pa \cdot m^2 \cdot s)$] is a sorption coefficient to be determined experimentally. This sorption coefficient should describe the sorption process, which is rapid in the beginning and slow close to equilibrium and for low temperatures. The sorption coefficient also depends on the moisture content and the step size according to the experience in Chapter 3. The resulting moisture transport equations become:

$$\psi \frac{\partial \rho_v}{\partial t} = \frac{\partial}{\partial x} \left(\delta_p \frac{\partial p}{\partial x} \right) - k(p - p^*) \quad (5.9)$$

$$\rho_0 \frac{\partial u^*}{\partial t} = k(p - p^*) \quad (5.10)$$

where ψ is the porosity of the material. The heat transport equation (including latent heat), is unchanged (Equation 5.6). The sorption model and the two nodes discussed are illustrated in Figure 5.15. Equation 5.8 represents a way of describing the slow sorption process that is obvious logically and therefore already suggested by several authors in different forms (see Chapter 3). The approach by (Håkansson, 1998) took another point of view by introducing the internal levels. The sorption equation given in Equation 5.8 is principally similar with his model with 1 internal node.

The implementation of item 2 in the model is yet to be proven, i.e. by further dividing the material node into sub-levels, as in (Håkansson, 1998), and depends on how this sorption equation is capable of modelling the retarded sorption alone.

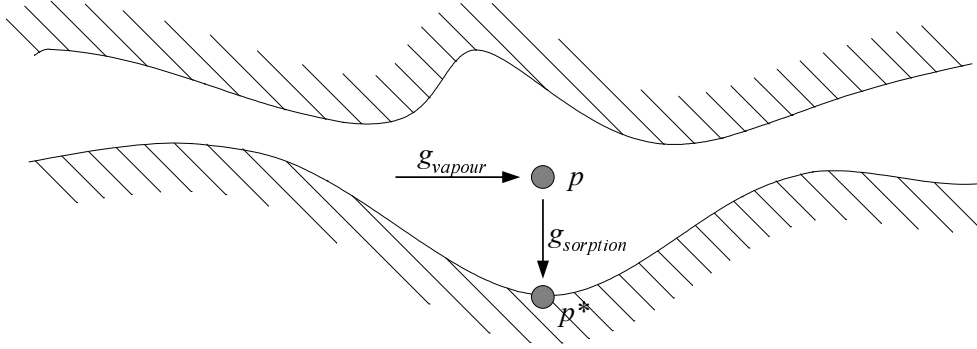


Figure 5.15: Illustration of the model where g_{vapour} is the Fickian diffusion of water vapour in air and $g_{sorption}$ the sorption between the air and the material node. • = nodes.

5.4.3 Determination of the sorption coefficient

The crucial part of the functionality of the new non-Fickian moisture transport model described in Section 5.4.2 is how to describe and determine the sorption coefficient k . Most of the earlier studies have taken k as being constant. In the following, a preliminary hypothetical approach for determining this coefficient experimentally is described.

The results from micro scale sorption experiments (Section 5.2.3) were in this case supposed to describe pure sorption, i.e. practically no water vapour diffusion occurred, due to the small size of the sample. All the transport between the ambient air (air node) and the material surface (material node) was supposed to be described by Equation 5.8 alone. It is understood here that using this assumption was in conflict with the assumptions for determining moisture diffusivities in Section 5.3, and was much simplified.

By using Equation 5.8, the sorption coefficient k can be determined easily:

$$k = \frac{g}{p - p^*} \quad (5.11)$$

The measured values for moisture content u are derived with respect to time to give g . The measured ambient relative humidity is transferred to water vapour pressure of the air node p via saturation vapour pressure p_{sat} , which is a function of the measured ambient temperature. p^* is determined as a product of the saturation vapour pressure p_{sat} for the actual temperature and the relative humidity determined by the equilibrium moisture content in material (i.e. sorption isotherm), where the equilibrium moisture content is equal with the actual moisture content in the material. The assumption of immediate equilibrium is hereby taken to be valid for *absorbed* moisture. The calculation model is given in Appendix D.2.

When k was calculated for a range of steps on different RH -levels (sorption experiments in Section 5.2.3), it could be determined as a function of relative humidity φ and the relative equilibrium p^*/p for absorption steps and as p/p^* for desorption steps. The idea of using the relative equilibrium as an independent variable for k was taken from (Krabbenhøft and Damkilde, 2002). Figure 5.16(a)-(c) shows linear approximation of k for flax for 5 % RH , 10 % RH and 20 % RH absorption steps.

As a result of this preliminary approach, some principal characteristics were already clear for absorption steps. The sorption coefficient k decreased when approaching equilibrium.

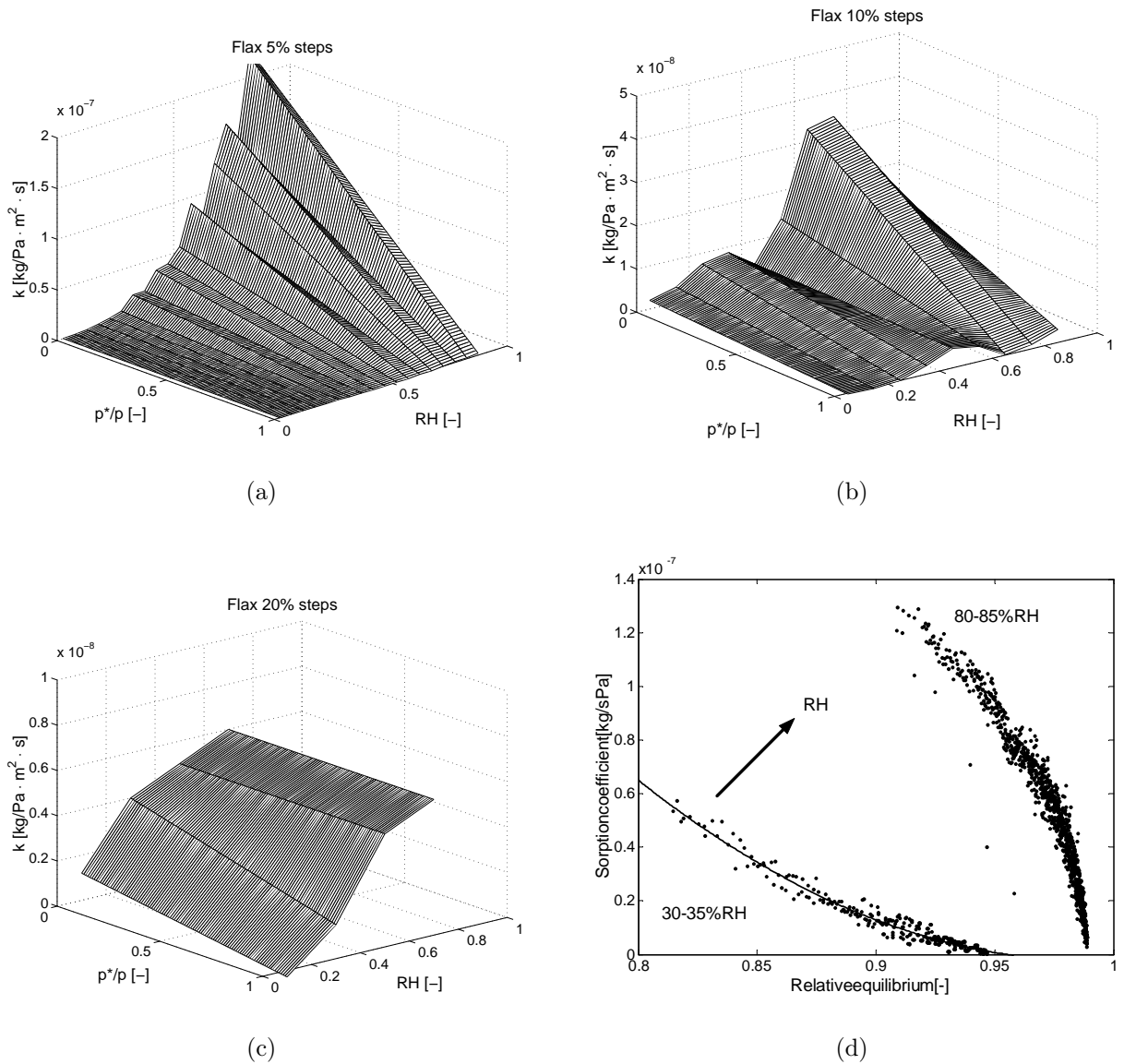


Figure 5.16: (a)-(c) The linear approximation of sorption coefficient k for **flax** as a function of relative humidity RH and the relative equilibrium p^*/p and the step size. Absorption steps 5 % RH , 10 % RH and 20 % RH for flax. The plot shows the trends for sorption coefficient for increasing RH and p^*/p , respectively. Note the very different scales. (d) Illustration of the principal shape of the sorption coefficient k as a function of relative equilibrium p^*/p for absorption steps at low and high RH . The solid line shows a fit of k for low RH .

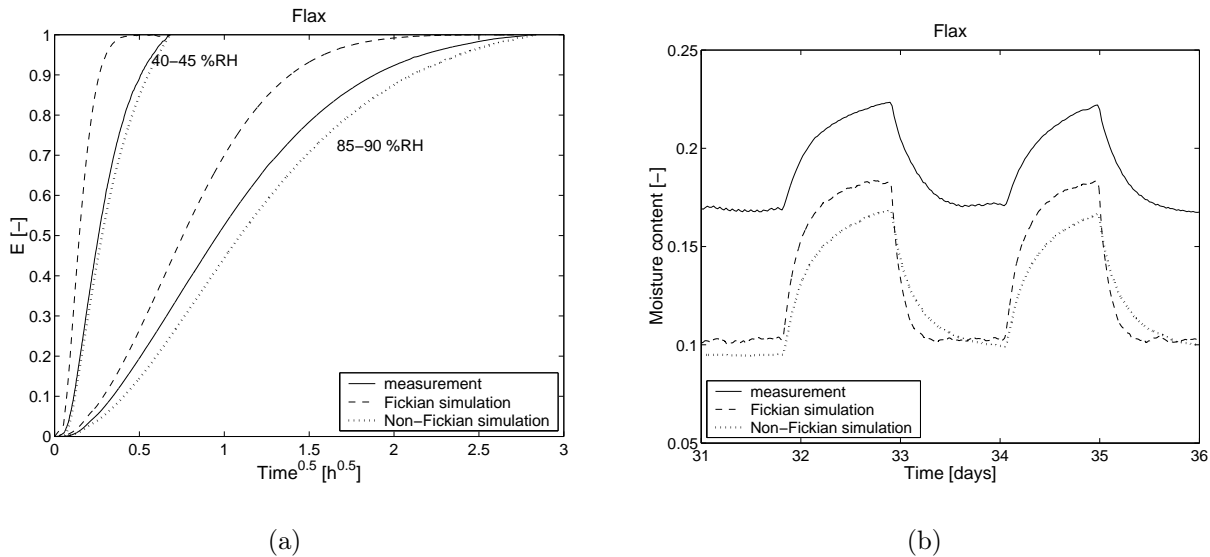


Figure 5.17: Measurements (—) compared with calculations with the Fickian model (- - -) and with the non-Fickian model ($\cdot\cdot\cdot$). (a) Absorption steps 40-45% RH and 85-90% RH for flax insulation with the IGAsorp equipment. (b) Steps between 75-85% RH (from Figure 5.5 for flax) Measurements from the Climate Chambers.

On the other hand, it increased with increasing relative humidity, when the equilibrium was not too close. By the end of the sorption process, the coefficient was relatively uniform and small for all moisture levels. Figure 5.16(d) shows an example of how the calculated sorption coefficient (dots) decreases for increasing equilibrium for two given relative humidity levels (here absorption steps 30-35 % RH and 80-85 % RH). A very interesting observation here is how the curves gradually changed slope and character for increasing RH . This observation corresponds well with the theoretical model in (Krabbenhøft and Damkilde, 2002) for high RH reproduced in Figure 3.9(a). Nevertheless, linear approximations are used for k in the defined RH -intervals.

On the basis of the literature study in Chapter 3, e.g. (Håkansson, 1998), it was pointed out that the transport coefficient in a non-Fickian model should depend also on the step size, because retarded sorption was most dominant for small steps. An approach to determine k as a function of step size is illustrated in Figure 5.16(a)-(c) for flax. Note the very different scales for the 3 different steps. It was clear that the sorption coefficient k determined from these measurements was extremely sensitive to the step size used and that the influence of step size on k was opposite to that found in literature. At this preliminary stage of the analysis, the step size will not be included in the model.

Surface moisture transfer resistance $Z_{p,c}$ was not used for determining k . The difference between k with and without $Z_{p,c}$ was checked for flax and it was non-significant.

5.4.4 Calculations with the new model

The new non-Fickian model described in Section 5.4.2 is documented shortly in Appendix D.1. To illustrate the function and the validity of the new model, some examples are given, where measurements are compared with the Fickian and the non-Fickian model in Figure 5.17. Both (a) consecutive absorption steps and (b) periodic steps are analysed for flax insulation.

The results in Figure 5.17 show that the new non-Fickian model slows down the sorption process, as desired. For the absorption step 40-45 %RH the non-Fickian simulation matches the measurements almost perfectly, while for the step 85-90 %RH the sorption process tends to be even too retarded. The periodic steps in Figure 5.17(b) are the most interesting for the actual validation of the non-Fickian model. Here, it is shown that the effect of retarded sorption works rather well both in ab- and desorption steps, even though there still exists too great an amplitude. However, there exists a strange deviation between the moisture content level for both simulations and measurements. An explanation could be that the measured sorption isotherm for flax gives moisture contents that are too low. More likely, an error could have been generated in the measurement of dry weight of the sample used for the periodic steps. Nevertheless, the non-Fickian model simulates the ab- and desorption process slightly better than the Fickian model.

No hysteresis was used in the model, but the average of ab- and desorption isotherms was employed for the periodic steps. In addition, the hysteresis effect was almost non-existent for flax insulation according to the measured isotherms in Appendix A.

5.5 Discussion

When determining the sorption coefficient in the manner mentioned above, a problem arises near to equilibrium. It is also a question of what the true equilibrium moisture content is in practice. Figure 5.16(d) illustrates this point in this actual case that the relative equilibrium never reached the value of 1: The IGAsorp equipment *predicted* the equilibrium moisture content, if the *measured* equilibrium moisture content was not reached within the maximum time of 8 hours. This *predicted* value was used for determining p^* .

Furthermore, the experimentally determined sorption coefficient also includes characteristics of the experimental set-up and not only the pure moisture uptake in the material.

In Equation 5.11, a potentially important mechanism, i.e. latent heat, is neglected. According to (Håkansson, 1998), the latent heat was of minor importance and subsequently neglected in his model. The role of latent heat should be studied further. However, in both the Fickian and the new non-Fickian model, latent heat is modelled as a part of the coupled equations. One should also be very careful, when determining coefficients on the basis of experimental data and just fitting the coefficients to match the actual measurements, without considering the true nature of the transport and sorption mechanisms. Models defined in this way will only be able to model the actual case. A future study should therefore also focus on the physical description of the sorption process, together with this numerical analysis of the experimental results. Nevertheless, no fitting of the coefficients has taken place in this work.

Hysteresis alone could also cause non-Fickian effects, i.e. a less steep slope of the intermediate curve also gives a reduced moisture capacity. But implementing hysteresis alone can not model all of the retarded sorption processes, like the effect of the step size. (Håkansson, 1998) made hysteresis coupled only to the most internal level, and together with his model described earlier, he achieved a better agreement with the measurements. Hysteresis was not applied here, but the effect of it is studied in Section 7.4.1. The hysteresis model is described in Appendix C.

Other experiences around the significance of hysteresis are rather divergent in the research literature. According to (Roels et al., 1999), it is more important to have a good expres-

sion of the sorption isotherm than to model hysteresis, although (Time, 1998) stated that including hysteresis gives better results for modelling ab- and desorption in wood. According to (Pedersen, 1990), the influence of hysteresis is dependent on the cyclic steps (amplitude and period) of the boundary conditions and the purpose of the simulation. However, in most cases, the use of an average sorption isotherm is sufficient, but to study moisture buffer effects, the hysteresis is probably important.

The significance of temperature, step size and convective moisture transfer coefficients between the material and the ambient air should also be considered. In general, non-isothermal effects may change the transport and sorption behaviour of the material and need to be studied, together with the importance of different transport forms.

5.6 Conclusion

In this Chapter an experimental and numerical approach has been used to analyse isothermal moisture ab- and desorption mechanisms. The experimental results show retarded sorption for almost all the materials analysed, particularly for the organic ones: cellulose, flax and wool insulation. An exception was cellular concrete, whose sorption behaviour showed almost only Fickian characteristics.

A model for non-Fickian moisture transport was also developed. The traditional assumption of immediate local moisture equilibrium was rejected when modelling dynamic moisture transport. This was in accordance with approaches of other studies presented in Chapter 3. Almost similar models with separate nodes for moisture in the air in the pores of porous materials and the absorbed moisture have been suggested by several other authors. The link between these nodes, which retards sorption, was described by a sorption equation. An approach for determining the sorption coefficient *experimentally* in this equation has been shown in this Chapter. This preliminary approach for determining a sorption coefficient, which can model retarded sorption, is encouraging.

Chapter 6

Non-Isothermal, steady state moisture transfer

The influence of temperature gradients on the flow of moisture through building materials has been the subject of much debate within the research community. However, the difficulty in experimentally measuring non-isothermal moisture transport and the influence of temperature gradients on the transfer coefficients, limit the inclusion of such properties within simulation models. The role of temperature in the moisture transfer process is usually limited to the temperature dependence of the saturation vapour pressure or concentration and the liquid viscosity.

Nevertheless, the question of the significance of the impact of temperature gradients on the resulting moisture transport rises occasionally. Recently, the introduction of some 'new' insulation materials, mainly of organic origin, has initiated discussion, at least in Denmark, on the existence of 'other transport processes' apart from water vapour pressure driven transport.

The experimental investigation in this Chapter will lead to some conclusions on the magnitude of moisture transport due to temperature gradient on a range of porous light-weight building materials. An experimental method has been developed in an attempt to separate this 'other' moisture transport from the total measured moisture flux, and to quantify its significance relative to the water vapour pressure-driven transfer.

6.1 Background

As stated in Equations 2.25 to 2.28, a moisture flux can exist (besides that caused by the water vapour pressure gradient), due to a temperature-, moisture content-, relative humidity- and/or capillary pressure gradient. This raises the question; "Is this 'other' moisture flux induced by the thermal gradient, by the suction pressure gradient, or by the moisture content gradient, and subsequently by the relative humidity gradient, or even by them all?" The direction of the moisture content gradient is usually from cold to warm in building envelopes. Also the direction of the thermal diffusion is theoretically from cold to warm (see Section 2.2.1). That these driving potentials can work in the same direction makes identification of the single contributions very complex.

However, in many simulation models, this possible 'other' movement of moisture through a porous, water-absorbent material exposed to both a temperature and a relative humidity

gradient, is not taken into account. Nevertheless, the assumption of water vapour pressure difference being the only driving force cannot be entirely correct, because this process will result in a gradient of absorbed moisture content within the material, which will tend to drive water in the opposite direction, even in the hygroscopic range (Padfield, 1999). Deviations between simulations and measurements reported in e.g. (Peuhkuri, 2000) for cellulose insulation, which is a very hygroscopic material, could be an indication of these phenomena.

The methods and results in (Kumaran, 1988), (Krus, 1995) and (Galbraith et al., 1998; Galbraith et al., 1999; Galbraith et al., 2000; Peuhkuri et al., 2003) have in many ways given the background and inspiration to the present analysis. Their works will be explained and referred further to under the discussion of results in Section 6.4.

6.2 Experimental set-up

The measurement strategy for this actual investigation of non-isothermal moisture transfer is presented in this Section together with the experimental apparatus, i.e. the so-called Megacup (described in Section 6.2.2), including the materials used.

6.2.1 Measurement strategy

The scope of this experimental work is to separate and quantify the transport forms involved in a non-isothermal moisture transport process. This was achieved experimentally where a temperature gradient together with different moisture gradients were created through a sample.

The material sample with a transmission area of 0.25 m^2 on the top of the Megacup, was exposed to a temperature gradient of 10 K and a given moisture gradient. The temperature on both sides of the sample was fixed for all measurements: $T_{room} = 22^\circ\text{C}$ and $T_{Megacup} = 12^\circ\text{C}$. The sample to be investigated was placed horizontally at the top of the Megacup with the cold climate underneath. In this way, one of the moisture transport forms, i.e. convection, could be excluded from the analysis as the natural convection due to the thermal buoyancy inside the sample was minimised.

The moisture flux in and out of the Megacup was registered continuously. In addition, developments in local relative humidity and temperature were followed at minute intervals using small sensors within and on both surfaces of the specimen, and in the ambient air, both in the Megacup and in the room (see Figure 6.3 for the principle placement of the sensors).

The moisture regulation strategy of the equipment depends on the desired moisture boundary conditions. One of the strategies to reveal any transport other than a water vapour pressure driven one, was to hold a constant weight of water in the moisture controller (see Figure 6.2(a)), which is equivalent to maintaining zero moisture flux through the specimen. The relative humidity inside the Megacup will reach the level where there is no flux, i.e. a value which should correspond to the same vapour pressure as the one in the room, assuming there is no 'other' transport than the vapour pressure-driven mechanism. On the other hand, keeping RH constant, but at different levels on each side, the boundary conditions are used to reveal any moisture transport due to the non-isothermal conditions. Altogether the used boundary conditions are:

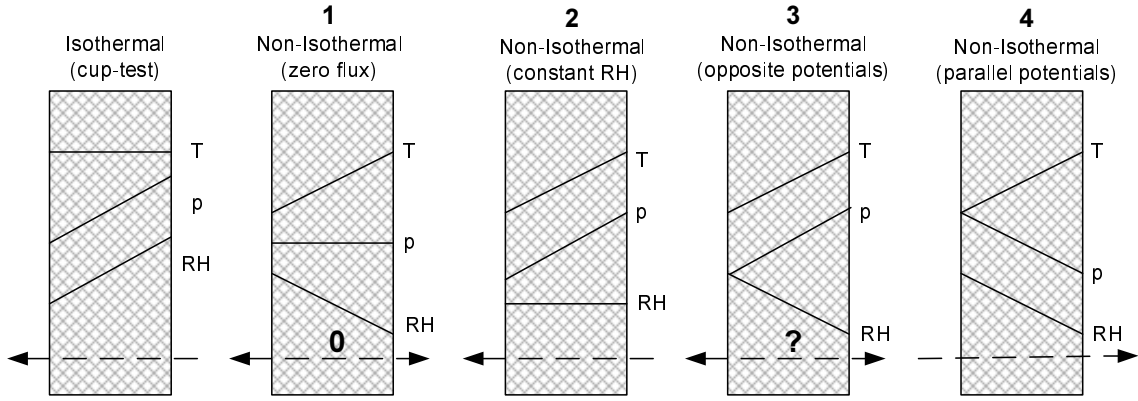


Figure 6.1: Illustration of the principle difference between isothermal and non-isothermal cup test on the moisture flow direction. The principal directions of gradients are shown for the four different measurement strategies. T is temperature, p water vapour pressure and RH relative humidity.

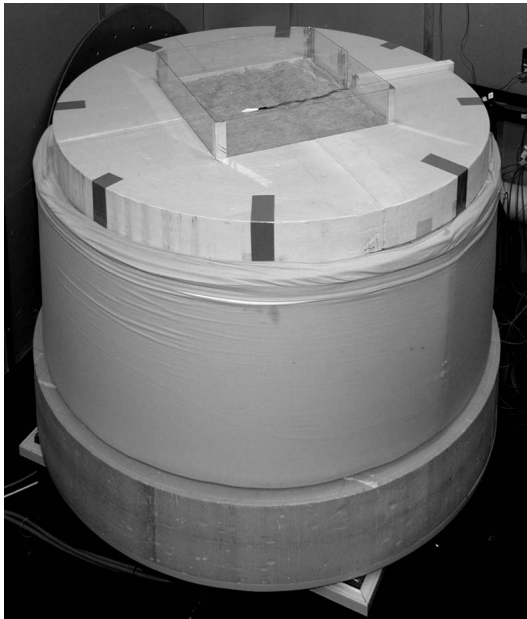
Table 6.1: Measurement strategy for non-isothermal, steady state measurements. The water vapour pressures are calculated from the temperatures and the relative humidities. $T_{room} = 22^{\circ}\text{C}$ and $T_{chamber} = 12^{\circ}\text{C}$. Water vapour pressure gradient Δp is set positive to the Megacup.

Measurement condition	RH	RH	p	p	Δp
	Megacup [%]	room [%]	Megacup [Pa]	room [Pa]	[Pa]
1 Zero flux	?	45	?	1191	?
2 Constant RH	50	50	702	1323	621
3 Opposite potentials	75	50	1053	1323	270
4 Parallel potentials	90	40	1263	1058	-205

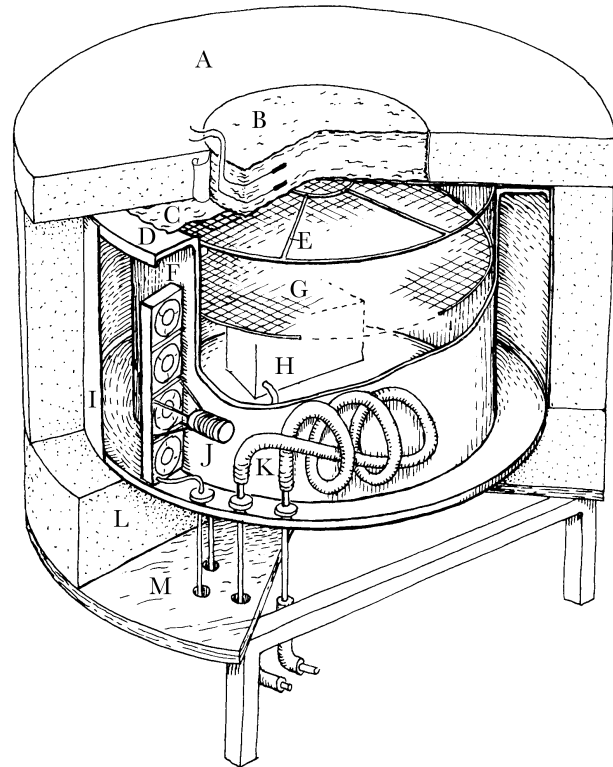
1. Zero flux: T - and RH -gradients are opposite, while p -gradient is supposed not to exist if there is only water vapour pressure-driven transport.
2. Constant relative humidity (RH): T - and p -gradients are in the same direction and there is no RH -gradient.
3. Opposite potentials: p - and RH -gradients are opposite, and T - gradient is in the same direction as p - gradient.
4. Parallel potentials: vapour pressure (p) and relative humidity (RH) gradients work parallel in the same direction, while T -gradient is opposite to the other gradients.

In general, in this Thesis *parallel* is synonymous with *in the same direction*.

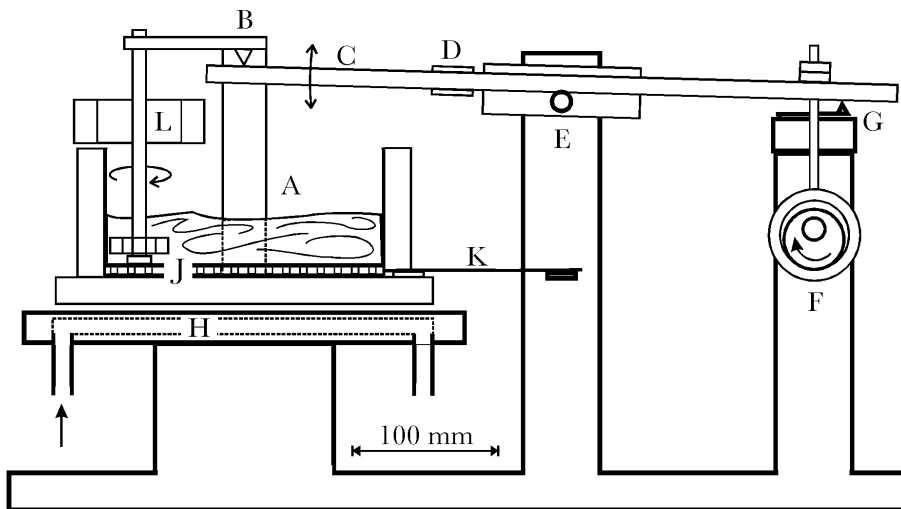
The impact of these gradients on the resulting moisture flux is presented in Figure 6.1, together with the illustration of the principal difference between isothermal and non-isothermal tests. Table 6.1 summarises the boundary conditions and the measurement strategy used.



(a)



(b)



(c)

Figure 6.2: (a) The overall set-up with the Megacup. The specimen under test is the square piece inserted in the top. All that is visible of the Megacup is the exterior insulation. (b) The cross section of the experimental set-up and the construction principles: **A** thermal guard insulation **B** sample (normally square) **C** vapour barrier under the guard insulation **D** flange over annular space **E** open grid **F** fans **G** another grid (not used) **H** moisture control unit **I** aluminium wall **J** heating (electric resistance) **K** cooling (water circulating in coil) **L** bottom insulation **M** table. (c) The moisture control unit: **A** water container (copper) **B** suspension points **C** beam **D** strain gauge bridge **E** fulcrum **F** turning cam **G** microswitch to break the circuit **H** heat sink **J** thermoelectric heat pump **K** flat spring conductors **L** wind driven propeller. The illustrations are from (Padfield et al., 2002).

6.2.2 The Megacup equipment

A special climate chamber was constructed (Padfield et al., 2002). Hereafter, this chamber was called Megacup due to the similarity of the measurement principle with ordinary cups for water vapour permeability measurements. The Megacup is a cylindrical well made of stainless steel (see Figure 6.2). The inner dimensions of the well are 793 mm (diameter) and 500 mm (depth). The test specimen was suspended horizontally at the top of the chamber. On the bottom of the well there is a removable tray with a moisture control unit, climate sensors, ventilators and electrical connections. As a part of the moisture controller there is a water flux control system: The mass of a small open water container is weighed with given intervals. As the rest of the inner surfaces of the well are inert, the flux of moisture through the specimen can be determined by the change in the mass of water in the container. The construction details of the Megacup are given in (Padfield et al., 2002). The steel well is enclosed by an annular outer chamber. Air is circulated in this outer chamber to ensure an even temperature in the well to avoid condensation on the walls. The temperature of this air is controlled by an electric heater and a finned copper tube containing re-circulating cold water. The chamber humidity is controlled by another cold water system, which cools a heat pump. The steel well is well insulated around the periphery and under the bottom plate.

The climate in the chamber, i.e. temperature T and relative humidity RH , and the state of the different elements of the climate control system are measured continuously. The data was collected every minute by a data logger connected to a computer. An active program analyses the data and sends control signals to the data logger. The climate inside the Megacup can either be constant in respect to both T and RH or oscillating, e.g. between 10-30°C and 40-95% RH . The overall set-up is illustrated in Figure 6.2(b). The lid of the chamber is made of rigid insulation, sealed vapour tight against the chamber. In the middle of the lid, there is a square hole of 0.5 x 0.5 meters where the test specimen was placed. The whole set-up was situated in a climate-controlled room, where temperature and relative humidity were held constant at the desired levels. The accuracy of the setup is given in Table 6.2. Although the accuracy of the set-up appeared to be quite good, it must be kept in mind that the investigated 'other' transport effects are supposed to be rather small, and therefore it might turn out that even this accuracy is insufficient. The uncertainties of the results are discussed in Section 6.4.3.

One of the objectives of this study was to investigate the local moisture distribution when a sample is exposed to a temperature gradient. Furthermore, the surface temperature and relative humidity conditions must be measured in order to reduce the uncertainties connected to the boundary layer effects. Therefore, small temperature and relative humidity sensors were inserted inside the material at 3 to 4 levels and on both surfaces (see Figure 6.3). Temperature was measured by K- and T-type thermocouples. Very small electronic relative humidity sensors¹, which do not disturb the moisture flux, were used. The relative humidity sensors measure voltage in a dielectric layer that is linearly dependent on the relative humidity of the ambient air. All the RH -sensors were individually calibrated, both in respect to relative humidity and temperature (see Appendix B.2). (Padfield, 1999) also used this type of capacitive relative humidity sensors and found them to be very reliable and sensitive. The unique feature with the set-up used was the possibility to measure the moisture flux into or out of the air of the chamber,

¹HIH-3610 Series from Honeywell. <http://content.honeywell.com/sensing/prodinfo/humiditymoisture>. Dimensions: 3.8 · 8.9 · 0.6mm

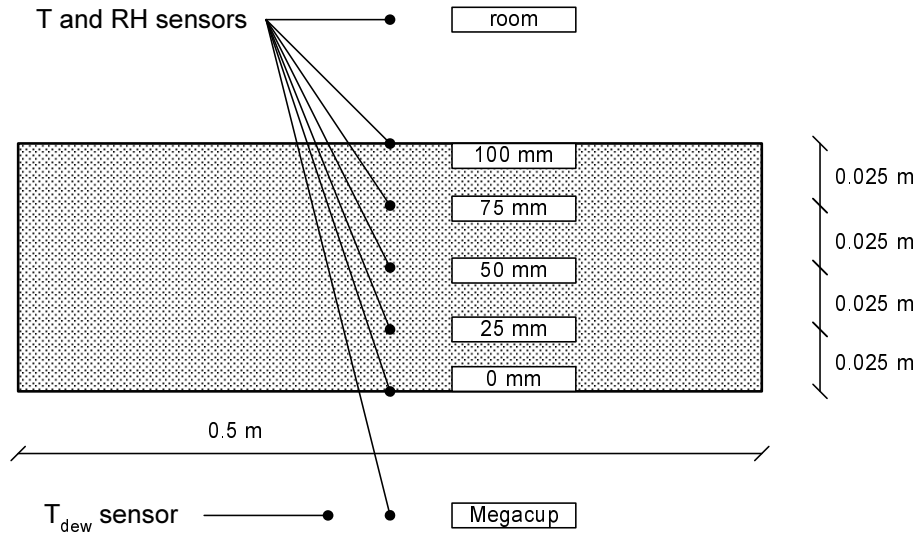


Figure 6.3: Location of the temperature and relative humidity sensors within the sample. Dimensions refer to samples with the thickness of 100 mm and sensors on 3 levels in the sample. Other thicknesses and sensor placements are used, too, but the names of the sensors used for the results are always given in same way: The distance from Megacup surface to room. Also the placement of the T_{dew} -sensor is given.

Table 6.2: Accuracy of the Megacup equipment and the used sensors. For humidity control the range in accuracy is due to the different accuracy on different RH -levels, the accuracy being best for low RH .

Component	Accuracy
Humidity control	$\pm 0.25 - 1.5\% RH$
Temperature control	$\pm 0.2^\circ C$
Moisture flux control	0.001 g
Temperature sensors	$\pm 0.2^\circ C$
Relative humidity sensors	$\pm 1.5\% RH$ (calibrated sensors)

$g [kg/(m^2s)]$ by weighing the moisture controller within the Megacup, as described in (Padfield et al., 2002). A data logger collected and averaged the 1-minute-measurements every 10 minutes. There was also an application, which made it possible for water to be removed or applied to the moisture controller without opening the set-up, if needed.

6.2.3 Materials

Thermal insulating materials are supposed to be most suitable for this non-isothermal investigation, as they are capable of maintaining a sufficient temperature gradient across the sample. With these materials also, the effect of the thermal boundary resistance is less dominant than for non-insulating materials, as experienced in Section 4.2.2. The materials selected for these tests were therefore; glass and rock wool insulation, cellular concrete and cellulose insulation.

Materials were chosen also with the anticipation that some materials would show 'other' moisture transport driven by temperature, while others would not. Moreover, these materials are rather common in building envelopes. Some more exotic insulation materials

Table 6.3: Materials used in the non-isothermal Megacup tests. Material parameters for rock wool, cellulose, flax and perlite are in general from (Hansen et al., 1999). Dry density for glass wool, cellular concrete and perlite are determined as a part of this work. The thermal conductivity for cellular concrete was determined as a part of student course work (Delfino and Giacchetti, 2001). Perlite was measured with 2 different sample thicknesses.

Material	Dry density	Thermal conductivity	Thickness of the sample
	ρ_0 [kg/m^3]	λ_0 [$W/m \cdot K$]	d [mm]
glass wool	70	0.037	100
rock wool	32	0.037	100
cellular concrete	450	0.11	100
cellulose	65	0.040	100
flax	30	0.040	90
perlite	100	0.050	100/140

Table 6.4: Isothermal water vapour permeability for the investigated materials. Isothermal permeabilities originate from (Hansen et al., 1999) (6 samples for each condition), except for glass wool (3 samples) and cellular concrete (4 samples) that have been determined as a part of this work with the same experimental set-up and conditions as in (Hansen et al., 1999). The isothermal permeabilities are values from wet-cup measurements: $50\% < RH < 93\%$.

Material	Isothermal permeability
	δ_p [$10^{-9} \cdot kg/(Pa \cdot m \cdot s)$]
glass wool	0.17 ± 0.01
rock wool	0.18 ± 0.03
cellular concrete	0.024 ± 0.0004
cellulose	0.11 ± 0.002
flax	0.15 ± 0.059
perlite	0.10 ± 0.015

were also included in the experiments; flax insulation and expanded perlite. Table 6.3 introduces some of the material parameters together with the sample dimensions. More detailed information on the investigated materials is found in Appendix A.

6.3 Measurement results

The results are in two parts, i.e. (a) the measured total moisture flux g [$kg/(m^2s)$] through the specimen and the calculated apparent permeabilities based on g and the measured boundary conditions, and (b) the distribution of temperature and relative humidity (and water vapour pressure) throughout the specimen and on both surfaces. Results for rock wool insulation are used as examples in the analysis.

The apparent water vapour permeability was calculated with Equation 4.1 under the assumption that water vapour pressure was the only driving force for moisture transport:

Table 6.5: Apparent water vapour permeability calculated from the non-isothermal Megacup test results, calculated under assumption of that the water vapour pressure gradient is the only driving force.

Material	Apparent non-isothermal permeability		
	Constant RH (condition 2) $\delta_{p,RH}$ [$10^{-9} \cdot kg / (Pa \cdot m \cdot s)$]	Opposite potentials (condition 3) $\delta_{p,opp}$ [$10^{-9} \cdot kg / (Pa \cdot m \cdot s)$]	Parallel potentials (condition 4) $\delta_{p,par}$ [$10^{-9} \cdot kg / (Pa \cdot m \cdot s)$]
glass wool	0.19	0.19	0.25 – 0.26
rock wool	0.19	0.17 – 0.21	0.39 – 0.48
cellular concrete	-	0.023 – 0.045	0.19
cellulose	0.13	0.12	0.50 – 1.0
flax	-	0.083 – 0.14	0.37
perlite	0.093	0.068 – 0.072	-

$$\delta_p = g \cdot \frac{d}{\Delta p} \quad (4.1)$$

where Δp is the water vapour pressure gradient calculated from the measured relative humidity and temperature on both surfaces of the sample. Table 6.5 shows the calculated apparent permeability under 3 different boundary conditions: constant RH , opposite and parallel potentials. These values can be compared with isothermal permeabilities in Table 6.4. According to the isothermal measurements reported in (Hansen et al., 1999), the isothermal permeability of rock wool, cellulose, wool, flax and perlite is not a function of relative humidity and therefore only a value for wet-cup measurements ($50\% < RH < 93\%$) is given here. Isothermal permeabilities for glass wool and cellular concrete have been measured as a part of the present work as dry-cup and wet-cup, and no significant dependence on relative humidity was found here, either. It is stressed that the determined apparent permeabilities for constant relative humidity $\delta_{p,RH}$, opposite $\delta_{p,opp}$ and parallel potentials $\delta_{p,par}$ only serve to give the first idea of the magnitudes, and are not seen as 'material parameters'.

These apparent permeabilities were plotted together with the isothermal permeabilities as a function of RH -distribution, see Figure 6.4. These measurements showed no correlation between RH and permeability, but they illustrated the effect of parallel potentials on the apparent permeability, i.e. $\delta_{p,par}$ was two to eight times greater than the one for opposite potentials $\delta_{p,opp}$. The values for opposite potentials and constant RH were relatively close to the isothermal permeability. The standard deviation² for calculated permeabilities is up to $\pm 4.4 \cdot 10^{-11}$, which makes $\delta_{p,opp}$ be treated as uniform with isothermal permeability, while $\delta_{p,par}$ is significantly different.

In addition, to illustrate that there exists a moisture flux induced by other driving forces than water vapour pressure gradient, the measured moisture flux g is plotted as a function of Δp , together with the 95% confidence intervals (Figure 6.5). The trend was clear, i.e. the trend line corresponding to the different magnitudes of water vapour pressure gradient and moisture flux intersected the zero vapour pressure difference not at the zero moisture

²Standard deviation for δ_p σ_{δ_p} is determined with an analytical expression, where both σ_g and $\sigma_{\Delta p}$ and the partial derivatives of δ_p are included.

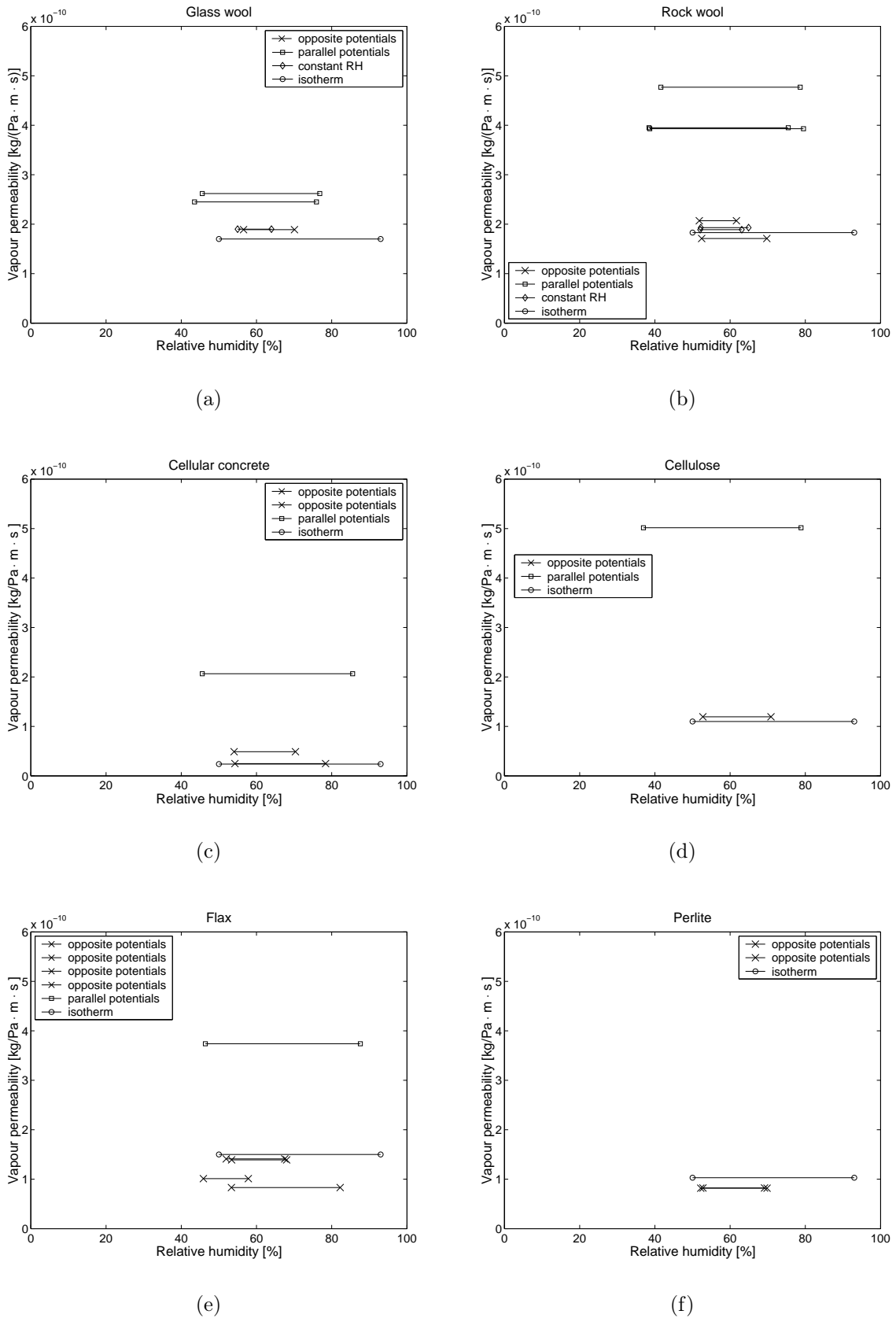


Figure 6.4: Measured isothermal and apparent permeabilities for (a) glass wool insulation, (b) rock wool insulation, (c) cellular concrete, (d) cellulose insulation, (e) flax insulation and (f) expanded perlite. Note: The absence of parallel potentials for perlite. Boundary conditions: constant RH (condition 2, only for glass wool and rock wool), opposite potentials (condition 3) and parallel potentials (condition 4).

Table 6.6: The measured relative humidity RH in Megacup is compared with the theoretical relative humidity in Megacup, which would be the case if the only driving potential is the gradient of water vapour pressure ∇p or water vapour concentration $\nabla \rho_v$, when there is no net moisture flux (condition 1). The RH -value measured with a dew point sensor inside the chamber, is closer to the 'true' RH than the small sensors and gives an indication for the great uncertainty of the measured values.

Material	Megacup relative humidity [%]			
	Measured		Theoretical	
	small RH -sensors	T_{dew} -sensor	$\nabla p=0$	$\nabla \rho_v=0$
glass wool	81	89	88	86
rock wool	81	89	88	86
cellular concrete	87	90	94	91
cellulose	80	87	88	85
flax	93	95	97	94
perlite	76	79	84	81

flux, but at a negative flux. This negative moisture flux at $\Delta p=0$ was seen as an indication that there is a transport against the p -gradient. The investigated materials seemed to belong to one of two groups. In the first group, rock wool and cellulose insulation showed rather significant 'other' transport, against the water vapour pressure gradient, while in the second group, the significance was minor for cellular concrete, perlite and glass wool, and almost non-existent for flax.

The distribution of RH and p in a material for different boundary conditions is given in Figure 6.6 for rock wool insulation. The profiles for all the materials are given in Appendix B.2 – Figures B.11 – B.16. The profiles can be compared with the principle profiles introduced in Figure 6.1. p -profiles should be linear through the specimen, if the water vapour pressure is the only governing driving potential and δ_p is constant. Linearity of temperature was assumed and used to localise the sensors within soft test specimens, as well as to check the placement in the more rigid materials. The resulting placement of the sensors was not exactly identical with the formalised model given in Figure 6.3.

Finally, for the condition where no net moisture flux was measured (condition 1), the deviation in the measured and theoretically determined $RH_{Megacup}$ is given in Table 6.6.

6.4 Discussion

The results given in Section 6.3 are discussed further in this Section together with relevant literature references. Also, the observed and possible uncertainties are treated in order to estimate the significance of the results.

The amount and the range of the measurements were not numerous enough to give a consistent idea of the dependence of different moisture processes on temperature and humidity levels. Therefore, the determined coefficients were assumed constant.

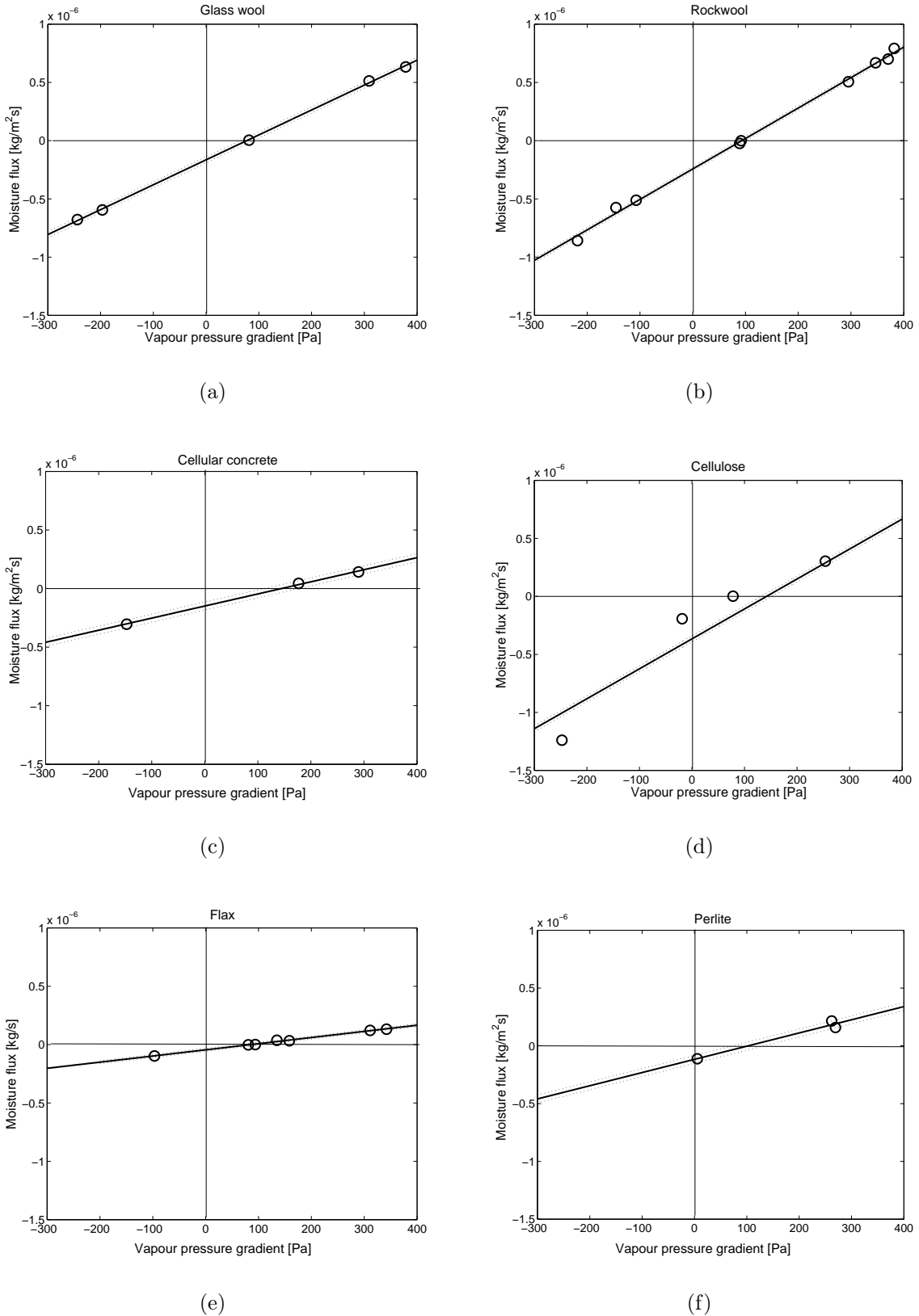


Figure 6.5: Moisture flux (g) as a function of water vapour difference (Δp) for (a) glass wool insulation, (b) rock wool insulation, (c) cellular concrete, (d) cellulose insulation, (e) flax insulation and (f) expanded perlite. All measurement conditions are used for the measured values (circles) and the linear trend lines (—). 95 % confidence intervals are given with (...). Confidence intervals were determined from the calculated standard deviation for flux measurements at $\sigma_g = 3 \cdot 10^{-8} \text{kg}/(\text{m}^2 \text{s})$ and the number of observations.

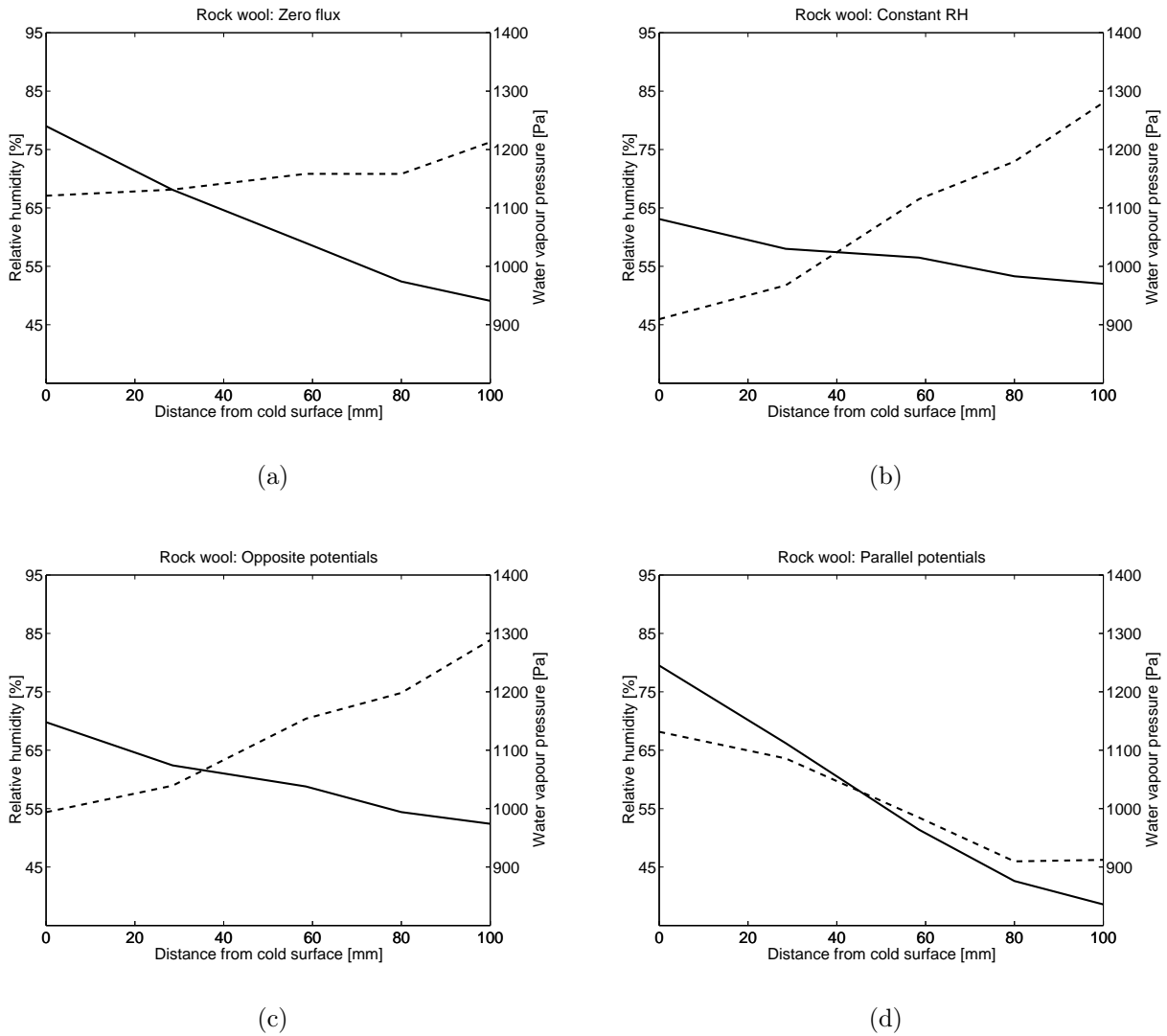


Figure 6.6: Measured relative humidity (solid line) and vapour pressure (dotted line) profiles for rock wool insulation for boundary conditions, where the profiles are a result of the given boundary conditions: (a) **1** zero flux, (b) **2** constant RH , (c) **3** opposite potentials and (d) **4** parallel potentials. Note that the resulting RH is not constant in case (b). This is due to a limited capacity of the moisture controller for reducing the $RH_{Megacap}$.

Table 6.7: The magnitude of moisture transport against vapour pressure gradient for the investigated materials. The 'other' transport is determined as the intersection with the y-axis of the trend line in Figure 6.5.

Material	'Other' transport [kg/(m ² s)]
glass wool	1.6 · 10 ⁻⁷
rock wool	2.4 · 10 ⁻⁷
cellular concrete	1.5 · 10 ⁻⁷
cellulose	3.7 · 10 ⁻⁷
flax	0.45 · 10 ⁻⁷
perlite	1.2 · 10 ⁻⁷

6.4.1 Assessment of the results

The deviation from zero flux for zero water vapour pressure in Figure 6.5 could be evaluated directly as 'other' moisture transport. The magnitude of this transport against vapour pressure gradient is given in Table 6.7. The goal of the analysis in this Section is to explain this 'other' transport and to draw some conclusions on the processes involved and their significance.

Apparent permeability

Results given in Figure 6.4 showed that the apparent permeability was two to eight times greater for the conditions where all the driving potentials were working in the same direction, in this case from cold to warm (condition **4**). This strongly indicated that there must exist other transport mechanisms than the water vapour pressure-driven one alone.

The apparent permeability calculated according to Equation 4.1 from the measured Δp describes *sensu stricto* only water vapour transport, but it was assumed here that it might also have included liquid transport. However, the separation of liquid and vapour contributions was not possible here on the basis of the measurements and therefore the 'other' transport is given as 'bulk' transport of vapour and liquid. The magnitude and driving forces responsible for this 'other' transport are analysed later in this Section, but already results in Figure 6.4 and Tables 6.4 and 6.5 indicated the following:

The isothermal permeability at $\delta_p=0.183 \cdot 10^{-9} \text{kg}/(\text{Pa} \cdot \text{m} \cdot \text{s})$ for rock wool and the apparent permeability for constant RH (condition **2**) at $\delta_{p,RH}=0.189\text{-}0.193 \cdot 10^{-9} \text{kg}/(\text{Pa} \cdot \text{m} \cdot \text{s})$ were identical within the accuracy of the measurements. Under isothermal conditions, p - and RH -gradients were parallel, and if any liquid transport occurred, it was in parallel with pure water vapour diffusion. Under constant RH , the T -gradient was parallel to the p -gradient. On the basis of these conditions it was not possible to conclude, which of the other gradients was driving the 'other' transport.

For opposite potentials (condition **3**) there was a T -gradient parallel with the p -gradient, while the RH -gradient was opposite. This condition gave the lowest apparent permeability at $\delta_{p,opp}=0.171\text{-}0.208 \cdot 10^{-9} \text{kg}/(\text{Pa} \cdot \text{m} \cdot \text{s})$ for rock wool, indicating that there must have been some transport driven by the RH -gradient.

Finally, when compared with the other conditions, the apparent permeability for condition **4** was high, i.e. $\delta_{p,par}=0.39\text{-}0.48 \cdot 10^{-9} \text{kg}/(\text{Pa} \cdot \text{m} \cdot \text{s})$ for rock wool, because now the

RH -gradient did not just work against the water vapour pressure-driven transport but supported it. The direction of the temperature gradient-driven transport was not known on the basis of this analysis, but it was perceived here that the direction of total flux in this case was from cold to warm.

Resulting relative humidity and vapour pressure profiles

Relative humidity and vapour pressure profiles in Figure 6.6 and in Appendix B.2 show that RH and p were almost linear for all materials. However, the slight tendency of p to non-linearity could be explained by the uncertainties in the measured RH , which gave a standard deviation for p at $34Pa$. It was seen that deviations from linearity for p were within this range and therefore the water vapour pressure profiles could be assumed as linear. The non-linear nature of saturation vapour pressure p_{sat} due to the strong temperature dependence plays a role for the RH -profiles, and makes RH decrease relatively quickly with increasing temperature. Therefore, this non-linearity of RH -profiles was expected and was not an indication of any other transport.

Resulting $RH_{Megacup}$

The investigation of the resulting relative humidity in the Megacup, when net moisture flux was zero, is presented in Table 6.6. If the RH measured with the dew point sensor – which is assumed to give more reliable values than the small RH -sensors – is compared with the theoretical RH for $\Delta p=0$, hardly any difference is found. The only materials showing any significant difference at all are cellular concrete and perlite. For $\Delta\rho_v=0$, even this significance disappears.

Therefore, the existence of a transport against Δp -gradient, which could make the resulting RH on the cold side lower than expected, making a building envelope more resistant to damage due to excessive moisture loads, cannot be confirmed with these observations. Also previous laboratory tests reported in (Vinha et al., 2002) showed that hygroscopic insulation materials like cellulose and flax performed not significantly better in avoiding high moisture levels than mineral wool in a building envelope structure without a vapour barrier.

Determination of transport coefficients

The transport coefficients given in Equations 2.25, 2.27 and 2.28 can be determined by calculating the water vapour pressure-driven transport g_p defined by the isothermal δ_p and the measured Δp first, and then by determining the other coefficient by solving following equations for each of the other coefficients. These equations are treated as totally individual models on non-isothermal moisture transport and have nothing in common with each others.

$$D_T = -\frac{g + \delta_p \frac{\partial p}{\partial x}}{\frac{\partial T}{\partial x}} \quad (6.1)$$

Table 6.8: Thermal moisture diffusion coefficient D_T , liquid conductivity coefficient D_φ and hydraulic conductivity K calculated from the non-isothermal Megacup test results with Equations 6.1, 6.2 and 6.3, respectively. The calculated coefficients are mean values for all the different boundary conditions.

Material	Thermal moisture diffusion coefficient D_T [$10^{-9} \cdot \text{kg}/(\text{K} \cdot \text{m} \cdot \text{s})$]	Liquid conduction coefficient D_φ [$10^{-9} \cdot \text{kg}/(\text{m} \cdot \text{s})$]	Hydraulic conductivity K [$10^{-15} \cdot \text{kg}/(\text{Pa} \cdot \text{m} \cdot \text{s})$]
glass wool	-0.93	-7.2	-0.03
rock wool	-1.8	-31	-0.13
cellular concrete	-0.64	-7.6	-0.03
cellulose	-2.8	-35	-0.15
flax	-1.1	-37	-0.15
perlite	-1.2	-810	-0.41

$$D_\varphi = -\frac{g + \delta_p \frac{\partial p}{\partial x}}{\frac{\partial \varphi}{\partial x}} \quad (6.2)$$

$$K = -\frac{g + \delta_p \frac{\partial p}{\partial x}}{P_c \frac{\partial \ln P_c}{\partial x}} \quad (6.3)$$

These coefficients, i.e. the calculated mean value of all the measured conditions, are given in Table 6.8. The calculations are found in Appendix B.2. However, there is a large standard deviation connected to these calculated coefficients. This deviation is illustrated in Table 6.9, where the coefficients are given for rock wool for each boundary condition before averaging the values.

It must be kept in mind that these coefficients are determined as a mean value of all the measured conditions, and therefore, any possible necessary conditions for the validity of determination of the coefficients are not fulfilled. The calculated values in Tables 6.8 and 6.9 serve mostly to illustrate the great sensitivity of the results with respect to the analytical method used.

The correct method of determining the coefficients is to make an experimental set-up where the boundary conditions are chosen in such a way that analysis is possible. In this case, only the conditions for determining D_T are present for condition **2**, i.e. constant RH . The average value of D_T for rock wool given in Table 6.8 can be compared with the 'correct' value in Table 6.9, and it is evident that there was no consistency of the values in between.

Identifying and quantifying the driving potentials

The presented results have so far given a strong indication that gradients of both T and RH also play a role in total non-isothermal moisture transport. In the following, a

Table 6.9: To illustrate the great deviation in the determined coefficients in Table 6.8, all 3 different transport coefficients for **rock wool** are given for every boundary condition. The coefficients are calculated from the non-isothermal Megacup test results with Equations 6.1, 6.2 and 6.3, respectively.

Boundary condition	Thermal moisture diffusion coefficient D_T [$10^{-9} \cdot \text{kg}/(\text{K} \cdot \text{m} \cdot \text{s})$]	Liquid conduction coefficient D_φ [$10^{-9} \cdot \text{kg}/(\text{m} \cdot \text{s})$]	Hydraulic conductivity K [$10^{-15} \cdot \text{kg}/(\text{Pa} \cdot \text{m} \cdot \text{s})$]
zero flux	-2.1	-62	-2.8
constant RH	0.3	20	0.81
opposite potentials	1.1	95	3.7
parallel potentials	-3.8	-85	-3.5

hypothesis is presented on how the 'other' transport could be allocated to the identified potentials, i.e. 3 single contributions to the total transport are given as

$$g = g_{diffusion} + g_{liquid} + g_{thermal} \quad (6.4)$$

where

$$g_{diffusion} = -\delta_p \frac{\partial p}{\partial x} \quad (6.5)$$

$$g_{liquid} = -K \cdot P_c \frac{\partial \ln P_c}{\partial x} \quad (6.6)$$

$$g_{thermal} = -D_T \frac{\partial T}{\partial x} \quad (6.7)$$

$g_{diffusion}$ stands for pure water vapour diffusion, while g_{liquid} represents any liquid transport and $g_{thermal}$ any transport induced by the temperature gradient. The suction pressure P_c is chosen as potential, together with water vapour pressure p and temperature T , because these are physical potentials, in contrast to relative humidity, for example. However, in the analysed hygroscopic range, P_c was determined by the Kelvin equation (Equation 2.6) from the measured temperature and relative humidity and was assumed to describe also surface diffusion, as well as capillary suction.

The unique separation of the temperature- or suction pressure-driven transport from water vapour pressure driven transport (given by Equation 6.4), is not supposed to be possible simultaneously, as all the gradients but the one investigated should be zero. However, by determining the water vapour pressure-driven transport defined by the isothermal δ_p first, then the 2 other coefficients can be determined by solving a set of linear equations (Matrix 6.8), each representing the n different measured conditions. The resulting matrix to be solved is Matrix 6.9.

Table 6.10: The determined transport coefficients for 'other' transport: K stands for a transport coefficient for any liquid transport and D_T for a transport coefficient for any temperature gradient induced transport. The coefficients were determined by solving Matrix 6.9.

Material	Liquid transport	Thermal transport
	K [$10^{-15} \cdot \text{kg}/(\text{Pa} \cdot \text{m} \cdot \text{s})$]	D_T [$10^{-9} \cdot \text{kg}/(\text{K} \cdot \text{m} \cdot \text{s})$]
glass wool	-0.36	2.2
rock wool	-0.61	2.7
cellular concrete	-0.56	3.6
cellulose	-1.1	5.8
flax	-0.27	0.74
perlite	-0.08	-0.68

$$\begin{bmatrix} \delta_p \frac{\partial p}{\partial x_1} & K \cdot P_c \frac{\partial \ln(P_c)}{\partial x_1} & D_T \frac{\partial T}{\partial x_1} \\ \delta_p \frac{\partial p}{\partial x_2} & K \cdot P_c \frac{\partial \ln(P_c)}{\partial x_2} & D_T \frac{\partial T}{\partial x_2} \\ \dots & \dots & \dots \\ \delta_p \frac{\partial p}{\partial x_n} & K \cdot P_c \frac{\partial \ln(P_c)}{\partial x_n} & D_T \frac{\partial T}{\partial x_n} \end{bmatrix} = \begin{bmatrix} g_1 \\ g_2 \\ \dots \\ g_n \end{bmatrix} \quad (6.8)$$

$$\begin{bmatrix} P_c \frac{\partial \ln(P_c)}{\partial x_1} & \frac{\partial T}{\partial x_1} \\ P_c \frac{\partial \ln(P_c)}{\partial x_2} & \frac{\partial T}{\partial x_2} \\ \dots & \dots \\ P_c \frac{\partial \ln(P_c)}{\partial x_n} & \frac{\partial T}{\partial x_n} \end{bmatrix} \begin{bmatrix} K & D_T \\ K & D_T \\ \dots & \dots \\ K & D_T \end{bmatrix} = \begin{bmatrix} g_1 - \delta_p \frac{\partial p}{\partial x_1} \\ g_2 - \delta_p \frac{\partial p}{\partial x_2} \\ \dots \\ g_n - \delta_p \frac{\partial p}{\partial x_n} \end{bmatrix} \quad (6.9)$$

The solving algorithm was based on a least squares method, and it was assumed that the coefficients were constant, even though it is understood that they may vary remarkably as a function of temperature and/or relative humidity.

The validity of Equation 6.4 is illustrated by using the isothermal permabilities δ_p (Table 6.4), the determined coefficients (Table 6.10), and the measured boundary conditions for a given set-up, i.e. Δp , $\Delta \ln P_c$ and ΔT , which should result in the measured total flux $g_{measured}$. An example of this is given in Figure 6.7 for rock wool. This example also gives a quantitative idea of the magnitudes of the different transport forms and the validity of the given equations. The measured boundary conditions and the resulting calculated fluxes together with diagrams for other materials are found in Appendix B.2.

In Figure 6.7, all the 4 different conditions are shown for rock wool. The calculated flux $g_{calculated}$ was very close to the measured total flux $g_{measured}$ for all cases. This is a general behaviour for all materials. Under certain conditions, there were deviations for some materials, (see Appendix B.2). The first bar in the diagrams depicts water vapour diffusion based on the isothermal permeability. It is quite clear that by taking only this part of the moisture transport into account, as some simplified models do, the real moisture transport is not predicted correctly at all. The next 2 bars correspond to liquid and thermal transport, and have different directions. The direction of liquid

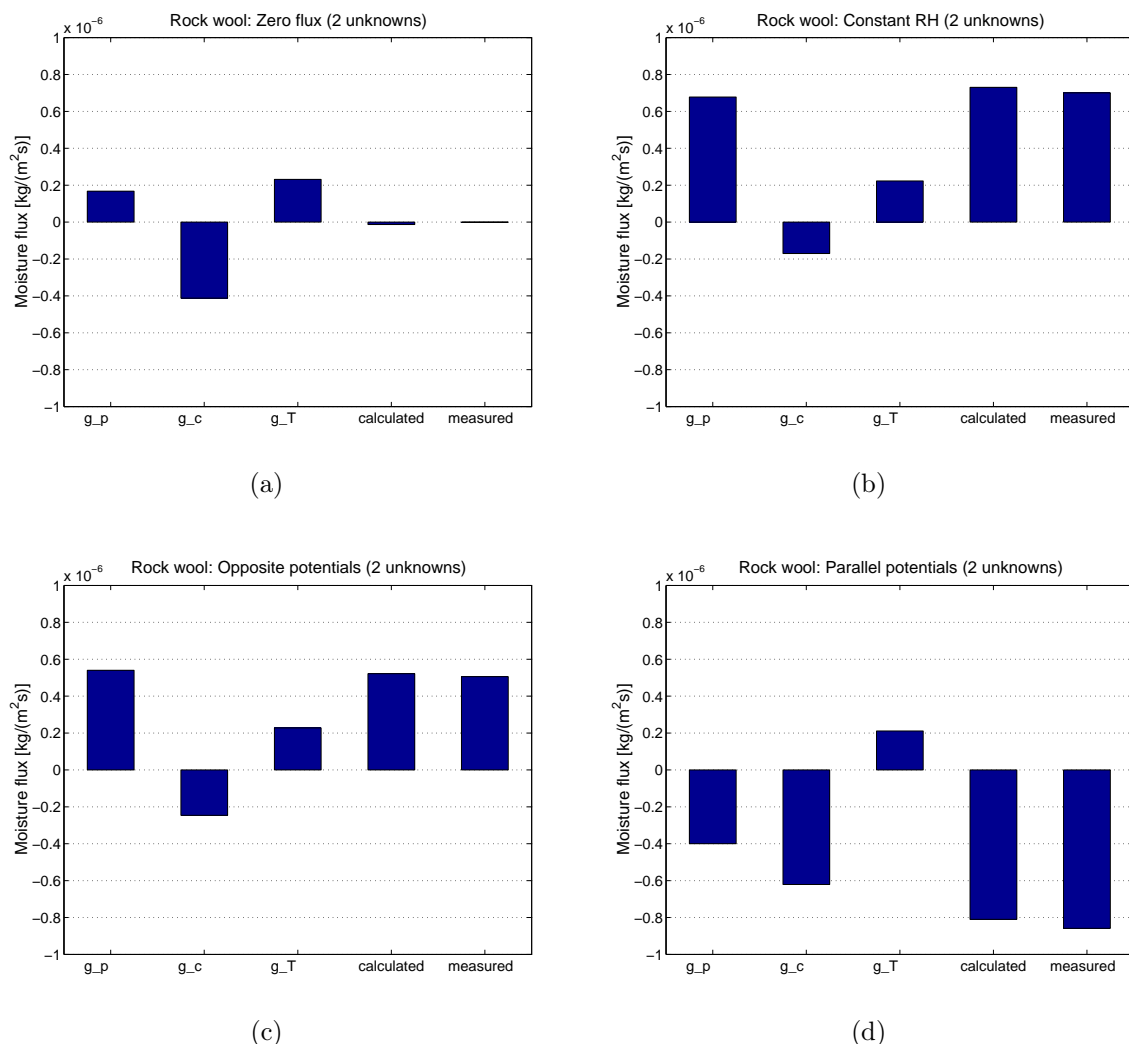


Figure 6.7: The identifying of the 'other' transport for **rock wool**, divided in 3 contributions: water vapour diffusion $g_{diffusion}$ (g_p), liquid transport g_{liquid} (g_c) and any temperature gradient induced transport $g_{thermal}$ (g_T). The water vapour pressure driven transport is based on the determined isothermal permeability and the actual boundary conditions. Liquid K and thermal D_T transport coefficients are determined by solving a set of linear equations with 2 unknowns with least squares method (Matrix 6.9). The calculated contributions $g_{calculated}$ are compared with the total measured transport $g_{measured}$. (a) zero flux (condition **1**), (b) constant RH (condition **2**), (c) opposite potentials (condition **3**) and (d) parallel potentials (condition **4**). The flux is positive from room to Megacup, i.e. from warm to cold.

transport is from the cold to the warm side, as expected, according to the hypothesis that moisture content plays a role in liquid transport. Thermal diffusion according to the classical definition also produces transport from cold to warm. However, the actual results showed that thermal effects, as defined here, made the moisture migrate parallel to the temperature gradient.

As a concluding remark, it must be stressed that the 3 different contributions in Equation 6.4 are not independent of each other, i.e. they can always be expressed with only 2 independent variables. This issue is discussed throughout in (Nicolajsen, 1973). In addition, the sharp distinction between vapour and liquid transport and thermal effects is not necessarily as simple as given in Equation 6.4. Nevertheless, the above analysis was attempted in order to open the discussion on how to separate some of the fluxes involved in this very complicated field of non-isothermal moisture transport.

Simultaneous determination of all the coefficients

In the previous Section, water vapour gradient-driven transport was supposed to be given by the isothermally determined δ_p and the other coefficients given by solving the Matrix 6.9. However, in Equation 6.4, it was assumed that g_p stood only for pure vapour transport, while the isothermal δ_p also might have included some liquid transport. In the following, an attempt to determine all the 3 coefficients simultaneously by using Matrix 6.8 is shown. An example of the results is given in Figure 6.8.

The magnitudes of the 3 different contributions become very different from the example with 2 unknowns. Still, the direction of g_{liquid} and $g_{thermal}$ is the same as before. But it is assumed to be an indication for the non-validity of this method that $g_{diffusion}$ has an opposite direction compared to the expected one: against the p -gradient!

6.4.2 Relevant observations in literature

Here, some of the most relevant studies in the literature are cited. They are divided into different research groups, because the references used are seen as representative for the work in the group.

Kumaran et. al

(Kumaran, 1988) reported investigations conducted on cellulose insulation. Slabs of cellulose insulation (50-60mm thick, $\rho_0 = 50\text{kg/m}^3$) were exposed to $\Delta T = 20 - 40\text{K}$ in a heat flow meter set-up. Initial moisture was added on the warm side and the moisture distribution during the moisture transport to the cold side was monitored using gamma-ray measurements. Glass wool insulation was also similarly tested.

At final steady state conditions, i.e. when no more moisture could be moved due to the T -gradient, there existed a measured moisture profile throughout the material. For comparison, a moisture content distribution in glass wool for corresponding boundary conditions showed that all the moisture had been transported to the cold side. (Kumaran, 1988) concluded that, based on the resulting moisture profile for cellulose insulation, a liquid phase transport against the water vapour gradient existed. Under the observed final steady state conditions this liquid transport was of same magnitude as the transport

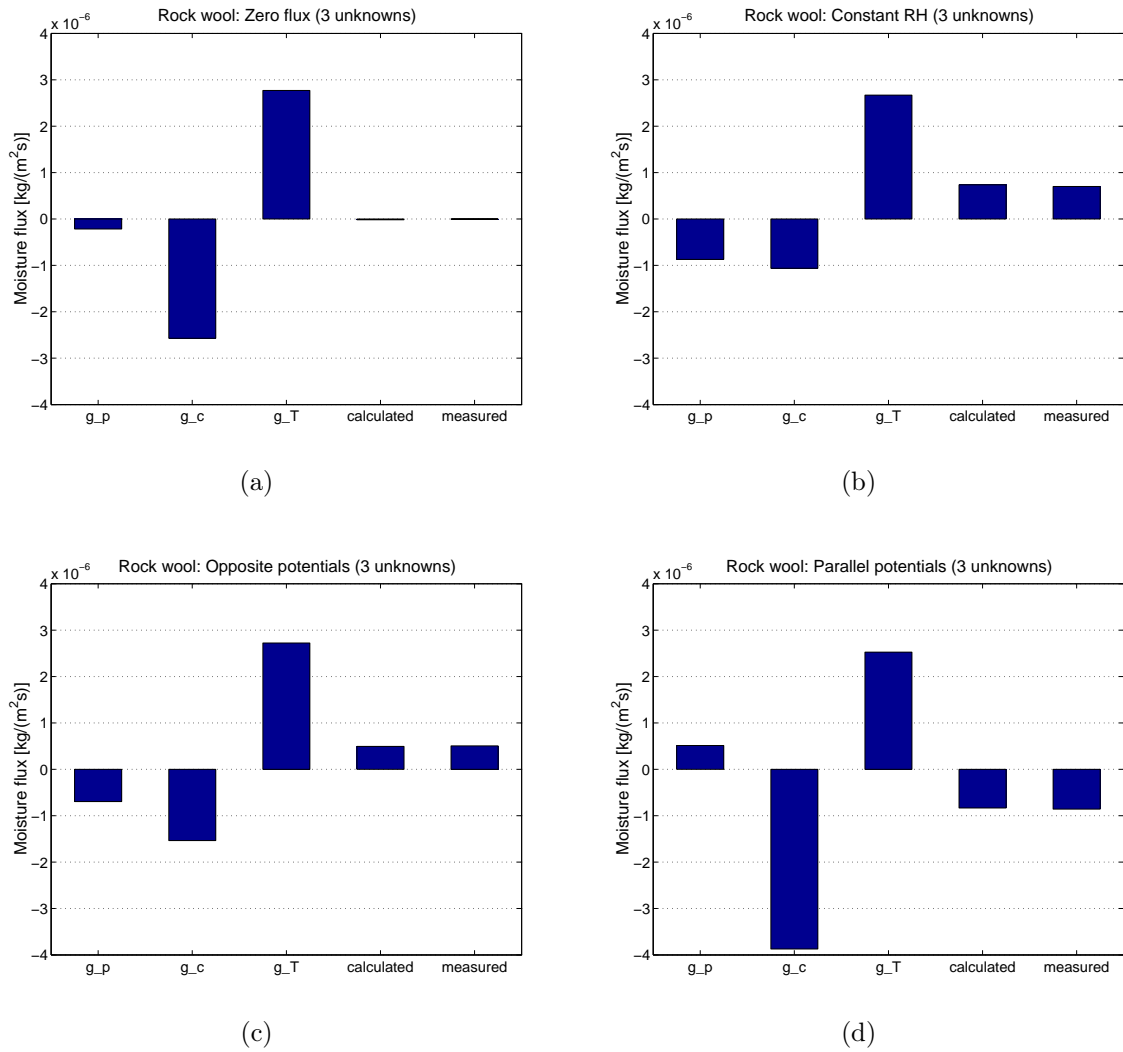


Figure 6.8: The simultaneous determining of transport coefficients for **rock wool** by solving a set of linear equations with 3 unknowns (Matrix 6.8) with least squares method, divided in 3 contributions: water vapour diffusion $g_{diffusion}$ (g_p), liquid transport g_{liquid} (g_c) and any temperature gradient induced transport $g_{thermal}$ (g_T). The calculated contributions $g_{calculated}$ are compared with the total measured transport $g_{measured}$. (a) zero flux (condition 1), (b) constant RH (condition 2), (c) opposite potentials (condition 3) and (d) parallel potentials (condition 4). The flux is positive from room to Megacup, i.e. from warm to cold.

driven by the water vapour pressure gradient, because the net transport was zero. The non-isothermal moisture transport can therefore be expressed by Equation 2.25.

Krus et. al

Among some other researches (Krus, 1995) argued for moisture content as the driving force for liquid transport, e.g. surface diffusion. For most materials, the use of a relative humidity gradient as the driving force (Künzel, 1995), is practically equivalent to using moisture content, as RH is more suitable for analysis of non-homogenous material structures, as discussed earlier.

(Krus, 1995) made a couple of different non-isothermal measurements on sandstone, gypsum board and chipboard to determine whether or not moisture content is a driving force for surface diffusion. He compared isothermal and non-isothermal transport and found that the moisture permeability decreases (as expected according to the hypothesis on moisture content as a driving force for surface diffusion), when the moisture content gradient was opposite to water vapour pressure gradient. A similar observation was achieved in the present study.

Another set-up in (Krus, 1995) was in principle similar to the particular condition in the present work, where the relative humidity in the Megacup was not set but resulted from the driving forces and conditions outside the Megacup. This experiment showed that there are indications for the moisture content being the driving force for wooden particle board also. When two small chambers with different temperatures were connected via the sample, RH in the cold one was maintained by a saturated salt solution. The dew point temperature T_{dew} was measured on both sides. The theory stated that if there was no other transport than water vapour diffusion, the dew point would be the same on both sides, when the system was in equilibrium, i.e. there is no net transfer of moisture. The experiment resulted in a dew point temperature on the warm side (23°C) that was 1-2 K higher than on the cold side (13°C). The RH range of the experiment was not mentioned. In this actual work, the differences in T_{dew} in the Megacup and the room were not significant.

Galbraith et. al

An extensive experimental programme on identifying primary and secondary temperature effects on various building materials is referred to in (Galbraith et al., 1998; Galbraith et al., 1999; Galbraith et al., 2000; Peuhkuri et al., 2003). Thermal diffusion was defined as a primary effect due to a temperature gradient, according to Equation 2.25, and as a secondary effect, the influence of different temperature levels, not gradients, on permeability.

The experimental work reported in (Galbraith et al., 1998) included non-isothermal small-scale test on two different set-ups for $\varphi < 0.76$. The results from the first set-up on particle board and polystyrene insulation showed no consistent thermal diffusion. By comparison, the second, improved set-up with a guard area for moisture transport, showed very clear evidence for the existence of thermal diffusion in plaster board and extruded polystyrene insulation. This temperature-induced transport made the total moisture transport higher, i.e. from warm to cold side. This is also seen for the actual analysis, e.g. Figure 6.7.

The tests in (Peuhkuri et al., 2003) were carried out under constant relative humidity with three different temperature gradients, and under 'zero' vapour pressure gradient with three different relative humidity ranges. The minimum temperature gradient maintained across each sample was $10K$. The secondary temperature effects were investigated with small-scale isothermal permeability cup tests carried out over a range of test temperatures ($10-30^{\circ}C$). The tested materials included phenolic foam, cement mortar, plywood, medium density fibre-board (MDF), plasterboard, chipboard, styrofoam and concrete.

The primary temperature effects were not measurable while the secondary effects according to (Galbraith et al., 1999) were most evident for the most hygroscopic materials like MDF and plywood, especially at higher relative humidity levels (see also Section 4.2). This supports the theory that, at increasing levels of moisture content within the material, the effects of a temperature gradient will become more pronounced. The presence of liquid moisture within the pore system of a material can act as a 'short-circuit' for increased moisture flow. Further, surface diffusion might support vapour transfer (Krus, 1995). Therefore, a temperature gradient, operating within a system that is already experiencing an increase in mass flux due to capillary condensation, could have a significantly greater effect upon the flow of moisture. The work in (Peuhkuri et al., 2003) also indicated that *vapour diffusion* is not significantly affected by temperature gradients, however, the combined effects of moisture content, hydraulic conductivity and ∇T , could have a greater significance for *liquid transfer*. Nevertheless, it remains unclear whether these observations are the sole explanation for very porous materials, as capillary transport is extremely limited, except for cellular concrete.

However, some experiments in (Peuhkuri et al., 2003) were performed on relatively thin and thermally well-conducting materials, apart from phenolic foam. As a result, the effect of heat and moisture transfer in the boundary layers was relatively large and measurements on insulating and thicker samples could reduce this type of error.

6.4.3 Sources for uncertainties

When evaluating the significance of the results, a possibility of uncertainties has to be recognised. In this Section, a range of possible errors and their impact on the results are discussed.

Moisture control

One of the main aims in the design of the Megacup was moisture control, where the water in the control unit is always the coldest place within the whole set-up. Using this method, no uncontrolled condensation occurs and the measured flux is an accurate representation of the actual flux produced by the driving potentials. The regulation strategy of the Megacup is ruled by computer programme, which is presently based on a rather simple algorithm using a first order PID-control. For some climate conditions, the relative humidity in the Megacup is oscillating ($\Delta RH = \pm 1.5\%$), while for other conditions, it is quite stable ($\Delta RH = \pm 0.25\%$). A 'window' of as stable environmental conditions as possible is used to obtain an accurately measurable flux. Unfortunately, the moisture controller has a limited capacity. In the present study, it was difficult to measure very permeable materials, therefore, thicker samples and smaller transmission areas should be used. The humidity in the room was controlled by a PID-controlled system connected

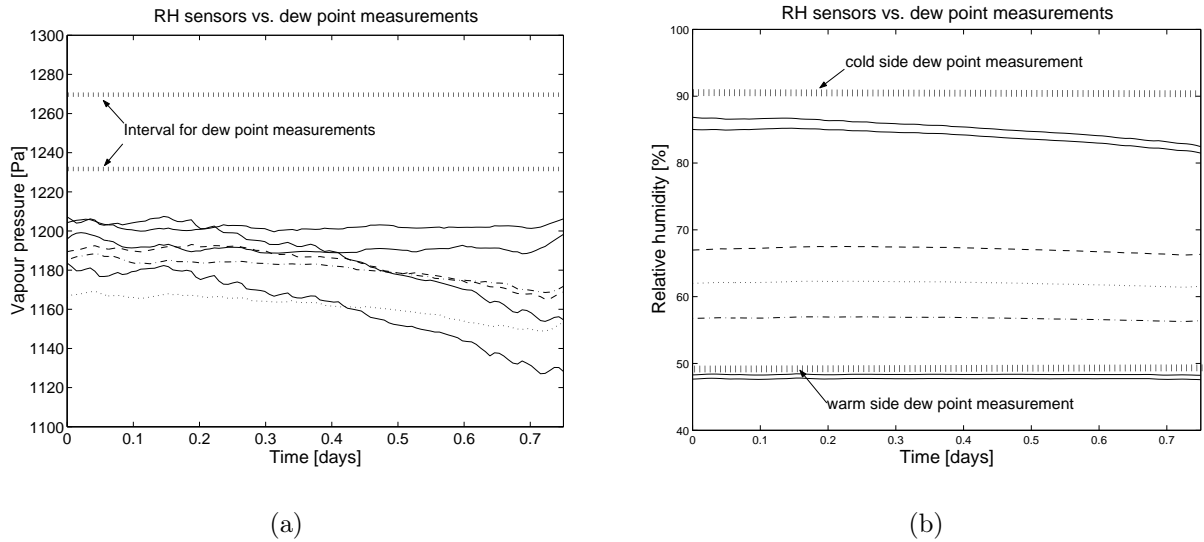


Figure 6.9: A measurement sequence for glass wool, where the T_{dew} both in room and in Megacup has been measured for the shown time period. The measured T_{dew} was practically uniform for all the cases. (a) The deviation in the vapour pressure based on measurements with the small relative humidity sensors is 50–100 Pa and lies clearly at a lower level than p according to dew point measurements. (b) Resulting RH shows that the RH measured with the small sensors on the warm side is very close to the dew point measurements, while the RH on the cold side is underestimated with the small sensors.

to a humidifier and a dehumidifier. This system performed satisfactorily enough but was not optimal in stability.

Furthermore, to make a final check of the results, the vapour pressure on the both sides of the specimen (room and Megacup) was also measured by a dew point measuring device. Air from the room or from the Megacup was circulated through the dew point meter. In this way one of the typical errors could be reduced, i.e. the use of different transducers for different measurements. This check was done by the end of all measurements and when a steady state had been reached. The result from this measurement showed (Figure 6.9) that when T_{dew} was uniform both in Megacup and in the room, the RH -sensors used gave a standard deviation in vapour pressure at around 35 Pa. Resulting standard deviation for the relative humidity sensors was 1.5 – 2.5% RH .

However, this 'final calibration' shows that the used relative humidity sensors underestimate heavily the RH on the cold side. This is also illustrated in Figure 6.10, where all the sensors are placed in a same climate and should therefore show the same relative humidity. While the small sensors agree quite well on the resulting RH , the 'true' level, measured with 2 different dew point sensors, is much higher for the low temperatures. Therefore, the RH -measurements are assumed to fulfill the expected standard deviation *relatively* to each other, while the *absolute* value on the cold side of the sample is very uncertain.

The influence of these observations on the assessment of the results so far will be shortly commented here. If it is assumed that the dew point sensor gives the true moisture conditions on the cold side, the used RH -value in the measurements is underestimated. This underestimation is realistically 5 % RH according to Figure 6.9(a). In Table 6.11 an example of the influence of this deviation on the resulting apparent permeabilities is given for glass wool insulation.

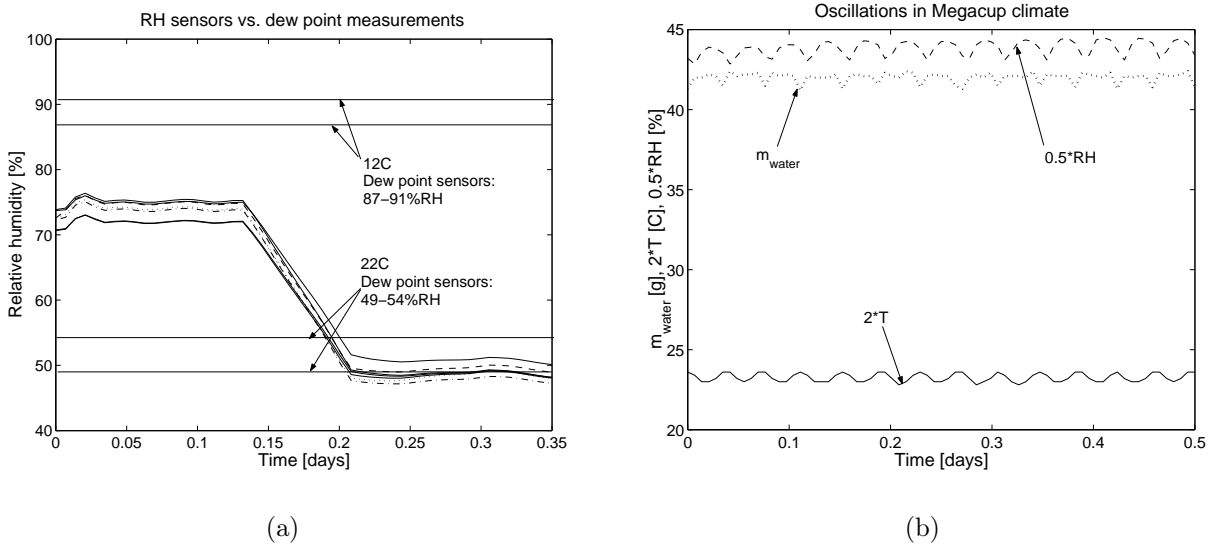


Figure 6.10: (a) A measurement sequence, where all the small RH -sensors together with 2 different dew point sensors have been first inside the Megacup (12°C) and then in the room (22°C). The deviation is very large on the cold side and the small RH -sensors underestimate the relative humidity to a great extent. (b) Illustration of the typical oscillations in Megacup climate. Note, that values for temperature T and relative humidity RH have been manipulated to suit the scale. The values are given *before* averaging.

Table 6.11: Apparent permeability for glass wool calculated on the basis of two different measurements of the boundary conditions: With the small RH -sensors (these measurements have been used for all the analysis in this Chapter) and with a T_{dew} -sensor.

Condition		Apparent permeability [$10^{-9}\cdot\text{kg}/(\text{Pa}\cdot\text{m}\cdot\text{s})$]	
		Small RH -sensors	T_{dew} -sensors
constant RH	$\delta_{p,RH}$	0.19	0.28
opposite potentials	$\delta_{p,opp}$	0.19	0.31
parallel potentials	$\delta_{p,par}$	0.26	0.18

Unfortunately, this apparently rather moderate deviation in the RH -measurement results in a totally opposite picture for the calculated apparent permeability compared to the results in Table 6.5: The apparent permeability is not highest for the conditions for parallel potentials but for the conditions, where RH either is constant or opposite to the vapour pressure gradient. This observation, if it is assumed to be correct, means that RH -gradient is *not* a driving potential, but that the T -gradient is. In addition, it is clear that the direction of the temperature-driven transport is from warm to cold.

On the other hand, it is difficult to conclude on the basis of this control measurement at the very end of the measurement approach, whether this deviation has existed for all the measurements or not. The small sensors were calibrated carefully before the measurement series, but not against the T_{dew} -sensor used for this final control. Nevertheless, there are strong indications for that there exists a consistent error in all the measurements, and therefore the conclusion on the driving forces has to be re-evaluated; i.e. that RH is not a driving force for the non-isothermal moisture transport while T is.

The accuracy of the strain gauges extended up to 0.001 g. However, the measured weight

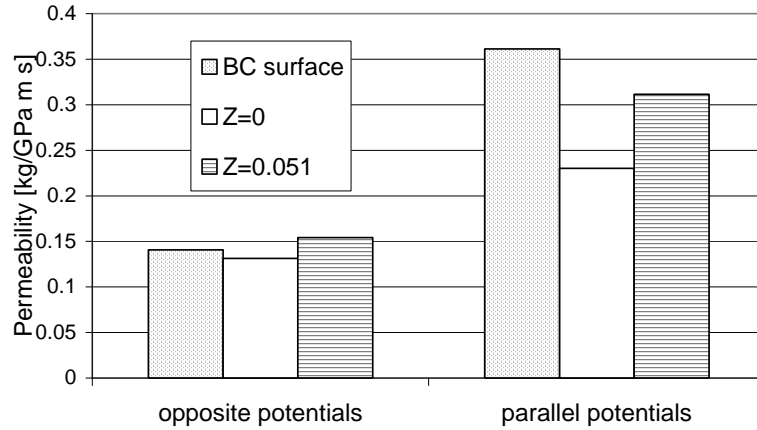


Figure 6.11: The effect of boundary conditions on the calculated permeability for flax under 2 different moisture resistances $Z = 0$ ($GPa \cdot m^2 \cdot s$)/kg and $Z = 0.05$ ($GPa \cdot m^2 \cdot s$)/kg and Δp based on the state of the ambient air. These cases are compared with the actual measurements, where the measured surface conditions are used directly to determine the permeability (BC surface).

of water showed a surprisingly high degree of oscillation, ± 0.5 g in Figure 6.10(b). Whether this was a result of weighing inaccuracy (more realistically ± 0.1 g), or due to the oscillating humidity or temperature in the Megacup, was not clear. In order to give a clearer picture of the behaviour, measurements were presented using running averages.

In the analysis, the moisture content of the Megacup air has been ignored. This results in no error as this moisture content is much smaller than the accuracy of the measurements.

Temperature control

The temperature in the Megacup was controlled as described in Section 6.2.2. The main disadvantage of this system was the asymmetry of regulation. Cooling was water-based and had a large thermal inertia, while heating was based on electrical resistance and had a very low inertia. Regulating this kind of system was very challenging and a certain temperature oscillation was accepted ($\Delta T = \pm 0.2K$). The resulting RH -oscillation became $\Delta RH = \pm 1\%RH$. Temperature in the room was very stable and maintained by a water-based heating and cooling aggregate.

Measurement of boundary conditions

Measurements in (Peuhkuri et al., 2003) (Section 6.4.2) showed the importance of measuring the surface temperature and moisture conditions as accurately as possible. An attempt to measure these surface conditions has been the aim for all the actual measurements with the Megacup. The unknown convective surface-moisture resistance will hereby be eliminated as a source of error. To illustrate the significance of this, an example is given in Figure 6.11, where apparent permeability was calculated based on measured surface conditions (BC surface) and compared with the apparent permeability calculated with 2 arbitrarily chosen different convective moisture transfer resistances ($Z = 0$ ($GPa \cdot m^2 \cdot s$)/kg and $Z = 0.05$ ($GPa \cdot m^2 \cdot s$)/kg), and Δp was based on the state of the ambient air. Equation 4.2 gives the permeability when there is a moisture transfer resistance Z on both surfaces:

$$\delta_p = \frac{d}{\frac{\Delta p}{g} - (Z_{p,in} + Z_{p,out})} \quad (4.2)$$

The resulting permeability obtains particularly where the case with parallel potentials is quite sensitive to how the boundary conditions are defined and measured.

6.5 Conclusion

It is widely accepted that temperature does have a pronounced effect for some materials on moisture content, hydraulic conductivity and liquid transfer. It is not unreasonable to assume, therefore, that the investigation of temperature gradients on the transfer of moisture through building materials, can have an important role. However, to-date, very few measurable or significant temperature-effects in published non-isothermal investigations have been found.

The measurement method and some results for a new approach for measuring the non-isothermal water vapour transmission in porous (light-weight) building materials have been described in this Chapter. The results until now showed that there exists some kind of 'other' transport against Δp in all the analysed materials. However, the results could not support field observations, where hygroscopic insulating materials, like cellulose insulation, are claimed to protect themselves from too excessive moisture levels on the cold side of a building envelope. Rather surprisingly, all the materials, as well the almost non-hygroscopic materials (e.g. rock wool) as the very hygroscopic materials (e.g. cellulose insulation) showed the same characteristics. However, the returned data suffered from unstable measurements and, subsequently, the amount of data cannot be seen as sufficient for drawing any definitive conclusions. Nevertheless, the trend of results seems rather convincing.

On the basis of the analysis of the measurement results, and especially the analysis of uncertainties, it can be concluded that the hypothesis of relative humidity being a driving force for non-isothermal moisture transport already in the hygroscopic could not be confirmed. On the contrary, there exist some indications for that the temperature gradient itself is driving the moisture from the warm towards the cold side.

An attempt to identify and quantify the single contributions of the different transport forms involved was also presented in this Chapter. The proposed model with 2 unknowns produced fairly consistent results and illustrated the error achieved if only water vapour diffusion based on isothermal permeability, and the water vapour pressure gradient are considered. Furthermore, it was shown how extremely sensitive the results are for the used analysis method. Therefore, great care must be taken when drawing any conclusions. The assumption of constant coefficients is understood by the author as being a rather simplified approach, and therefore future works should include a larger range of humidity and temperature levels.

Chapter 7

Non-Isothermal, dynamic moisture transfer

This Chapter continues the investigations presented in Chapters 5 and 6, involving dynamic moisture transport in a range of porous, light-weight building materials under isothermal conditions, and non-isothermal transport under steady state conditions, respectively. A unique experimental set-up and results are described: The set-up (the non-isothermal Megacup already described in Chapter 6), allows the creation of a dynamic climate on the cold side of the sample. This experimental set-up is comparable with full-scale field experiments, although in the Megacup the conditions are very well regulated and designed. Most importantly also, the resulting moisture flux as well as the hygrothermal states around and within the material are monitored.

The aim of these actual measurements is to identify the dynamic moisture response of a material exposed to a temperature gradient. It is understood that this way of presenting the problem is complex, as both the size of the moisture sorption capacity and the existence of the 'other' possible transport forms affect the resulting moisture transport and the distribution of moisture. Nevertheless, these measurements will help to understand moisture conditions in building envelopes. The experimental results are compared with dynamic simulations partly with (i) a 'conventional' model, and (ii) with a model where some of the findings in Chapter 5 have been implemented.

7.1 Background

The moisture characterisation of porous building materials is a result of a series of different standardised experimental investigations. The most central methods include; determination of water vapour permeability, hydraulic conductivity and moisture retention. One thing common for all these methods is that they represent the material under steady state or equilibrium conditions.

Dynamic simulation of the hygrothermal performance of building envelopes is widely used as a part of the building design process. The aim of these simulations is to predict how the designed construction will perform when exposed over the years to naturally varying temperature and humidity loads. The materials are represented in the simulation models by their measured moisture properties, as mentioned above. Although the used boundary conditions are dynamic, the common simulation models assume that there exists

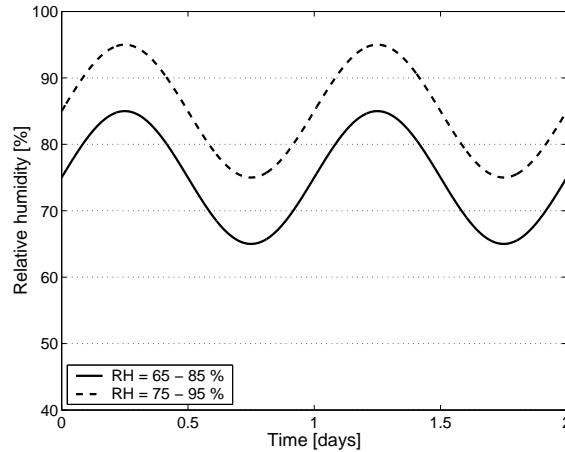


Figure 7.1: The sinusoidal variation in the relative humidity of the Megacup air $RH_{Megacup}$. Two different variations are used: $65 < RH < 85\%$ and $75 < RH < 95\%$.

local hygrothermal equilibrium within the material. This assumption makes it possible, e.g. to convert local vapour pressure to moisture content of the material via a sorption isotherm. While it is widely accepted that this assumption is not absolutely correct, for many materials the resulting error is considered being small. However, the assumption of immediate local moisture equilibrium ignores a possible time delay in the sorption processes, which can introduce significant errors in modelling the effects of rapid climate change.

Therefore, the central problem of these simulation models is the conflict between steady state material properties and the dynamic boundary conditions. For instance, the water vapour permeability of porous, absorbent materials is based on steady state measurements using the cup method. Such measurements do not involve water absorption by the material and are really just a measure of gas transmission through the physical pore structure. In practice, materials in a building envelope are exposed to naturally varying, non-isothermal conditions on both daily and annual time scales.

Another discussion exists around the potentials driving moisture transport under non-isothermal conditions, and the use of material properties determined under isothermal conditions for non-isothermal conditions. These questions have arisen again in connection to the (re)introduction of a group of hygroscopic insulation materials, and in predicting the hygrothermal behaviour of the constructions with dynamic simulations.

7.2 Experimental set-up

This Section presents the measurement strategy for the dynamic experiments. A special constructed climate chamber was used, where the sample was exposed to a temperature and a dynamic moisture gradient. The change in local relative humidity was followed non-destructively by small built-in sensors within the specimen.

The description of the apparatus, i.e. Megacup, as well as the analysed materials, is identical to the description in Section 6.2.2 and is not repeated here. The instrumentation of the sample is also identical (Section 6.2.2), see Figure 6.3.

The use of relative humidity sensors to measure the moisture conditions around and within the specimen is based on the assumption of local equilibrium, where the relative

Table 7.1: Materials and measurement strategy for non-isothermal, dynamic measurements. $T_{room} = 22^{\circ}\text{C}$ and $T_{Megacup} = 12^{\circ}\text{C}$. Materials are the same as in Chapter 6, where also some of the material parameters are given. More detailed material information is found in Appendix A.

Material	RH interval	
	65 – 85%RH	75 – 95%RH
glass wool		x
rock wool	x	
cellular concrete	x	x
cellulose	x	
flax	x	x
perlite	x	

humidity in the pores of a porous material is in equilibrium with the water content of the material. As already discussed in Chapter 3, this assumption is not necessarily correct under dynamic conditions, nor in steady state, due to hysteresis. The measurement strategy presented in this Chapter was based on dynamic conditions. Therefore, the local moisture content could not be fully estimated with the relative humidity sensors used.

7.2.1 Measurement strategy

The measurement strategy for these dynamic, non-isothermal tests was to expose a material sample to a sinusoidal change in relative humidity on the cold side with a period of 24 hours – see Figure 7.1 for the sinusoidal development in $RH_{Megacup}$. There were measurements at two different relative humidity levels: $65 < RH < 85\%$ and $75 < RH < 95\%$. The resulting dynamic moisture sorption and transport process was then followed by built-in temperature and relative humidity sensors, together with the measurement of the net moisture flux through the sample.

The sinusoidal relative humidity change and the period at 24 hours was chosen for the following reasons:

1. To illustrate the effect of daily oscillations in relative humidity on the distribution and transport of moisture.
2. A regular and smooth sinusoidal development is easier to analyse than random development as a result of natural climate.
3. In a sinusoidal development, no sudden changes are needed. Sudden changes would demand almost unlimited capacity of the moisture control system.

For the sake of simplicity, the temperature was kept constant on both sides of the sample: $T_{room} = 22^{\circ}\text{C}$ and $T_{Megacup} = 12^{\circ}\text{C}$.

From the beginning, the plan was to test the materials at two different moisture levels, i.e. high and low dynamic relative humidity, to see if there existed any separate dynamic phenomenon for the high relative humidities. Unfortunately, it turned out during the tests that the temperature control of the equipment was not as stable as in the initial phase. This resulted in unwanted condensation on the Megacup inner walls, when $RH > 90\%$.

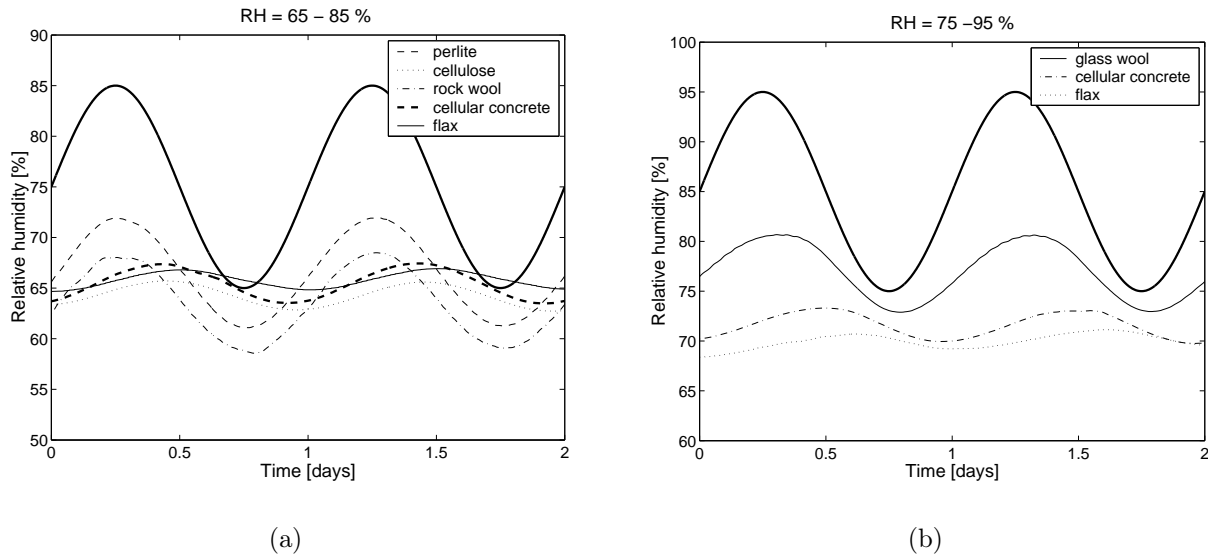


Figure 7.2: The measured relative humidity approximately 28mm from the cold surface for sinusoidal variation (a) $RH = 65 - 85\%$ and (b) $RH = 75 - 95\%$ in Megacup (thick solid line). Exact distances are: Cellulose 26mm , cellular concrete 27.5mm , perlite 28mm , rock wool 28.5mm , flax 29mm and glass wool 30mm .

Therefore the relative humidity conditions were not the same for all the materials, as seen in Table 7.1.

In Table 6.3 some of the material parameters together with the sample dimensions were given. The thickness of the samples was chosen in a way that the samples were close to "natural" dimensions in a building envelope that is under a temperature gradient. Materials were chosen with the anticipation that they will respond very differently under dynamic conditions.

7.3 Measurement results

The experimental results are given in this Section. The results are presented as the distribution of relative humidity in different materials during the dynamic moisture transport and sorption process, when the specimen was exposed to a periodically oscillating climate on the cold side of the Megacup. The measured total moisture flux is presented also. The measured boundary conditions, i.e. temperature, relative humidity and moisture flux, were used as an input to numerical simulations reported in the next Section. Not all the results for all the materials are presented in this Section, but the complete results are found in Appendix B.3.

7.3.1 Measured distribution of RH

Figures 7.3 and 7.4 show the development in relative humidity in the different layers of the samples during a 48-hour-period. Values in Figure 7.3 are a result of a sinusoidal oscillation in RH_{Megacup} between 65 and $85\%RH$ while they in Figure 7.4 come from oscillations between 75 and $95\%RH$. Note that the layers are not identical from material

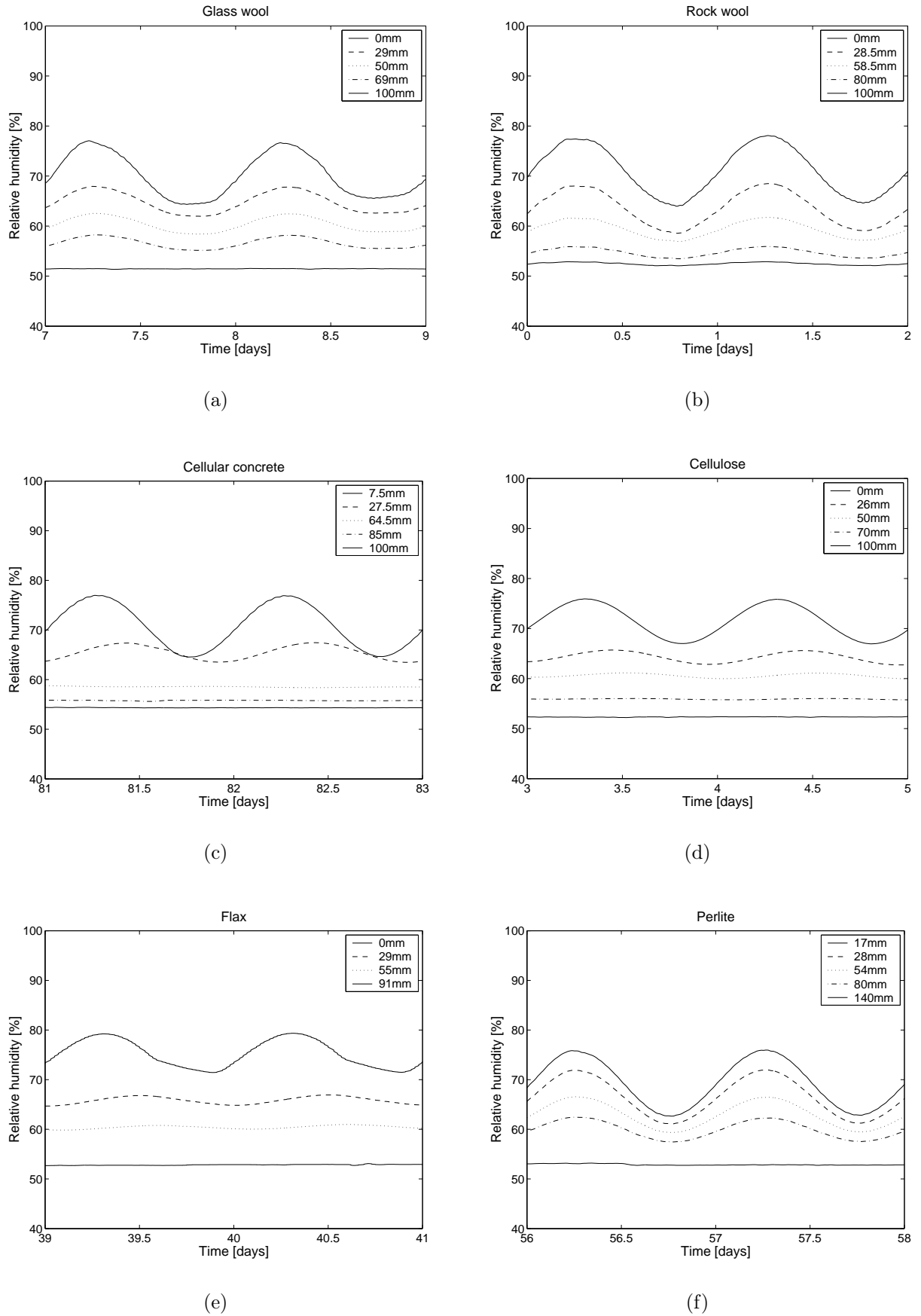


Figure 7.3: The measured distribution of relative humidity for sinusoidal variation $RH = 65 - 85\%$ for (a) glass wool insulation, (b) rock wool insulation, (c) cellular concrete, (d) cellulose insulation, (e) flax insulation and (f) expanded perlite. Note that the sinusoidal variation for flax is not symmetrical. This is due to problems with the capacity of the moisture controller. Legends stand for the sensor distance from the cold surface of the sample.

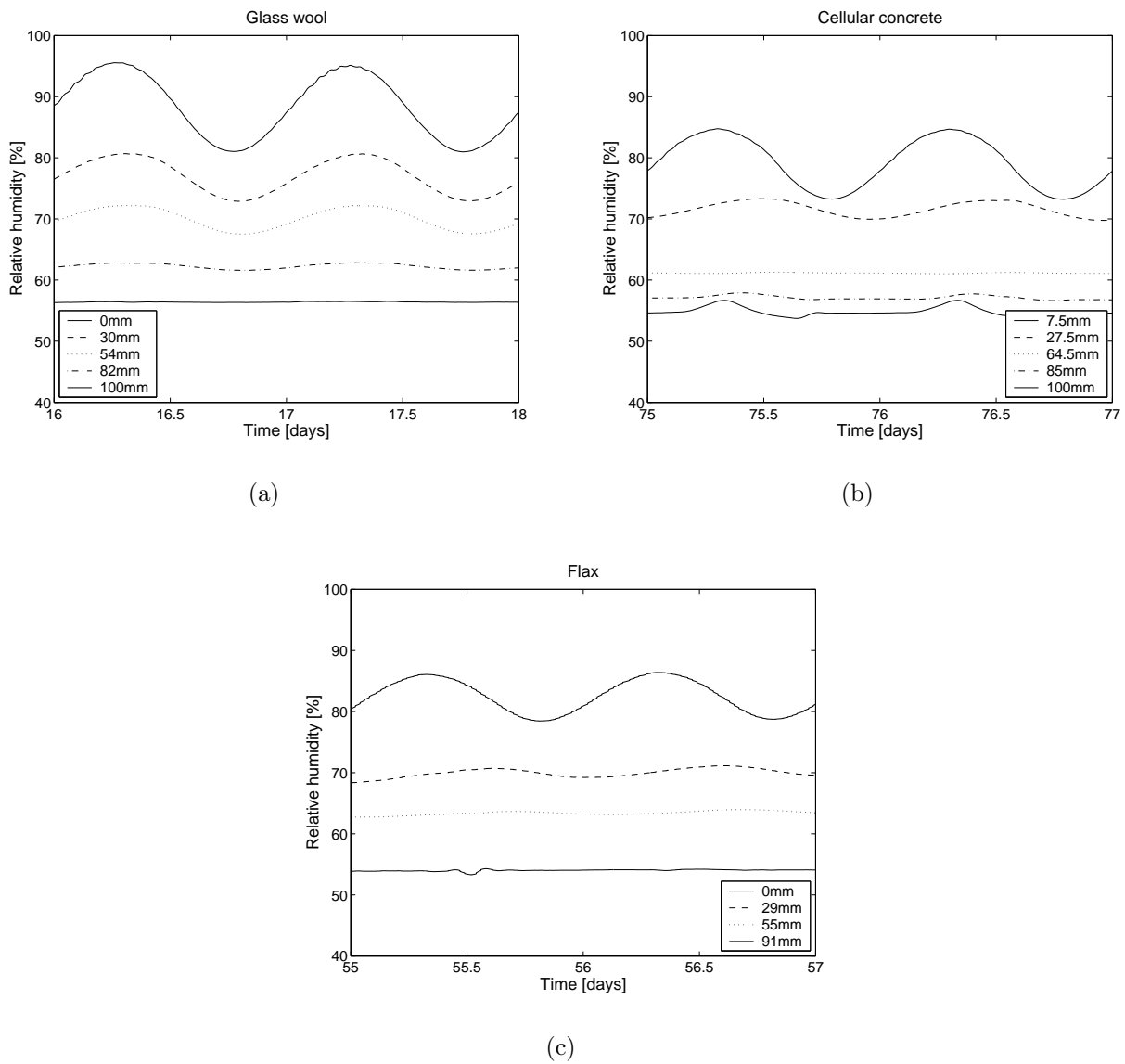


Figure 7.4: The measured distribution of relative humidity for sinusoidal variation $RH = 75 - 95\%$ for (a) glass wool (b) cellular concrete (c) flax.

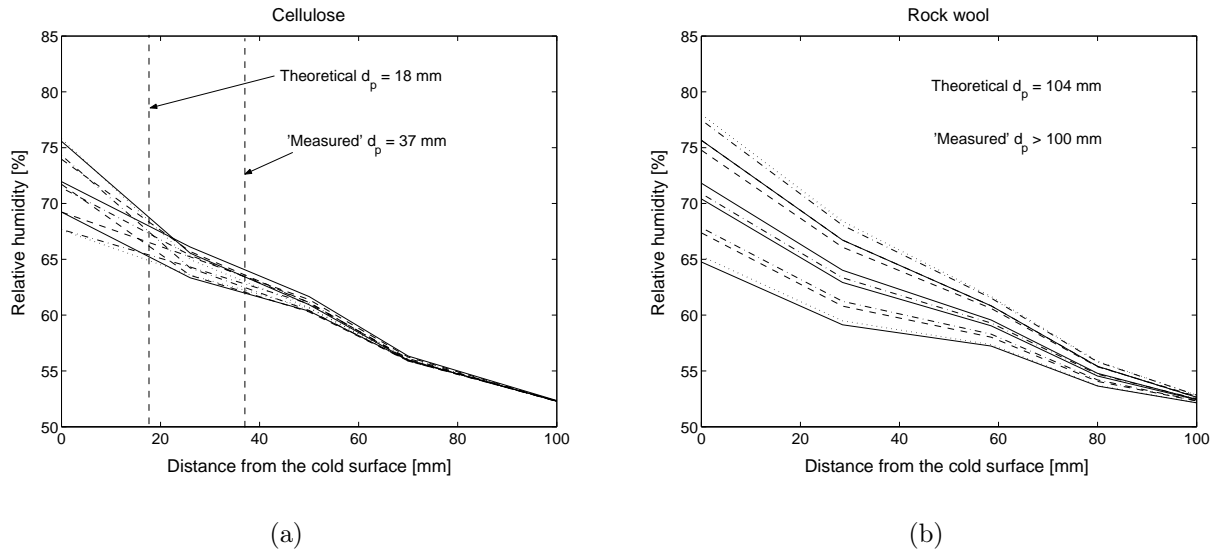


Figure 7.5: The measured relative humidity as a function of distance from the cold surface for sinusoidal variation in the Megacup 65 – 85%RH for (a) cellulose and (b) rock wool. The different curves are values for different times during a 24-hour-period. Also the 'measured' and theoretical penetration depth is given.

to material. Furthermore, $RH_{Megacup}$ does not follow the designed variation in all cases (see e.g. Figure 7.7).

A comparison of the dynamic response on the cold side of the sample for each material is illustrated in Figure 7.2. For the interior of each material, the curves are quite similar. The development in relative humidity shown corresponds to locations 26 – 30mm from the cold surface. There were 2 main observations:

1. The response was remarkably more buffered for cellulose, cellular concrete and flax insulation than for perlite, glass wool and rock wool.
2. The phase delay was greatest for cellulose, descending thereafter for flax, cellular concrete, glass wool, rock wool and finally perlite, which showed no phase delay at all

The phase delay for cellulose at 26mm was about 0.4 days which corresponds to 9.5 hours. The phase delay for cellulose, cellular concrete and flax insulation increased with distance from the cold surface and the oscillating climate.

7.3.2 Penetration depth

Another way of representing differences between the materials is to determine their penetration depth, both as a measured value and a theoretical value¹. These depths are given in Table 7.2 for $RH = 65 - 85\%$.

¹This theoretical definition of penetration depth is identical to the definition given in Chapter 2, where d_p is defined as a depth in a material, where the oscillations are 36.7% of the oscillations on the material surface.

Table 7.2: The measured and theoretical 'penetration depth' d_p for non-isothermal, sinusoidal oscillations in the Megacup $RH = 65 - 85\%$. The measured d_p is a result of a fitting of the measured p -distribution (calculated from the measured RH and T) with the theoretical solution for a slab according to Equations 7.1 - 7.3. The penetration depth was defined as a depth from the cold side, where the oscillations in RH were 36.7 % of the oscillations on the material surface, here the cold side. The theoretical d_p was determined from Equation 2.38.

Material	Penetration depth [mm]	
	measured	theoretical
glass wool	55	52
rock wool	>100	104
cellular concrete	32	9
cellulose	37	18
flax	35	27
perlite	85	90

The 'measured' d_p is determined on the basis of theory for periodic solutions for temperature in a homogenous slab according to (Hagentoft, 2001). An analogy between temperature and vapour pressure (and the superposition principle) is used in the present analysis. Vapour pressure p has been calculated from the measured T and RH .

The cold surface is exposed to a sinusoidal variation $p_{1,t}$, which is the measured p on the surface *minus* the average p_{mean} . The warm side of the slab with a thickness d is kept on the constant p_2 , which is the average of the measured values. The distribution of the $p_{t,x}$ as a function of distance x and time is determined with Equations 7.1 to 7.3.

$$p_{1,t} = p - p_{mean} \quad (7.1)$$

$$p_{t,x} = p_{1,t} \frac{\sinh [(1+i) \cdot (d-x)/d_p]}{\sinh [(1+i) \cdot d/d_p]} \quad (7.2)$$

$$p_{t,x} = p_{t,x} + p_{mean} + \frac{x}{d}(p_2 - p_{mean}) \quad (7.3)$$

This calculated p -distribution is then given as RH by using the theoretical distribution of temperature in the same way as in Equations 7.1 to 7.3. d_p is determined by fitting the resulting RH -distribution with the measured distribution until they agree to defined accuracy.

Theoretical d_p is defined from Equations 2.38 and 4.10:

$$d_p = \sqrt{\frac{D_w t_p}{\pi}} = \sqrt{\frac{\delta_p \cdot p_{sat} \cdot t_p}{\rho_0 \cdot \xi \cdot \pi}} \quad (2.38) + (4.10)$$

The main observation was that the 'measured' penetration depth d_p , defined as a measure for the sinusoidal oscillations being less than 36.7% of the oscillations on the cold surface of the material at this location, was greatest for rock wool and perlite, and smallest for materials like cellular concrete, cellulose and flax insulation. This means that the material

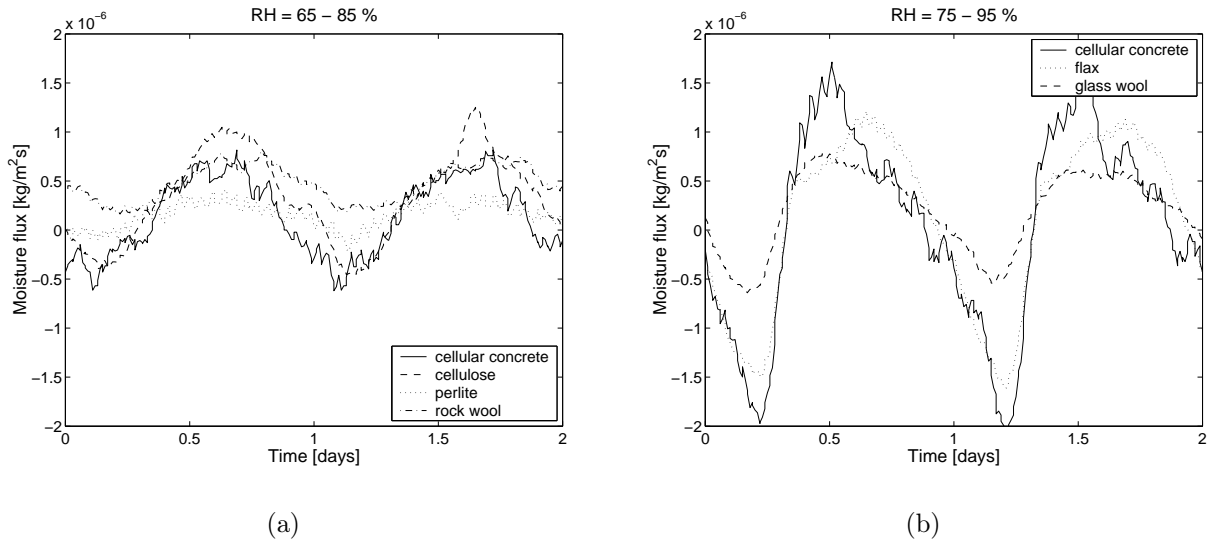


Figure 7.6: Comparison of the measured moisture flux [$\text{kg/m}^2\text{s}$] for the different materials. (a) Sinusoidal variation $RH = 65 - 85\%$ (b) Sinusoidal variation $RH = 75 - 95\%$.

that was on the 'warm side' of this depth could not 'feel' more than about one third of the changes in the relative humidity in the Megacup. Subsequently, within this 'inactive' part of the materials there existed almost steady state conditions in terms of moisture ab- and desorption. The measured RH -range involved inside the material during a period of 24 hours is illustrated in Figure 7.5 for cellulose and rock wool, together with the 'measured' and theoretical penetration depth.

The theoretical d_p is significantly smaller than the 'measured' one for the materials like cellular concrete and cellulose insulation. For the materials like glass wool, rock wool, flax and perlite there is almost no difference.

7.3.3 Measured moisture flux

The resulting total net moisture flux was calculated from the weight change of the moisture controller and is illustrated for every analysed material in Appendix B.3, (Figures B.22 and B.23). The resulting moisture flux for different materials is compared in Figure 7.6. The amount of moisture involved in the interaction between the material and the air in Megacup as a response to the oscillations is in this way illustrated. It was quite obvious that for rock wool, glass wool and perlite samples, there was much less moisture involved than for the other materials. Furthermore, cellulose and cellular concrete impelled more water movement than flax. The curve for glass wool is not totally comparable with the other materials as RH_{room} for glass wool tests was higher, which made the flux smaller also. The non-symmetry of the moisture flux for the alternating ab- and desorption processes could be caused by hysteresis.

7.4 Simulation results

The measurements are compared with the results from numerical simulations. The simulation model – identical with the one presented in Chapter 5 – was developed in the

Simulink-environment. Many of the structural choices in the model are the results of discussions during a parallel development of an international building physics toolbox in Simulink (Weitzmann et al., 2003). The 'conventional' model was based on the same partial differential equations and material parameters as in the MATCH model (Rode, 1991). The only principal difference was that the boundary conditions inside Megacup in the Simulink model were not only the measured temperature and relative humidity for all simulations, but also the measured moisture flux. The relative humidity in Megacup was therefore not fixed for the simulation with the measured flux as a boundary condition, but a result of the moisture flux, room conditions and the material's hygrothermal performance. These two types of simulation strategies were used in this section for the calculations with the 'conventional' model. The documentation of the conventional simulation model is found in detail in (Peuhkuri, 2002), which is also attached as Appendix C.

The conventional model was developed further when analysing the results from isothermal dynamic experiments. The model is here tested under non-isothermal conditions.

Tables with material properties used for simulations and the measured sorption isotherms are given in Appendix A. In general, average of ab- and desorption isotherms have been used. The significance of hysteresis was investigated on a single material. Calculation nodes were in general identical with sensor placements.

7.4.1 Conventional model

The simulations with the conventional model represent Fickian behaviour, as defined in Chapters 2 and 3. The simulation results for selected materials with typical behaviour given in Figure 7.7 are based on the measured *relative humidity* in Megacup, while the results in Figure 7.8 are based on the measured *moisture flux* to the Megacup. Simulation results are plotted together with measurement results to illustrate the deviations between actual measurements and the model. Results for all the materials are given in Figures B.24 to B.27.

Measured *RH* as a boundary condition

The simulation results with the measured relative humidity as the boundary condition show (see Figures 7.7 and B.24 to B.25), that there was a fairly good agreement between the actual measurements and the simulations for cellulose, perlite and flax insulation. A slight phase delay was seen in the simulation results for all materials. This indicated a smaller moisture capacity in the dynamic case than the one determined from the slope of the sorption isotherm or the existence of remarkable hysteresis effect. The results could also indicate that the permeability of the materials was greater than the value determined with isothermal cup-measurements, which is the permeability used in the model. A larger deviation between measurements and simulations was seen for cellular concrete, where the simulated development in relative humidity on the cold side oscillated much less than according to measurements. The deviations for glass wool were of a slightly different nature than for the other materials, but the main observation was still that the true moisture capacity was slightly smaller than the one assumed for simulation.

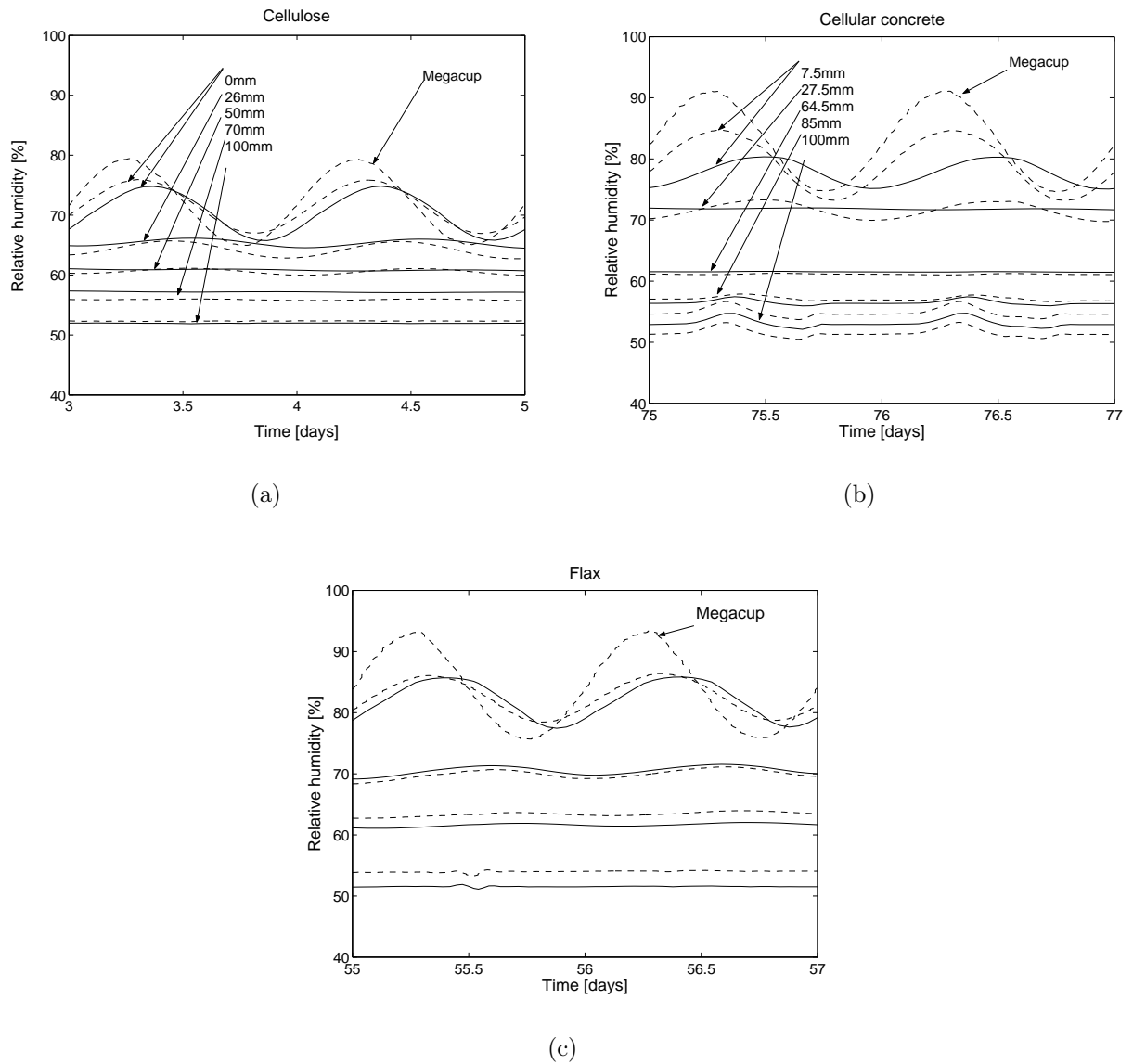


Figure 7.7: Measured RH as a boundary condition. Comparison of measured (---) and simulated (—) distribution of relative humidity. The measured relative humidity has been used as boundary condition in the Megacup. (a) Cellulose $RH = 65 - 85\%$ (Note, that RH in the Megacup never reaches 85%, nor 95% for some of the measurement series. This is probably caused by the drifting of the used RH -sensors or by moisture capacity problems of the equipment.), (b) cellular concrete $RH = 75 - 95\%$ and (c) flax $RH = 75 - 95\%$.

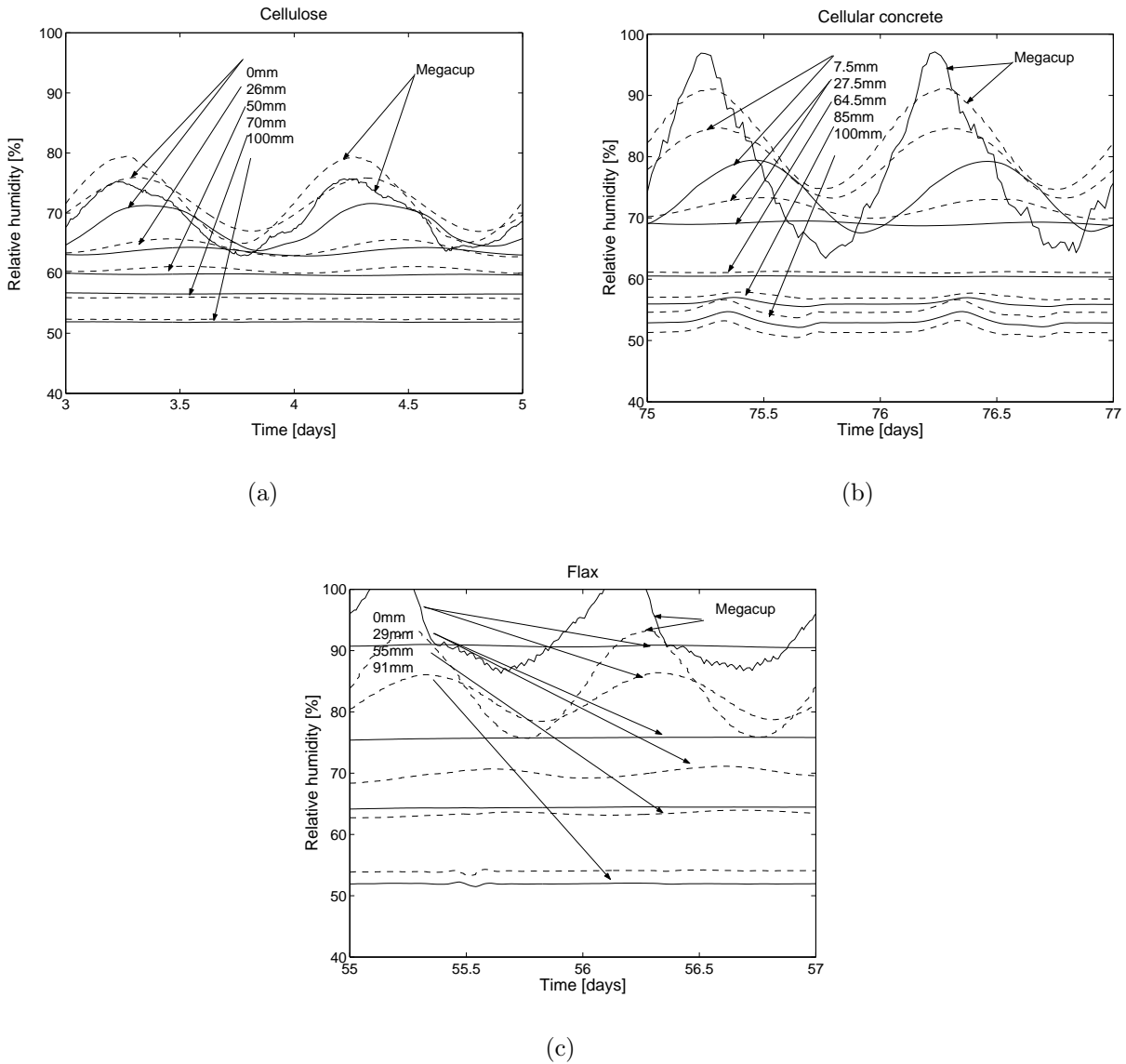


Figure 7.8: Measured flux as a boundary condition. Comparison of measured (---) and simulated (—) distribution of relative humidity. The measured moisture flux has been used as boundary condition in the Megacup. (a) Cellulose $RH = 65 - 85\%$, (b) cellular concrete $RH = 75 - 95\%$ and (c) flax $RH = 75 - 95\%$.

Measured flux as a boundary condition

The simulation results with the measured moisture flux as boundary condition in the Megacup showed a very different picture, i.e. there existed a large deviation between the measurements and simulations for almost all the materials (see Figures 7.8 and B.26 to B.27). The deviation was smallest for perlite and glass wool. The biggest deviations existed for cellulose and flax insulation and partly for cellular concrete, although the simulation results underestimated the relative humidity for cellulose and cellular concrete while they overestimated it for flax insulation.

The simulated relative humidity distribution for cellulose on the cold side was shown to be much lower than the measured one. One explanation could be that the amount of moisture cellulose can absorb under these non-steady conditions is much less than the equilibrium moisture content. The size of the moisture capacity seems to be significantly smaller in the measured cases than in the simulated cases, where the slope of the sorption isotherm has been used.

The high and very much more buffered simulated relative humidity for flax indicated also that the moisture capacity of the material was smaller in reality than in simulation with the moisture capacity given by the slope of the sorption isotherm. Also, the amount of moisture the material can absorb was greater in this dynamic case than according to the sorption isotherm determined as the equilibrium moisture content. This last observation was hardly possible, even though a minor part of the explanation can be found in the possible temperature dependence of the sorption isotherms, i.e. the equilibrium moisture content increases for decreasing temperatures. In this case, the sorption isotherms were measured at 20°C and therefore it could be expected that the equilibrium moisture content was higher for $T=12^{\circ}\text{C}$, i.e. the cold side, and subsequently the resulting relative humidity was lower.

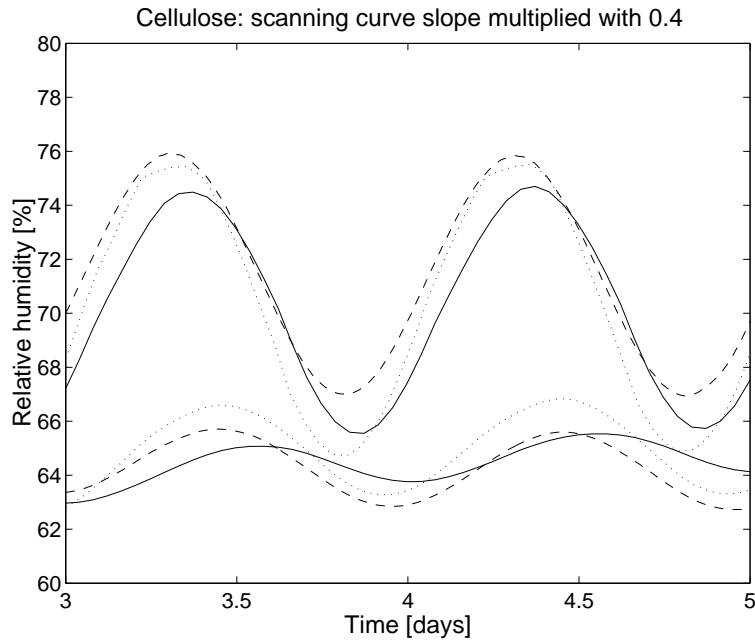
Significance of hysteresis

In the simulations so far, averages of ab- and desorption isotherms have been used. Some of the observed deviations between measurements and simulations might be explained by the hysteresis effect. The significance of hysteresis will be illustrated here for a single material, i.e. cellulose insulation (see Figure 7.9) for two different multiplication's of the slope of the scanning curve:

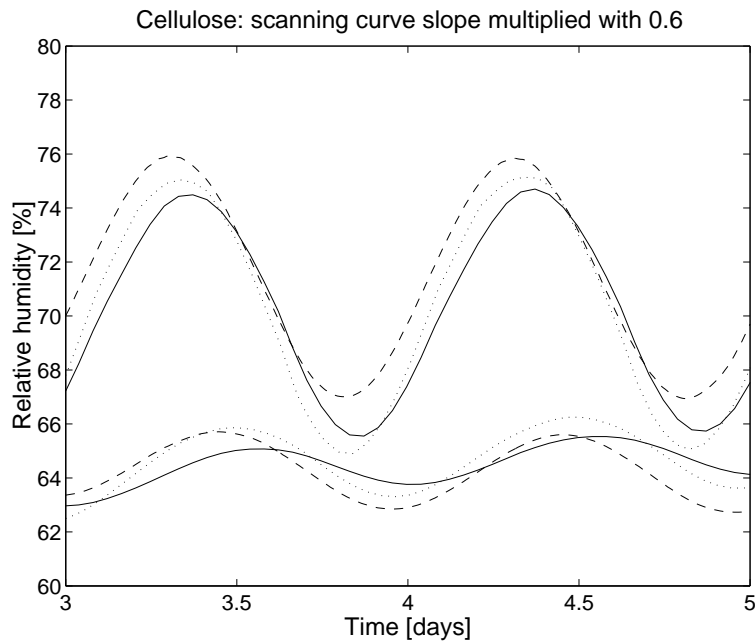
resulting scanning curve slope = 0.4 or 0.6 times scanning curve slope.

The resulting scanning curve is illustrated in Figure 7.10 where u is given as a function of φ for a period of 24 hours. Also the measured ab- and desorption isotherms are given. The measured ab- and desorption isotherms are found in Appendix A. The hysteresis model is described in Appendix C together with the entire model. Also found here is a discussion about the choice of the slope of the scanning curve, which according to (Chomcharn and Skaar, 1983) is recommended to be multiplied by 0.4.

Figure 7.9(a) illustrates how a hysteresis model with a slope multiplied by 0.4 almost eliminates the phase delay compared to the model without hysteresis. This is due to the reduced moisture capacity as a result of this reduced slope. However, the reduced moisture capacity also results in an increased amplitude of RH . Figure 7.9(b) shows



(a)



(b)

Figure 7.9: Comparison of measurements (---), simulations without (—) and with hysteresis (...) for cellulose. RH -oscillations are given for locations: $0mm$ and $26mm$. Conventional model is used. Simulation without hysteresis uses an average of ab- and desorption isotherms. Hysteresis is investigated for 2 different slopes of the scanning curve: The *resulting* scanning curve slope (a) = 0.4 times the scanning curve slope and (b) = 0.6 times the scanning curve slope.

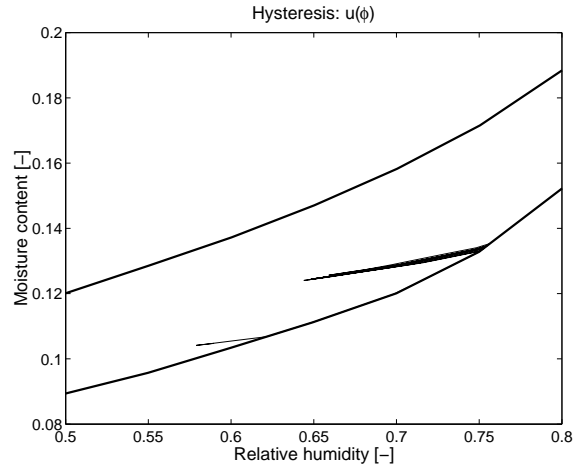


Figure 7.10: Scanning curve $u(\varphi)$ for cellulose together with ab- and desorption isotherms. Period of 24 hours.

how the increased moisture capacity (slope multiplied with 0.6) results in a deviation in phase delay between measurements and simulations that is however, not as large as for the model without hysteresis.

Therefore, including hysteresis in the model reduces the deviations between modelling and measurements to some extent, but do not explain the deviations fully.

7.4.2 Non-Fickian model

The non-Fickian model developed in Section 5.4.2 is here used to investigate how this model taking account the retarded sorption in materials will be able to predict the relative humidity in a material sample exposed both on a temperature gradient and dynamic change in the relative humidity boundary conditions. No comprehensive study on this subject has taken place, the example in Figure 7.11 for flax gives just a preliminary idea of the function of the models.

It is obvious that while the conventional Fickian model overestimates the moisture capacity of the materials, the non-Fickian model – with the determined sorption coefficient k from measurements in Chapter 5 – underestimates it. This result leads to a conclusion that the method for determination of sorption coefficient k presented in Section 5.4.2 is not perfect.

7.5 Discussion

The observations in previous Sections, both the measured and calculated, are discussed in this Section. In particular, the consequences of the observed behaviour on the performance of the tested materials in building envelopes exposed to dynamic non-isothermal moisture transports are presented under the following headings.

Uncertainties due to the experimental set-up and instrumentation that might affect the results were already discussed in Section 6.4.3 and are not repeated here.

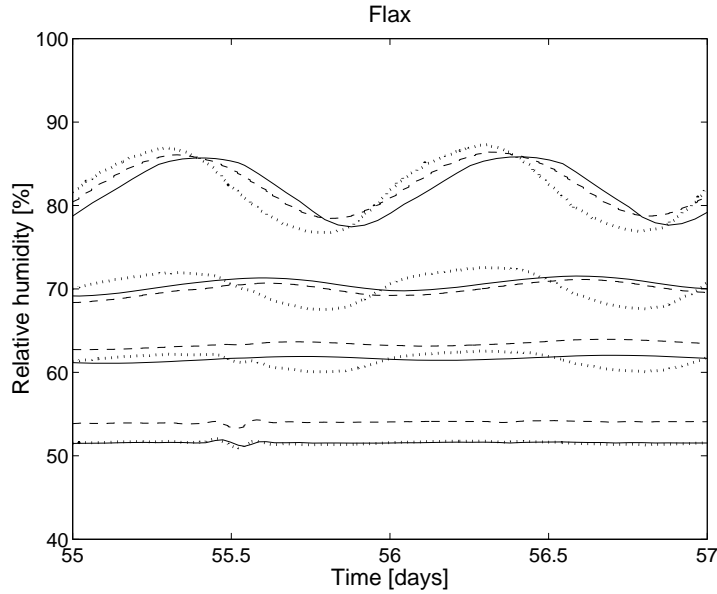


Figure 7.11: Comparison of measurements (- -) and simulations with the conventional Fickian (—) and the new non-Fickian model (...) for flax insulation. Hysteresis has not been included in the models.

7.5.1 Buffer capacity

Penetration depth, given in Table 7.2, can be used to give an indication for how much moisture is involved in the dynamic moisture transport process, together with the moisture capacity. Consequently, materials with a large penetration depth and a high moisture capacity involves lots of moisture under a dynamic ab- and desorption process while the reverse holds true for materials with small penetration depths and poor moisture capacity. These mechanisms have already been discussed in Chapter 5.

The buffer capacity of the materials can be determined as the moisture accumulation capacity b_m [$kg/(m^2 Pa\sqrt{s})$] theoretically given by Equation 2.37.

$$b_m = \sqrt{\frac{\delta_p \cdot \rho_0 \cdot \xi}{p_{sat}}} \quad (2.37)$$

By rearranging, this equation can be expressed as Equation 7.4, which includes the 'measured' d_p . In this way the moisture accumulation capacity b_m can also be given as a 'measured' value. Both the theoretical and the measured values for b_m are given in Table 7.3 and in Figure 7.12.

$$b_m = \frac{d_p \cdot \rho_0 \cdot \xi}{p_{sat}} \sqrt{\frac{\pi}{t_p}} \quad (7.4)$$

The moisture buffer capacity of the materials is also calculated from Equation 2.39 for both theoretically and as a 'measured' value. d_p for the 'measured' case is the measured value and the theoretical d_p for the theoretical case given in Table 7.2. These theoretical

Table 7.3: Theoretical and 'measured' values for moisture accumulation capacity b_m . Theoretical values are calculated from Equation 2.37 and the 'measured' ones from Equation 7.4. The slope of the sorption isotherm is determined from the isothermal sorption experiments presented in Chapter 5. The 'measured' penetration depth is given in Table 7.2. Values are valid for $RH = 65 - 85\%$.

Material	Slope of sorption isotherm [-] average	Moisture accumulation capacity b_m [$10^{-7}kg/(m^2Pa\sqrt{s})$]	
		measured	theoretical
glass wool	0.057	6	5
rock wool	0.036	3	3
cellular concrete	0.045	17	5
cellulose	0.32	20	10
flax	0.46	12	9
perlite	0.008	2	2

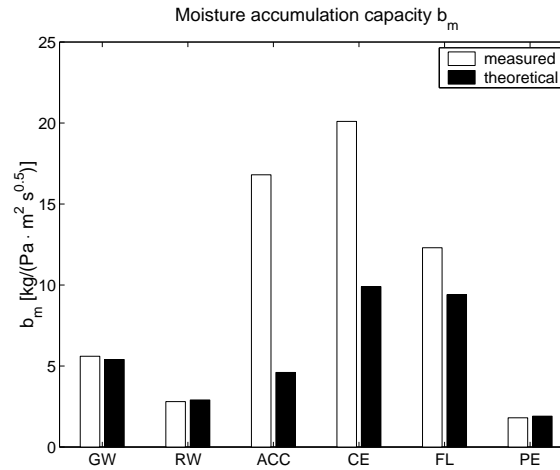


Figure 7.12: Theoretical and 'measured' values for moisture accumulation capacity b_m for all the measured materials. Values are valid for $RH = 65 - 85\%$. GW = glass wool insulation, RW = rock wool insulation, ACC = cellular concrete, CE = cellulose insulation, FL = flax insulation and PE = perlite.

and 'measured' values for Δm_w are compared in Table 7.4. The moisture capacity ξ in both cases is determined from the equilibrium moisture content.

$$\Delta m_w = \rho_0 \cdot \xi \cdot \Delta \varphi \cdot d_p \quad (2.39)$$

What does this buffer capacity of the material actually mean? The answer is that materials with a large buffer capacity like cellulose and flax insulation and cellular concrete are able to moderate the oscillations in relative humidity. However, for cellular concrete it is clear that according to *measurements* the material hardly moderates the variations in ambient RH at all compared to *simulations*, see Figure 7.7(b). Oscillations in relative humidity in a building construction is usually not dangerous as such, but high oscillations also often mean high peaks in relative humidity. Figure 7.2 illustrates this. Here, a moderated RH results also in lower peak values of the relative humidity. For instance, the resulting relative humidity peak value $28mm$ from the cold side is up to $5\%RH$ lower for a construction with cellular concrete or flax, and up to $7-8\%RH$ lower for a

Table 7.4: The available water calculated from Equation 2.39. The slope of the sorption isotherm is determined from the isothermal sorption experiments presented in Chapter 5. Penetration depth is measured from the non-isothermal tests in the Megacup given in Table 7.2. These dynamic, non-isothermal values are compared with the theoretical values based on the theoretical d_p given by Equations 2.38 and 4.10. $\Delta RH = 10\%$ has been chosen as an arbitrary value for comparison. Values are valid for $RH = 65 - 85\%$.

Material	Available water [$g/(m^2 \cdot 10\%RH \cdot 24h)$]	
	measured	theoretical
glass wool	22	21
rock wool	11	11
cellular concrete	65	18
cellulose	78	39
flax	48	36
perlite	7	7

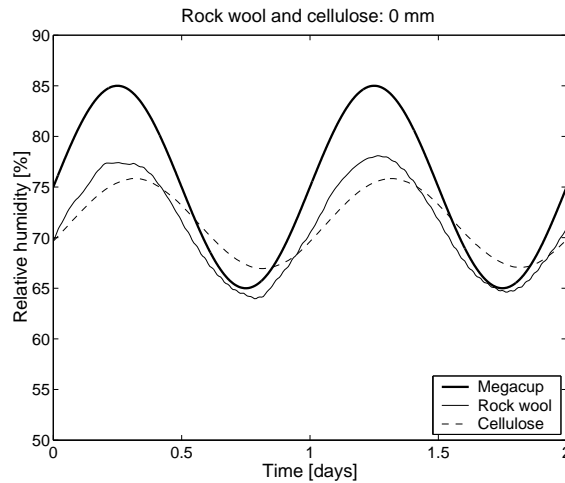


Figure 7.13: The measured response of cold – and the most critical – surface of rock wool and cellulose insulation on a sinusoidal variation in the relative humidity of the Megacup air at $65 < RH < 85\%$.

construction with cellulose, than a construction with expanded perlite insulation or glass wool.

A comparison of resulting relative humidity on the cold surface, at $0mm$, would be most interesting, but this was not possible for all the materials due to the different locations of the sensors. The moisture response on this cold surface is here illustrated with rock wool and cellulose insulation in Figure 7.13. Consequently, materials with a good buffer capacity, are slightly more resistant to damage due to high moisture loads than constructions with glass wool and perlite, but this is not significant, especially on the cold, and most critical surface. Here, the difference in peak values in-between these very different materials is only $2\%RH$, which can be regarded as a non-significant difference due to the uncertainties of the measurements discussed in Section 6.4.3.

In addition, it seems that there has been a drift in the measured RH towards a lower RH -level during the measurement series. Therefore, the comparison of the different materials might be misleading.

7.5.2 Phase delay

The main reason for the deviation between the measured and simulated phase delay of RH is the moisture capacity of the material. In other words, the greater deviation where the simulated development is delayed compared to the measured, the bigger is the simulated moisture capacity compared to the 'true' capacity. This was illustrated by the effect of the hysteresis. A small deviation was seen for all the investigated materials and a more remarkable one for cellular concrete.

Another possible explanation for this deviation could be the use of relative humidity sensors and the assumption of the local equilibrium between the absorbed moisture and the humid air in the simulation model. The true moisture content of the material does not necessarily correspond to the measured RH , while in the simulation model they correspond perfectly. Therefore, the measured RH changes slightly more rapidly than the corresponding moisture content of the material. This observation can also be seen as an indication that the true moisture capacity is smaller than the mathematical one, the reason being either non-Fickian behaviour and/or the hysteresis effect.

7.5.3 The modelling

In the following, reasons for deviations between the measured and simulated development are further discussed.

Not all the material parameters have been defined explicitly for all materials. However, the most important moisture parameters, e.g. water vapour permeability and moisture retention curves, have been determined as a part of this work or earlier on these very same batch of materials.

For the simulations, where the measured moisture flux has been used as a boundary condition, the large deviations between the measured and simulated relative humidity in different layers of the samples might also originate from the uncertainties in the measured moisture flux based on the weighed mass of the water in the moisture controller. There also exists the possibility that there have been leaks for vapour transport in the set-up and the resulting flux might therefore not have been the true flux.

The exclusion of latent heat in the models is often pointed out as an explanation for deviations. However, the present model includes latent heat for all cases. The significance of latent heat on temperature distribution is illustrated in Figure 7.14(a), where the measured and simulated temperature distribution for a period with sinusoidal variation is given for cellulose insulation. Figure 7.14(b) shows the negligible effect on the simulated RH , when including or omitting the latent heat in the model.

Other common explanations for deviations are according to (Roels et al., 1999): the experiments are not totally one-dimensional and there might be air gaps in the materials that are assumed homogenous. Also, the statistical variability of material properties is a source for inaccuracy of the results (Holm and Künzle, 2002).

The use of the isothermal permeability in the model has been mentioned as one of the explanations for the deviations between measurements and simulations. Unfortunately, Chapter 6 could not give any clarity to the question of existing driving forces.

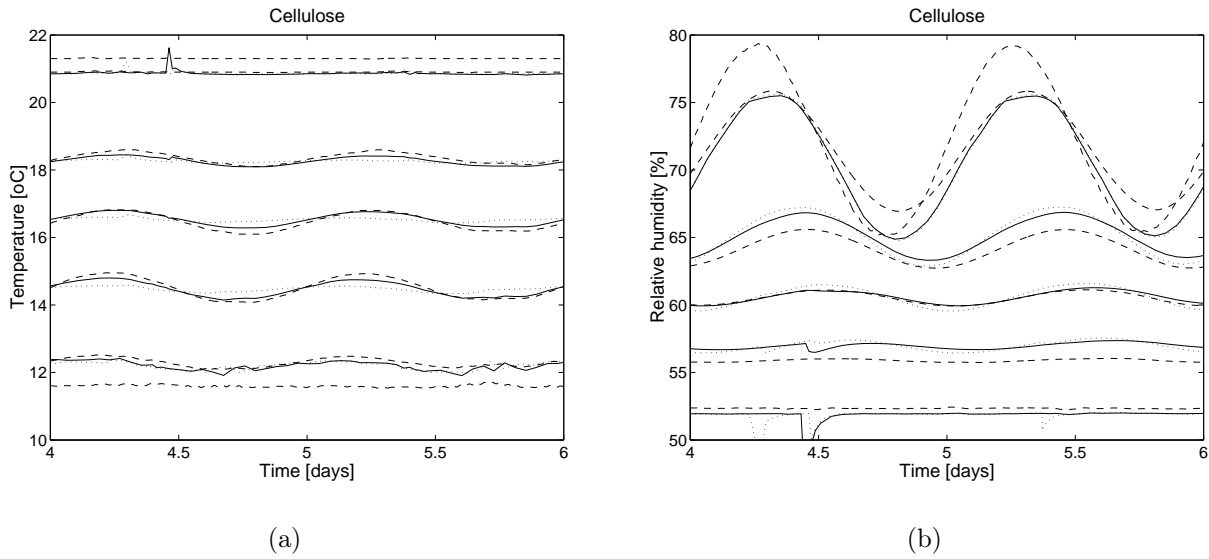


Figure 7.14: (a) Measured (---) and simulated – with latent heat (—) and without latent heat (...) – temperature distribution for a period with sinusoidal variation for cellulose insulation. (b) Measured (---) and simulated – with latent heat (—) and without latent heat (...) – relative humidity for the same period. Model with hysteresis.

7.6 Conclusion

The special constructed non-isothermal set-up, i.e. the Megacup, has been used to investigate the hygrothermal response of selected lightweight building materials. Homogenous materials were exposed to a temperature gradient of $10K$ and sinusoidal oscillations in relative humidity on the cold side, over a period of 24 hours.

Materials like cellulose and flax insulation and cellular concrete were able to moderate the oscillations, and as the most relevant observation of all for the performance of building envelope constructions, the moderated RH also resulted in a slightly lower level of peak values of relative humidity. For instance, the resulting peak relative humidity $28mm$ from the cold side is up to $5\%RH$ lower for a construction with cellular concrete or flax, and up to $7-8\%RH$ lower for a construction with cellulose than a construction with expanded perlite insulation or glass wool. This difference between the materials, however, is not assumed to be significantly unambiguous, especially when the discussed accuracy of the small RH -sensors used in Section 6.4.3 is considered.

Moisture buffer capacity of the materials was also assessed. It turned out that the 'measured' buffer capacity was higher than the theoretical buffer capacity for the materials with good buffer capacity: flax and cellulose insulation and cellular concrete. There was no difference for materials with poor buffer capacity: glass wool, rock wool and perlite.

The comparison of the measured and simulated results showed that, for most materials there exists a fairly good agreement with the used conventional Fickian model. A minor phase delay on simulated results compared to measured RH indicated that the true moisture capacity of the materials was lower than the mathematical one, i.e. the slope of the sorption isotherm. Implementing a hysteresis model increased the agreement between measurements and simulations but was not able to remove all the deviation. Implementing the non-Fickian model for this non-isothermal set-up did not give any good

agreement with the measurements: The non-Fickian model made the moisture transport too retarded.

Chapter 8

Discussion on the major findings

In this research work, two central focus areas have been presented: (i) The moisture response of porous materials to a dynamic change in the ambient air relative humidity and (ii) The question of the driving forces existing for moisture transport, across a simultaneous temperature gradient. In this chapter, the major findings of the experimental and analytical approaches are gathered and discussed. The significance of uncertainties is also treated. Finally, an outlook is given on the future of these research topics.

8.1 Retarded sorption and non-Fickian transport

It was hypothesised that the assumption of immediate local moisture equilibrium would lead to overestimation of the real moisture capacity. The conventional way to present a moisture capacity of the materials in simulation models is with the slope of the sorption isotherm. Therefore, the time dependence of the sorption process was investigated experimentally with ab- and desorption steps.

The time dependence of the sorption process was naturally rather different from material to material. The changes in moisture content were most rapid for perlite and slowest for cellulose and flax insulation. When considering a single material, moisture uptake was slowest for both very high and very low relative humidities, and most rapid for moderate *RH*'s. Together, these observations indicated that the sorption process is a function of the *amount of moisture* to be ab- or desorbed. In other words, moisture uptake was slowest for the most hygroscopic materials and under conditions where the moisture capacity of the materials was highest. Further, absorption was slightly slower than desorption for most materials.

The well-known indication for the existence of non-Fickian behaviour is the divergence between permeability determined by steady-state cup measurements and by the dynamic sorption approach. The measured steady-state permeabilities were up to ten times greater than the dynamically determined permeabilities. An exception was cellular concrete, where the deviation was deemed non-significant.

Another way of studying retarded sorption is to relate measurement results to Fickian simulations. This comparison showed clear non-Fickian behaviour for the organic materials: flax, cellulose and wool insulation.

It was also hypothesised that it is possible to quantify this time-dependence of the sorption mechanisms. The results of the presented numerical approach showed that by rejecting the conventional assumption of the immediate local moisture equilibrium, and by introducing a sorption coefficient that gives the connection between the humidity in air and the absorbed moisture, a better agreement was achieved between the measured and the simulated moisture uptake. The central part of the definition of this new non-Fickian model was the determination of the sorption coefficient from the experimental results. Unfortunately, this coefficient (using the applied analysis method), was found to be very sensitive to the step size of the measurements used.

When analysing the dynamic measurements over an applied temperature gradient, a minor phase delay was found for all materials in simulated RH (Fickian simulations without hysteresis) compared to measured RH . This delay indicated that the moisture capacity of the materials was overestimated when using the slope of sorption isotherm and the assumption of immediate local moisture equilibrium. Applying hysteresis (which also gives a minor moisture capacity but is not time dependent), removed the phase delay but made the amplitude of the RH -changes too high. Applying the non-Fickian model did not produce a good agreement with the measurements as it overly retarded the moisture transport. However, the new model must be considered as a preliminary approach and therefore, it is still possible that the non-Fickian model will be able to describe dynamic behaviour under non-isothermal conditions also.

8.2 Driving potentials for non-isothermal transport

Another part of the hypothesis referred to the definition of the driving forces for moisture transport under non-isothermal conditions. The resulting measured moisture flux and measured boundary conditions were used in an attempt to identify and separate the involved driving forces.

The results strongly indicated that there existed some 'other' transport, besides the water vapour gradient-driven transport for all materials analysed. This was quite surprising as the materials have very different moisture properties. The identification of the driving forces was hampered by the observed inaccuracy of the RH -sensors used, as in the worst case, diametric conclusions resulted. However, on the basis of the analysis of the measurement results, and especially the analysis of uncertainties, it can be concluded that the hypothesis of relative humidity being a driving force for non-isothermal moisture transport already in the hygroscopic range could not be confirmed. On the contrary, indications existed that the temperature gradient itself was driving the moisture from the warm side towards the cold side.

The presented approach for identifying and quantifying the fluxes involved, produced consistent results, under the assumption of using isothermal water vapour permeability to determine the moisture transport due to the vapour pressure gradient. These results also confirmed observations that a temperature-driven transport existed from warm to cold.

8.3 Buffer capacity of materials

Different methods for defining an expression that could indicate a material's ability to buffer for changes in ambient relative humidity were presented. All the methods 'ranked' the materials in more or less the same order, but it was not indifferent if the parameters were determined from steady state or dynamic measurements, or what method was used: When using steady state parameters:

1. When analysing isothermal step measurements, the moisture buffer capacity was overestimated compared to the dynamic case where determined moisture diffusivity was used.
2. When analysing dynamic, non-isothermal measurements – using the 'measured' penetration depth for the dynamic case – the moisture buffer capacity was underestimated for those materials with good buffer capacity, e.g. flax and cellulose insulation and cellular concrete, while there was no difference for materials with poor buffer capacity such as glass wool, rock wool and perlite.

It must be stressed here that the moisture buffer capacity of the insulation materials analysed only refer to the conditions *inside* a construction, because the insulation is 'hidden' behind e.g. a plasterboard and a vapour retarder.

8.4 Significance of uncertainties

8.4.1 Uncertainty of measurements

Isothermal tests

No strong indications exist to doubt the accuracy of the advanced sorption apparatus IGAsorp. This is one of the reasons, why only one sample has been used per material, as concluded in (Kelly, 2002). For statistically reliable results however, the experiment should have been conducted using several replicate samples. In addition, if the sample did not reach equilibrium within 8 hours, a predicted value for *EMC* was given by the apparatus. This value might not necessarily have been the real *EMC*. The consequences of this on the analysis were discussed in Section 5.5.

On the other hand, the accuracy of the periodic step measurements could be a source for errors. It was observed in Figure 5.17 that the measured and simulated moisture content were not comparable. This deviation could best be explained by an error in the determination of the dry density of the material.

Non-isothermal tests

The validity of the non-isothermal results has already been discussed. There are two major sources for uncertainty, i.e. weighing the water for determination of moisture flux, and the relative humidity sensors. The large deviation observed between the small *RH*-sensors used and the dew point sensors used in control measurements created great doubt

about the validity of the results in Chapter 6 and especially the validity of the determined transport coefficients. The control measurements indicated that there in the calculations were used RH 's that were too low on the cold side of the sample. Unfortunately, it could not be confirmed if this deviation existed for all the measurements performed. However, the significance of this deviation is high for the results, as mentioned in Section 6.4.3: The original conclusion on the existing driving forces, i.e. that ΔRH must be a driving potential, was replaced with an opposite conclusion. Instead, ΔT drives the moisture migration from warm to cold, while the role of ΔRH as a driving force was not confirmed.

Nevertheless, when compared with simulations, the dynamic measurements showed that the validity of the relative humidity measurements (relatively to each other), was, in fact rather good. It is open to discussion if the RH 's used as boundary conditions in the simulations were realistic values, nevertheless, all the sensors within the sample measured values in accordance with the expected accuracy.

It has already been discussed that the measured effects might be so small that they can hardly be separated due to the uncertainty of the measurements. But how significant are the results for the practical use in building simulation tools? It has not been possible in the frame of this work to employ any comprehensive uncertainty analysis. However, a systematic study on the significance of different types of uncertainty sources was reported in (Holm and Künzel, 2002): Two different stochastic uncertainty analysis methods (differential sensitivity analysis and Monte Carlo analysis) were applied to determine the significant parameters for a transient hygrothermal simulation of drying of a cellular concrete roof. The analyses showed that uncertainties due to climatic conditions, including surface transfer coefficients were more significant, or at least comparable with the uncertainty of material properties. Some of the uncertainties derived from properties like water vapour permeability and liquid transfer coefficient for surface diffusion, while liquid water uptake and moisture content at free saturation were the most sensitive parameters.

In the present work, the effects of surface transfer coefficients have been eliminated. Therefore, the main uncertainty lies in the determination of the transport coefficients.

8.4.2 Uncertainty of modelling

The modelling approach has not been the major focus in this work, however, it is relevant when discussing any possible source of error to the simulation results.

The models used in this work were made in a Simulink environment, i.e. one of the Matlab-Toolboxes. One of the strengths of using Simulink as a modelling tool is that numerical problem-solving is optimised and ready-to-use.

No model gives a better output than the quality of the input parameters. In this work, great care has been taken that most important moisture parameters, e.g. water vapour permeability and moisture retention curves, have been determined as a part of this work or earlier on these very same batch of materials. For most of the other parameters, standard values from the literature or even dummy values have been used. The material parameters used are given in Appendix A. However, as every material parameter has not been measured explicitly for all the materials, this could have caused deviations between the measurements and simulations.

In (Roels et al., 1999), sources of uncertainty in simulations were discussed. One of the conclusions was that differences in modelling results using different tools are mainly due

to the way they handle approximate analytic relationships for the material properties. Approximate analytical material parameters are used to fill gaps in measurements and to create continuous functions, in order to be able to derive them. In the current work, the sorption isotherms have been defined very carefully with measurement points throughout the relative humidity range. On the contrary, the determination of transport coefficients was more or less based on constant values.

Another source of error in simulations was the used surface transfer coefficients. However, it was concluded in (Pedersen, 1990) that, when the drying is in the vapour transfer phase, as in the studied hygroscopic range, the convective surface transfer coefficient does not play any role as the internal resistance of the material is much higher. Finally, the degree of discretisation is known to affect the simulation results, i.e. the finest grid of nodes produces the best results. In the current work, the degree of discretisation has not been assessed, and a rather coarse grid of nodes has been used for the non-isothermal analysis. Nevertheless, when keeping the observed experimental uncertainty in mind, it was assumed that the possible deviations due to the lack in discretisation have been suppressed by the general level of accuracy.

8.5 Recommendations for future works

The work in this Thesis has not only given some answers to the field of moisture transport and dynamics under iso- and non-isothermal conditions, but has also made it possible to point out subjects where additional analysis is needed.

8.5.1 Additional measurements

Further work with non-isothermal experiments could include some investigations about the effect of temperature gradients on materials with different, and also high moisture contents and with several different magnitudes of gradients. This will link the presence of liquid moisture within the material to an increase in flux, which could be more greatly influenced than pure vapour diffusion. In addition, the investigation of non-isothermal transport should be executed at different temperatures and sizes of gradient to extract the effect of these on the resulting moisture flux.

The reliability of the results from the Megacup set-up could be increased by modifying it to a double flux chamber, where flux on both sides of the sample could be controlled. The observed great uncertainty of the *RH*-sensors used could be eliminated by using another (more expensive) type of sensor, which could be even more carefully calibrated than has been the case for the actual work. In addition, control measurements should be conducted more often to relieve any drift of the measurements.

One of the original experimental plans was to use X-ray measurements to determine the possible non-agreement on the assumption of the local moisture equilibrium in the dynamic case. The local moisture content and the local relative humidity could be measured simultaneously in the same specimen by X-ray and the built-in *RH*-sensors, respectively. The preliminary experiments with X-ray, however, did not succeed, most probably due to too low a moisture content of the materials in the hygroscopic range. Nevertheless, by using more sensitive X-ray-apparatus, or other similar methods, the existence of local equilibrium could be confirmed or rejected.

8.5.2 Additional modelling

Even though the focus in this work has been on experimental investigations, it was also a goal to use the analysis of the experimental results on developing some new simulation models for combined heat and moisture transport. The numerous problems with the time-consuming experimental work, however, reduced the possibilities to fulfil this modelling task. However, a preliminary modelling approach was carried out, albeit with non-consistent results.

The developed hysteresis model was not fully numerically stable for all conditions. This instability did not affect the results shown in Figure 7.9, but further development is needed for the hysteresis model.

The preliminary analysis in Chapter 5 showed that the new non-Fickian model was better able to predict the moisture uptake and release than a conventional Fickian model. However, implementing this non-Fickian model for the set-up presented in Chapter 7 did not confirm the experience in Chapter 5: The resulting moisture capacity of the analysed material (flax) was far too small. A more comprehensive study on the modelling approach is needed to draw any final conclusion on the method presented for modelling non-Fickian behaviour, and most importantly the method for experimentally determining the sorption coefficient k .

Furthermore, to complete the analysis on the non-isothermal moisture transport, a model should be developed that implements all the different ways of considering the driving forces for non-isothermal moisture transport presented in Chapter 6. The final validity of any of these models for non-isothermal moisture transport, possibly together with the non-Fickian model, need to be confirmed with simulations with such a dynamic simulation model.

Chapter 9

Conclusion

The overall scope of this Thesis has been to characterise how the porous insulation materials investigated performed under conditions similar to those in a typical building envelope. From a hygrothermal respect, materials in building envelopes are exposed to an impact in part by the indoor air and partly by the natural weather outside. It is characteristic for this type of exposure that there typically exists a temperature gradient over the materials in an envelope, which dynamically absorb and release moisture as a result of exterior changes in temperature and moisture conditions. Although the impact of these conditions on the resulting moisture transport and moisture content of the materials is a complex subject, it has been studied in this Thesis using controlled laboratory tests.

Isothermal, dynamic tests were used to quantify the moisture response of the materials. Retarded sorption was found for the most of the materials, particularly for the organic ones. A modelling approach with a non-Fickian model, where air in the pores and absorbed moisture were separated into different nodes, and where a sorption coefficient between these nodes was determined experimentally, gave a strong indication that taking the time-dependence of moisture ab- and desorption into account will improve the agreement between measurements and simulations.

Steady state experiments, where the material sample was exposed to a temperature gradient, were used to identify the governing driving potentials in a building envelope. Experimental results gave a strong indication that there existed (even within the studied hygroscopic range), some 'other' transport against the water vapour pressure gradient. However, this phenomenon was detected for all the materials and therefore, together with the observed experimental inaccuracy, drawing any final conclusion on this subject was difficult. Nevertheless, an approach was shown for identifying the driving potentials and quantifying the resulting contribution of these to the total transport.

The same non-isothermal set-up was also subjected to a sinusoidal dynamic change in relative humidity on the cold side of the sample. These results were used to compare the responses of the materials to simultaneous exposure to a temperature gradient and dynamic conditions. The comparison of the measured and simulated results showed that for most materials there exists a fairly good agreement with the conventional Fickian model used. A minor phase delay on simulated results indicated that the true moisture capacity of the materials was lower than the mathematical one, i.e. the slope of the sorption isotherm. Implementing a hysteresis model increased the agreement between measurements and simulations but was not able to remove all the deviation.

Furthermore, the materials' ability to serve as moisture 'buffers' for changes in ambient

relative humidity has been assessed analytically. The analysis was undertaken with results from both isothermal and non-isothermal dynamic tests. The importance of the choice of the material parameters for the resulting moisture buffer capacity (based on parameters determined from either steady state or dynamically), was also pointed out. For example, the moisture buffer capacity will be greatly overestimated when steady state material parameters are used in stead of dynamically determined moisture diffusivity. When the penetration depth of the materials was determined on the basis of non-isothermal dynamic measurements, this depth and therefore also the 'measured' buffer capacity was higher than the theoretical buffer capacity for the materials with good buffer capacity, e.g. flax and cellulose insulation and cellular concrete. There was no difference for materials with poor buffer capacity: glass wool, rock wool and perlite.

The main conclusion on the performance of different insulation materials in building envelopes is, in the practical sense, that very hygroscopic materials like cellulose and flax insulation and cellular concrete are able to moderate peak values in relative humidity to some extent. In addition, a conventional simulation model for coupled heat and moisture transport is able to predict for most practical situations the moisture conditions in a building envelope. However, in the academic sense, including latent heat and hysteresis in the simulation models leads to a better agreement between measurements and the simulations. The positive effect of rejecting the common assumption of immediate local equilibrium was shown for simulation of isothermal step-response experiments, while the same model did not perform as expected for the simulation of non-isothermal, dynamic set-up.

References

- Bomberg, M., Pazera, M., Haghghat, F. and Grunewald, J. (2002). Modified cup for testing of water vapour transmission through thick, permeable materials, *6th Symposium on Building Physics in the Nordic Countries*, Trondheim.
- Chomcharn, A. and Skaar, C. (1983). Dynamic sorption and hygroexpansion of wood wafers exposed to sinusoidally varying humidity, *Wood Science and Technology* **17**: 259–277.
- Christensen, G. N. and Kelsey, K. E. (1959). Die Geschwindigkeit der Wasserdampfsorption durch Holz, *Holz als Roh- und Werkstoff* **17**: 178–188.
- Crank, J. (1975). *The Mathematics of Diffusion*, Oxford at the Clarendon Press.
- Cunningham, M. J. (1995). A model to explain "anomalous" moisture sorption in wood under step function driving forces, *Wood and Fibre Science* **27**(3): 265–277.
- Delfino, S. and Giacchetti, G. (2001). Assignment in master course, '11546 Experimental Mechanics' at Department of Civil Engineering at Technical University of Denmark.
- EN-ISO (1999). European standard EN ISO 12571: Hygrothermal performance of building materials - determination of hygroscopic sorption properties, European Committee for Standardization.
- EN-ISO (2001). European standard EN ISO 12572: Hygrothermal performance of building materials and products - determination of water vapour transmission properties, European Committee for Standardization.
- Fick, A. (1855). Über diffusion, *Annalen der Physik und Chemie* **94**: 59–86.
- Galbraith, G. H., Guo, J. S. and McLean, R. C. (2000). The effect of temperature on the moisture permeability of building materials, *Building Research and Information* **28**(4): 245–259.
- Galbraith, G. H., Guo, J. S., McLean, R. C., Lee, C. K. and Kelly, D. J. (1999). The temperature dependence of moisture permability, *CIB W40 Conference*, Prague.
- Galbraith, G. H., McLean, R. C., Gillespie, I., Guo, J. S. and Kelly, D. (1998). Non-isothermal moisture diffusion in porous building materials, *Building Research and Information* **26**(6): 330–339.
- Galbraith, G. H., McLean, R. C. and Guo, J. S. (1997). Moisture permeability data as a mathematical function applicable to heat and moisture transfer models, *5th International IBPSA Conference*, Prague.

- Hagentoft, C.-E. (2001). *Introduction to building physics*, Studentlitteratur.
- Håkansson, H. (1998). *Retarded sorption in wood*, Ph.d thesis (Report TABK-98/1012), Department of Building Science, Lund Institute of Technology, Lund University.
- Hansen, E. J., Hansen, K. K. and Padfield, T. (1999). Measured moisture properties for alternative insulation products, *5th Symposium on Building Physics in the Nordic Countries*, Göteborg.
- Hansen, K. K. and Lund, H. B. (1990). Cup method for determination of water vapour transmission properties of building materials. Sources of uncertainty in the method, *2nd Symposium on Building Physics in the Nordic Countries*, Trondheim.
- Hedenblad, G. (1996). *Materialdata för fugttransportberäkningar*, Byggeforskningsrådet.
- Hens, H. (1992). Vapour permeability: Moisture dependent or not (T3-B-92/04), *IEA Annex 24 Hamtie, Task 1: Modelling & Task 3: Material properties*.
- Hens, H. (1996). Final report, volume 1: Task 1: Modelling, *IEA Annex 24 Hamtie*.
- Hens, H., Vanherck, K. and Goddeau, M. (1993). Vapour permeability of lightweight concrete and expanded polystyrene: Isothermal and non-isothermal measurements (T3-B-93/01), *IEA Annex 24 Hamtie, Task 3: Material properties*.
- Holm, A. H. and Künzeli, H. M. (2002). Practical application of an uncertainty approach for hygrothermal building simulations - drying of an AAC flat roof, *Building and Environment* **37**: 883–889.
- Janz, M. (2000). *Moisture transport and fixation in porous materials at high moisture levels*, Ph.d thesis (Report TVBM-1018), Lund Institute of Technology, Division of Building Materials, Lund University.
- Kelly, D. J. (2002). *Rapid experimental methods for the evaluation of material moisture permeability*, PhD thesis, School of Built and Natural Environment, Glasgow Caledonian University.
- Koponen, S. and Liu, L. (1999). Modeling of moisture transfer in wood based on cell structure, *5th Symposium on Building Physics in the Nordic Countries*, Göteborg.
- Krabbenhøft, K. and Damkilde, L. (2002). Non-fickian moisture transfer in wood. Part 1: Mathematical model, *Holzforschung (Submitted)*.
- Krus, M. (1992). Does vapour diffusion really depend on moisture content (T3-D-92/02), *IEA Annex 24 Hamtie, Task 3: Material properties*.
- Krus, M. (1995). *Feuchtetransport- und Speicherkoeffizienten poröser mineralischer Baustoffe. Theoretische Grundlagen und neue Meßtechniken*, PhD thesis, Fakultät Bauingenieur- und Vermessungswesen der Universität Stuttgart.
- Kumaran, M. K. (1988). Comparison of simultaneous heat and moisture transport through glass-fibre and spray-cellulose insulations, *Journal of Thermal Insulation* **12**: 6–16.
- Kumaran, M. K. (1996). Final report, Volume 3: Task 3: Material properties, *IEA Annex 24 Hamtie*.

- Künzel, H. M. (1995). *One and two-dimensional calculation of the simultaneous heat and moisture transport in building components, using simple parameters*, PhD thesis, Fraunhofer Institute for Building Physics.
- Künzel, H. M. and Kiessl, K. (1990). Bestimmung des Wasserdampfdiffusionswiderstandes von mineralischen Baustoffen aus Sorptionsversuchen, *Bauphysik* 12.
- Luikov, A. V. (1966). *Heat and Mass Transfer in Capillary-porous Bodies*, Pergamon Press.
- Mukhopadhyaya, P., Kumaran, K. and Lackey, J. (2001). Temperature dependency of water vapour transmission through building materials, *CIB W40: Heat and moisture transfer in buildings*, Wellington, New Zealand.
- Nicolajsen, A. (1973). *Fugttransportkoefficienter for gasbeton*, Moisture transport coefficients for cellular concrete. Report 25, Thermal Insulation Laboratory, Technical University of Denmark.
- Padfield, T. (1999). *The role of absorbent building materials in moderating changes of relative humidity*, Ph.d thesis (Report no.54), Department of Structural Engineering and Materials, Technical University of Denmark.
- Padfield, T., Peuhkuri, R., Rode, C. and Hansen, K. K. (2002). Non-isothermal water vapour transmission through porous insulation. Part 1: Equipment, *6th Symposium on Building Physics in the Nordic Countries*, Trondheim.
- Pedersen, C. R. (1990). *Combined Heat and Moisture Transfer in Building Constructions*, Ph.d. thesis (Report no.214), Thermal Insulation Laboratory, Technical University of Denmark.
- Peuhkuri, R. (2000). *Isoleringsmaterialers fugttekniske egenskaber i klimaskærm (Moisture performance of insulation materials in building envelopes)*, Master's Thesis, Technical University of Denmark, Department of Buildings and Energy.
- Peuhkuri, R. (2002). SIMULINK model of coupled heat and moisture transport in material layers, *Report SR-02-02, Department of Civil Engineering, Technical University of Denmark*.
- Peuhkuri, R., Rode, C., Hansen, K. K., Kelly, D. J., Baker, P. H., Galbraith, G. H. and McLean, R. C. (2003). Comparison of experimental methods for the measurement of non-isothermal moisture transport, *2nd International Conference on Research in Building Physics*, Leuven.
- Philip, J. R. and De Vries, D. A. (1957). Moisture movement in porous materials under temperature gradient, *Trans. Am. Geophysical Union*, Vol 39, no. 5.
- Rode, C. (1991). Description of the model MATCH. Theoretical background, equations (T1-DK-91/01), *IEA Annex 24 Final report, Volume 1: Task 1: Modelling*.
- Roels, S., Depraetere, W., Carmelit, J. and Hens, H. (1999). Simulating non-isothermal water vapour transfer: An experimental validation on multi-layered building components, *Journal of Thermal Envelopes & Building Science* 23: 17–40.
- Salin, J.-G. (1996a). Mass transfer from wooden surfaces, *10th International Drying Symposium*, Krakow, Poland.

- Salin, J.-G. (1996b). Mass transfer from wooden surfaces and internal moisture non-equilibrium, *Drying Technology* **14**(10): 2213–2224.
- Salin, J.-G. (2002). Theoretical analysis of mass transfer from wooden surfaces, *13th International Drying Symposium*, Beijing, China, pp. 1826–.
- Salin, J.-G. (2003). *COST Action E15 Advances in Drying of Wood*, Editor: P. Perré, chapter 5-6.
- Scarpa, F. and Milano, G. (2002). The role of adsorption and phase change phenomena in the thermophysical characterization of moist porous materials, *International Journal of Thermophysics* **23**(4): 1033–1046.
- Schascheck, H. (1956). Bewegungsmechanismus von Wasserdampf in porösen blattförmigen Materialien, *Chemie-Ingenieur-Technik* **28**: 698–702.
- Strømdahl, K. (2000). *Water Sorption in Wood and Plant Fibres*, Ph.d thesis (Report R No 78), Department of Structural Engineering and materials, Technical University of Denmark.
- Time, B. (1998). *Hygroscopic Moisture Transport in Wood*, PhD thesis, Department of Building and Construction Engineering, Norwegian University of Science and Technology.
- Vinha, J., Käkelä, P. and Lindberg, R. (2002). Moisture transport in timber-framed external wall structures in nordic climate. Laboratory tests, *6th Symposium on Building Physics in the Nordic Countries*, Trondheim.
- Wadsö, L. (1993). *Studies of Water Vapor Transport and Sorption in Wood*, PhD thesis, Department of Building Science, Lund Institute of Technology, Lund University.
- Weitzmann, P., Kalagasidis, A. S., Nielsen, T. R., Peuhkuri, R. and Hagentoft, C.-E. (2003). Presentation of the International Building Physics Toolbox for SIMULINK, *Building Simulation 2003, 8th International IBPSA Conference*, Eindhoven, pp. 1369–1376.

APPENDIX

Appendix A

Material parameters

In this appendix, the material parameters used in the simulation models are given. Many of the parameters are given as dummy values. That means that these parameters have NOT been measured, but are only qualified guesses, based on catalogue values for similar materials. The material library in MATCH (Rode, 1991) has been used as a main "catalogue".

Measured values originate from following sources

- measured as a part of this project
- (Hansen et al., 1999)
- data from the manufacturer

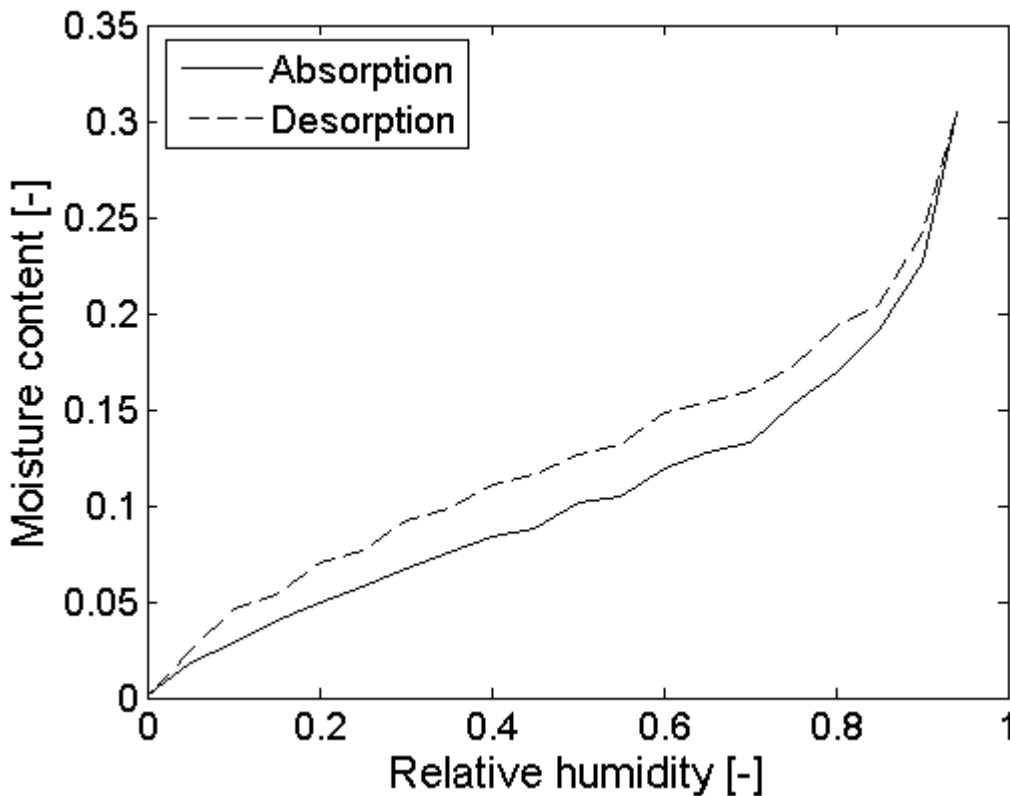
Wool insulation

Manufacturer	Heraklith, Austria/Germany
Trade name	Herawool NF 040
Composition	Sheep wool + 2-4% boron salts

	Symbol	Value	Unit	Reference
Dry density	ρ_0	25	kg/m ³	Heraklith
Heat capacity	c_p	1382	J/(kg·K)	MATCH
Dry thermal conductivity	λ_{10}	0.040	W/(m·K)	Heraklith
Temperature dependent part of the thermal conductivity	λ_T	0	W/(m·K ²)	MATCH
Moisture dependent part of the thermal conductivity	λ_u	0	W/(m·K)	MATCH
Critical moisture content	u_{cr}	10	kg/kg	MATCH

Sorption isotherm

Measured at 20°C with IGAcorp equipment as a part of this project.
Determination of the dry mass at 0% RH and 20 °C.



APPENDIX A: MATERIAL PARAMETERS

Absorption		Desorption	
RH [-]	u [kg/kg]	RH [-]	u [kg/kg]
0.00	0.001	0.94	0.305
0.05	0.018	0.90	0.242
0.10	0.029	0.85	0.205
0.15	0.040	0.80	0.193
0.20	0.049	0.75	0.172
0.25	0.058	0.70	0.160
0.30	0.067	0.65	0.154
0.35	0.076	0.60	0.148
0.40	0.084	0.55	0.132
0.45	0.088	0.50	0.127
0.50	0.102	0.45	0.116
0.55	0.105	0.40	0.111
0.60	0.119	0.35	0.098
0.65	0.128	0.30	0.092
0.70	0.133	0.25	0.077
0.75	0.153	0.20	0.070
0.80	0.169	0.15	0.054
0.85	0.191	0.10	0.046
0.90	0.227	0.05	0.025
0.94	0.305	0.00	0.000
Reference:	This project		

Relative humidity	Water vapour permeability	Moisture content	Water vapour permeability
[-]	[10 ⁻¹⁰ kg/(Pa·m·s)]	[-]	[10 ⁻¹⁰ kg/(Pa·m·s)]
0.000	1.9	0.60	1.9
0.495	1.9	11.86	1.9
0.505	1.9		
0.940	1.9		
Reference:	Hansen et.al 1999	Reference:	MATCH

Logarithmic suction pressure	Moisture content
[ln(Pa)]	[-]
-10.00	10.99
14.786	0.8458
Reference:	MATCH

Moisture content	Hydraulic conductivity
[-]	[10 ⁻¹⁰ kg/(Pa·m·s)]
0.8466	10 ⁻⁴⁰
10.99	10 ⁻⁴⁰
Reference:	MATCH

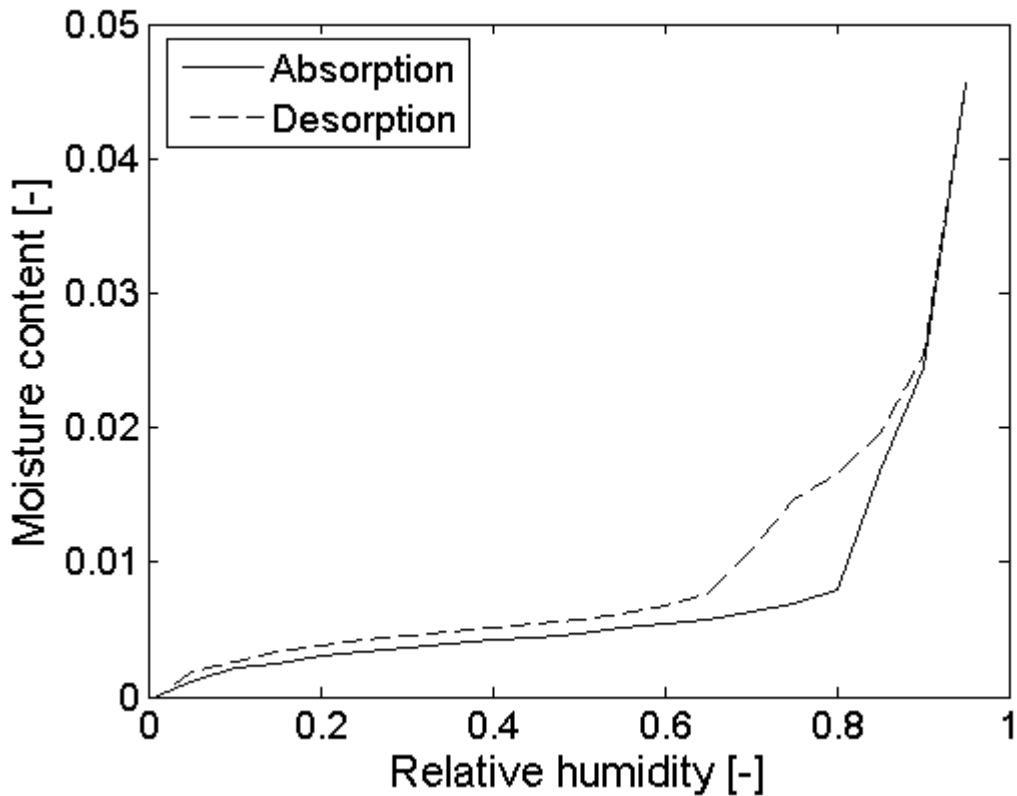
Glass wool

Manufacturer	Saint-Gobain Isover
Trade name	Isover Ground Batt
Composition	glass fibers (mostly recycled glass and sand) + 5% binding agents

	Symbol	Value	Unit	Reference
Dry density	ρ_0	70	kg/m ³	Isover
Heat capacity	c_p	800	J/(kg·K)	MATCH
Dry thermal conductivity	λ_{10}	0.037	W/(m·K)	Isover
Temperature dependent part of the thermal conductivity	λ_T	$1.50 \cdot 10^{-4}$	W/(m·K ²)	MATCH
Moisture dependent part of the thermal conductivity	λ_u	0.043	W/(m·K)	MATCH
Critical moisture content	u_{cr}	10	kg/kg	MATCH

Sorption isotherm

Measured at 20°C with IGA-sorp equipment as a part of this project.
Determination of the dry mass at 0% RH and 20 °C.



APPENDIX A: MATERIAL PARAMETERS

Absorption		Desorption	
RH [-]	u [kg/kg]	RH [-]	u [kg/kg]
0.01	0.0001	0.95	0.0456
0.05	0.0011	0.90	0.0253
0.10	0.0021	0.85	0.0196
0.15	0.0024	0.80	0.0166
0.20	0.0031	0.75	0.0146
0.25	0.0034	0.70	0.0110
0.30	0.0037	0.65	0.0077
0.35	0.0039	0.60	0.0067
0.40	0.0042	0.55	0.0062
0.45	0.0044	0.50	0.0058
0.50	0.0047	0.45	0.0055
0.55	0.0051	0.40	0.0052
0.60	0.0054	0.35	0.0048
0.65	0.0058	0.30	0.0045
0.70	0.0063	0.25	0.0042
0.75	0.0069	0.20	0.0038
0.80	0.0079	0.15	0.0034
0.85	0.0167	0.10	0.0026
0.90	0.0245	0.05	0.0018
0.95	0.0456	0.01	0.0000
Reference:	This project		

Relative humidity	Water vapour permeability	Moisture content	Water vapour permeability
[-]	[10 ⁻¹⁰ kg/(Pa·m·s)]	[-]	[10 ⁻¹⁰ kg/(Pa·m·s)]
0.00	1.7	0.0000	1.7
0.60	1.7	0.0417	1.7
Reference:	This project	Reference:	MATCH

Logarithmic suction pressure	Moisture content
[ln(Pa)]	[-]
-10.00	13
14.786	0.0253
Reference:	MATCH

Moisture content	Hydraulic conductivity
[-]	[10 ⁻¹⁰ kg/(Pa·m·s)]
0	10 ⁻⁴⁰
13	10 ⁻⁴⁰
Reference:	MATCH

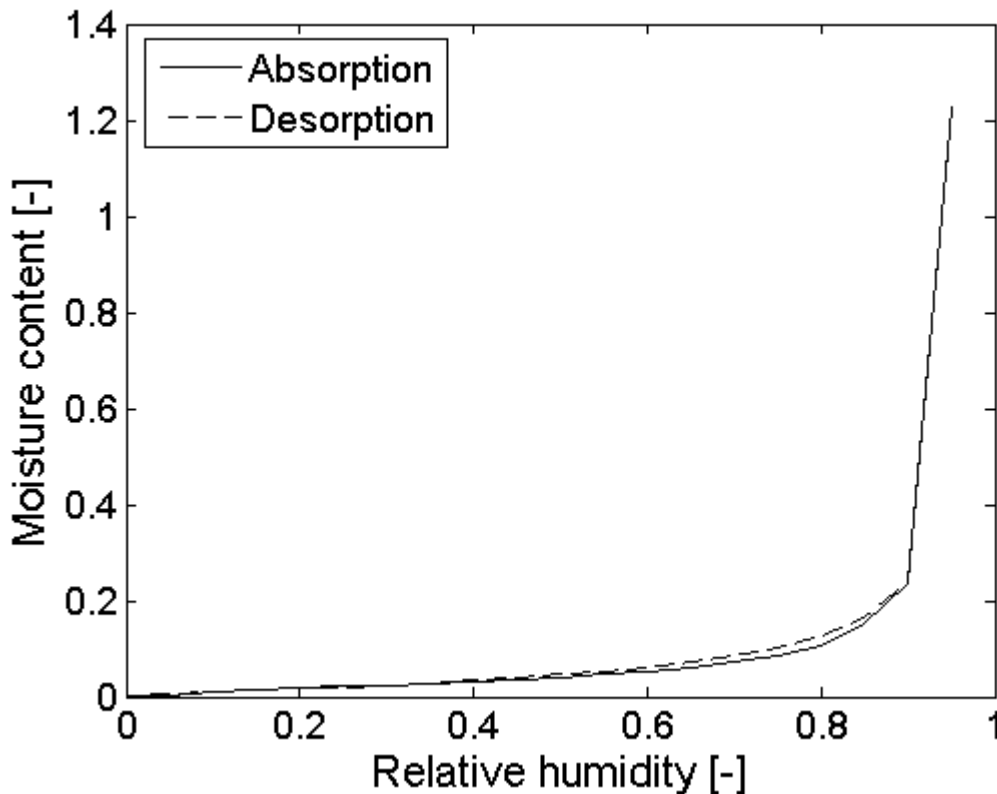
Flax insulation

Manufacturer	Heraklith, Austria/Germany
Trade name	Heraflax SF 040
Composition	Flax fibres + 8% ammonium phosphate/sulphate

	Symbol	Value	Unit	Reference
Dry density	ρ_0	30	kg/m ³	Heraklith
Heat capacity	c_p	1382	J/(kg·K)	MATCH
Dry thermal conductivity	λ_{10}	0.040	W/(m·K)	Heraklith
Temperature dependent part of the thermal conductivity	λ_T	0	W/(m·K ²)	MATCH
Moisture dependent part of the thermal conductivity	λ_u	0	W/(m·K)	MATCH
Critical moisture content	u_{cr}	10	kg/kg	MATCH

Sorption isotherm

Measured at 20°C with IGAsorp equipment as a part of this project.
Determination of the dry mass at 0% RH and 20 °C.



APPENDIX A: MATERIAL PARAMETERS

Absorption		Desorption	
RH [-]	u [kg/kg]	RH [-]	u [kg/kg]
0.00	0.000	0.95	1.228
0.05	0.004	0.90	0.241
0.10	0.009	0.85	0.164
0.15	0.013	0.80	0.126
0.20	0.017	0.75	0.102
0.25	0.021	0.70	0.085
0.30	0.025	0.65	0.073
0.35	0.029	0.60	0.061
0.40	0.033	0.55	0.054
0.45	0.036	0.50	0.047
0.50	0.041	0.45	0.040
0.55	0.046	0.40	0.036
0.60	0.053	0.35	0.029
0.65	0.061	0.30	0.025
0.70	0.071	0.25	0.020
0.75	0.085	0.20	0.017
0.80	0.108	0.15	0.013
0.85	0.152	0.10	0.010
0.90	0.234	0.05	0.005
0.95	1.228	0.00	0.001
Reference:	This project		

Relative humidity	Water vapour permeability	Moisture content	Water vapour permeability
[-]	[10 ⁻¹⁰ kg/(Pa·m·s)]	[-]	[10 ⁻¹⁰ kg/(Pa·m·s)]
0.00	1.5	0.0000	1.67
0.72	1.5	0.8466	1.67
Reference:	Hansen et.al 1999	Reference:	MATCH

Logarithmic suction pressure	Moisture content
[ln(Pa)]	[-]
-10.00	10.99
14.786	0.8458
Reference:	MATCH

Moisture content	Hydraulic conductivity
[-]	[10 ⁻¹⁰ kg/(Pa·m·s)]
0	10 ⁻⁴⁰
0.8466	10 ⁻⁴⁰
Reference:	MATCH

Cellular concrete

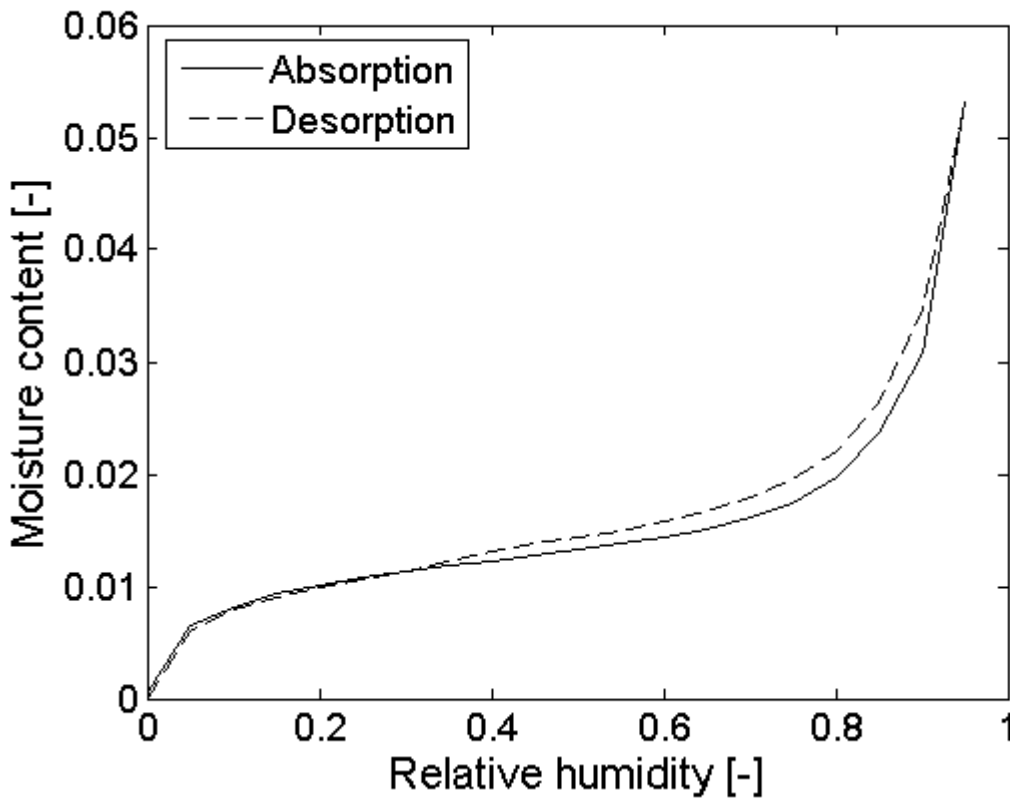
Manufacturer -
 (quality sent to several laboratories in Europe, North America and Japan in 1999 as a part of the CIB W40 TG on Material characterization and model bench-marking)

Trade name -

	Symbol	Value	Unit	Reference
Dry density	ρ_0	450	kg/m ³	This project
Heat capacity	c_p	900	J/(kg·K)	MATCH
Dry thermal conductivity	λ_{l0}	0.11	W/(m·K)	Delfino, 2001
Temperature dependent part of the thermal conductivity	λ_T	$4.0 \cdot 10^{-4}$	W/(m·K ²)	MATCH
Moisture dependent part of the thermal conductivity	λ_u	0.40	W/(m·K)	MATCH
Critical moisture content	u_{cr}	0.8466	kg/kg	MATCH

Sorption isotherm

Measured at 20°C with IGAsorp equipment as a part of this project.
 Determination of the dry mass at 0% RH and 20 °C.



APPENDIX A: MATERIAL PARAMETERS

Absorption		Desorption	
RH [-]	u [kg/kg]	RH [-]	u [kg/kg]
0.00	0.0005	0.95	0.0531
0.05	0.0065	0.90	0.0347
0.10	0.0082	0.85	0.0263
0.15	0.0093	0.80	0.0220
0.20	0.0101	0.75	0.0196
0.25	0.0108	0.70	0.0180
0.30	0.0114	0.65	0.0167
0.35	0.0119	0.60	0.0158
0.40	0.0123	0.55	0.0150
0.45	0.0128	0.50	0.0144
0.50	0.0133	0.45	0.0138
0.55	0.0138	0.40	0.0132
0.60	0.0144	0.35	0.0123
0.65	0.0151	0.30	0.0113
0.70	0.0161	0.25	0.0106
0.75	0.0174	0.20	0.0099
0.80	0.0197	0.15	0.0091
0.85	0.0236	0.10	0.0079
0.90	0.0308	0.05	0.0060
0.95	0.0531	0.00	0.0000
Reference:	This project		

Relative humidity	Water vapour permeability	Moisture content	Water vapour permeability
[-]	[10 ⁻¹⁰ kg/(Pa·m·s)]	[-]	[10 ⁻¹⁰ kg/(Pa·m·s)]
0.00	0.2	0.4183	0.24
0.60	0.2	1.5	1.1·10 ⁻⁶
0.98	0.24		
Reference:	This project	Reference:	MATCH

Logarithmic suction pressure	Moisture content	Moisture content	Hydraulic conductivity
[ln(Pa)]	[-]	[-]	[10 ⁻¹⁰ kg/(Pa·m·s)]
-10.00	0.7000	0.40	1.21·10 ⁻²
4.00	0.6848	0.70	6.53
7.00	0.6299	1.50	6.53
9.00	0.5607		
11.00	0.4591		
13.00	0.3198		
14.00	0.2345		
14.786	0.1650		
Reference:	MATCH	Reference:	MATCH

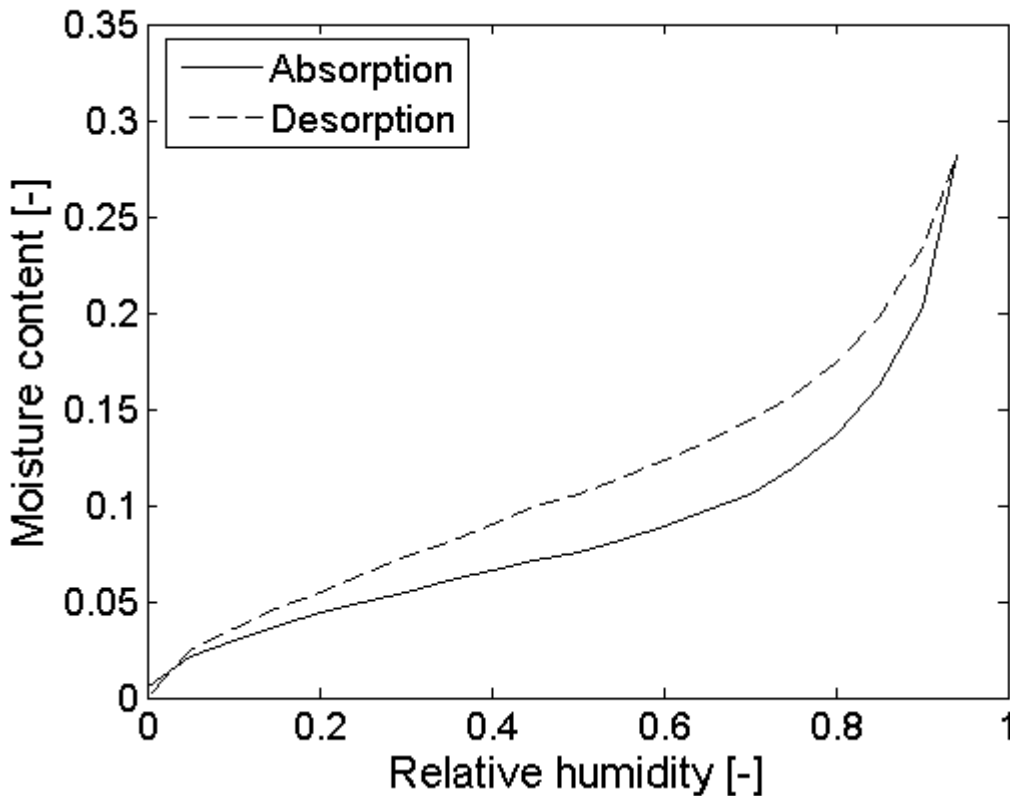
Cellulose insulation

Manufacturer	Ekofiber, Sweden
Trade name	Ekofiber Vind
Composition	cellulose fibres + 18% boron salts

	Symbol	Value	Unit	Reference
Dry density	ρ_0	65	kg/m ³	This project
Heat capacity	c_p	1382	J/(kg·K)	MATCH
Dry thermal conductivity	λ_{10}	0.040	W/(m·K)	Ekofiber
Temperature dependent part of the thermal conductivity	λ_T	0	W/(m·K ²)	MATCH
Moisture dependent part of the thermal conductivity	λ_u	0	W/(m·K)	MATCH
Critical moisture content	u_{cr}	10	kg/kg	MATCH

Sorption isotherm

Measured at 20°C with IGAsorp equipment as a part of this project.
Determination of the dry mass at 0% RH and 20 °C.



APPENDIX A: MATERIAL PARAMETERS

Absorption		Desorption	
RH [-]	u [kg/kg]	RH [-]	u [kg/kg]
0.00	0.005	0.94	0.282
0.05	0.021	0.90	0.234
0.10	0.030	0.85	0.197
0.15	0.037	0.80	0.174
0.20	0.044	0.75	0.157
0.25	0.050	0.70	0.144
0.30	0.055	0.65	0.133
0.35	0.061	0.60	0.123
0.40	0.066	0.55	0.114
0.45	0.071	0.50	0.106
0.50	0.076	0.45	0.099
0.55	0.082	0.40	0.090
0.60	0.089	0.35	0.081
0.65	0.097	0.30	0.073
0.70	0.106	0.25	0.064
0.75	0.119	0.20	0.055
0.80	0.137	0.15	0.046
0.85	0.162	0.10	0.036
0.90	0.203	0.05	0.025
0.94	0.282	0.00	0.000
Reference:	This project		

Relative humidity	Water vapour permeability	Moisture content	Water vapour permeability
[-]	[10 ⁻¹⁰ kg/(Pa·m·s)]	[-]	[10 ⁻¹⁰ kg/(Pa·m·s)]
0.00	1.1	0.4183	1.1
0.60	1.1	1.5	1.1
0.98	1.1		
Reference:	Hansen et.al 1999	Reference:	MATCH

Logarithmic suction pressure	Moisture content
[ln(Pa)]	[-]
-10.00	10.99
14.7860	0.8458
Reference:	MATCH

Moisture content	Hydraulic conductivity
[-]	[10 ⁻¹⁰ kg/(Pa·m·s)]
0.00	10 ⁻⁴⁰
0.8466	10 ⁻⁴⁰
Reference:	MATCH

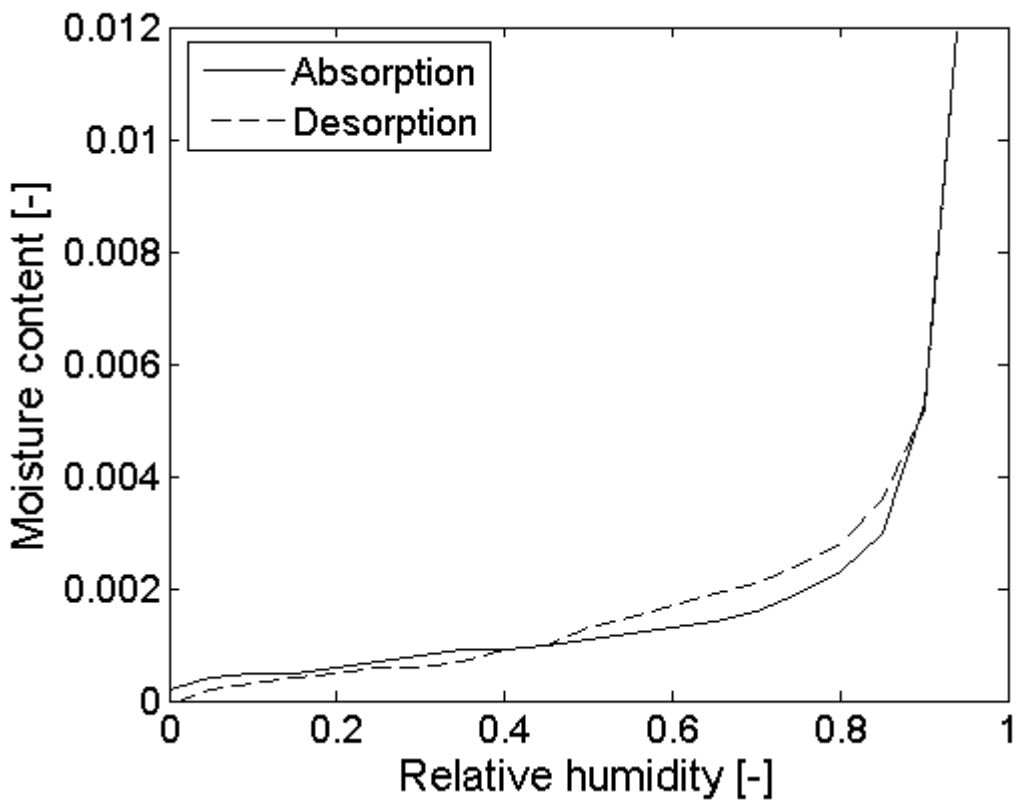
Perlite

Importer	Nordisk Perlite
Trade name	Perlite SC
Composition	expanded volcanic glass + 0.2% silicon resin

	Symbol	Value	Unit	Reference
Dry density	ρ_0	100	kg/m ³	This project
Heat capacity	c_p	1000	J/(kg·K)	MATCH
Dry thermal conductivity	λ_{10}	0.050	W/(m·K)	Perlite
Temperature dependent part of the thermal conductivity	λ_T	0	W/(m·K ²)	MATCH
Moisture dependent part of the thermal conductivity	λ_u	0	W/(m·K)	MATCH
Critical moisture content	u_{cr}	1	kg/kg	MATCH

Sorption isotherm

Measured at 20°C with IGAsorp equipment as a part of this project.
Determination of the dry mass at 0% RH and 20 °C.



APPENDIX A: MATERIAL PARAMETERS

Absorption		Desorption	
RH [-]	u [kg/kg]	RH [-]	u [kg/kg]
0.00	0.0002	0.94	0.0119
0.05	0.0004	0.90	0.0052
0.10	0.0005	0.85	0.0036
0.15	0.0005	0.80	0.0028
0.20	0.0006	0.75	0.0024
0.25	0.0007	0.70	0.0021
0.30	0.0008	0.65	0.0019
0.35	0.0009	0.60	0.0017
0.40	0.0009	0.55	0.0015
0.45	0.0010	0.50	0.0013
0.50	0.0011	0.45	0.0010
0.55	0.0012	0.40	0.0009
0.60	0.0013	0.35	0.0007
0.65	0.0014	0.30	0.0006
0.70	0.0016	0.25	0.0006
0.75	0.0019	0.20	0.0005
0.80	0.0023	0.15	0.0004
0.85	0.0030	0.10	0.0003
0.90	0.0053	0.05	0.0002
0.94	0.0119	0.01	0.0000
Reference:	This project		

Relative humidity	Water vapour permeability	Moisture content	Water vapour permeability
[-]	[10 ⁻¹⁰ kg/(Pa·m·s)]	[-]	[10 ⁻¹⁰ kg/(Pa·m·s)]
0.00	1.03	0.4183	1.03
0.60	1.03	1.5	1.03
0.98	1.03		
Reference:	Hansen et.al 1999	Reference:	MATCH

Logarithmic suction pressure	Moisture content
[ln(Pa)]	[-]
-10.00	10.99
14.7860	0.8458
Reference:	MATCH

Moisture content	Hydraulic conductivity
[-]	[10 ⁻¹⁰ kg/(Pa·m·s)]
0.00	10 ⁻⁴⁰
0.8466	10 ⁻⁴⁰
Reference:	MATCH

Rock wool

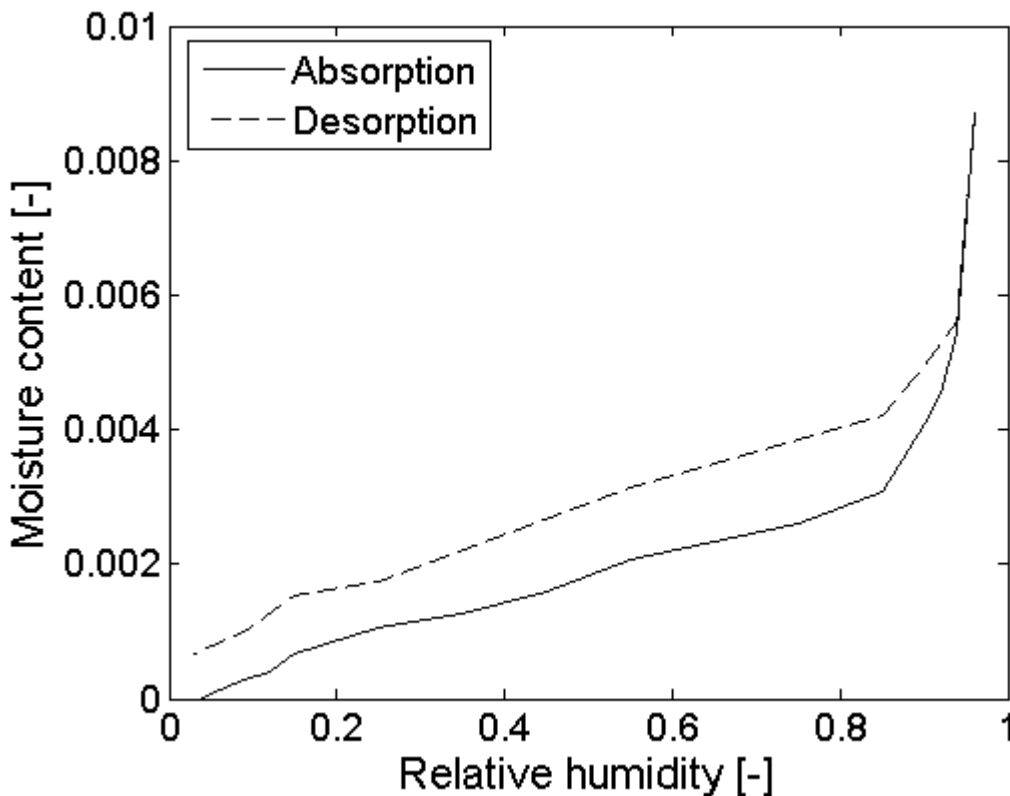
Manufacturer	Rockwool, Denmark
Trade name	Flexi A-batt
Composition	Mineral fibres + binders + 0.5% silicon oil

	Symbol	Value	Unit	Reference
Dry density	ρ_0	32	kg/m ³	Rockwool
Heat capacity	c_p	800	J/(kg·K)	MATCH
Dry thermal conductivity	λ_{10}	0.037	W/(m·K)	Rockwool
Temperature dependent part of the thermal conductivity	λ_T	$1.5 \cdot 10^{-4}$	W/(m·K ²)	MATCH
Moisture dependent part of the thermal conductivity	λ_u	0.03	W/(m·K)	MATCH
Critical moisture content	u_{cr}	10	kg/kg	MATCH

Sorption isotherm

Measured at 20°C (Hansen et.al, 1999)

Determination of the dry mass at 0-1% RH and 20 °C.



APPENDIX A: MATERIAL PARAMETERS

Absorption		Desorption	
RH [-]	u [kg/kg]	RH [-]	u [kg/kg]
0.03	-0.0001	0.96	0.0087
0.06	0.0001	0.94	0.0056
0.09	0.0003	0.90	0.0050
0.12	0.0004	0.85	0.0042
0.15	0.0007	0.55	0.0031
0.25	0.0011	0.25	0.0017
0.35	0.0013	0.15	0.0015
0.45	0.0016	0.09	0.0010
0.55	0.0021	0.03	0.0007
0.65	0.0023		
0.75	0.0026		
0.85	0.0031		
0.90	0.0041		
0.92	0.0046		
0.94	0.0054		
0.96	0.0087		
Reference:	Hansen et.al 1999		

Relative humidity	Water vapour permeability	Moisture content	Water vapour permeability
[-]	[10 ⁻¹⁰ kg/(Pa·m·s)]	[-]	[10 ⁻¹⁰ kg/(Pa·m·s)]
0.00	1.83	0.4183	1.83
0.60	1.83	1.5	1.83
0.98	1.83		
Reference:	Hansen et.al 1999	Reference:	MATCH

Logarithmic suction pressure	Moisture content
[ln(Pa)]	[-]
-10.00	10.99
14.7860	0.8458
Reference:	MATCH

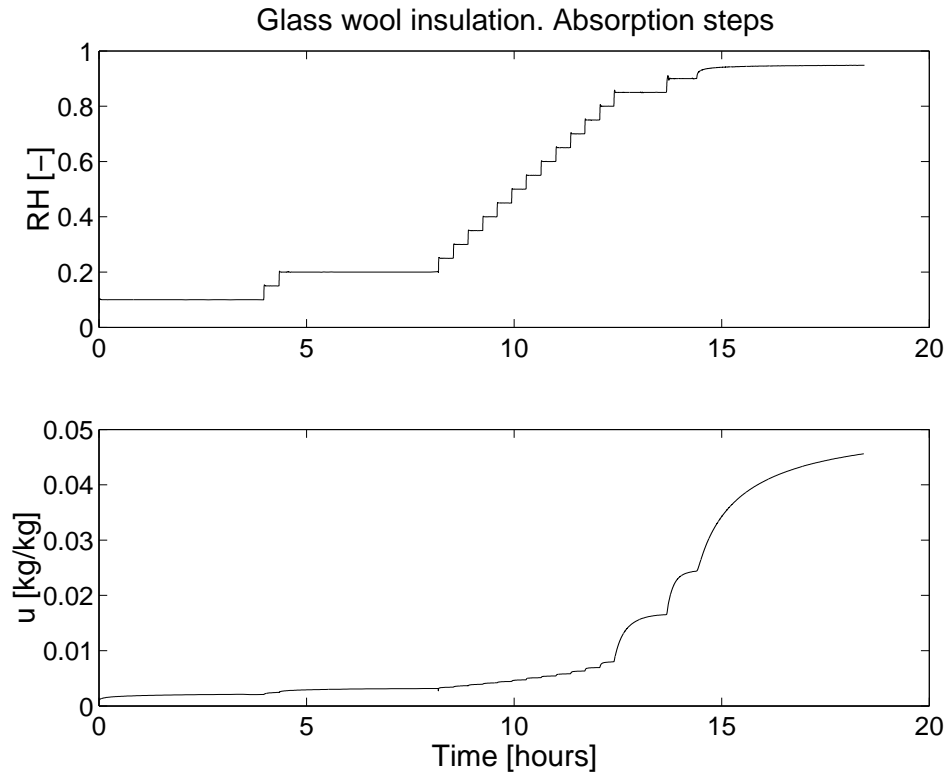
Moisture content	Hydraulic conductivity
[-]	[10 ⁻¹⁰ kg/(Pa·m·s)]
0.00	10 ⁻⁴⁰
0.8466	10 ⁻⁴⁰
Reference:	MATCH

Appendix B

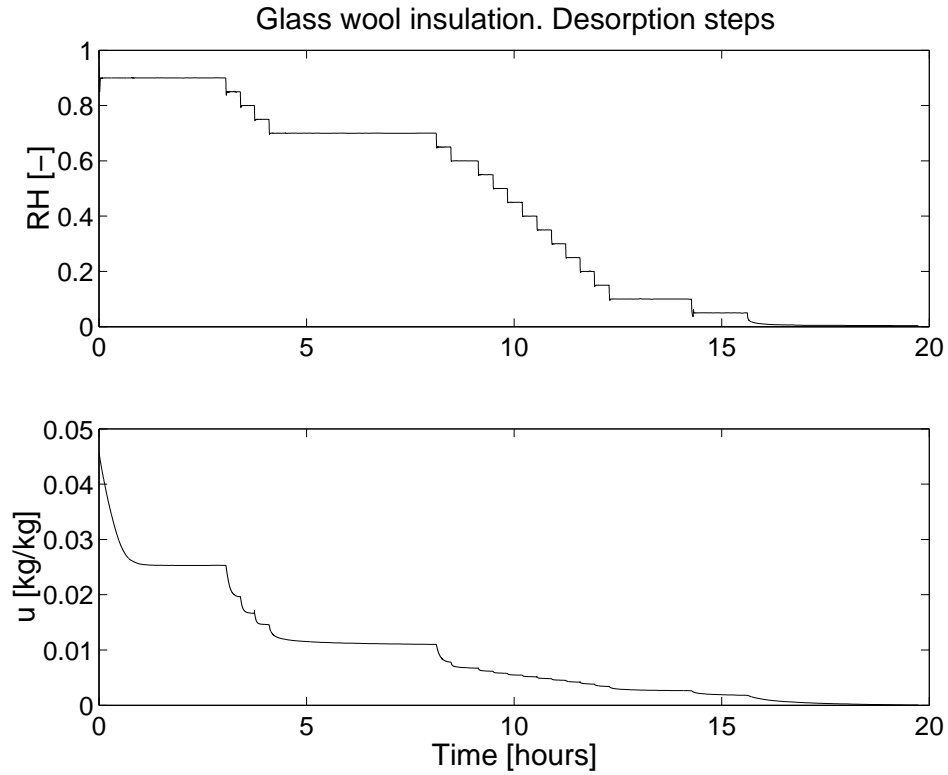
Additional results

B.1 Isothermal, dynamic moisture transport

B.1.1 Measurements with IGAsorp and Climate Chambers



(a)



(b)

Figure B.1: IGAsorp measurements. Measured moisture content in **glass wool** as a result of 5% - steps in relative humidity. Temperature 20°C. (a) Absorption steps and (b) desorption steps.

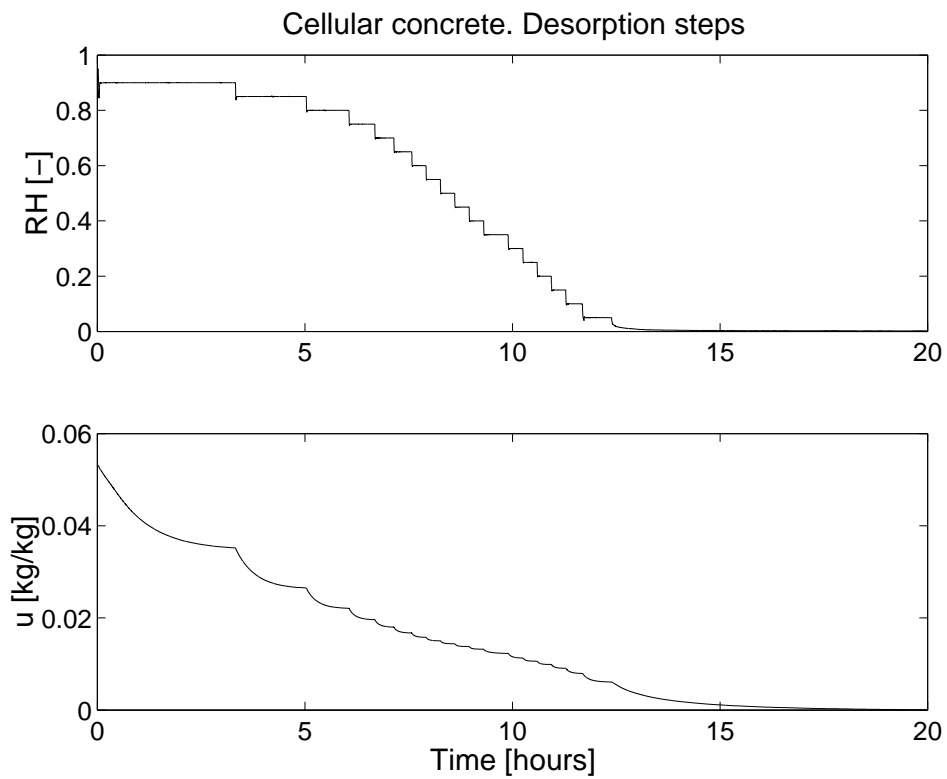
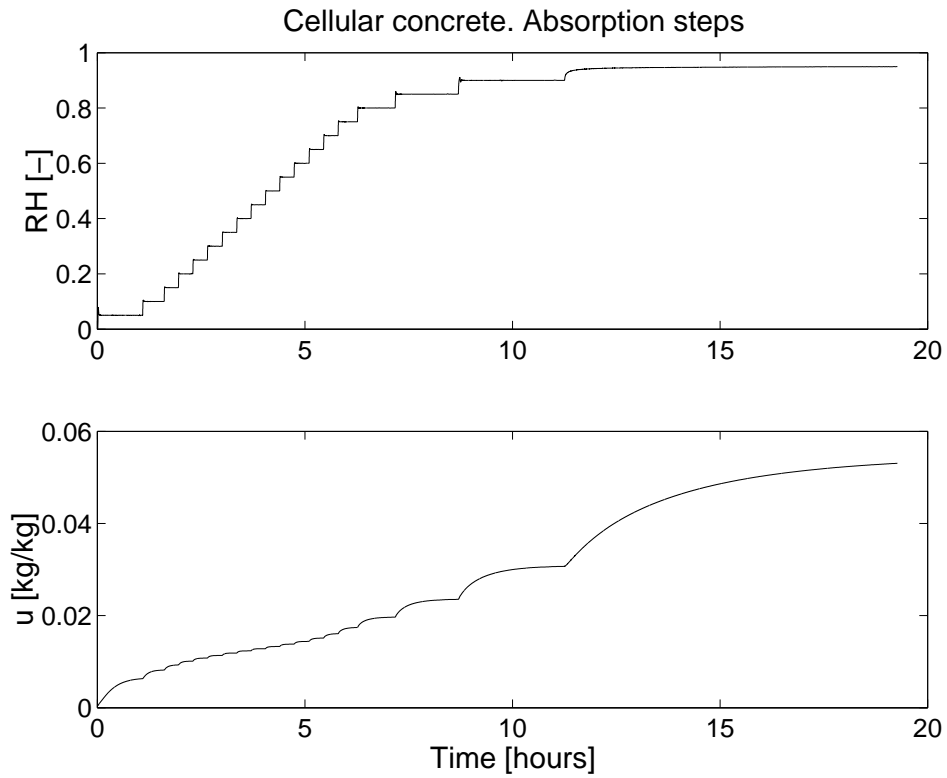
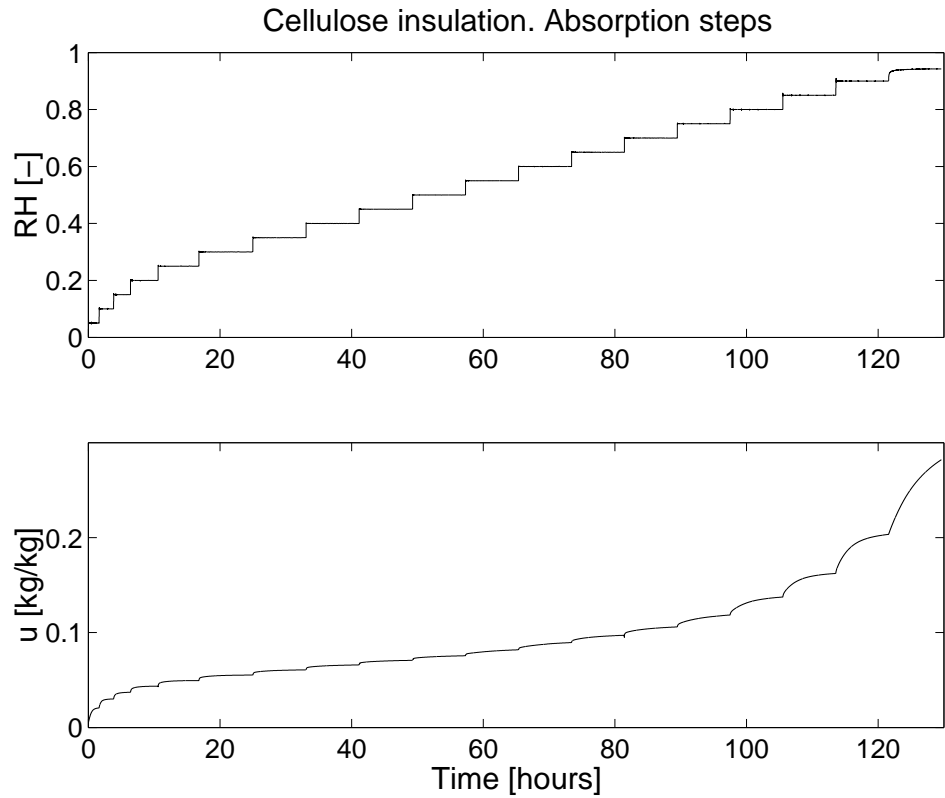
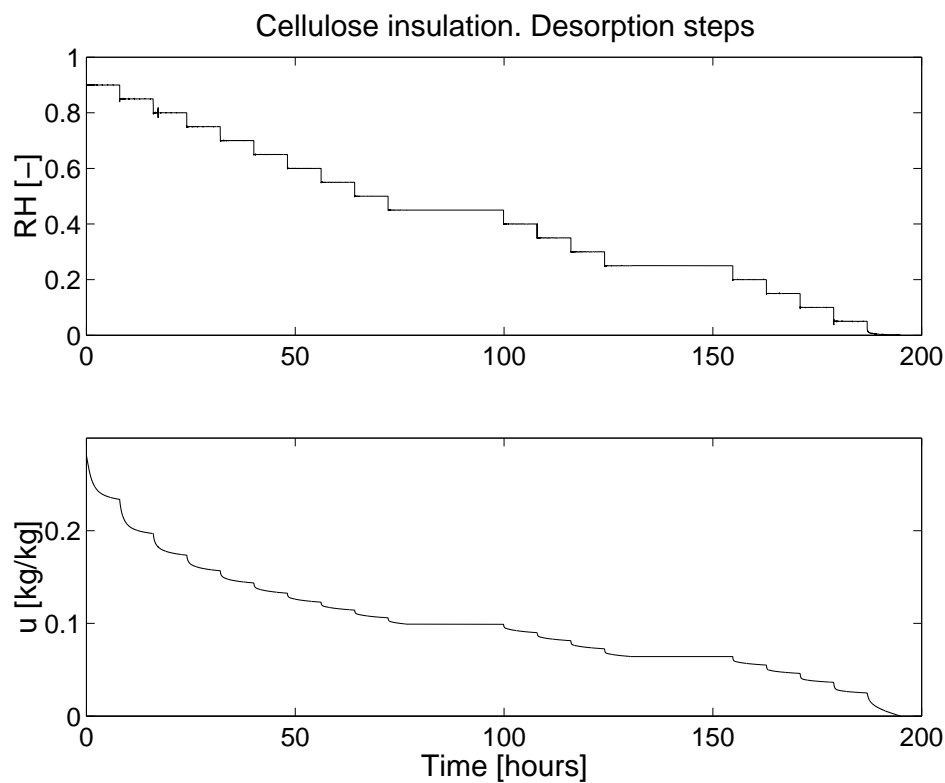


Figure B.2: IGAsorp measurements. Measured moisture content in **aerated cellular concrete** as a result of 5% - steps in relative humidity (a) Absorption steps and (b) desorption steps.



(a)



(b)

Figure B.3: IGAsorp measurements. Measured moisture content in **cellulose insulation** as a result of 5% - steps in relative humidity (a) Absorption steps and (b) desorption steps.

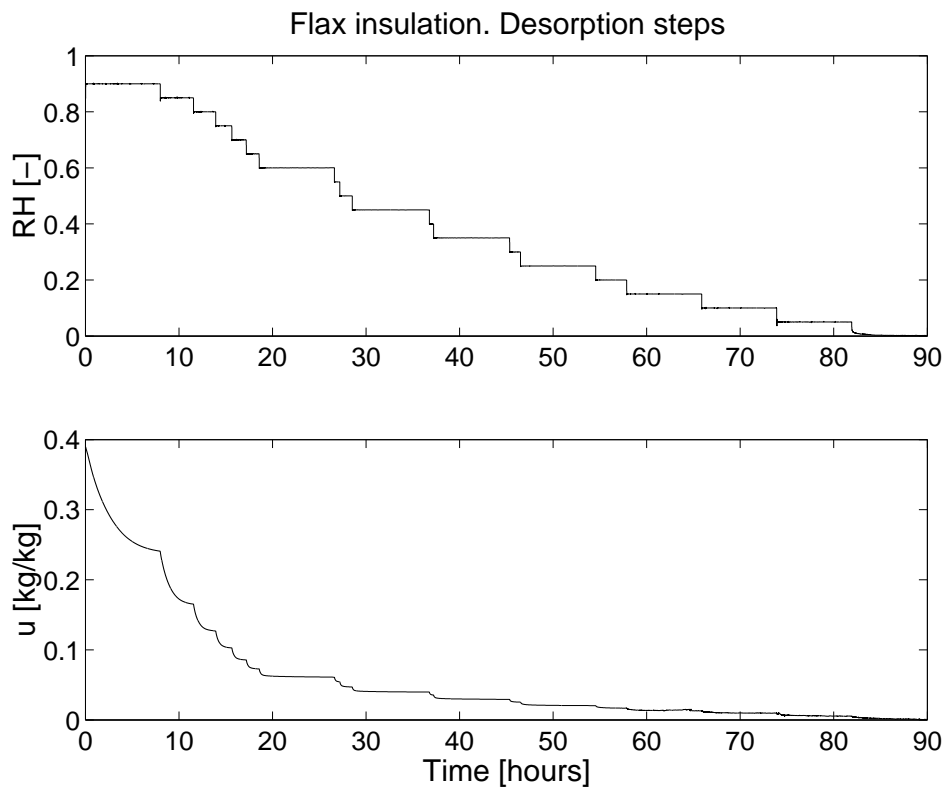
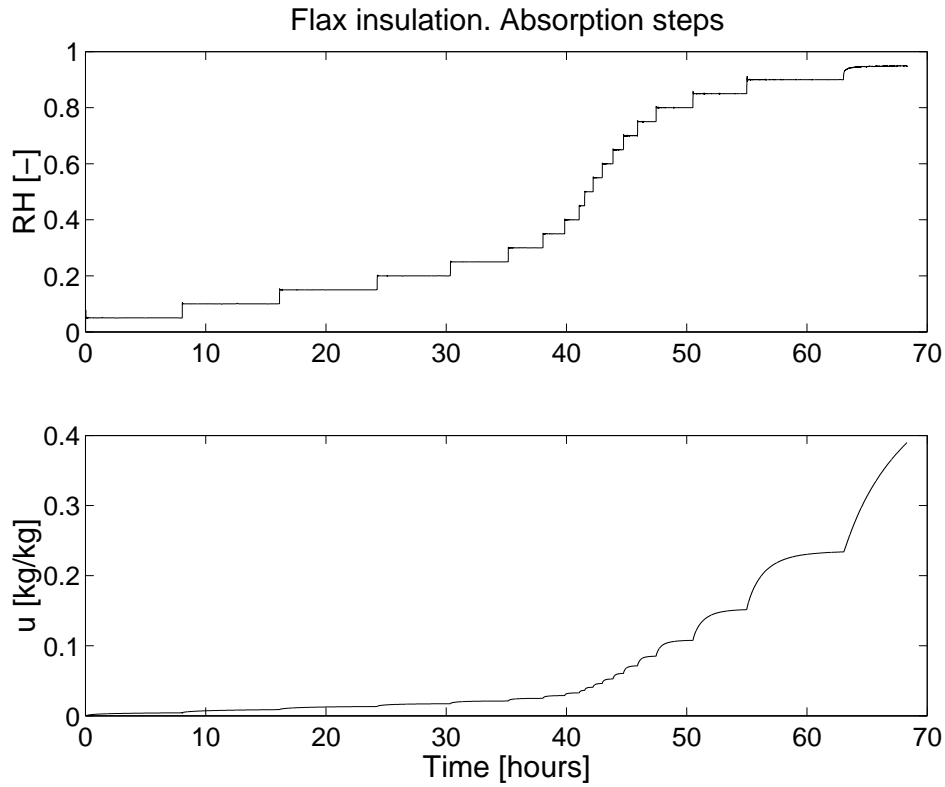


Figure B.4: IGAsorp measurements. Measured moisture content in **flax insulation** as a result of 5% - steps in relative humidity (a) Absorption steps and (b) desorption steps.

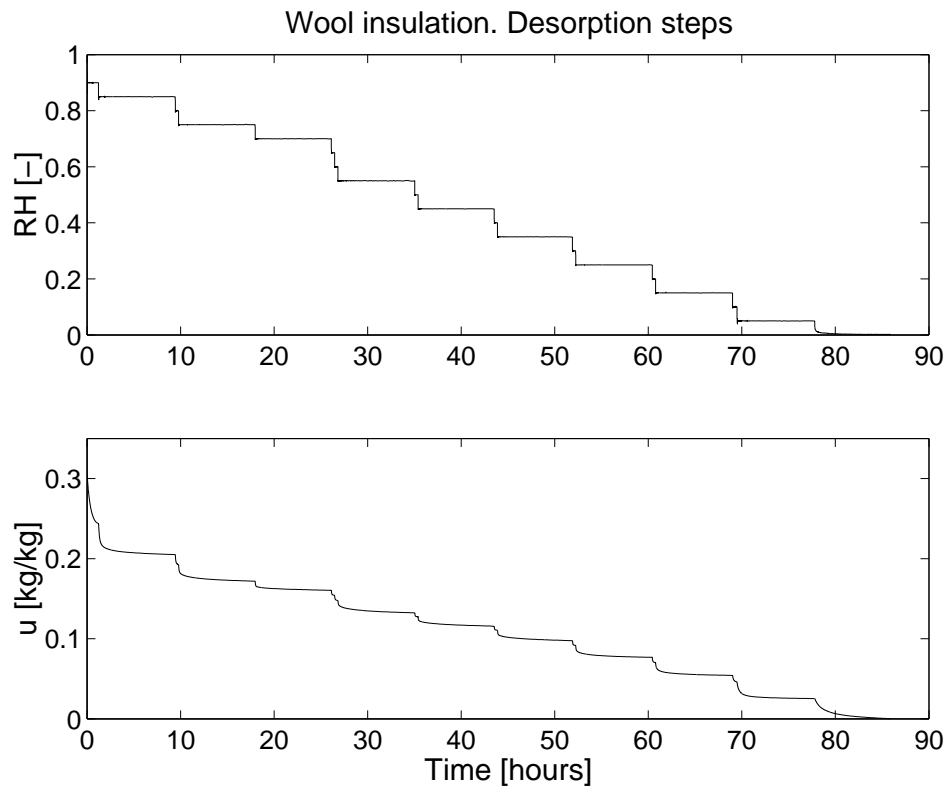
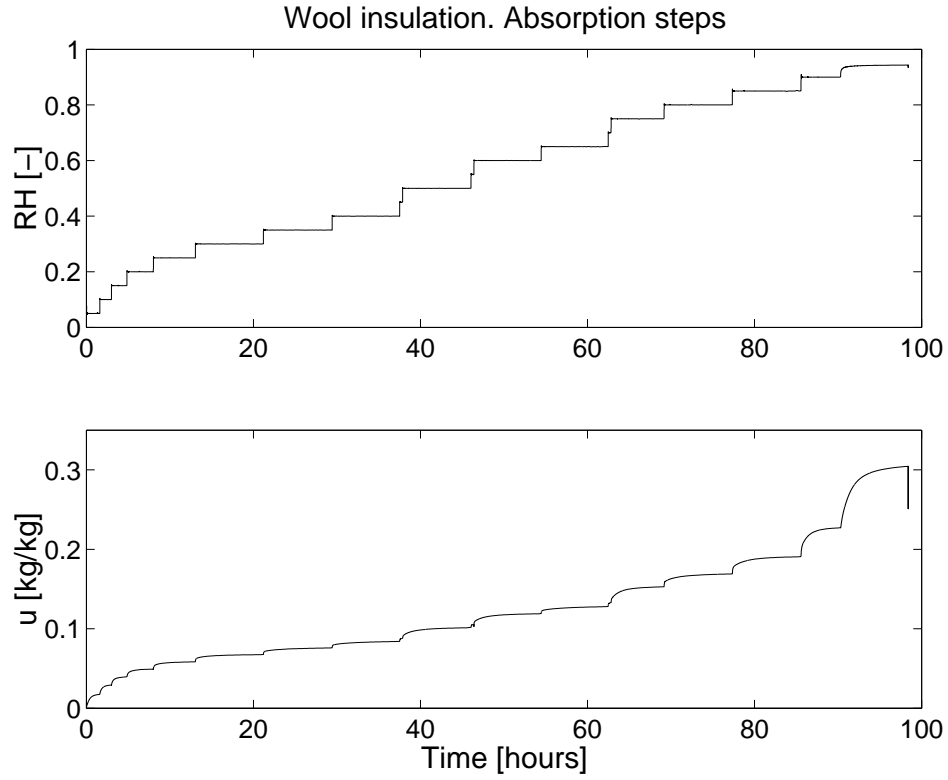
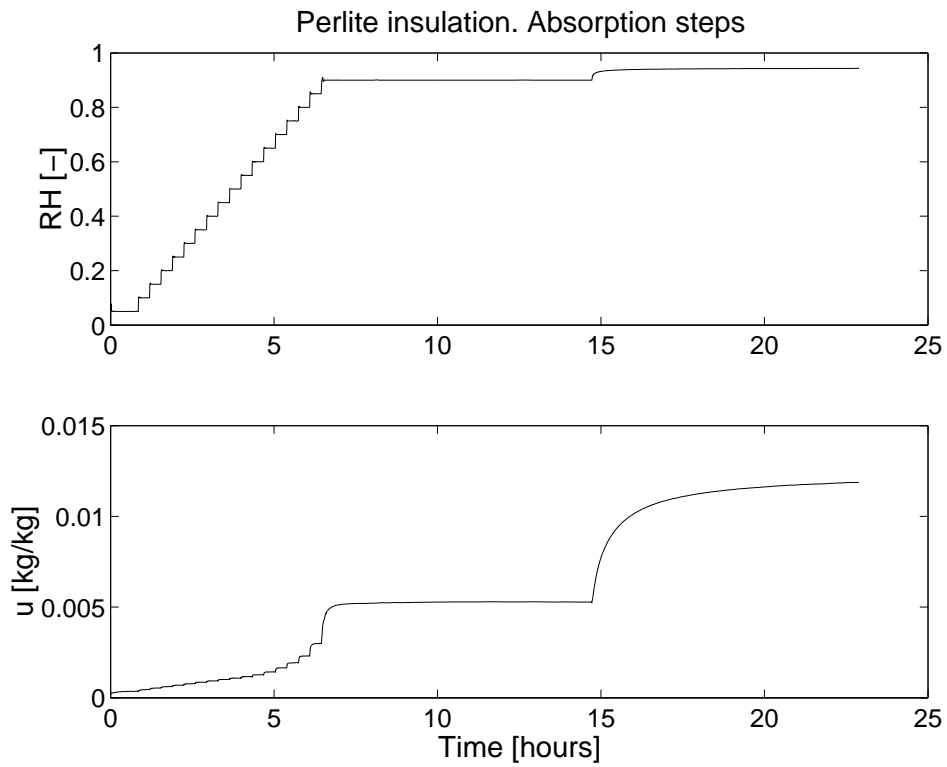
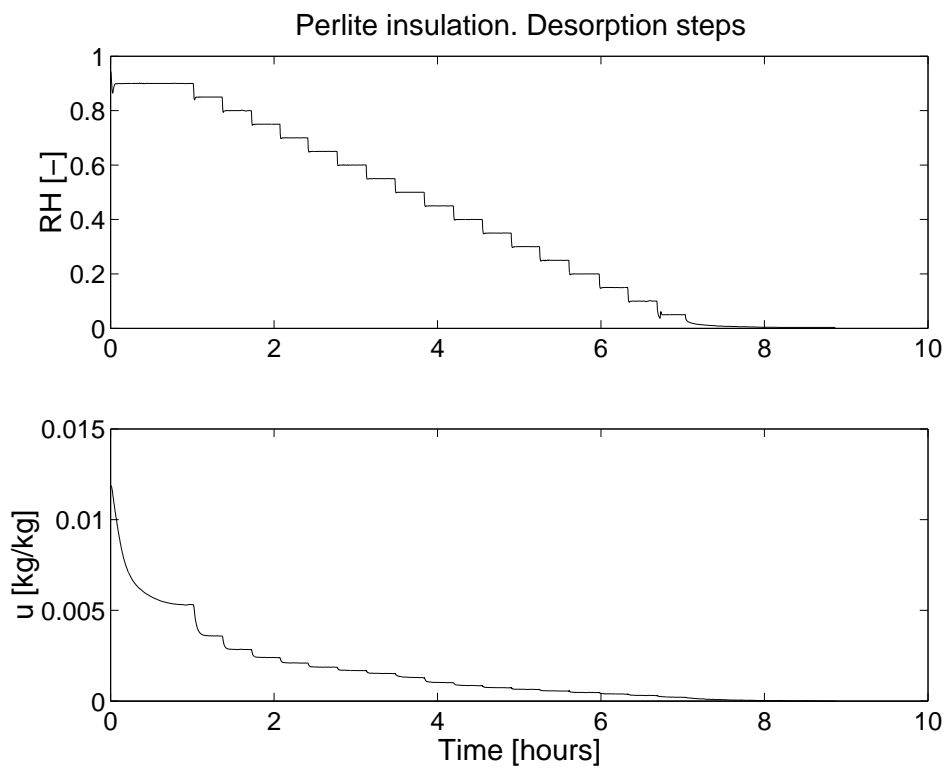


Figure B.5: IGAsorp measurements. Measured moisture content in **wool insulation** as a result of 5% - steps in relative humidity (a) Absorption steps and (b) desorption steps.

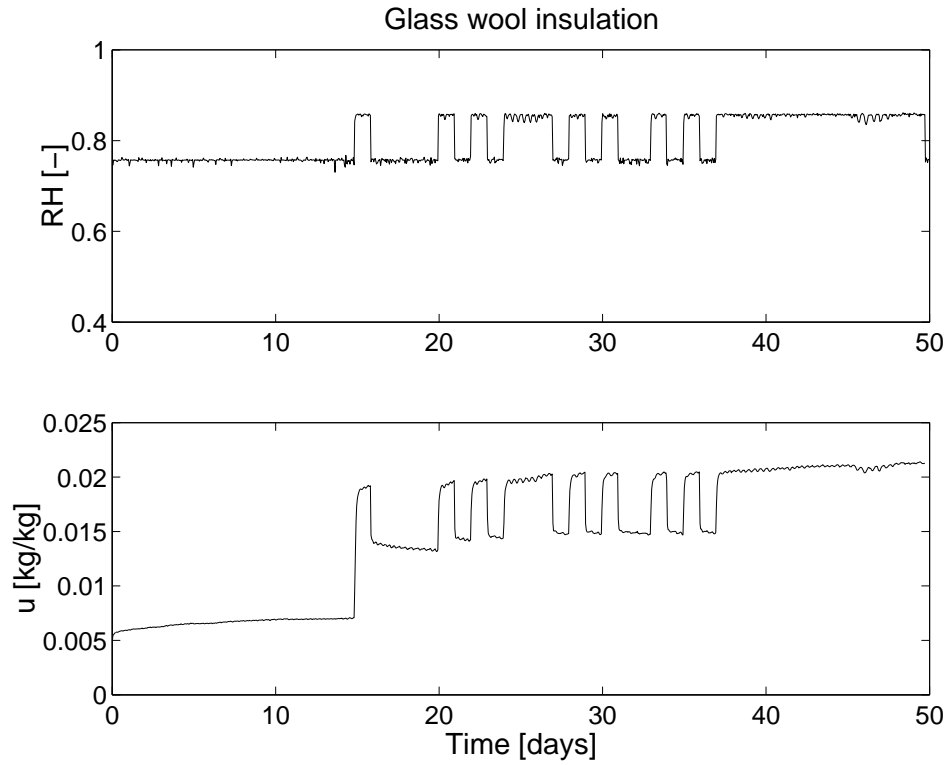


(a)

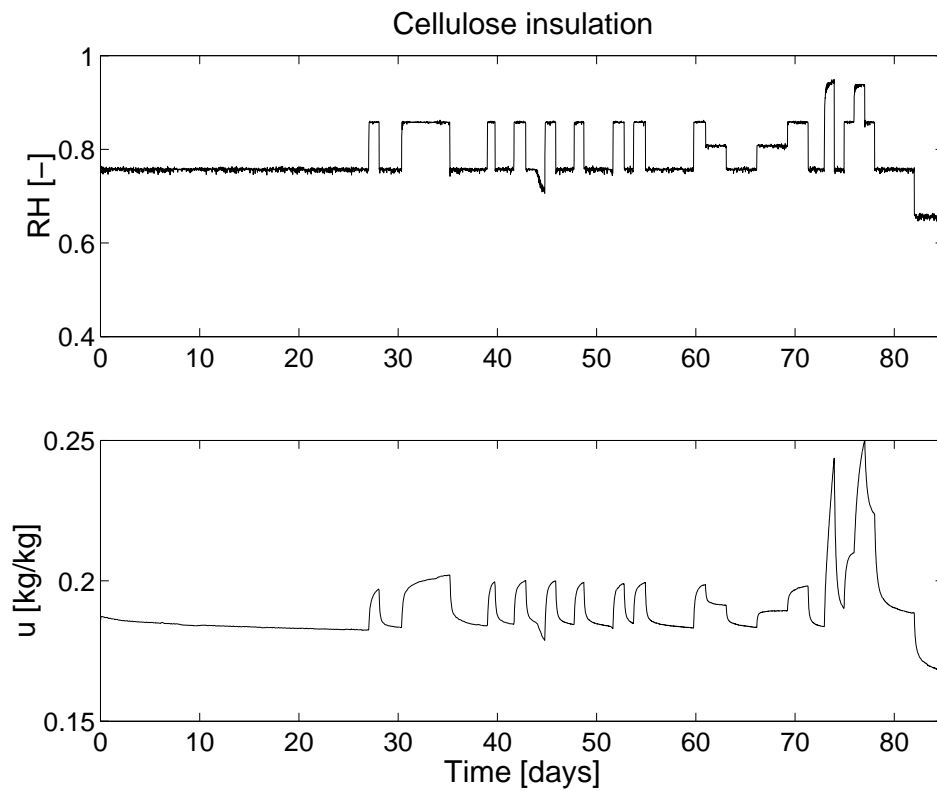


(b)

Figure B.6: IGAsorp measurements. Measured moisture content in **expanded perlite** as a result of 5% - steps in relative humidity (a) Absorption steps and (b) desorption steps.



(a)



(b)

Figure B.7: Climate chamber measurements. Measured moisture content as a result of cyclic steps in relative humidity. Temperature 20°C. (a) **Glass wool insulation** and (b) **cellulose insulation**.

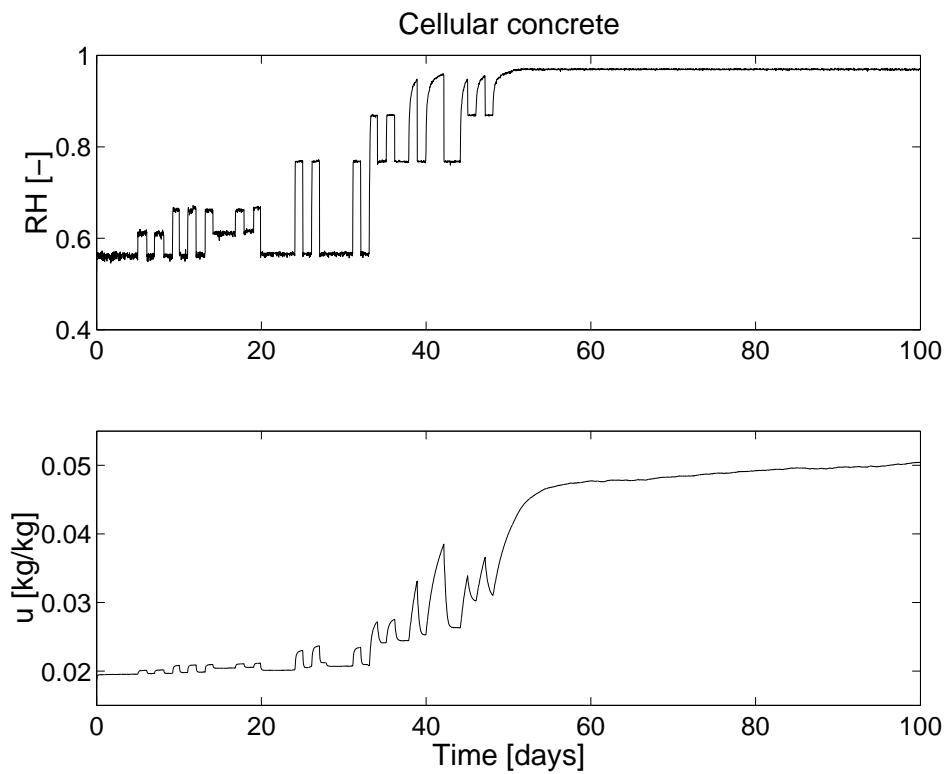
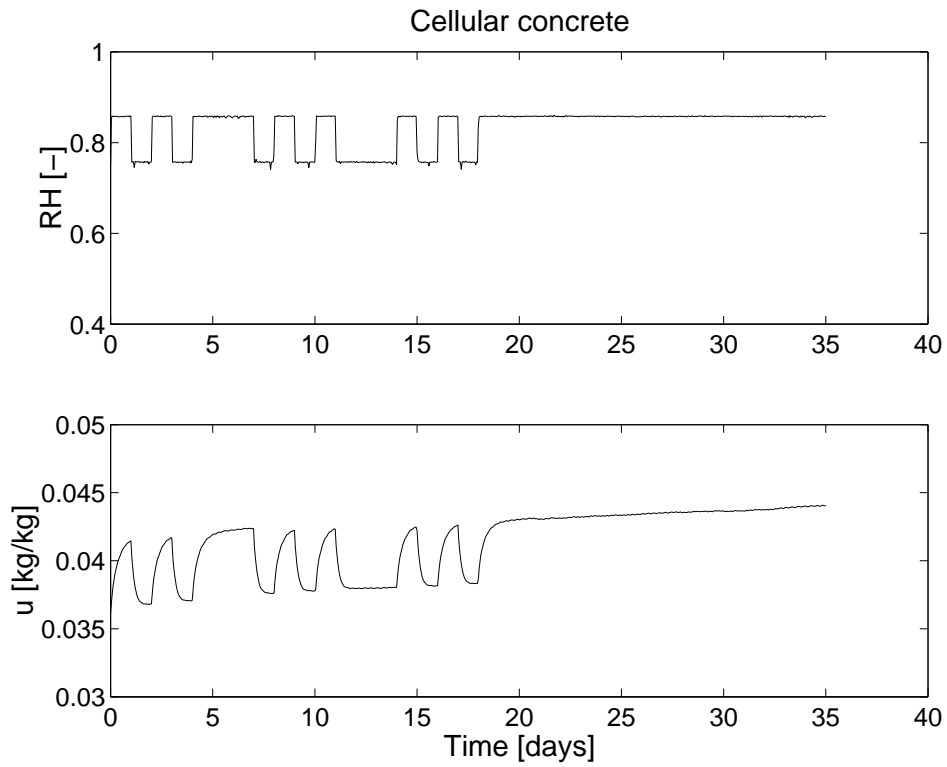


Figure B.8: Climate chamber measurements. Measured moisture content as a result of cyclic steps in relative humidity. Temperature 20°C. (a) **Cellular concrete** and (b) **cellular concrete**.

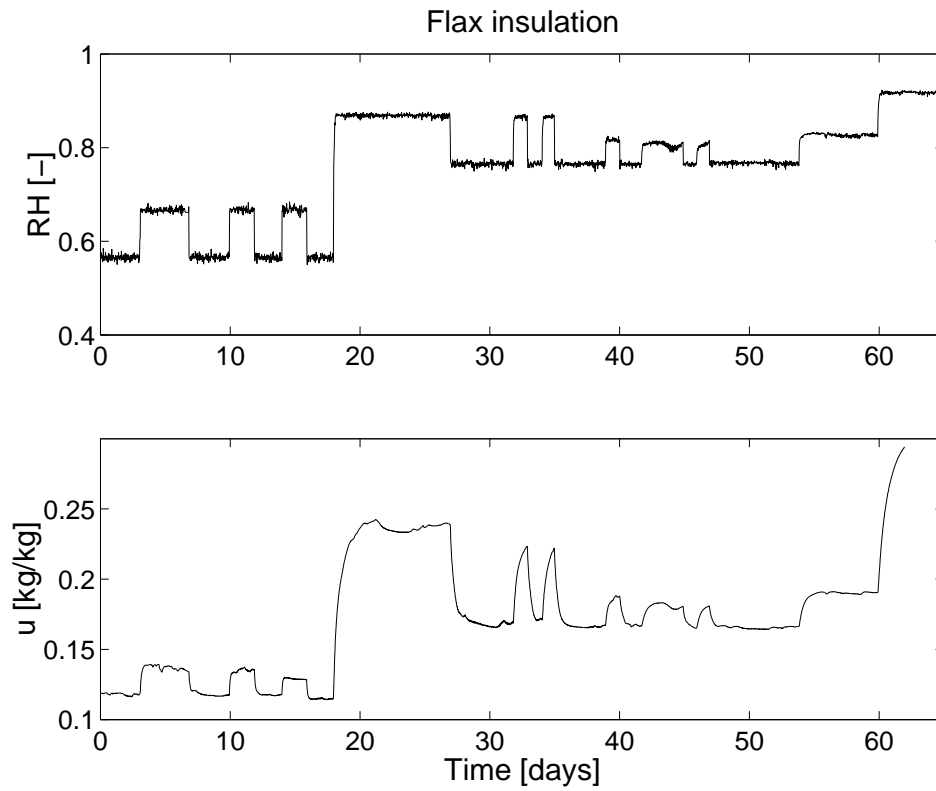


Figure B.9: Climate chamber measurements. Measured moisture content as a result of cyclic steps in relative humidity. Temperature 20°C. **Flax insulation.**

B.1.2 Non-dimensional absorption steps

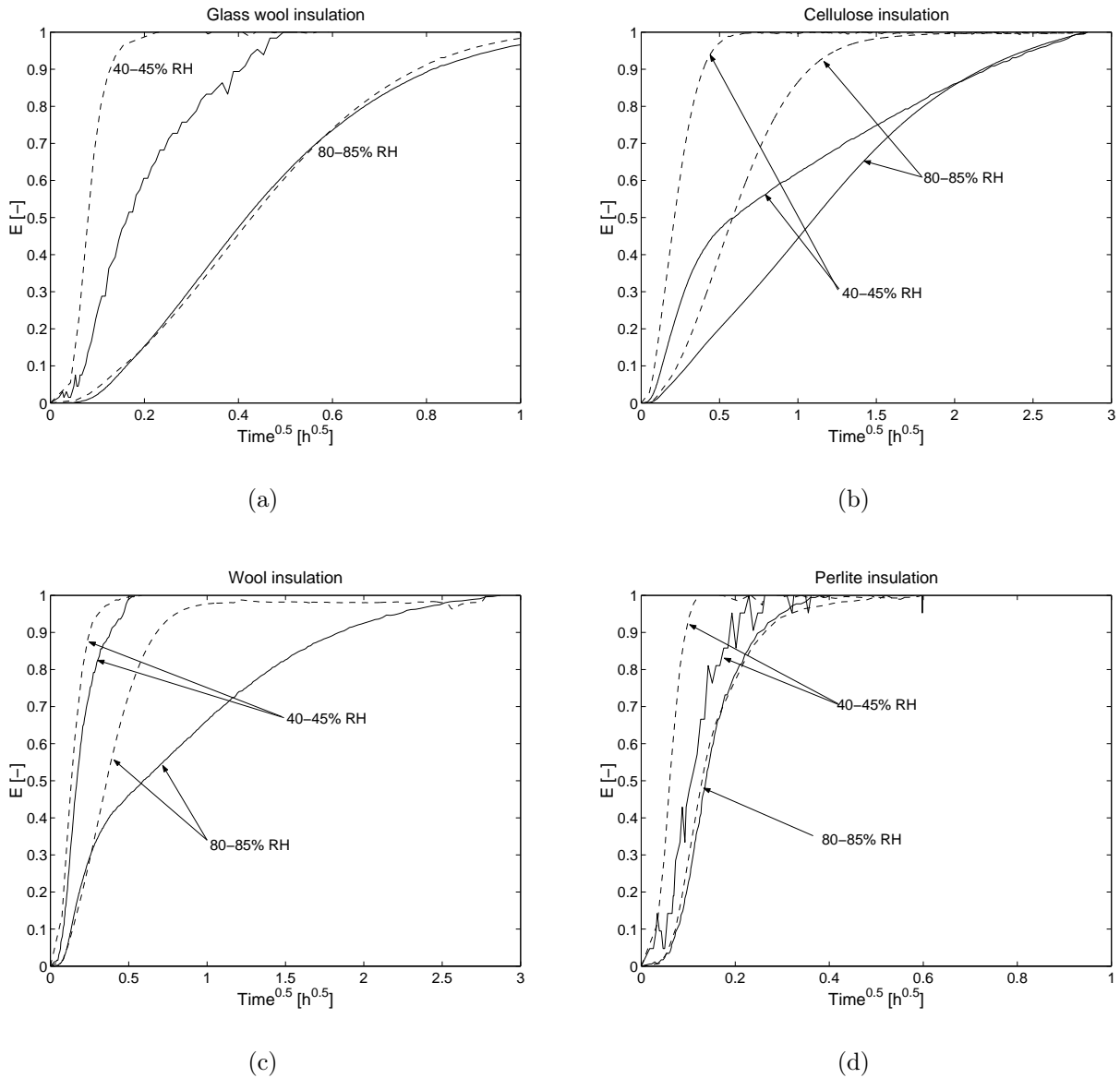


Figure B.10: Measurements with the IGAsorp equipment (—) compared with calculations with the Fickian model (- -). Absorption steps 40-45% *RH* and 80-85% *RH*. (a) Glass wool insulation, (b) cellulose insulation, (c) wool insulation and (d) perlite insulation

B.2 Non-Isothermal steady-state moisture transport

B.2.1 Relative humidity and vapour pressure profiles

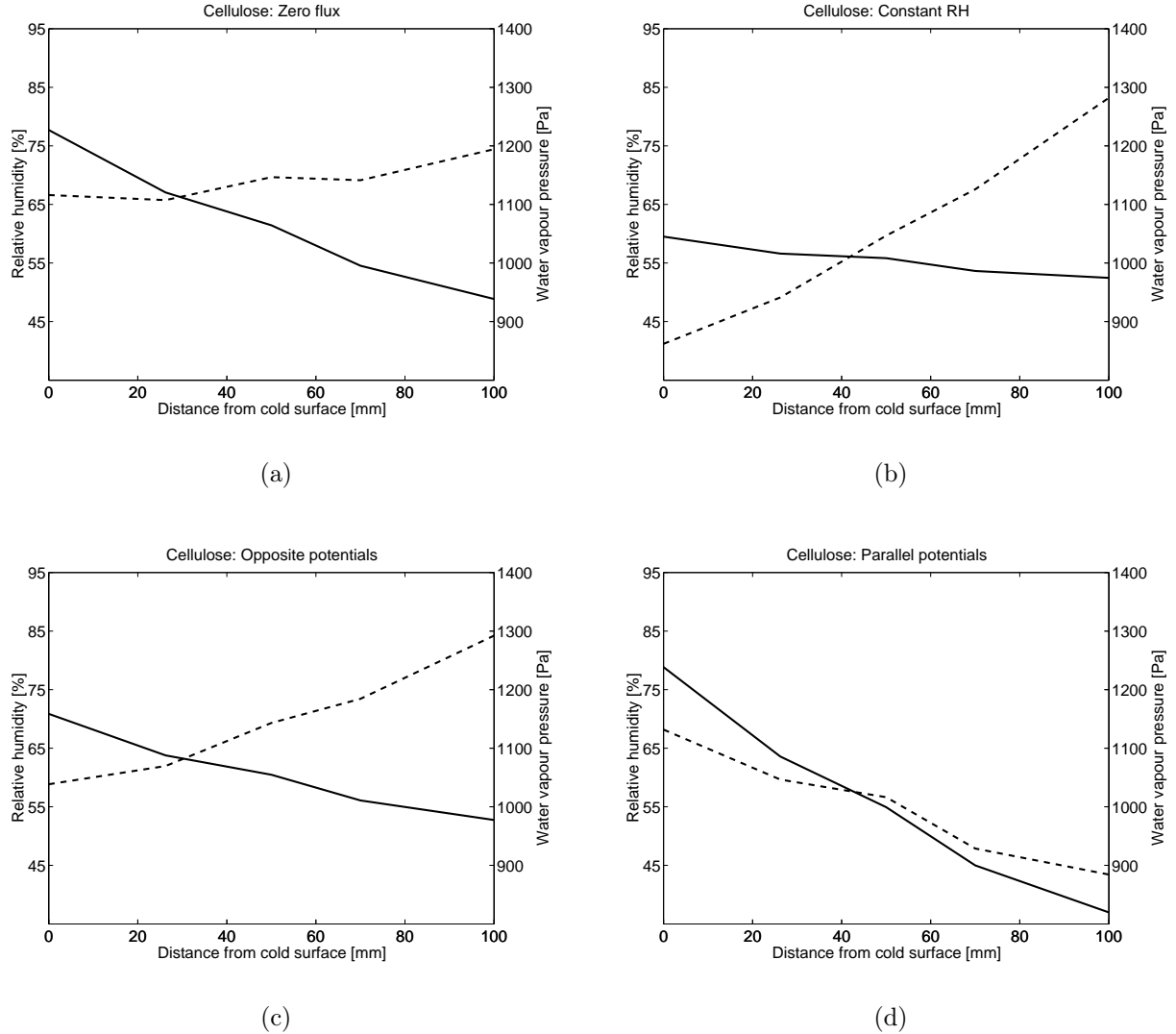


Figure B.11: Measured relative humidity (solid line) and vapour pressure (dotted line) profiles for **cellulose insulation** for boundary conditions, where the profiles are a result of the given boundary conditions: (a) **1** zero flux, (b) **2** constant RH , (c) **3** opposite potentials and (d) **4** parallel potentials.

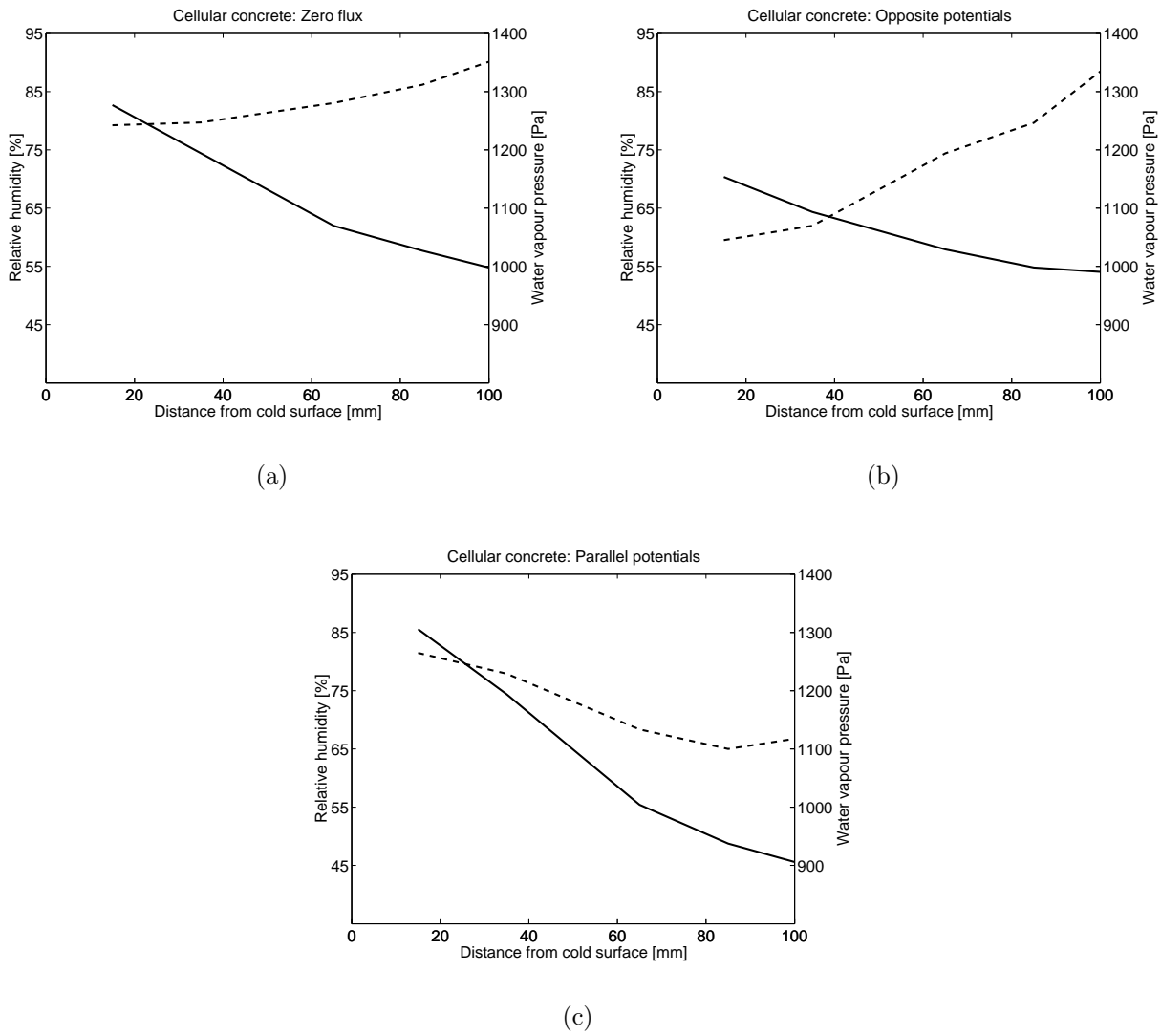


Figure B.12: Measured relative humidity (solid line) and vapour pressure (dotted line) profiles for **cellular concrete** for boundary conditions, where the profiles are a result of the given boundary conditions: (a) **1** zero flux, (b) **3** opposite potentials and (c) **4** parallel potentials.

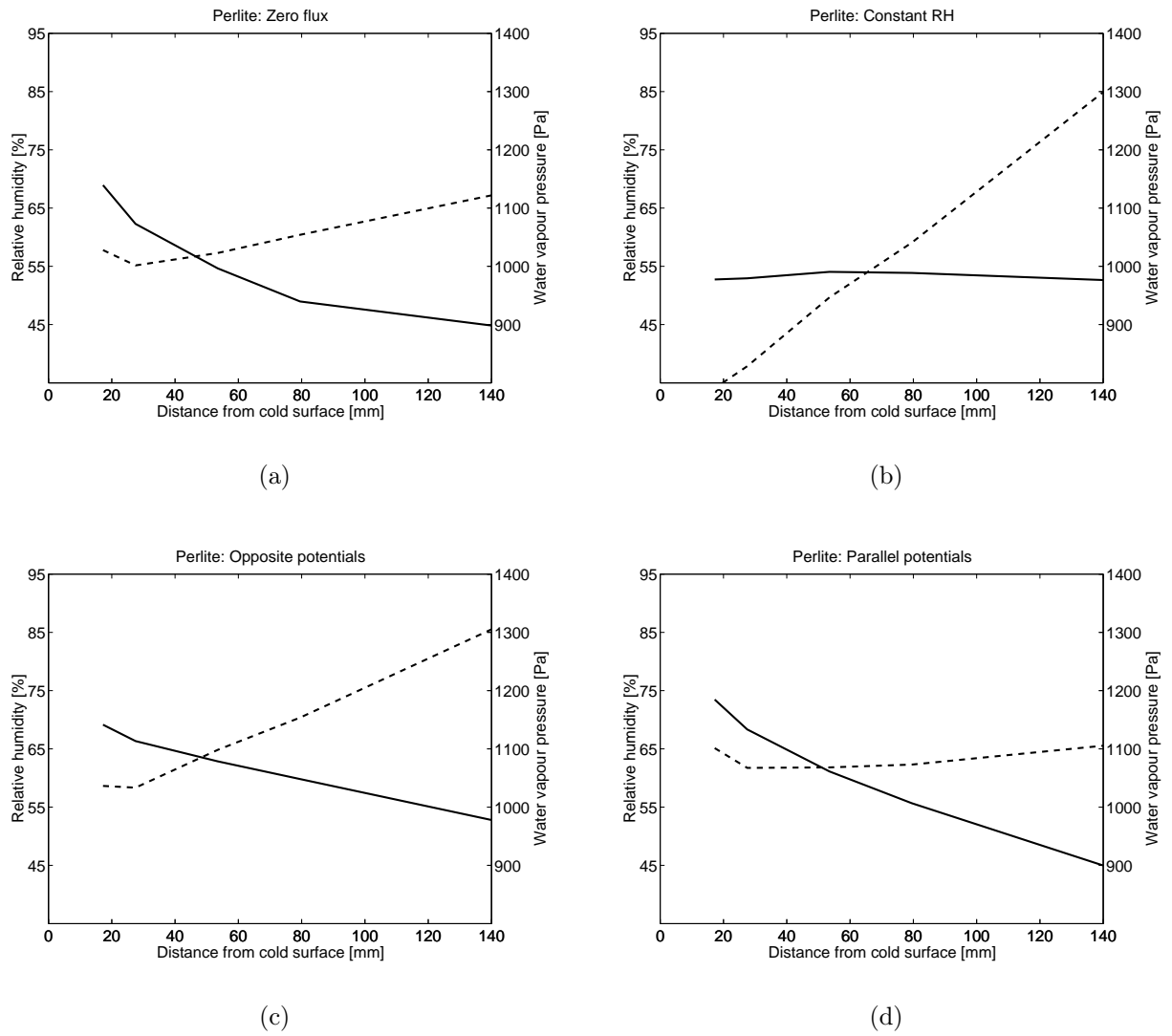


Figure B.13: Measured relative humidity (solid line) and vapour pressure (dotted line) profiles for **expanded perlite insulation** for boundary conditions, where the profiles are a result of the given boundary conditions: (a) **1** zero flux, (b) **2** constant RH , (c) **3** opposite potentials and (d) **4** parallel potentials.

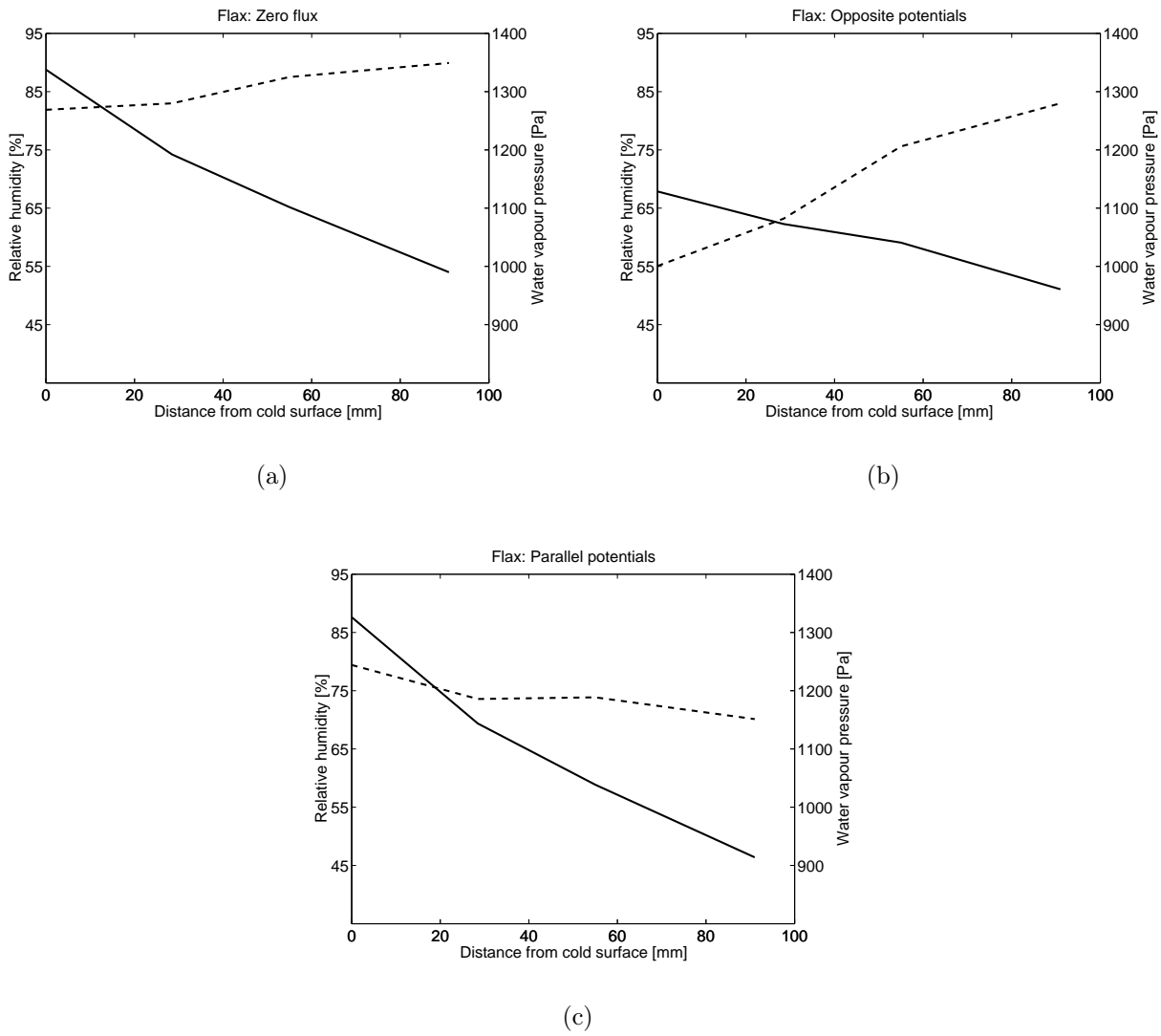


Figure B.14: Measured relative humidity (solid line) and vapour pressure (dotted line) profiles for **flax insulation** for boundary conditions, where the profiles are a result of the given boundary conditions: (a) **1** zero flux, (b) **3** opposite potentials and (c) **4** parallel potentials.

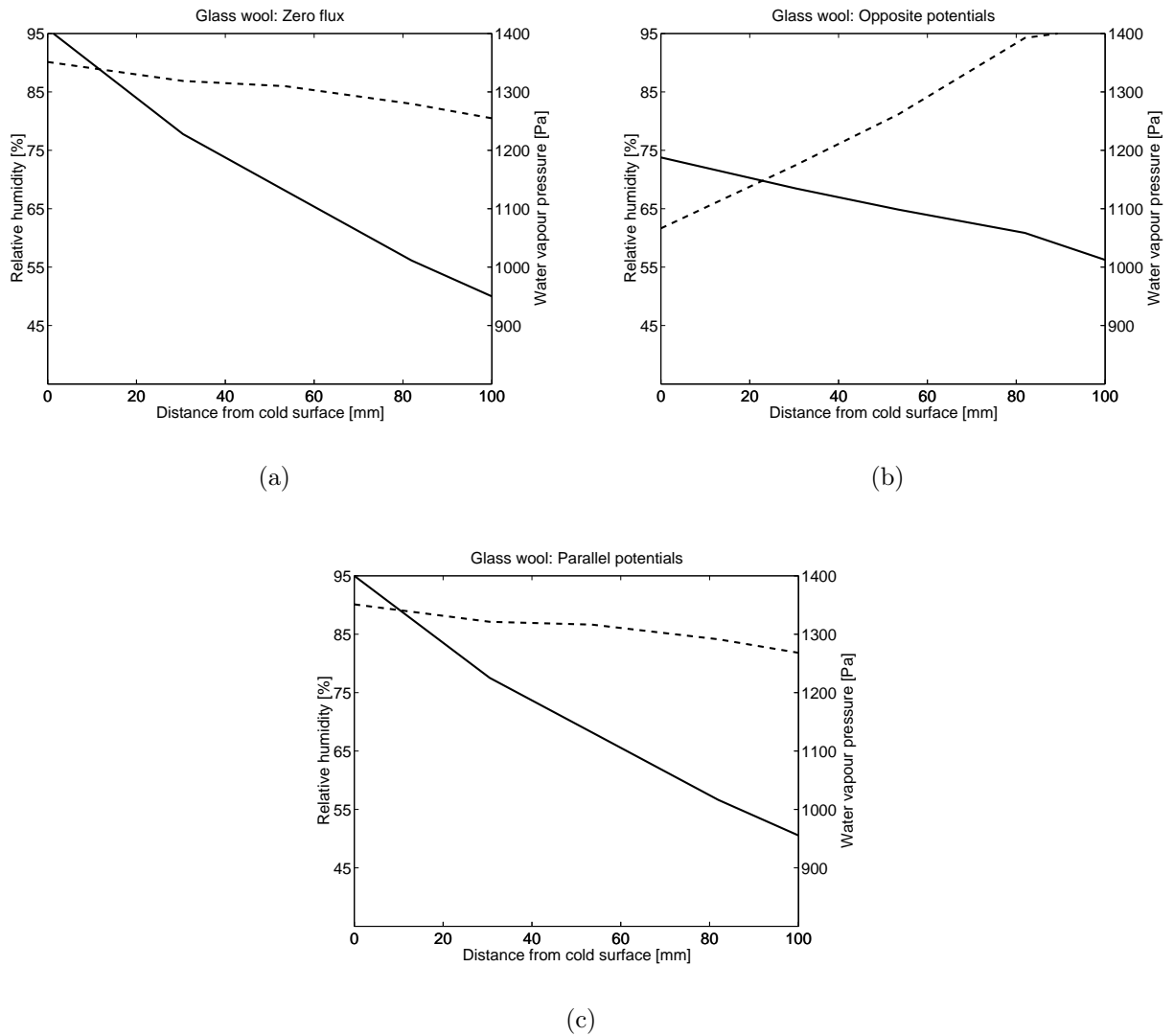


Figure B.15: Measured relative humidity (solid line) and vapour pressure (dotted line) profiles for **glass wool insulation** for boundary conditions, where the profiles are a result of the given boundary conditions: (a) **1** zero flux, (b) **3** opposite potentials and (c) **4** parallel potentials.

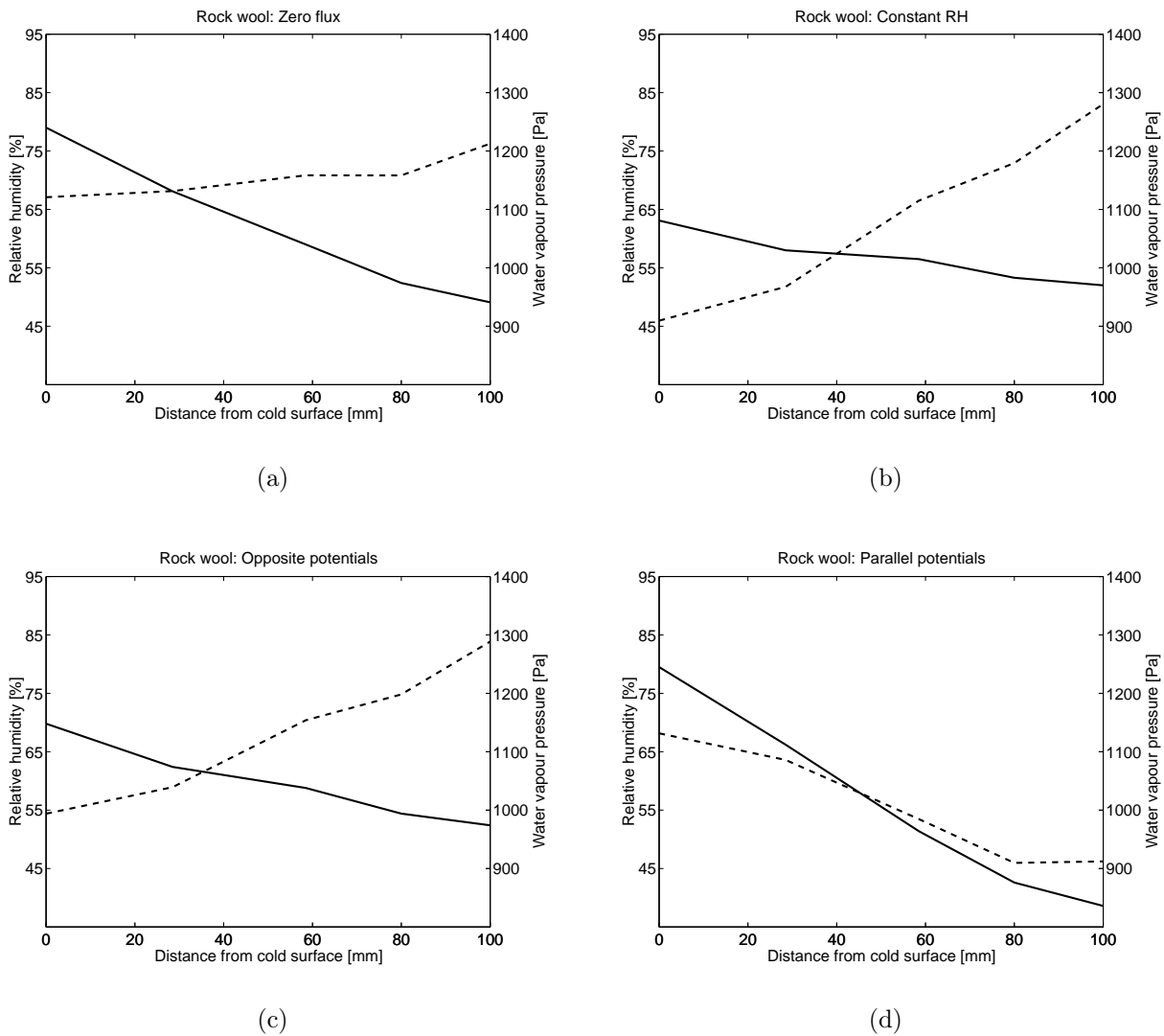


Figure B.16: Measured relative humidity (solid line) and vapour pressure (dotted line) profiles for **rock wool insulation** for boundary conditions, where the profiles are a result of the given boundary conditions: (a) **1** zero flux, (b) **2** constant RH , (c) **3** opposite potentials and (d) **4** parallel potentials.

B.2.2 Determination of transport coefficients

APPENDIX B.2.2: DETERMINATION OF TRANSPORT COEFFICIENTS

	Glass wool	Glass wool	Glass wool	Glass wool	Glass wool	Rock-wool
	zero flux	constant RH	opposite potentials	parallel potentials	parallel potentials	zero flux
days	6--6.5	13--13.5	4--4.5	1--1.5	12--12.5	10--10.2
dx	0.069	0.069	0.069	0.069	0.069	0.1
g_measured	3.98E-09	6.33E-07	5.13E-07	-6.78E-07	-5.95E-07	-2.39E-08
p-p	35	230	187	-191	-157	89
RH_cold	79.5	64.0	70.1	75.9	76.8	79.3
RH_warm	55.6	55.0	56.6	43.5	45.6	49.1
RH-RH	23.9	9.0	13.5	32.4	31.2	30.1
T_cold	12.1	12.3	12.2	12.1	12.0	12.1
T_warm	18.1	18.2	18.2	17.7	17.7	20.9
T-T	6.0	5.8	6.0	5.6	5.7	8.7
lnPc_cold	17.2	17.9	17.7	17.4	17.4	17.2
lnPc_warm	18.2	18.2	18.2	18.5	18.5	18.4
lnPc-lnPc	1.0	0.3	0.5	1.1	1.1	1.1
Pc	5.21E+07	6.92E+07	6.08E+07	6.85E+07	6.52E+07	5.92E+07
g_"other"	-8.23E-08	6.63E-08	5.28E-08	-2.07E-07	-2.08E-07	-1.87E-07
delta_p_isothermal	1.70E-10	1.70E-10	1.70E-10	1.70E-10	1.70E-10	1.83E-10
gradients:						
dp/dx	508	3334	2708	-2771	-2272	890
dT/dx	87.40	84.58	87.15	81.05	82.10	87.12
0.01*dRH/dx	3.46	1.30	1.96	4.70	4.53	3.01
Pc.dlnPc/dx	7.26E+08	3.13E+08	4.35E+08	1.12E+09	1.05E+09	6.80E+08

Verifying Eq. 6.4 with Eq. 6.9

g_diffusion	8.63E-08	5.67E-07	4.60E-07	-4.71E-07	-3.86E-07	1.63E-07
g_liquid	-2.60E-07	-1.12E-07	-1.55E-07	-4.00E-07	-3.76E-07	-4.14E-07
g_thermal	1.91E-07	1.85E-07	1.91E-07	1.77E-07	1.80E-07	2.31E-07
g_total	1.80E-08	6.40E-07	4.96E-07	-6.93E-07	-5.83E-07	-2.03E-08
g_measured	3.98E-09	6.33E-07	5.13E-07	-6.78E-07	-5.95E-07	-2.39E-08
K	-3.58E-16					-6.09E-16
D_T	2.19E-09					2.65E-09

Verifying Eq. 6.4 with Eq. 6.8

g_diffusion	2.51E-07	1.65E-06	1.34E-06	-1.37E-06	-1.12E-06	-2.09E-07
g_liquid	1.48E-06	6.39E-07	8.87E-07	2.28E-06	2.14E-06	-2.58E-06
g_thermal	-1.72E-06	-1.66E-06	-1.71E-06	-1.59E-06	-1.61E-06	2.77E-06
g_total	1.46E-08	6.26E-07	5.14E-07	-6.85E-07	-5.93E-07	-2.47E-08
g_measured	3.98E-09	6.33E-07	5.13E-07	-6.78E-07	-5.95E-07	-2.39E-08
delta_p	4.95E-10					-2.35E-10
K	2.04E-15					-3.80E-15
D_T	-1.97E-08					3.18E-08

Verifying Eqs. 2.25, 2.27 and 2.28

D_T	-9.42E-10	7.84E-10	6.06E-10	-2.56E-09	-2.54E-09	-2.14E-09
D_RH	-2.38E-08	5.09E-08	2.69E-08	-4.41E-08	-4.60E-08	-6.20E-08
D_K	-1.13E-16	2.12E-16	1.22E-16	-1.85E-16	-1.98E-16	-2.75E-16
g_p	8.63E-08	5.67E-07	4.60E-07	-4.71E-07	-3.86E-07	1.63E-07
g_T	6.85E-08	6.63E-08	6.83E-08	6.35E-08	6.44E-08	2.94E-08
g_RH	-2.05E-15	-1.35E-14	-1.09E-14	1.12E-14	9.19E-15	-9.64E-15
g_c	-5.76E-14	-3.78E-13	-3.07E-13	3.14E-13	2.58E-13	1.09E-22
Equation 2.24	1.55E-07	6.33E-07	5.29E-07	-4.08E-07	-3.22E-07	1.92E-07
Equation 2.26	8.63E-08	5.67E-07	4.60E-07	-4.71E-07	-3.86E-07	1.63E-07
Equation 2.27	8.63E-08	5.67E-07	4.60E-07	-4.71E-07	-3.86E-07	1.63E-07
g_measured	3.98E-09	6.33E-07	5.13E-07	-6.78E-07	-5.95E-07	-2.39E-08

APPENDIX B.2.2: DETERMINATION OF TRANSPORT COEFFICIENTS

Rock- wool zero flux	Rock- wool constant RH	Rock- wool constant RH	Rock- wool opposite potentials	Rock- wool opposite potentials	Rock- wool parallel potentials	Rock- wool parallel potentials	Rock- wool parallel potentials
12--12.5	12.9--13.3	14--14.3	6.8--7.2	9--9.3	3.5--4.2	5--5.2	16--16.5
0.1	0.1	0.1	0.1	0.1	0.1	0.1	0.1
-1.05E-09	7.00E-07	6.69E-07	7.92E-07	5.06E-07	-5.12E-07	-8.59E-07	-5.75E-07
92	370	347	382	295	-107	-218	-146
79.0	63.1	64.9	61.7	69.8	78.6	79.5	75.5
49.1	52.0	52.2	51.8	52.4	41.6	38.6	38.4
29.9	11.1	12.7	9.9	17.3	37.1	40.9	37.0
12.2	12.4	12.4	12.5	12.2	12.2	12.2	12.1
20.9	20.8	20.8	20.8	20.8	20.6	20.2	20.4
8.7	8.4	8.4	8.3	8.6	8.4	7.9	8.3
17.2	17.9	17.9	18.0	17.7	17.3	17.2	17.4
18.4	18.3	18.3	18.3	18.3	18.6	18.7	18.7
1.1	0.4	0.4	0.3	0.6	1.3	1.4	1.3
5.96E+07	7.38E+07	7.16E+07	7.58E+07	6.59E+07	6.80E+07	7.03E+07	7.52E+07
-1.69E-07	2.25E-08	3.42E-08	9.34E-08	-3.45E-08	-3.15E-07	-4.59E-07	-3.09E-07
1.83E-10	1.83E-10	1.83E-10	1.83E-10	1.83E-10	1.83E-10	1.83E-10	1.83E-10
917	3704	3467	3819	2951	-1073	-2185	-1456
87.21	84.00	83.77	83.47	85.72	84.13	79.50	82.78
2.99	1.11	1.27	0.99	1.73	3.71	4.09	3.70
6.77E+08	2.79E+08	3.13E+08	2.55E+08	4.04E+08	9.00E+08	1.02E+09	9.41E+08
1.68E-07	6.78E-07	6.34E-07	6.99E-07	5.40E-07	-1.96E-07	-4.00E-07	-2.66E-07
-4.12E-07	-1.70E-07	-1.91E-07	-1.56E-07	-2.46E-07	-5.49E-07	-6.21E-07	-5.73E-07
2.31E-07	2.23E-07	2.22E-07	2.22E-07	2.28E-07	2.23E-07	2.11E-07	2.20E-07
-1.32E-08	7.31E-07	6.66E-07	7.65E-07	5.21E-07	-5.22E-07	-8.10E-07	-6.20E-07
-1.05E-09	7.00E-07	6.69E-07	7.92E-07	5.06E-07	-5.12E-07	-8.59E-07	-5.75E-07
-2.16E-07	-8.71E-07	-8.15E-07	-8.98E-07	-6.94E-07	2.52E-07	5.14E-07	3.42E-07
-2.57E-06	-1.06E-06	-1.19E-06	-9.70E-07	-1.53E-06	-3.42E-06	-3.87E-06	-3.58E-06
2.77E-06	2.67E-06	2.66E-06	2.65E-06	2.72E-06	2.67E-06	2.53E-06	2.63E-06
-1.61E-08	7.36E-07	6.58E-07	7.84E-07	4.95E-07	-4.96E-07	-8.32E-07	-6.03E-07
-1.05E-09	7.00E-07	6.69E-07	7.92E-07	5.06E-07	-5.12E-07	-8.59E-07	-5.75E-07
-1.94E-09	2.68E-10	4.08E-10	1.12E-09	-4.03E-10	-3.75E-09	-5.77E-09	-3.73E-09
-5.64E-08	2.04E-08	2.69E-08	9.47E-08	-1.99E-08	-8.52E-08	-1.12E-07	-8.33E-08
-2.50E-16	8.06E-17	1.09E-16	3.66E-16	-8.55E-17	-3.50E-16	-4.50E-16	-3.28E-16
1.68E-07	6.78E-07	6.34E-07	6.99E-07	5.40E-07	-1.96E-07	-4.00E-07	-2.66E-07
2.95E-08	2.84E-08	2.83E-08	2.82E-08	2.90E-08	2.84E-08	2.69E-08	2.80E-08
-9.93E-15	-4.01E-14	-3.75E-14	-4.14E-14	-3.20E-14	1.16E-14	2.37E-14	1.58E-14
1.08E-22	4.46E-23	5.00E-23	4.08E-23	6.45E-23	1.44E-22	1.63E-22	1.50E-22
1.97E-07	7.06E-07	6.63E-07	7.27E-07	5.69E-07	-1.68E-07	-3.73E-07	-2.39E-07
1.68E-07	6.78E-07	6.34E-07	6.99E-07	5.40E-07	-1.96E-07	-4.00E-07	-2.66E-07
1.68E-07	6.78E-07	6.34E-07	6.99E-07	5.40E-07	-1.96E-07	-4.00E-07	-2.66E-07
-1.05E-09	7.00E-07	6.69E-07	7.92E-07	5.06E-07	-5.12E-07	-8.59E-07	-5.75E-07

APPENDIX B.2.2: DETERMINATION OF TRANSPORT COEFFICIENTS

	Cellular concrete	Cellular concrete	Cellular concrete	Cellular concrete	Cellulose	Cellulose
	opposite potentials	opposite potentials	parallel potential	zero flux	opposite potentials	parallel potentials
days	82.5--83.5	96--98	115--116	65.5--66.5	17.5--18.5	7.5--8.5
dx	0.0925	0.0925	0.0925	0.0925	0.1	0.1
g_measured	4.42E-08	1.42E-07	-3.04E-07	1.06E-08	3.03E-07	-1.93E-07
p-p	177	290	-147	111	254	-19
RH_cold	78.4	70.4	85.6	82.6	70.9	80.0
RH_warm	54.3	54.0	45.6	54.8	52.8	45.6
RH-RH	24.1	16.3	40.0	27.8	18.1	34.5
T_cold	12.9	12.9	12.8	13.0	12.7	12.2
T_warm	20.9	20.9	20.8	20.9	20.7	20.8
T-T	8.0	8.0	8.0	7.8	8.1	8.6
lnPc_cold	17.3	17.7	16.8	17.0	17.6	17.2
lnPc_warm	18.2	18.2	18.5	18.2	18.3	18.5
lnPc-lnPc	0.9	0.6	1.6	1.2	0.6	1.3
Pc	5.50E+07	6.35E+07	5.64E+07	5.02E+07	6.43E+07	6.22E+07
g_"other"	-1.69E-09	6.66E-08	-2.66E-07	-1.81E-08	2.40E-08	-1.73E-07
delta_p_isothermal	2.40E-11	2.40E-11	2.40E-11	2.40E-11	1.10E-10	1.10E-10
gradients:						
dp/dx	1912	3132	-1592	1196	2539	-187
dT/dx	86.73	86.62	86.09	84.55	80.88	85.86
0.01*dRH/dx	2.61	1.76	4.32	3.01	1.81	3.45
Pc.dlnPc/dx	5.63E+08	4.03E+08	1.00E+09	6.38E+08	4.16E+08	8.02E+08

**Verifying Eq. 6.4
with Eq. 6.9**

g_diffusion	4.59E-08	7.52E-08	-3.82E-08	2.87E-08	2.79E-07	-2.06E-08
g_liquid	-3.16E-07	-2.26E-07	-5.63E-07	-3.58E-07	-4.66E-07	-8.99E-07
g_thermal	3.14E-07	3.13E-07	3.11E-07	3.06E-07	4.72E-07	5.02E-07
g_total	4.35E-08	1.62E-07	-2.90E-07	-2.37E-08	2.85E-07	-4.18E-07
g_measured	4.42E-08	1.42E-07	-3.04E-07	1.06E-08	3.03E-07	-1.93E-07
K	-5.61E-16				-1.12E-15	
D_T	3.62E-09				5.84E-09	

**Verifying Eq. 6.4
with Eq. 6.8**

g_diffusion	1.55E-06	2.54E-06	-1.29E-06	9.70E-07	-3.29E-06	2.42E-07
g_liquid	3.16E-06	2.27E-06	5.64E-06	3.59E-06	-4.86E-06	-9.36E-06
g_thermal	-4.67E-06	-4.66E-06	-4.63E-06	-4.55E-06	8.29E-06	8.80E-06
g_total	4.58E-08	1.44E-07	-2.86E-07	4.30E-09	1.40E-07	-3.19E-07
g_measured	4.42E-08	1.42E-07	-3.04E-07	1.06E-08	3.03E-07	-1.93E-07
delta_p	8.11E-10				-1.30E-09	
K	5.62E-15				-1.17E-14	
D_T	-5.38E-08				1.02E-07	

**Verifying Eqs.
2.25, 2.27 and 2.28**

D_T	-1.95E-11	7.69E-10	-3.09E-09	-2.14E-10	2.96E-10	-2.01E-09
D_RH	-6.50E-10	3.78E-08	-6.16E-08	-6.00E-09	1.32E-08	-5.01E-08
D_K	-3.01E-18	1.65E-16	-2.65E-16	-2.83E-17	5.75E-17	-2.15E-16
g_p	4.59E-08	7.52E-08	-3.82E-08	2.87E-08	2.79E-07	-2.06E-08
g_T	6.67E-08	6.66E-08	6.62E-08	6.50E-08	8.67E-08	9.20E-08
g_RH	-1.56E-08	-1.06E-08	-2.59E-08	-1.81E-08	-5.31E-08	-1.01E-07
g_c	-5.41E-14	-8.87E-14	4.51E-14	-3.39E-14	-5.36E-08	-1.03E-07
Equation 2.24	1.13E-07	1.42E-07	2.80E-08	9.37E-08	3.66E-07	7.15E-08
Equation 2.26	3.02E-08	6.46E-08	-6.42E-08	1.06E-08	2.26E-07	-1.21E-07
Equation 2.27	4.59E-08	7.52E-08	-3.82E-08	2.87E-08	2.26E-07	-1.24E-07
g_measured	4.42E-08	1.42E-07	-3.04E-07	1.06E-08	3.03E-07	-1.93E-07

APPENDIX B.2.2: DETERMINATION OF TRANSPORT COEFFICIENTS

Cellulose	Cellulose	Cellulose	Flax	Flax	Flax	Flax	Flax
parallel potentials	constant RH	zero flux	opposite potentials	opposite potentials	opposite potentials	opposite potentials	parallel potential
43--44	38--39	33.5--34.5	25--25.5	46--46.5	51.5--52.5	72.5--73.5	33--34
0.1	0.1	0.1	0.09	0.09	0.09	0.09	0.09
-1.24E-06	5.50E-07	1.45E-09	4.88E-07	1.49E-07	5.29E-07	1.52E-07	-3.84E-07
-247	420	78	311	161	342	135	-93
78.8	59.5	77.7	67.5	82.3	68.0	57.8	87.6
37.0	52.5	48.9	51.9	53.3	53.4	45.9	46.4
41.9	7.0	28.9	15.6	28.9	14.6	11.9	41.2
12.3	12.5	12.3	12.6	12.2	12.5	15.2	12.2
20.4	20.7	20.7	21.0	21.1	21.0	20.9	21.0
8.0	8.2	8.4	8.5	8.8	8.5	5.7	8.8
17.3	18.0	17.3	17.8	17.1	17.7	18.1	16.7
18.7	18.3	18.4	18.3	18.3	18.3	18.5	18.5
1.5	0.2	1.1	0.5	1.2	0.5	0.4	1.8
7.30E+07	7.76E+07	6.12E+07	6.89E+07	5.20E+07	6.68E+07	8.82E+07	5.35E+07
-9.69E-07	8.81E-08	-8.46E-08	-3.10E-08	-1.20E-07	-4.14E-08	-7.33E-08	-2.30E-07
1.10E-10	1.10E-10	1.10E-10	1.50E-10	1.50E-10	1.50E-10	1.50E-10	1.50E-10
-2474	4202	782	3458	1791	3802	1503	-1028
80.17	82.23	83.61	93.99	98.29	94.35	63.33	97.51
4.19	0.70	2.89	1.73	3.21	1.63	1.33	4.58
1.07E+09	1.90E+08	6.56E+08	4.14E+08	6.93E+08	3.84E+08	3.65E+08	1.06E+09
-2.72E-07	4.62E-07	8.60E-08	5.19E-07	2.69E-07	5.70E-07	2.25E-07	-1.54E-07
-1.19E-06	-2.13E-07	-7.35E-07	-1.13E-07	-1.88E-07	-1.04E-07	-9.91E-08	-2.89E-07
4.68E-07	4.80E-07	4.88E-07	6.98E-08	7.30E-08	7.01E-08	4.71E-08	7.25E-08
-9.97E-07	7.29E-07	-1.61E-07	4.76E-07	1.53E-07	5.36E-07	1.73E-07	-3.71E-07
-1.24E-06	5.50E-07	1.45E-09	4.88E-07	1.49E-07	5.29E-07	1.52E-07	-3.84E-07
			-2.72E-16				
			7.43E-10				
3.21E-06	-5.45E-06	-1.01E-06	8.56E-07	4.44E-07	9.42E-07	3.72E-07	-2.55E-07
-1.24E-05	-2.22E-06	-7.66E-06	1.79E-07	2.99E-07	1.66E-07	1.57E-07	4.59E-07
8.22E-06	8.43E-06	8.57E-06	-5.62E-07	-5.88E-07	-5.64E-07	-3.79E-07	-5.83E-07
-1.01E-06	7.59E-07	-1.04E-07	4.73E-07	1.55E-07	5.43E-07	1.51E-07	-3.79E-07
-1.24E-06	5.50E-07	1.45E-09	4.88E-07	1.49E-07	5.29E-07	1.52E-07	-3.84E-07
			2.48E-10				
			4.32E-16				
			-5.98E-09				
-1.21E-08	1.07E-09	-1.01E-09	-3.30E-10	-1.22E-09	-4.39E-10	-1.16E-09	-2.36E-09
-2.31E-07	1.25E-07	-2.93E-08	-1.79E-08	-3.72E-08	-2.54E-08	-5.53E-08	-5.03E-08
-9.09E-16	4.63E-16	-1.29E-16	-7.49E-17	-1.73E-16	-1.08E-16	-2.01E-16	-2.16E-16
-2.72E-07	4.62E-07	8.60E-08	5.19E-07	2.69E-07	5.70E-07	2.25E-07	-1.54E-07
8.59E-08	8.81E-08	8.96E-08	-1.09E-07	-1.14E-07	-1.09E-07	-7.33E-08	-1.13E-07
-1.23E-07	-2.06E-08	-8.46E-08	-5.71E-08	-1.06E-07	-5.37E-08	-4.38E-08	-1.51E-07
-1.37E-07	-2.45E-08	-8.46E-08	-5.26E-13	-2.73E-13	-5.79E-13	-2.29E-13	1.56E-13
-1.86E-07	5.50E-07	1.76E-07	4.10E-07	1.55E-07	4.61E-07	1.52E-07	-2.67E-07
-3.95E-07	4.42E-07	1.45E-09	4.62E-07	1.63E-07	5.17E-07	1.82E-07	-3.05E-07
-4.09E-07	4.38E-07	1.45E-09	5.19E-07	2.69E-07	5.70E-07	2.25E-07	-1.54E-07
-1.24E-06	5.50E-07	1.45E-09	4.88E-07	1.49E-07	5.29E-07	1.52E-07	-3.84E-07

APPENDIX B.2.2: DETERMINATION OF TRANSPORT COEFFICIENTS

	Flax	Perlite	Perlite	Perlite	Perlite	Perlite
	zero flux	opposite potentials	opposite potentials	parallel potential	constant RH	zero flux
days	19--20	16.9--17.2	52.5--53	55.5--56	53.9--54.2	3--4
dx	0.09	0.083	0.123	0.123	0.123	0.083
g_measured	6.69E-09	2.15E-07	1.58E-07	-1.12E-07	3.84E-07	-2.57E-09
p-p	81	262	269	5	509	92
RH_cold	88.8	69.8	69.1	73.5	52.7	80.5
RH_warm	54.0	52.2	52.8	45.0	52.6	51.5
RH-RH	34.8	17.6	16.4	28.5	0.1	28.9
T_cold	12.3	13.0	13.0	13.0	13.0	12.9
T_warm	21.1	21.1	20.9	20.8	20.9	21.1
T-T	8.8	8.1	7.9	7.8	7.9	8.2
lnPc_cold	16.6	17.7	17.7	17.5	18.3	17.2
lnPc_warm	18.2	18.3	18.3	18.5	18.3	18.3
lnPc-lnPc	1.7	0.6	0.6	1.0	0.0	1.1
Pc	4.51E+07	6.62E+07	6.63E+07	7.01E+07	8.58E+07	5.56E+07
g_"other"	-1.28E-07	-1.11E-07	-6.71E-08	-1.16E-07	-4.17E-08	-1.17E-07
delta_p_isothermal	1.50E-10	1.03E-10	1.03E-10	1.03E-10	1.03E-10	1.03E-10
gradients:						
dp/dx	895	3159	2190	44	4135	1113
dT/dx	97.69	97.85	64.24	63.47	63.88	98.80
0.01*dRH/dx	3.86	2.12	1.33	2.32	0.01	3.49
Pc.dlnPc/dx	8.39E+08	4.95E+08	3.10E+08	5.58E+08	2.06E+07	7.66E+08
Verifying Eq. 6.4 with Eq. 6.9						
g_diffusion	1.34E-07	3.25E-07	2.26E-07	4.49E-09	4.26E-07	1.15E-07
g_liquid	-2.28E-07	-4.08E-08	-2.55E-08	-4.59E-08	-1.70E-09	-6.31E-08
g_thermal	7.26E-08	-6.14E-08	-4.03E-08	-3.99E-08	-4.01E-08	-6.20E-08
g_total	-2.11E-08	2.23E-07	1.60E-07	-8.13E-08	3.84E-07	-1.05E-08
g_measured	6.69E-09	2.15E-07	1.58E-07	-1.12E-07	3.84E-07	-2.57E-09
K		-8.23E-17				
D_T		-6.28E-10				
Verifying Eq. 6.4 with Eq. 6.8						
g_diffusion	2.22E-07	3.31E-07	2.29E-07	4.56E-09	4.33E-07	1.17E-07
g_liquid	3.62E-07	-3.39E-08	-2.12E-08	-3.81E-08	-1.41E-09	-5.24E-08
g_thermal	-5.84E-07	-7.34E-08	-4.82E-08	-4.76E-08	-4.79E-08	-7.41E-08
g_total	-5.73E-10	2.23E-07	1.60E-07	-8.12E-08	3.83E-07	-9.99E-09
g_measured	6.69E-09	2.15E-07	1.58E-07	-1.12E-07	3.84E-07	-2.57E-09
delta_p		1.05E-10				
K		-6.83E-17				
D_T		-7.50E-10				
Verifying Eqs. 2.25, 2.27 and 2.28						
D_T	-1.31E-09	-1.13E-09	-1.05E-09	-1.84E-09	-6.54E-10	-1.19E-09
D_RH	-3.30E-08	-5.21E-08	-5.05E-08	-5.03E-08	-6.21E-06	-3.36E-08
D_K	-1.52E-16	-2.23E-16	-2.16E-16	-2.09E-16	-2.03E-15	-1.53E-16
g_p	1.34E-07	3.25E-07	2.26E-07	4.49E-09	4.26E-07	1.15E-07
g_T	-1.13E-07	-6.39E-08	-4.20E-08	-4.15E-08	-4.17E-08	-6.46E-08
g_RH	-1.28E-07	-7.64E-08	-4.78E-08	-8.33E-08	-2.42E-10	-1.25E-07
g_c	-1.36E-13	-4.82E-13	-3.34E-13	-6.64E-15	-6.31E-13	-1.70E-13
Equation 2.24	2.12E-08	2.61E-07	1.84E-07	-3.70E-08	3.84E-07	5.01E-08
Equation 2.26	6.69E-09	2.49E-07	1.78E-07	-7.88E-08	4.26E-07	-1.07E-08
Equation 2.27	1.34E-07	3.25E-07	2.26E-07	4.49E-09	4.26E-07	1.15E-07
g_measured	6.69E-09	2.15E-07	1.58E-07	-1.12E-07	3.84E-07	-2.57E-09

APPENDIX B.2.2: DETERMINATION OF TRANSPORT COEFFICIENTS

Perlite	Perlite	Perlite
zero flux	zero flux	zero flux
5--6	8.5--9.5	74--76
0.083	0.083	0.123
-5.73E-10	-7.66E-10	6.94E-10
89	94	82
71.4	68.9	74.4
46.2	44.8	49.1
25.2	24.1	25.3
13.0	12.9	13.0
21.1	21.1	20.7
8.1	8.2	7.7
17.6	17.7	17.5
18.5	18.5	18.4
0.9	0.8	0.9
7.12E+07	7.55E+07	6.44E+07
-1.11E-07	-1.18E-07	-6.82E-08
1.03E-10	1.03E-10	1.03E-10
1073	1134	669
98.01	98.42	62.36
3.03	2.90	2.06
7.35E+08	7.25E+08	4.74E+08
1.10E-07	1.17E-07	6.89E-08
-6.05E-08	-5.97E-08	-3.90E-08
-6.15E-08	-6.18E-08	-3.92E-08
-1.15E-08	-4.72E-09	-9.26E-09
-5.73E-10	-7.66E-10	6.94E-10
1.12E-07	1.19E-07	7.00E-08
-5.02E-08	-4.95E-08	-3.24E-08
-7.35E-08	-7.38E-08	-4.68E-08
-1.15E-08	-4.74E-09	-9.15E-09
-5.73E-10	-7.66E-10	6.94E-10
-1.13E-09	-1.19E-09	-1.09E-09
-3.66E-08	-4.05E-08	-3.32E-08
-1.51E-16	-1.62E-16	-1.44E-16
1.10E-07	1.17E-07	6.89E-08
-6.41E-08	-6.43E-08	-4.08E-08
-1.09E-07	-1.04E-07	-7.40E-08
-1.64E-13	-1.73E-13	-1.02E-13
4.64E-08	5.24E-08	2.82E-08
1.35E-09	1.23E-08	-5.10E-09
1.10E-07	1.17E-07	6.89E-08
-5.73E-10	-7.66E-10	6.94E-10

B.2.3 Identifying driving potentials

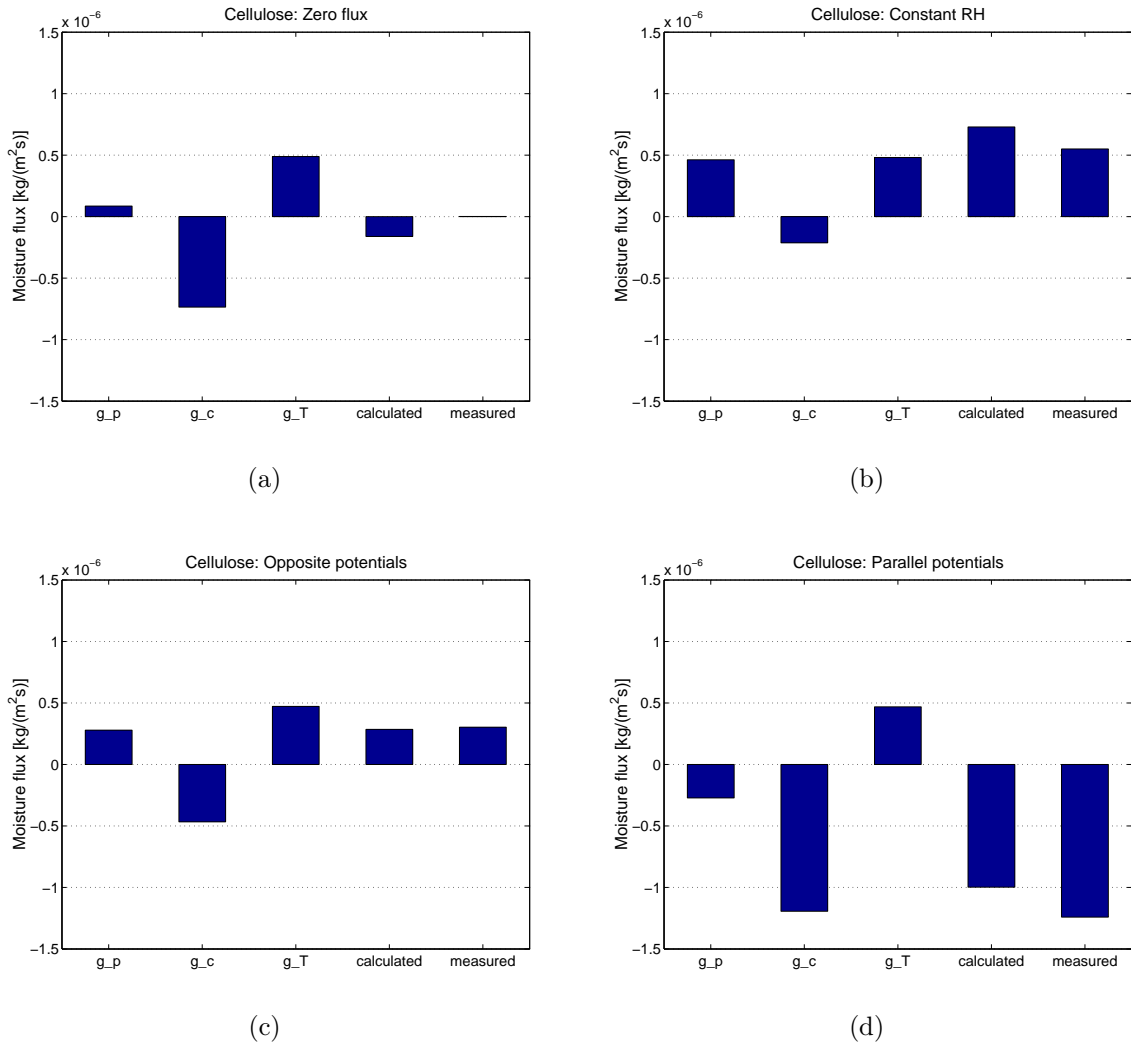


Figure B.17: The identifying of the 'other' transport for **cellulose**, divided in 3 contributions: water vapour diffusion $g_{diffusion}$ (g_p), liquid transport g_{liquid} (g_c) and any temperature gradient induced transport $g_{thermal}$ (g_T). The water vapour pressure driven transport is based on the determined isothermal permeability and the actual boundary conditions. Liquid K and thermal D_T transport coefficients are determined by solving a set of linear equations with 2 unknowns with least squares method (Matrix 6.9). The calculated set contributions $g_{calculated}$ are compared with the total measured transport $g_{measured}$. (a) zero flux (condition **1**), (b) constant RH (condition **2**), (c) opposite potentials (condition **3**) and (d) parallel potentials (condition **4**). The flux is positive from room to Megacup, i.e. from warm to cold.

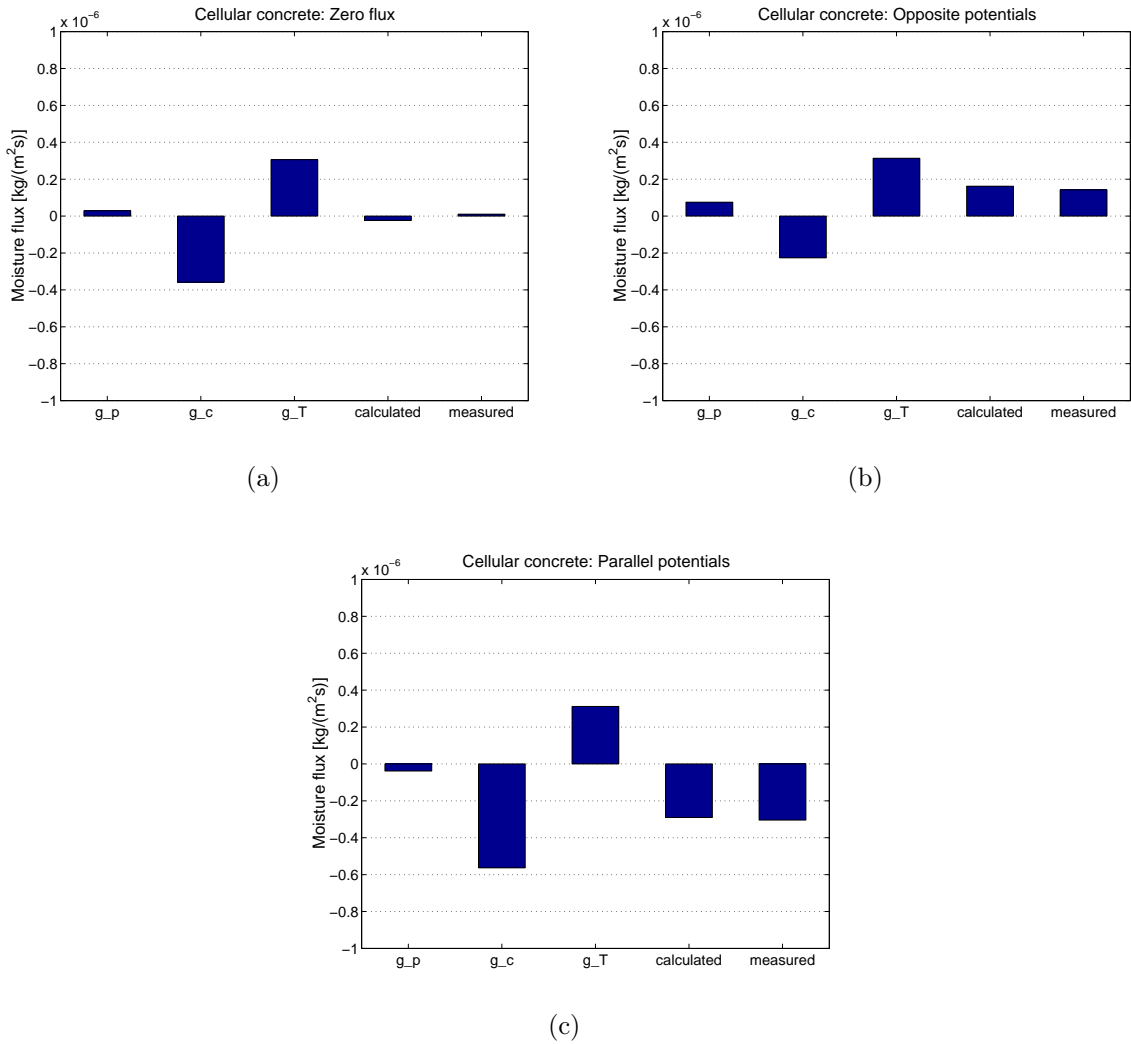


Figure B.18: The identifying of the 'other' transport for **cellular concrete**, divided in 3 contributions: water vapour diffusion $g_{diffusion}$ (g_p), liquid transport g_{liquid} (g_c) and any temperature gradient induced transport $g_{thermal}$ (g_T). The water vapour pressure driven transport is based on the determined isothermal permeability and the actual boundary conditions. Liquid K and thermal D_T transport coefficients are determined by solving a set of linear equations with 2 unknowns with least squares method (Matrix 6.9). The calculated contributions $g_{calculated}$ are compared with the total measured transport $g_{measured}$. (a) zero flux (condition **1**), (b) opposite potentials (condition **3**) and (c) parallel potentials (condition **4**). The flux is positive from room to Megacup, i.e. from warm to cold.

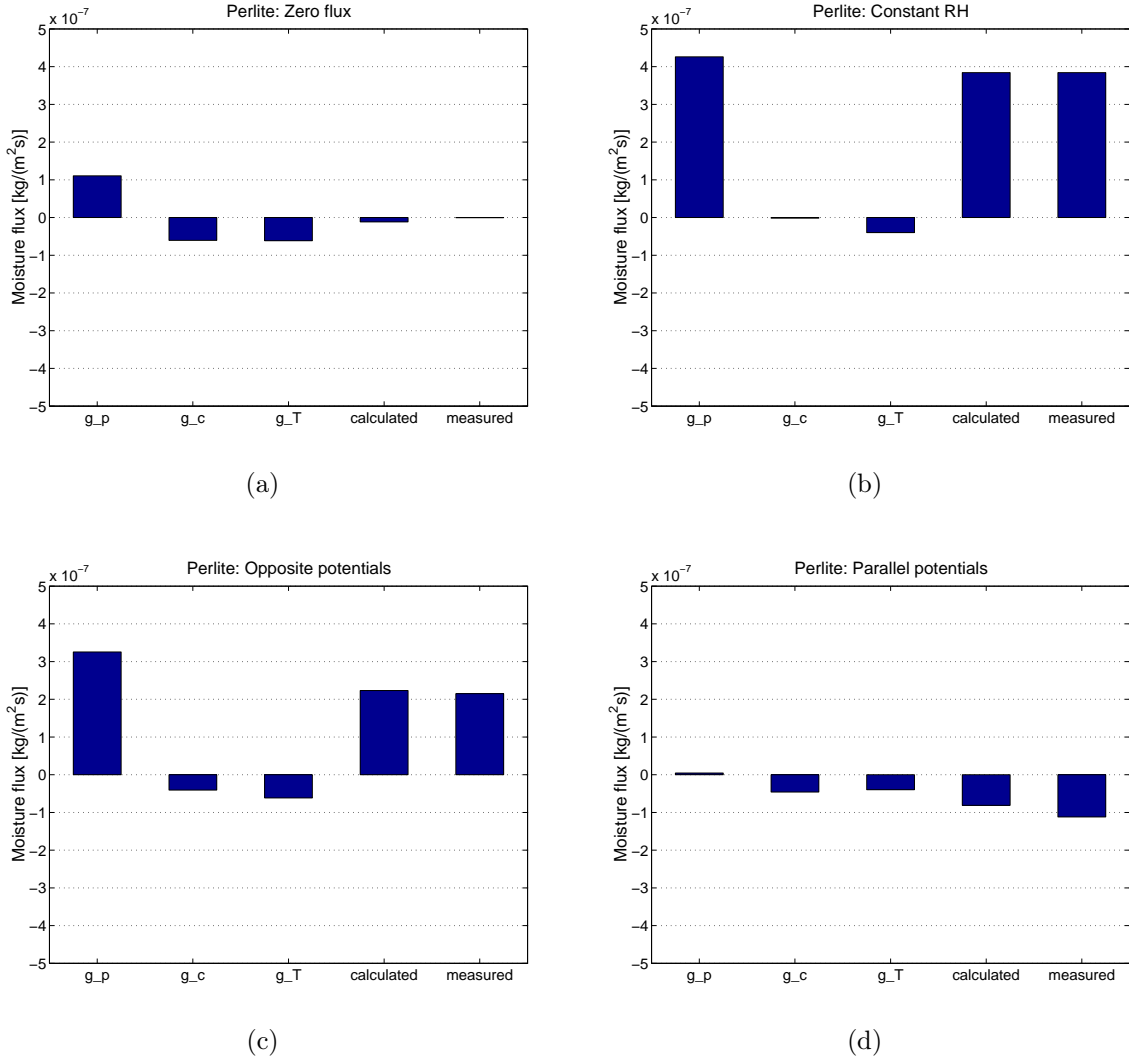


Figure B.19: The identifying of the 'other' transport for **perlite**, divided in 3 contributions: water vapour diffusion $g_{diffusion}$ (g_p), liquid transport g_{liquid} (g_c) and any temperature gradient induced transport $g_{thermal}$ (g_T). The water vapour pressure driven transport is based on the determined isothermal permeability and the actual boundary conditions. Liquid K and thermal D_T transport coefficients are determined by solving a set of linear equations with 2 unknowns with least squares method (Matrix 6.9). The calculated contributions $g_{calculated}$ are compared with the total measured transport $g_{measured}$. (a) zero flux (condition **1**), (b) constant RH (condition **2**), (c) opposite potentials (condition **3**) and (d) parallel potentials (condition **4**). The flux is positive from room to Megacup, i.e. from warm to cold.

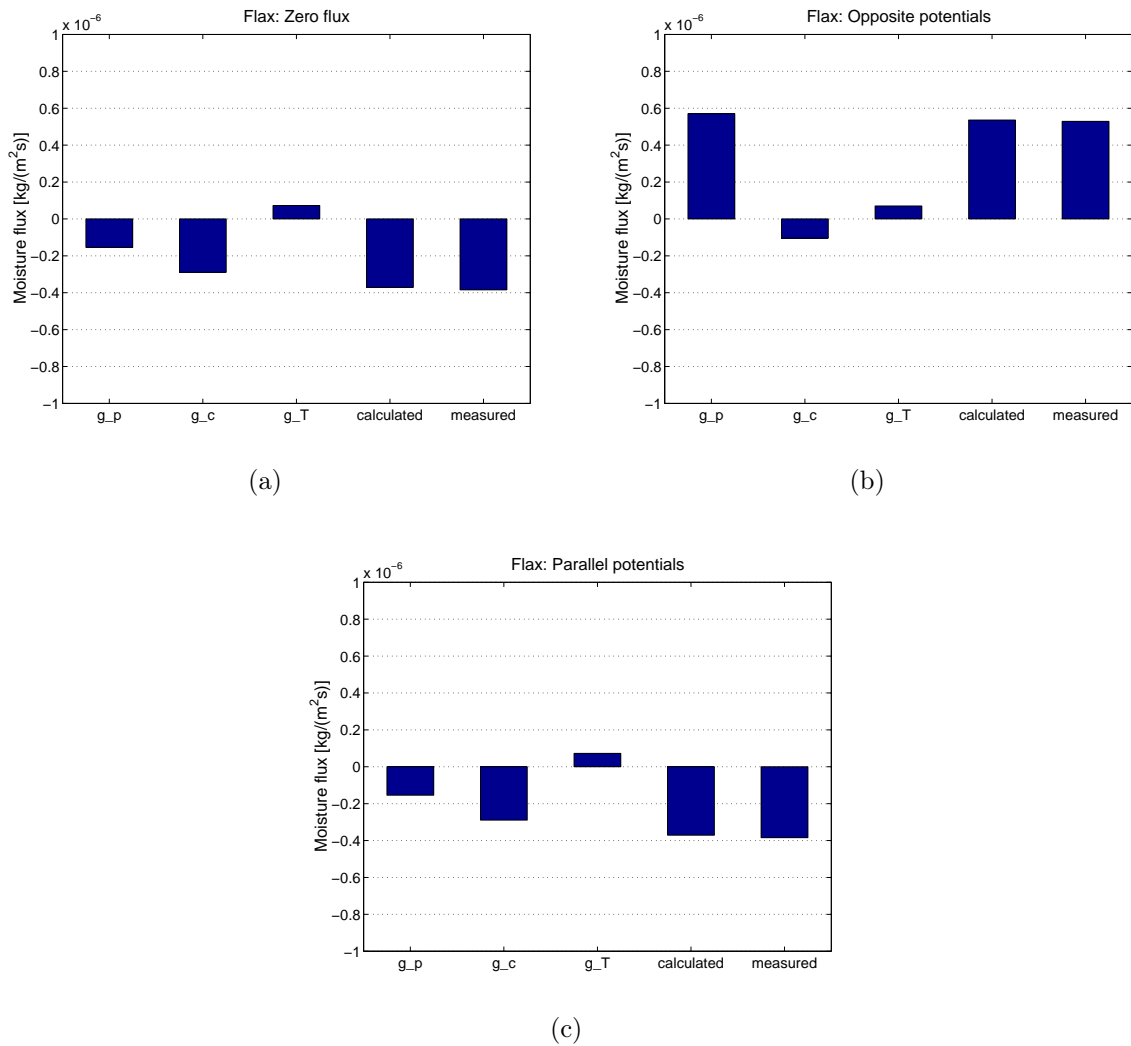


Figure B.20: The identifying of the 'other' transport for **flax**, divided in 3 contributions: water vapour diffusion $g_{diffusion}$ (g_p), liquid transport g_{liquid} (g_c) and any temperature gradient induced transport $g_{thermal}$ (g_T). The water vapour pressure driven transport is based on the determined isothermal permeability and the actual boundary conditions. Liquid K and thermal D_T transport coefficients are determined by solving a set of linear equations with 2 unknowns with least squares method (Matrix 6.9). The calculated contributions $g_{calculated}$ are compared with the total measured transport $g_{measured}$. (a) zero flux (condition **1**), (b) opposite potentials (condition **3**) and (c) parallel potentials (condition **4**). The flux is positive from room to Megacup, i.e. from warm to cold.

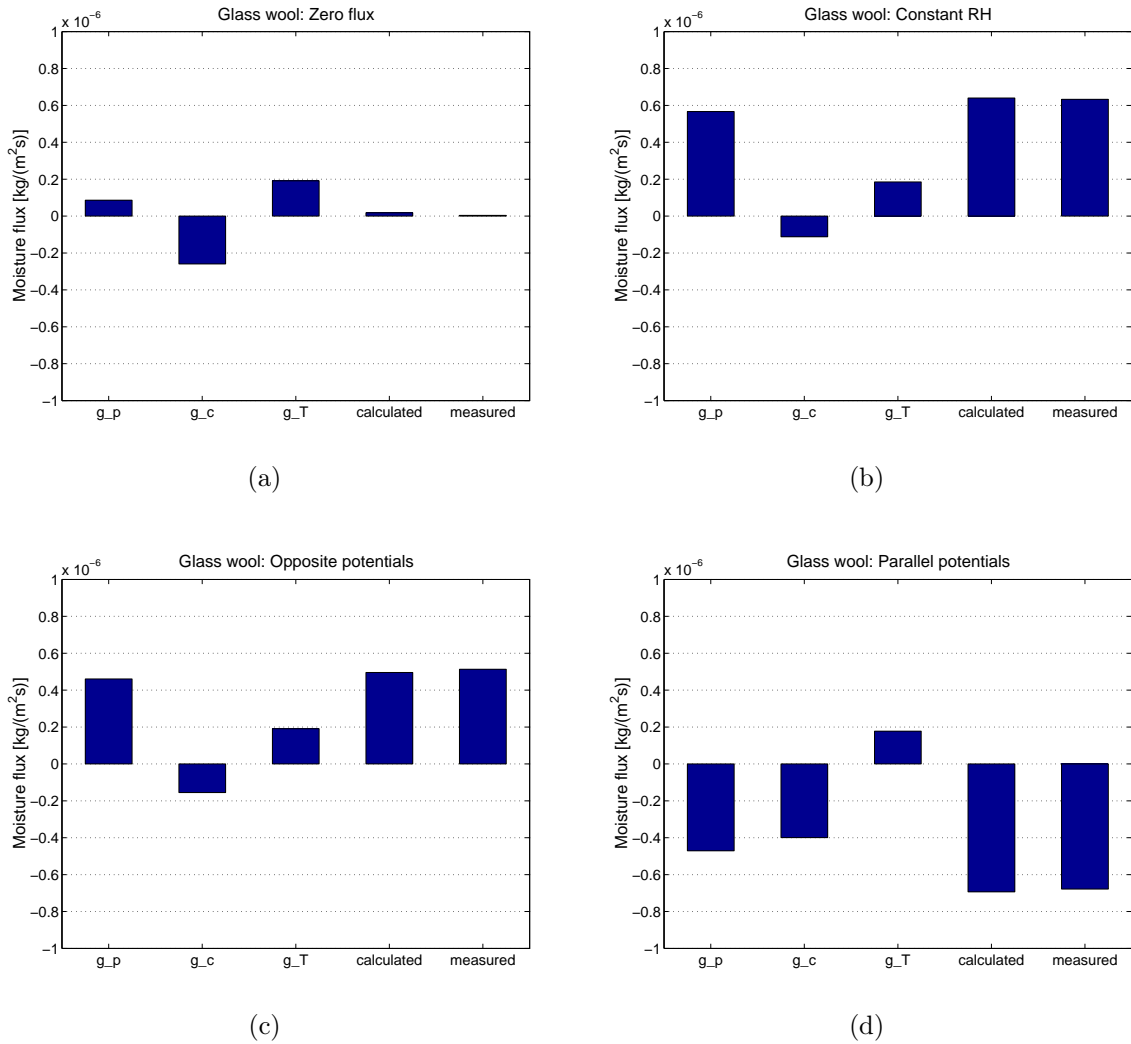


Figure B.21: The identifying of the 'other' transport for **glass wool**, divided in 3 contributions: water vapour diffusion $g_{diffusion}$ (g_p), liquid transport g_{liquid} (g_c) and any temperature gradient induced transport $g_{thermal}$ (g_T). The water vapour pressure driven transport is based on the determined isothermal permeability and the actual boundary conditions. Liquid K and thermal D_T transport coefficients are determined by solving a set of linear equations with 2 unknowns with least squares method (Matrix 6.9). The calculated contributions $g_{calculated}$ are compared with the total measured transport $g_{measured}$. (a) zero flux (condition **1**), (b) constant RH (condition **2**), (c) opposite potentials (condition **3**) and (d) parallel potentials (condition **4**). The flux is positive from room to Megacup, i.e. from warm to cold.

B.2.4 Calibration of RH sensors

Calibration of small RH-sensors

The used small electronic relative humidity sensors (HIH-3610 Series from Honeywell) were individually calibrated, both in respect to relative humidity (RH) and temperature (T). The relative humidity sensors measure voltage V_{out} in a dielectric layer that is linearly dependent on the relative humidity and the temperature of the ambient air. Their dimensions are $3.8 \cdot 8.9 \cdot 0.6$ mm, why they do not disturb the moisture flux.

There are conducted 2 measurements series:

1. Different RH's (45 – 95% RH) at one temperature level (20°C) in a small climate chamber. See Figure 1 with a measurement sequence.
2. Different RH's (33, 75 and 97%RH) at different temperature levels (0 – 20°C). See Figure 2 with a measurement sequence. Saturated salt solutions were used to produce the humidity in a small climate chamber.

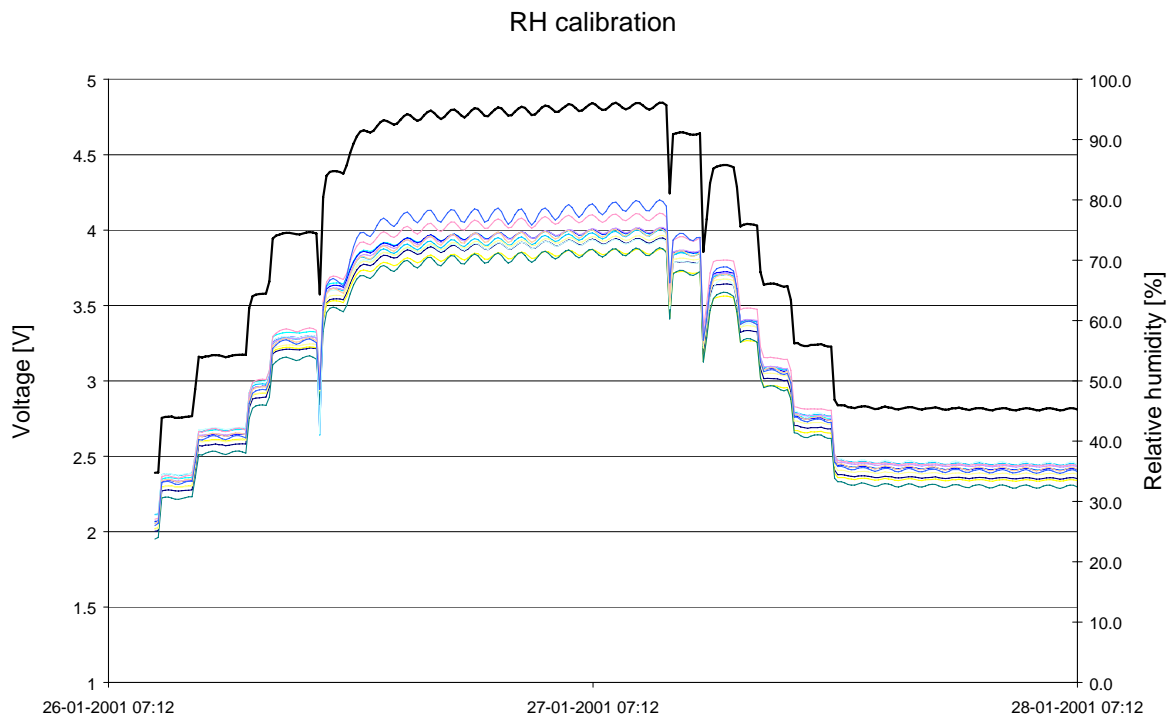


Figure 1: A measurement sequence at 20°C. Relative humidity steps. The thick solid line gives the variations in relative humidity of the climate chamber air. Thin lines give the output voltage of the sensors. Mean values for a given sequence is used for determination of the calibration constants.

The measured mean values for every condition were used in linear regression analysis that produced the individual calibration coefficients (a – d) for the sensors. The calibration expression is

$$RH(T) = \frac{a \cdot V_{out}(20^{\circ}C) + b}{c \cdot T + d}$$

where T is given as °C.

T calibration at 75 % RH

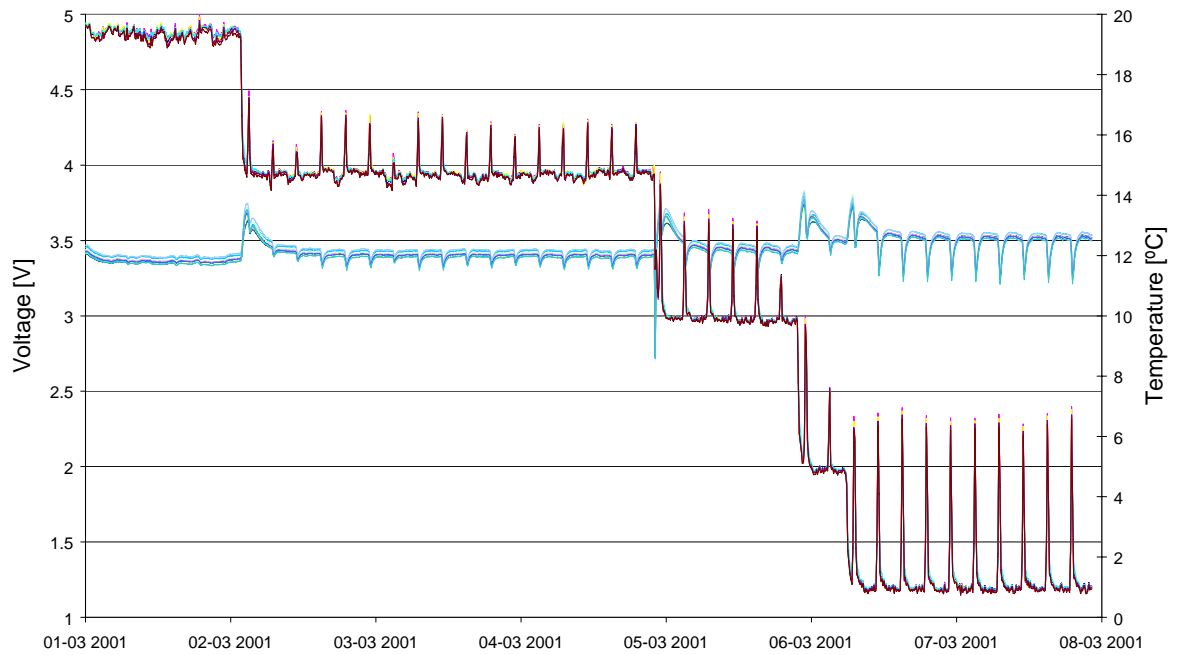


Figure 2: A measurement sequence at 75%RH. Steps in temperature 0 – 20°C. The output voltage of the sensors is only slightly increasing for decreasing temperature.. Mean values, without the peaks, for a given sequence is used for determination of the calibration constants.

Figure 3 shows the resulting deviation between the RH given by the calibrated sensors with the calibrated expression and the ‘true’ relative humidity. There is a moderate tendency to the small sensors showing less than the ‘true’ relative humidity for temperature range 10 – 20°C.

Error in RH at 75%
RH as a function of temperature

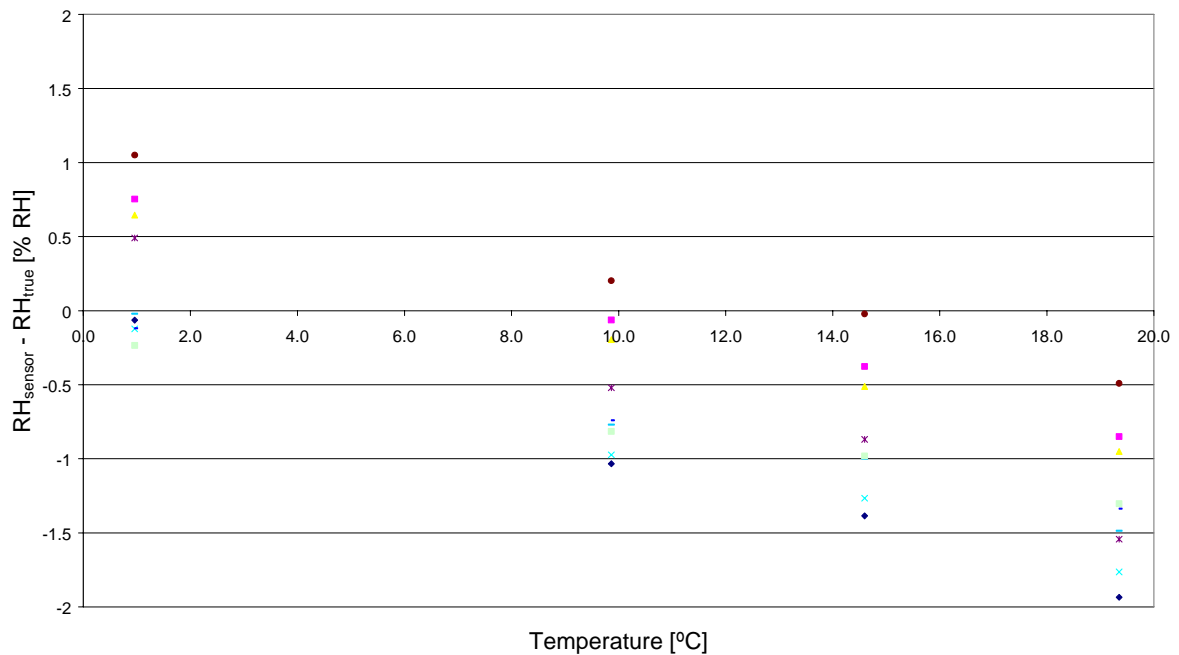


Figure 3 The deviation between the RH given by the calibrated sensors with the calibrated expression and the ‘true’ relative humidity

B.3 Non-Isothermal dynamic moisture transport

B.3.1 Measurements of moisture flux

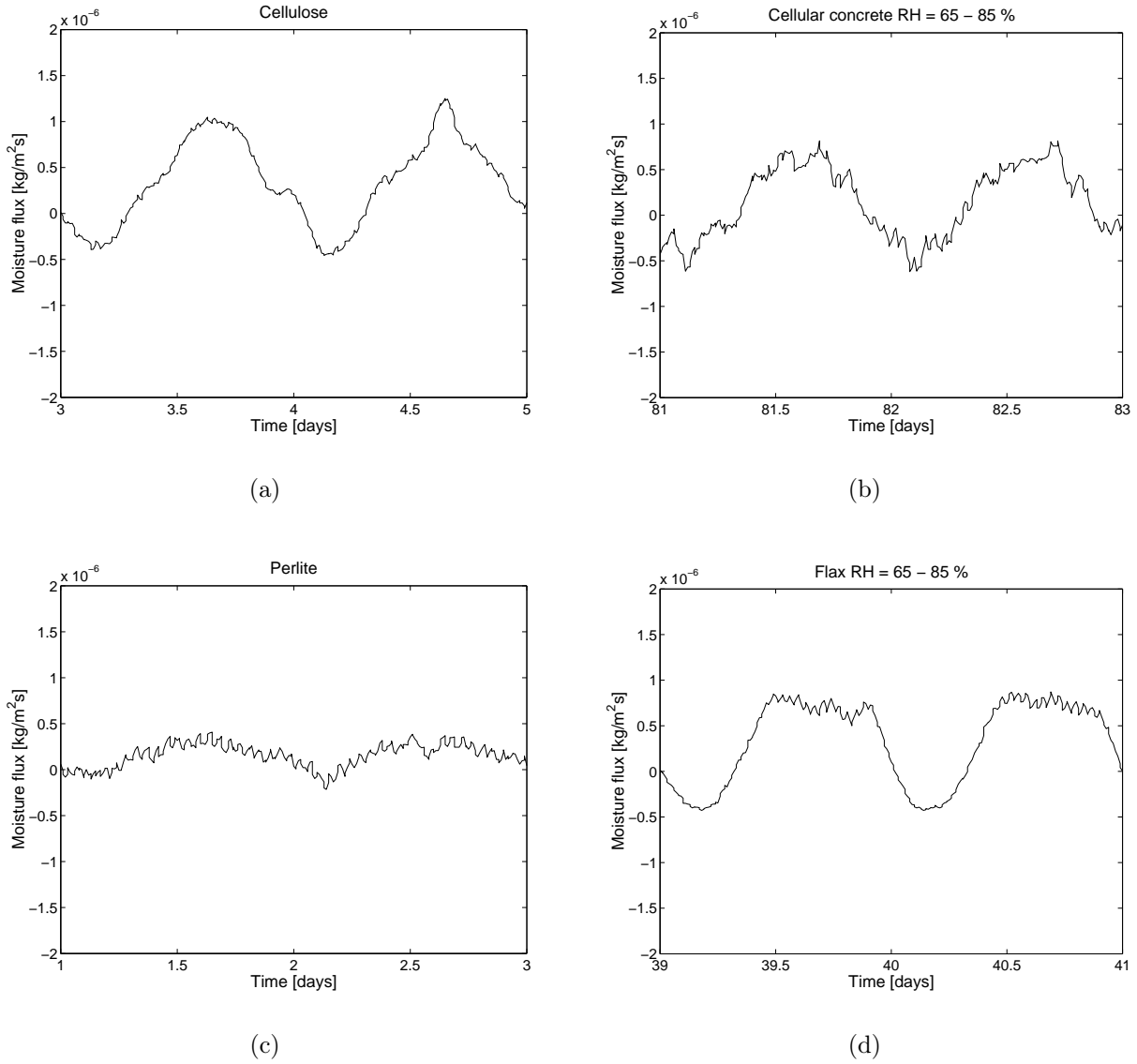


Figure B.22: The measured moisture flux $[kg/m^2s]$ for sinusoidal variation $RH = 65 - 85\%$ for (a) cellulose (b) cellular concrete (c) perlite and (d) flax.

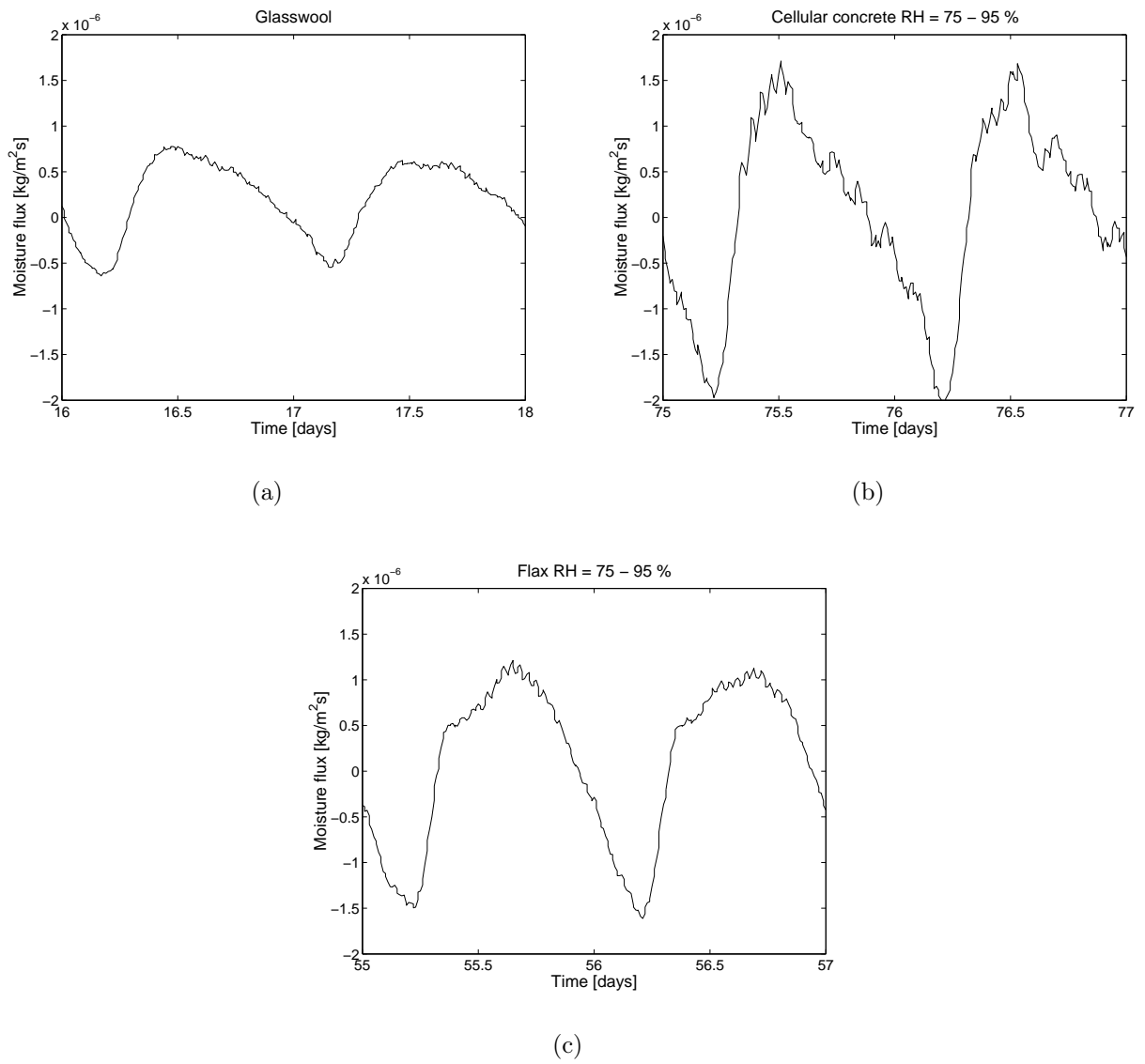


Figure B.23: The measured moisture flux $[kg/m^2s]$ for sinusoidal variation $RH = 75 - 95\%$ for (a) glass wool (b) cellular concrete (c) flax.

B.3.2 Measurements vs. Simulations

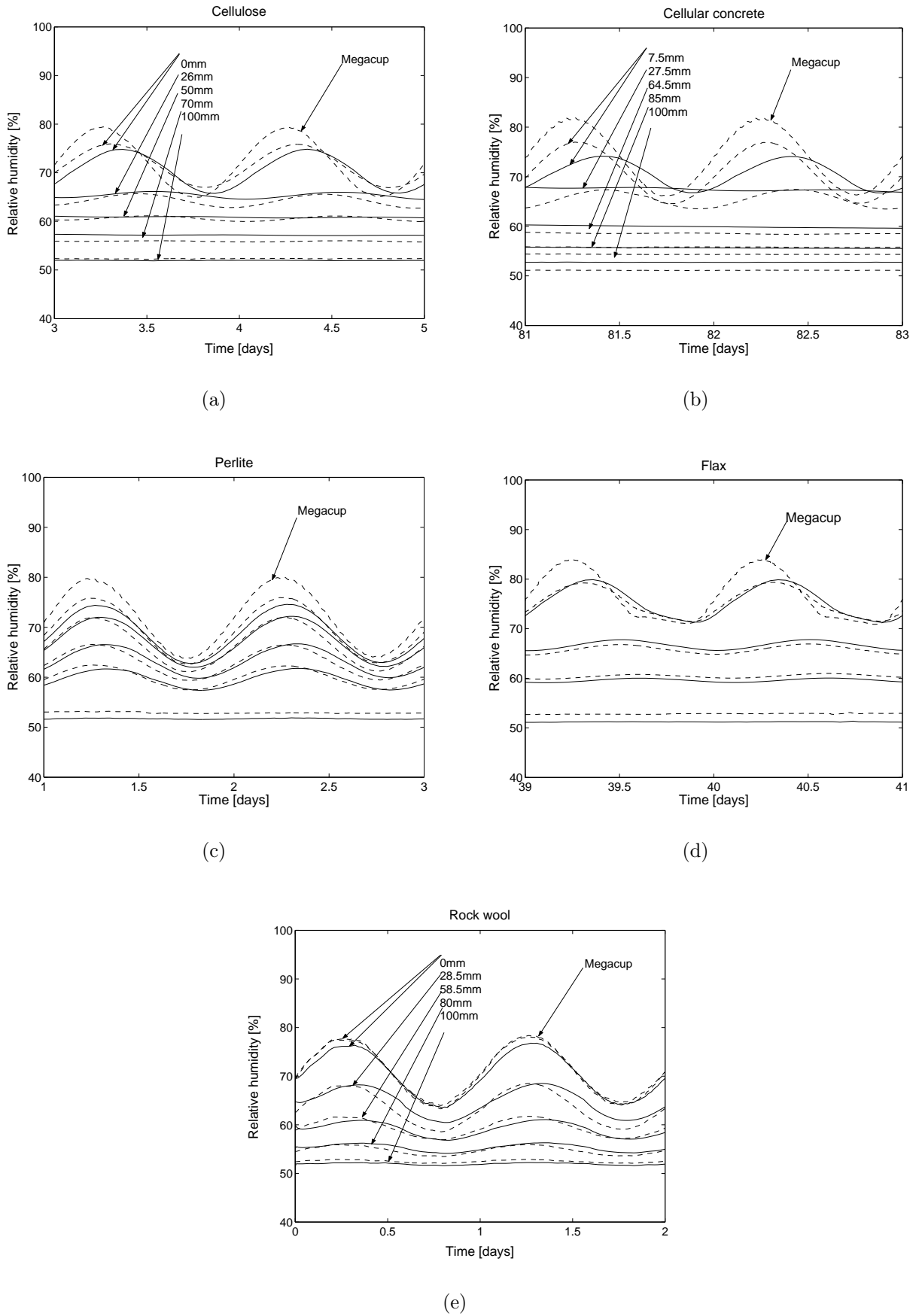


Figure B.24: Comparison of measured (dotted lines) and simulated (solid lines) distribution of relative humidity for $RH = 65 - 85\%$. The measured relative humidity has been used as boundary condition in the Megacup. (a) Cellulose, (b) cellular concrete, (c) perlite and (d) flax.

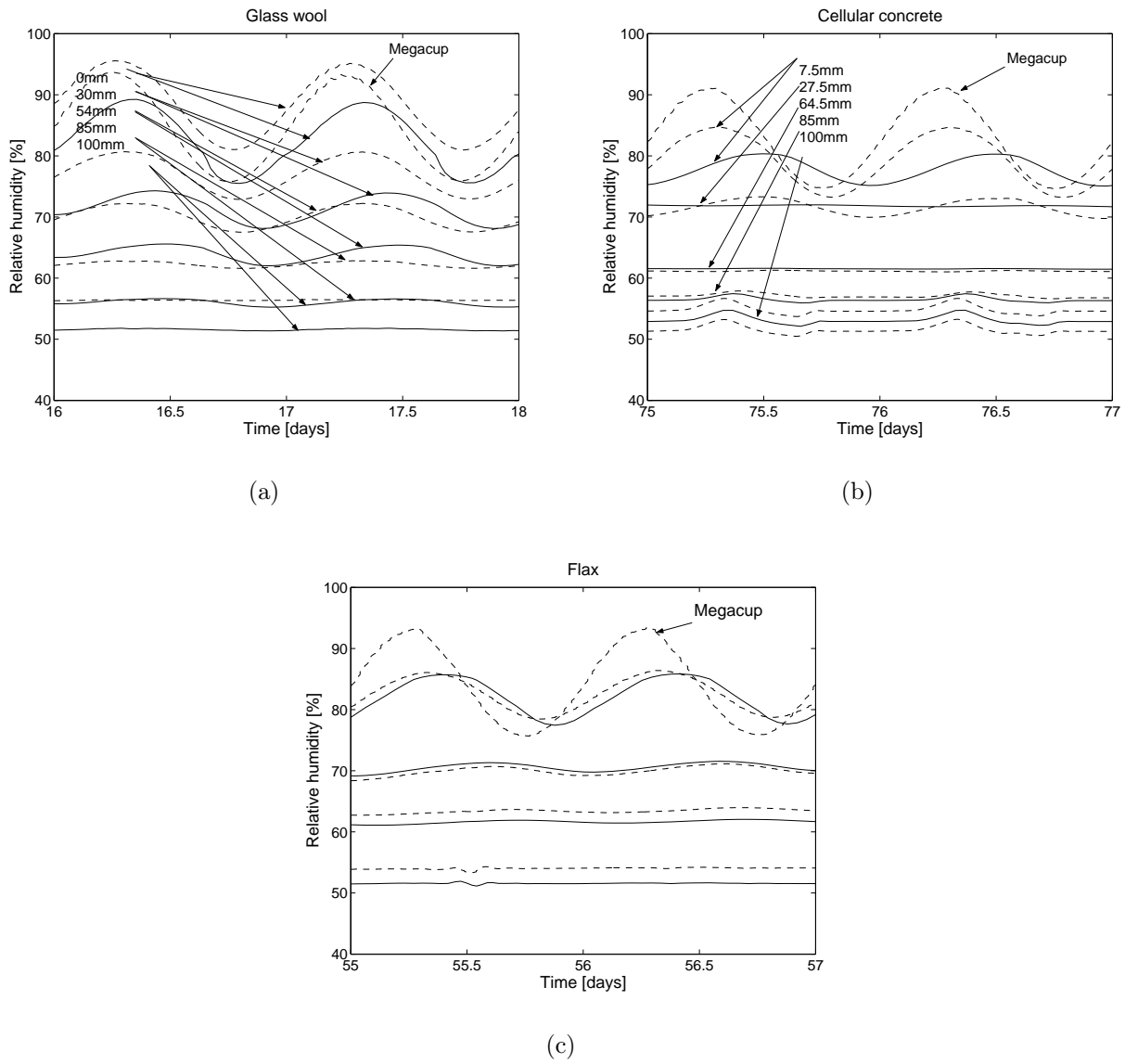


Figure B.25: Comparison of measured (dotted lines) and simulated (solid lines) distribution of relative humidity for $RH = 75 - 95\%$. The measured relative humidity has been used as boundary condition in the Megacup. (a) Glass wool, (b) cellular concrete and (c) flax.

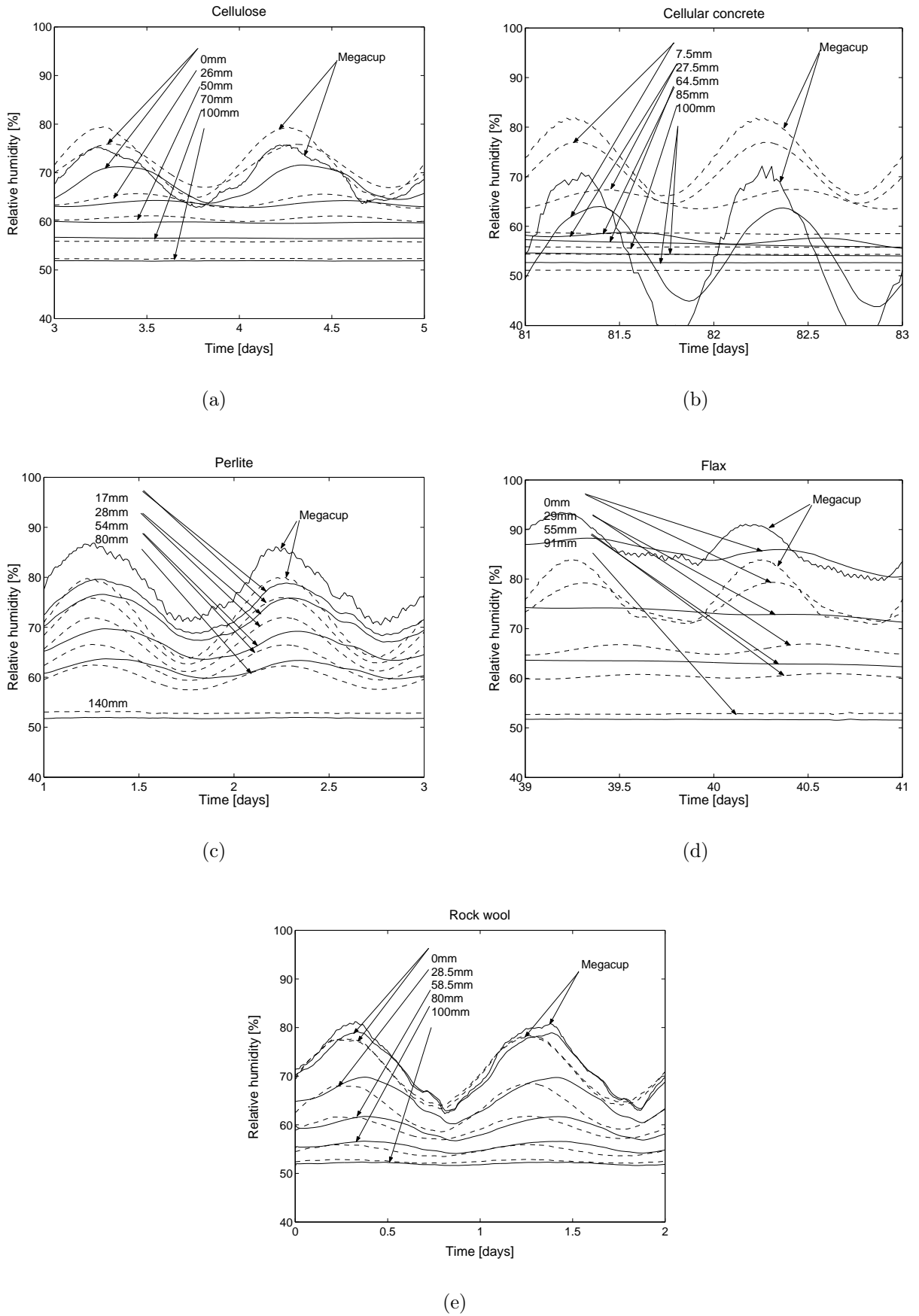


Figure B.26: Comparison of measured (dotted lines) and simulated (solid lines) distribution of relative humidity for $RH = 65 - 85\%$. The measured moisture flux has been used as boundary condition in the Megacup. (a) Cellulose, (b) cellular concrete, (c) perlite and (d) flax.

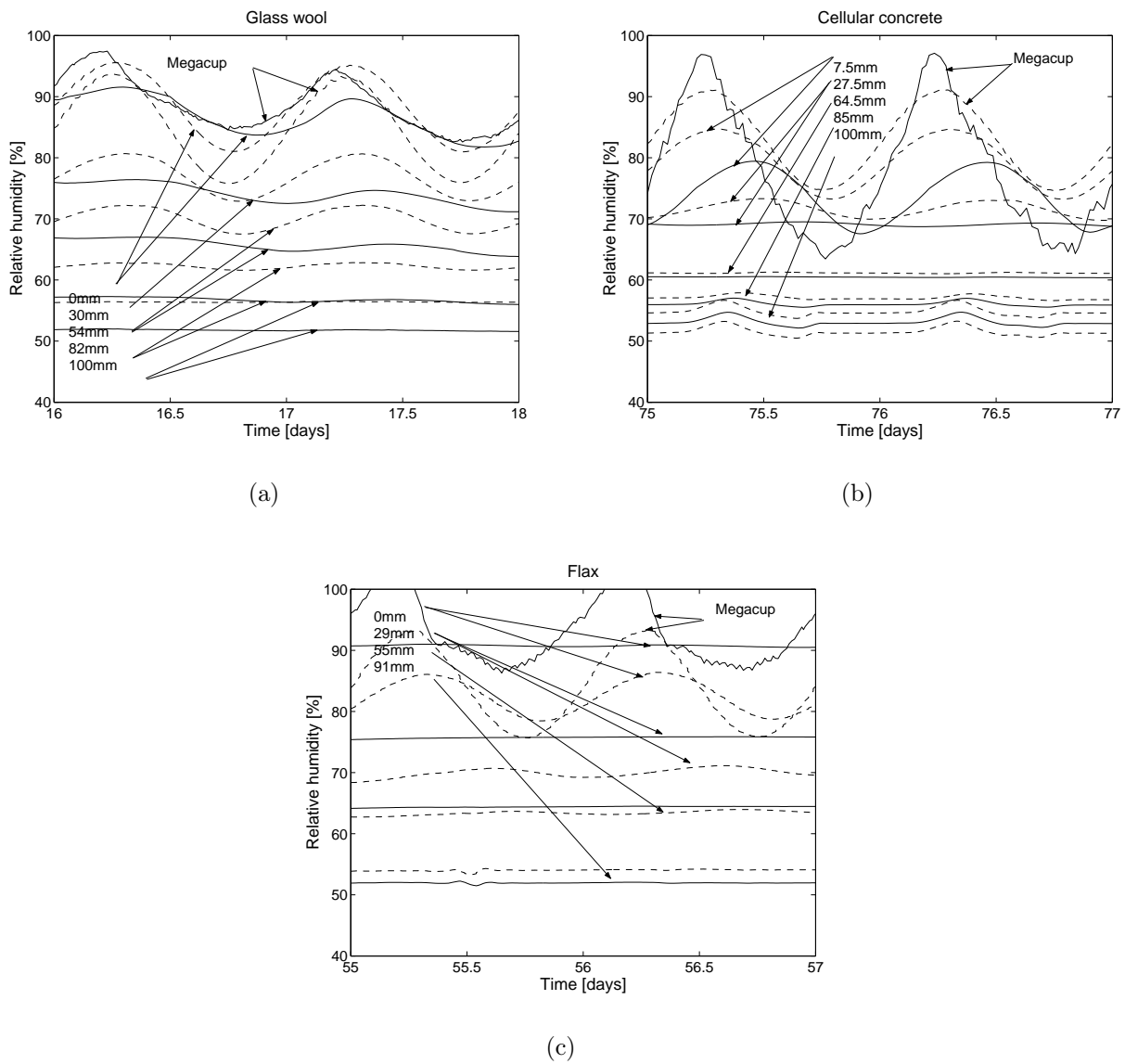


Figure B.27: Comparison of measured (dotted lines) and simulated (solid lines) distribution of relative humidity for $RH = 75 - 95\%$. The measured moisture flux has been used as boundary condition in the Megacup. (a) Glass wool, (b) cellular concrete and (c) flax.

Appendix C

SIMULINK model

Ruut Peuhkuri

*SIMULINK model of coupled
heat and moisture transport in
material layers*

DANMARKS
TEKNISKE
UNIVERSITET



Sagsrapport
BYG·DTU SR-02-02
2002

Contents

1.	INTRODUCTION	209
	<i>Simulink as modelling tool</i>	210
2.	DESCRIPTION	210
3.	INPUT AND OUTPUT	211
4.	USER INTERFACE: MASK	212
5.	REQUIRED MATLAB FILES	213
6.	VARIABLES	213
	MATHEMATICAL MODEL	214
7.	SIMULINK EQUATIONS AND CORRESPONDING BLOCK DIAGRAMS.....	215
	<i>The heat balance</i>	215
	<i>The moisture balance</i>	215
	<i>Surface layer</i>	216
	<i>Moisture source G as boundary condition</i>	217
	<i>Hysteresis</i>	217
	<i>Moisture flux</i>	217
	<i>Block diagrams</i>	218
8.	HANDLING MATERIAL PARAMETERS	224
	<i>The material parameters</i>	224
	Water vapour permeability.....	224
	Hydraulic conductivity.....	225
	Sorption isotherm and hysteresis	225
	Suction pressure	226
	<i>Material database</i>	227
9.	VALIDATION	228
	<i>The physical model</i>	228
	<i>The boundary conditions</i>	228
	<i>The model in Simulink</i>	229
	<i>Results</i>	229
10.	REFERENCES	231

1. Introduction

As a part of the author's Ph.D- work, a model of the coupled heat and moisture transport in material layers was created. This material model is based on finite difference method, where the investigated material layer is divided into control volumes (CV). The properties and states of these CVs are defined in a node as a lumped model.

The purpose of the modelling was not to create a superior model of heat and moisture transport problems, but a flexible open source tool, which freely can be modified for special problems. During 2001 there was started an inspiring modelling co-operation based on Simulink environment, as well locally at the Department and internationally. As a part this co-operation, a group of research students at the Department started to develop different submodels, which could work together [Nielsen et al. 2002]. The first versions of this material model of coupled heat and moisture transport were created to be part of a ventilated cavity model created by [Gudum 2002].

The material model is constructed as a node, which has separate temperature and moisture "subnodes". These subnodes are coupled to each others and the nodes to their "neighbours". As a major initialising inspiration was used the thermal model described in [Hagentoft 2001]. The overall structure of the node model is illustrated in Figure 1.

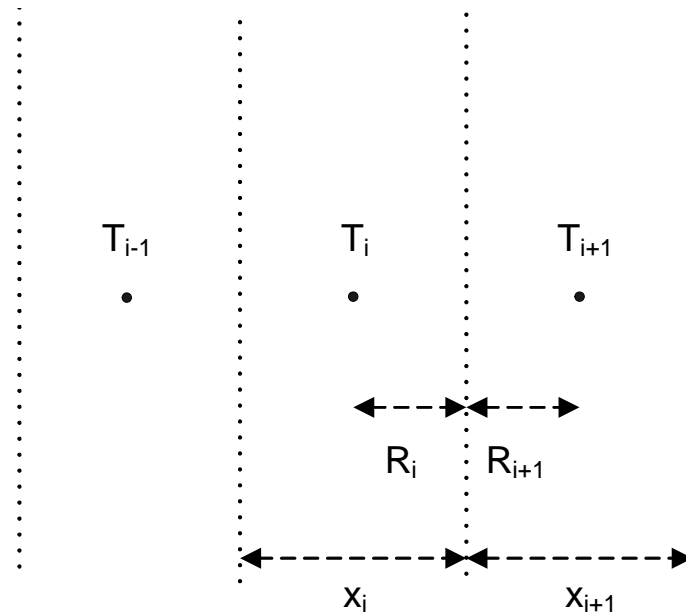


Figure 1: Material layer model with node

In this report, the basic model is described in detail, including the documentation of the Simulink-blocks and the validation. It is my aim to modify the model as a part of the ongoing Ph.D.-work, but the fundamental Simulink modelling will not be changed and is fully described only here. The mechanisms in this basic model are as identical as possible with the ones in simulation tool MATCH [Rode 1991].

Simulink as modelling tool

Simulink is a tool integrated with Matlab (www.mathworks.com) for modeling, simulating, and analyzing dynamic systems. Simulink was chosen as a modelling tool mainly because of the co-operative perspectives mentioned above. In addition, the graphical presentation of the mathematical formulas is clear and logical.

The numerical solution in Simulink is totally in-built: Simulink uses different types of very advanced and effective Matlab ordinary differential equation (ODE) solvers. All the “numerics” one has to do is for example the discretization and to choose the solver suitable to the problem. All the considerations on the matrix systems, time steps and the solvers are done by the Matlab/Simulink. One just has to define the partial differential equations in the way that Simulink can understand.

2. Description

The Simulink model of the coupled heat and moisture transport is built on a basis of the differential equations introduced in Chapter 6. The numerical method is the finite difference method with a network node model of the opaque material layer with a lumped heat and moisture capacity located in the node. Only one-dimensional heat and moisture transfer is considered here. The defined node structure is illustrated in Figure 1.

The transfer mechanisms included in model are (including the driving force):

- Heat conductivity (temperature)
- Latent heat (vapour pressure)
- Water vapour diffusion (vapour pressure)
- Liquid transfer (suction pressure)

The **material layer** block calculates the temperature and the moisture content in the middle of the node. To be able to connect this material layer to the boundary conditions (BC), e.g. a room air and an outdoor air node, a special **BC and surface layer** block is also defined. Here the lumped capacity is on the material surface facing the boundary conditions and the interaction with the construction and the environment takes place. A wall structure consisting of different material layers can be built with these blocks.

For the further analysis of the simulation results, a **moisture flux** and a **surface moisture flux** block are defined.

3. Input and output

A **material layer** node communicates with other nodes by the input and output arrays. In this case the input and the output arrays are identical: The output from a node is directly input to another node.

Table 1: Input and output array for material layer

Symbol	Description	Unit
R	thermal resistance	m ² K/W
T	Temperature	K
Z	moisture resistance	Pa·s·m ² /kg
P	vapour pressure	Pa
K	hydraulic conductivity	kg/(Pa·m·s)
LnPsuc	logarithmic suction pressure	Pa
C	volumetric heat capacity pr. m ²	J/(K·m ²)
CM	mass pr. m ²	kg/m ²

The input array from the boundaries to the **surface layer** is identical to the component array defined in [Report 2002] and is described in Table 2. Only 4 first values are used at the time being.

Table 2: Construction and system array

Symbol	Description	Unit
Rc	Convective thermal surface resistance	m ² K/W
Ts	Surface temperature	°C
Rp	Moisture surface resistance	Pa·s·m ² /kg
Ps	Surface vapour pressure	Pa
Ra	Air flow conductance	m ³ /(s Pa)
Pa	Air pressure	Pa
Qsun	Transmitted solar energy	W/m ²
ε	Surface emittance	-
Tair	Inlet temperature of air flow	°C
φair	Relative humidity of air flow	-

At the moment the only input to the model is temperature and relative humidity of the surroundings. These are collected in the **BC and surface layer** block from a file, where values are as in Table 3. In the long run the array structure should follow the guidelines in [Report 2002].

Table 3 Array with conditions of the surroundings

Row	Symbol	Description	Unit
1	t	time	s, h, days,...
2	T _a	Air temperature	°C
3	φ _a	Relative humidity	-

Output from the **material layer** block and the **BC and surface layer** block is the temperature and relative humidity in the lumped node. Output from the **moisture flux** and surface **moisture flux** is the moisture flux/m². The unit for flux depends on the time definitions of boundary conditions as in Table 3.

4. User interface: Mask

The Simulink model is built of hierarchical subsystems and the top level of the node is very simple, see Figure 4. In a Simulink model it is possible to work either in the user or in the developer level. In the user level the only visible is the mask of the model, see Figure 2. In this case, only the material, thickness of the layer and initial values for temperature, relative humidity and moisture content has to be defined. The amplifier defining the unit for time array has to be set, as well. E.g. amplifier = 1 for time running in seconds. For the **BC and surface layer** block, the convective heat and moisture resistances have to be defined, too.

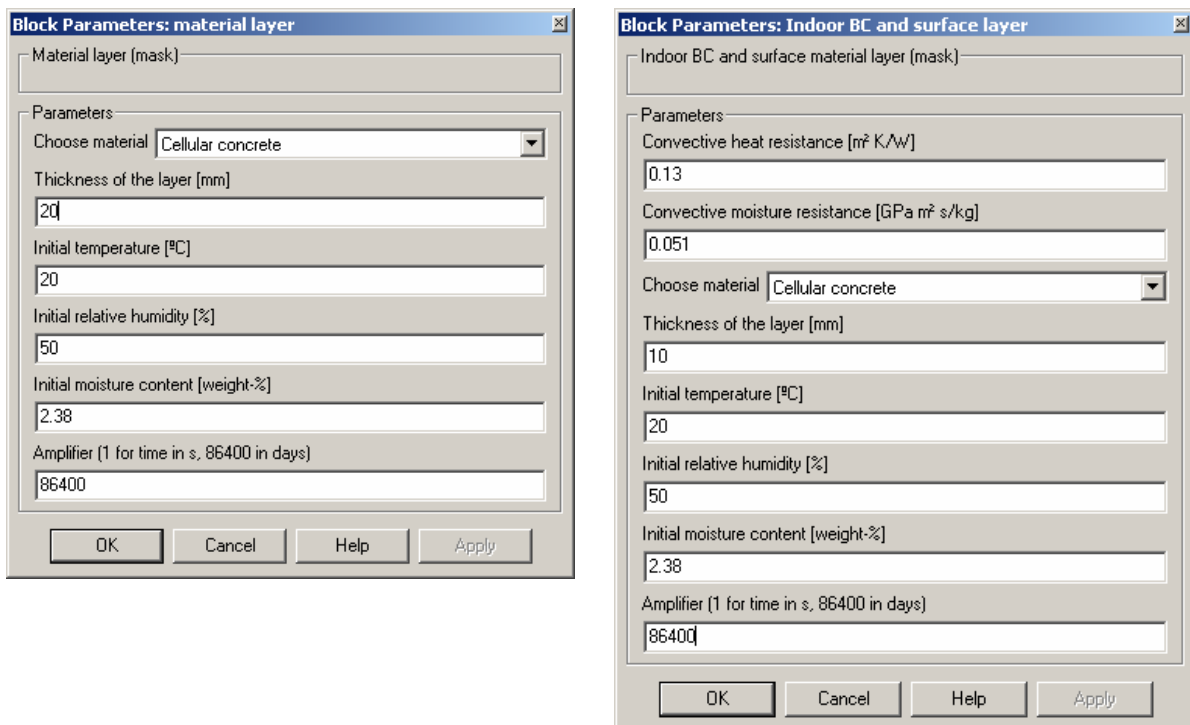


Figure 2: The **material layer** block and **BC and surface layer** block user interface (the mask).

If the user wants to check or modify the model, this is easy: Unlock the library and look under the mask.

Matlab ODE-solver ODE23s is most suitable to running a simulation of a system based on these blocks. The maximal time step in the simulation should not exceed the timestep of the boundary conditions.

5. Required Matlab files

DATABASE.m has to be in the same library with the model when running a simulation. This file is initialised automatically by the block masks.

6. Variables

c_{air}	water vapour concentration of air [kg/m ³]
c_p	specific heat capacity of the material [J/(kg·K)]
$c_{p,0}$	specific heat capacity of the dry material [J/(kg·K)]
$c_{p,w}$	specific heat capacity of water [J/(kg·K)]
g	total moisture flux density [kg/m ² ·s]
g_v	vapour flux density [kg/ m ² ·s]
g_l	liquid flux density [kg/ m ² ·s]
G	moisture flux [kg/s]
Δh	phase change enthalpy for vapour/liquid [J/kg]
k	hydraulic conductivity [kg/(Pa·m·s)]
K	hydraulic conductivity of a half layer [(m ² ·s)/kg]
p	water vapour pressure [Pa]
p_s	saturation vapour pressure [Pa]
P_{suc}	suction pressure [Pa]
R	heat conduction resistance of a half layer [m ² ·K/W]
R_v	gas constant for water vapour: 461.5 J/(kg·K)
T	temperature [K]
T_{ref}	reference temperature: 283.15 K
t	time [s]
u	moisture content, kg water per kg dry material [-]
V	volume [m ³]
x	space coordinate [m]
Z	water vapour resistance of a half layer [(Pa·m ² ·s)/kg]
δ_p	water vapour permeability [kg/(m·s·Pa)]
λ	heat conductivity [W/(m·K)]
λ_{l0}	heat conductivity of a dry material [W/m·K]
λ_T	heat conductivity coefficient for temperature dependency [W/m·K ²]
λ_w	heat conductivity coefficient dependent on water content [W/m·K]
φ	relative humidity [-]
ρ_0	dry density of the material [kg/m ³]

Mathematical model

The model of the coupled heat and moisture transport is based on the well-known laws of Fourier, Fick and Darcy. No further discussion on the theory finds place here; the equations are just accepted and used. By using the continuity equations and the equations of the state, beside the laws of transport, the equations for dynamic model are determined.

The basic model includes the same features as in the model MATCH, which is used for validation. Hysteresis is also included, just in a slightly different way.

The coupled equations are:

$$\rho_0 c_p(u) \frac{\partial T}{\partial t} = \frac{\partial}{\partial x} \left(\lambda(u, T) \frac{\partial T}{\partial x} \right) + \Delta h \frac{\partial}{\partial x} \left(\delta_p(u) \frac{\partial p}{\partial x} \right) \quad (1)$$

$$\rho_0 \frac{\partial u}{\partial t} = \frac{\partial}{\partial x} \left(\delta_p(u) \frac{\partial p}{\partial x} \right) + \frac{\partial}{\partial x} \left(k(u) P_{suc} \frac{\partial \ln P_{suc}}{\partial x} \right) \quad (2)$$

where

$$\lambda(u, T) = \lambda_{10} + u \cdot \lambda_w + (T - T_{ref}) \cdot \lambda_T \quad (3)$$

$$c_p(u) = c_{p,0} + u \cdot c_{p,w} \quad (4)$$

The connection between the actual water vapour pressure and the material moisture content is determined by the sorption isotherm as a function of the relative humidity φ , which is given by:

$$\varphi = \frac{P}{p_s} \quad (5)$$

The saturation vapour pressure p_s is given by the empirical formula:

$$p_s(T) = \exp \left(23.5771 - \frac{4042.90}{T - 37.58} \right) \quad (6)$$

The water vapour permeability δ_p is dependent on the relative humidity on the hygroscopic range and on the moisture content on the higher moisture levels.

7. Simulink equations and corresponding block diagrams

The heat balance

A Simulink model of the heat balance is based on a discretised form of the equation (1), which by introducing a resistance of a half of a layer for heat conduction R and for water vapour diffusion Z :

$$R_i = \frac{x_i}{2 \cdot \lambda_i} \quad (7)$$

$$Z_i = \frac{x_i}{2 \cdot \delta_i} \quad (8)$$

gets the form:

$$\frac{\rho_0 \cdot c_p \cdot \Delta x}{\Delta t} (T_i^{new} - T_i^{old}) = \frac{(T_{i-1} - T_i)}{R_{left}} + \frac{(T_{i+1} - T_i)}{R_{right}} + \Delta h \left[\frac{(p_{i-1} - p_i)}{Z_{left}} + \frac{(p_{i+1} - p_i)}{Z_{right}} \right] \quad (9)$$

where

$$R_{left} = R_{i-1} + R_i \text{ and } R_{right} = R_{i+1} + R_i \quad (10)$$

$$Z_{left} = Z_{i-1} + Z_i \text{ and } Z_{right} = Z_{i+1} + Z_i$$

After some rearranging, the equation becomes the final Simulink-equation for heat balance:

$$\frac{dT_i}{dt} = \frac{1}{C_i} \left[\left(\frac{(T_{i-1} - T_i)}{R_{i-1} + R_i} + \frac{(T_{i+1} - T_i)}{R_{i+1} + R_i} \right) + \Delta h \left(\frac{(p_{i-1} - p_i)}{Z_{i-1} + Z_i} + \frac{(p_{i+1} - p_i)}{Z_{i+1} + Z_i} \right) \right] \quad (11)$$

where

$$C_i = \rho_0 \cdot c_p \cdot x_i \quad (12)$$

Equation (11) represents one node of the material.

The moisture balance

In the same way, the equation 2 is discretized and rearranged, by introducing hydraulic conductivity of a half of a layer for liquid transport K_i :

$$K_i = \frac{x_i}{2 \cdot k_i \cdot P_{suc,i}} \quad (13)$$

gets a form

$$\frac{\rho_0 \Delta x}{\Delta t} (u_i^{new} - u_i^{old}) = \frac{(p_{i-1} - p_i)}{Z_{left}} + \frac{(p_{i+1} - p_i)}{Z_{right}} + \frac{(\ln P_{suc,i-1} - \ln P_{suc,i})}{K_{left}} + \frac{(\ln P_{suc,i+1} - \ln P_{suc,i})}{K_{right}} \quad (14)$$

where

$$K_{left} = K_{i-1} + K_i \text{ and } K_{right} = K_{i+1} + K_i \quad (15)$$

And the final Simulink equation becomes:

APPENDIX C: SIMULINK MODEL

$$\frac{du}{dt} = \frac{1}{CM_i} \left[\frac{(p_{i-1} - p_i)}{Z_{i-1} + Z_i} + \frac{(p_{i+1} - p_i)}{Z_{i+1} + Z_i} + \frac{(\ln P_{suc,i-1} - \ln P_{suc,i})}{K_{i-1} + K_i} + \frac{(\ln P_{suc,i+1} - \ln P_{suc,i})}{K_{i+1} + K_i} \right] \quad (16)$$

where

$$CM_i = \rho_0 \cdot x_i \text{ is the mass per m}^2. \quad (17)$$

Surface layer

The **surface materiale layer** is basically identical with the **material layer**, with some alternations: the convective heat and resistance gives another half of the heat and moisture resistances in equations 11 and 16. Furthermore, the model is prepared to be extended with additional heat (radiation) and moisture (driving rain) fluxes on the surface. The connections around the surface node are illustrated in figure below:

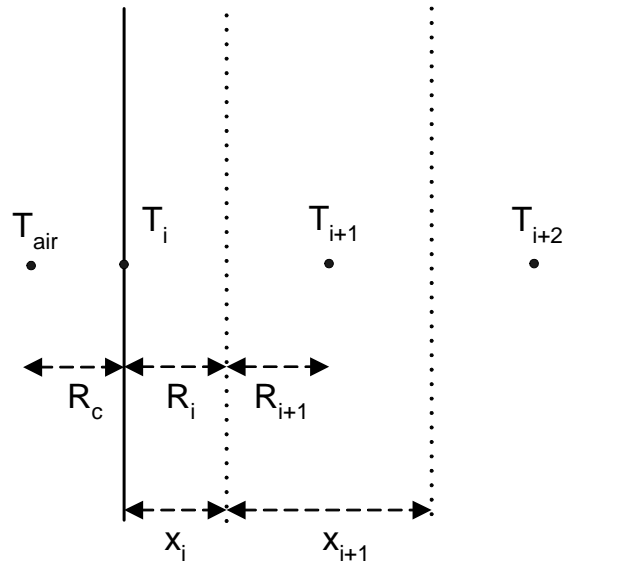


Figure 3 Placement of nodes on surface of material

The final Simulink-equation for *heat balance*, solving the temperature on the surface T_i , becomes:

$$\frac{dT_i}{dt} = \frac{1}{C_i} \left[\left(\frac{(T_{air} - T_i)}{R_c} + \frac{(T_{i+1} - T_i)}{R_{i+1} + R_i} \right) + \Delta h \left(\frac{(p_{air} - p_i)}{Z_c} + \frac{(p_{i+1} - p_i)}{Z_{i+1} + Z_i} \right) \right] \quad (18)$$

where subscript $i+1$ indicates the neighbouring material layer and subscript *air* states of the surrounding air node. Subscript *c* stands for convective. Attention must be paid here to the thickness of the layer used in the resistance, which is the whole thickness for the surface layer. This is handled by multiplying resistances with 2 after material parameters have been calculated.

In the same way, the Simulink –equation for *moisture balance* becomes:

$$\frac{du}{dt} = \frac{1}{CM_i} \left[\frac{(p_{air} - p_i)}{Z_c} + \frac{(p_{i+1} - p_i)}{Z_{i+1} + Z_i} + \frac{(\ln P_{suc,i+1} - \ln P_{suc,i})}{K_{i+1} + K_i} \right] \quad (19)$$

where there is no liquid transfer between surface and the air node.

Moisture source G as boundary condition

So far, the boundary conditions have been given by a temperature and relative humidity of the air node. For a problem, where the **moisture flux** G [kg/s] is preferred as boundary condition for moisture, the moisture balance becomes:

$$V_{air} \frac{dc_{air}}{dt} = \frac{A(p_{surface} - p)}{Z_c} + G \quad (20)$$

where c_{air} [kg/m³] is the water vapour concentration of air and V [m³] the volume of the air node, e.g. a room.

Hysteresis

Following equations make the hysteresis model. Slopes of the absorption (subscript a) and desorption (subscript d) isotherms $\partial u / \partial \varphi$ are defined by

$$\frac{\partial u}{\partial \varphi_a} = \frac{u_{a,i-2} - u_{a,i-1}}{\varphi_{i-2} - \varphi_{i-1}} \quad (21)$$

$$\frac{\partial u}{\partial \varphi_d} = \frac{u_{d,i-2} - u_{d,i-1}}{\varphi_{i-2} - \varphi_{i-1}} \quad (22)$$

where subscripts $i-1$ means the previous time step and $i-2$ the time step before that.

Slope of the intermediate scanning curve:

$$\frac{\partial u}{\partial \varphi_{hys}} = 0.4 \cdot \left[\frac{\partial u}{\partial \varphi_a} \left(1 - \frac{|u_i - u_{a,i-1}|}{u_{d,i-1} - u_{a,i-1}} \right) + \frac{\partial u}{\partial \varphi_d} \left(1 - \frac{|u_i - u_{d,i-1}|}{u_{d,i-1} - u_{a,i-1}} \right) \right] \quad (23)$$

where subscripts i means the actual time step. The new relative humidity is found by

$$\varphi_i = \varphi_{i-1} + \frac{u_i - u_{i-1}}{\frac{\partial u}{\partial \varphi_{hys}}} \quad (24)$$

After this it is checked that the value is inside the absorption and desorption isotherms.

Moisture flux

The total moisture **flux** density g between two material layer nodes – also surface layer – is defined as a sum of vapour and liquid flow:

APPENDIX C: SIMULINK MODEL

$$g = g_v + g_l = \frac{(p_i - p_{i-1})}{Z_i + Z_{i-1}} + \frac{(\ln P_{suc,i} - \ln P_{suc,i-1})}{K_i + K_{i-1}} \quad (25)$$

The flow is defined positive from right to left node. The surface moisture flux does not include liquid transfer; hence the flux density becomes:

$$g_{surface} = g_{v,surface} = \frac{(p_i - p_{air})}{Z_c} \quad (26)$$

Block diagrams

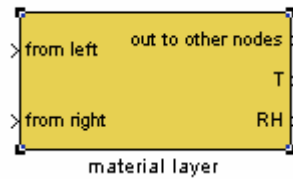


Figure 4: The **material layer** block

Figure 4 shows the top level of the **material layer** block. The block has got 2 input ports (from left and from right) and 3 output ports (to other nodes, T and RH). Output ports T (temperature) and RH (relative humidity) are just for monitoring the results, while there is only one output that is used by other nodes. The next level under the top level is seen in Figure 5 with 3 subsystems: The heat and moisture balance and a system, which calculates the material properties dependent on temperature and/or moisture in every time step. This **hygrothermal material properties** block also calculates the data array sent to neighbour nodes and the node itself, see Figure 6.

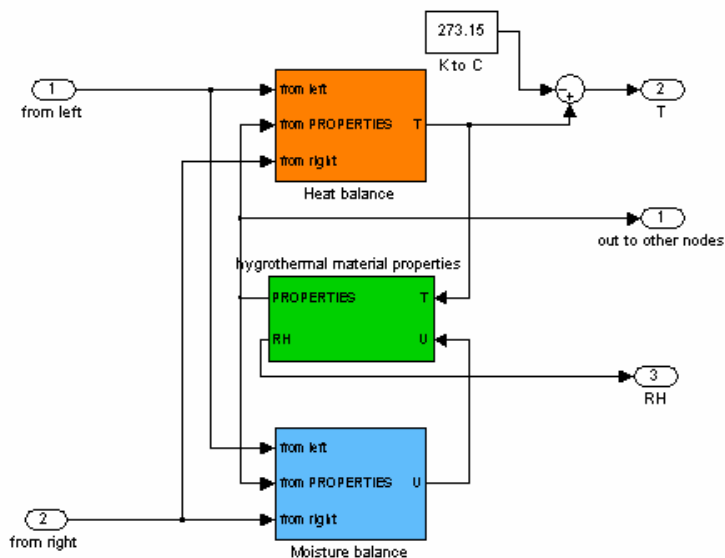


Figure 5: The **material layer** block under the top level: The block consists of 3 subsystems: The **heat and moisture balance** and a system which calculates the material properties dependent on temperature and/or moisture. The **hygrothermal material properties** block also calculates the data array sent to other nodes and the node itself.

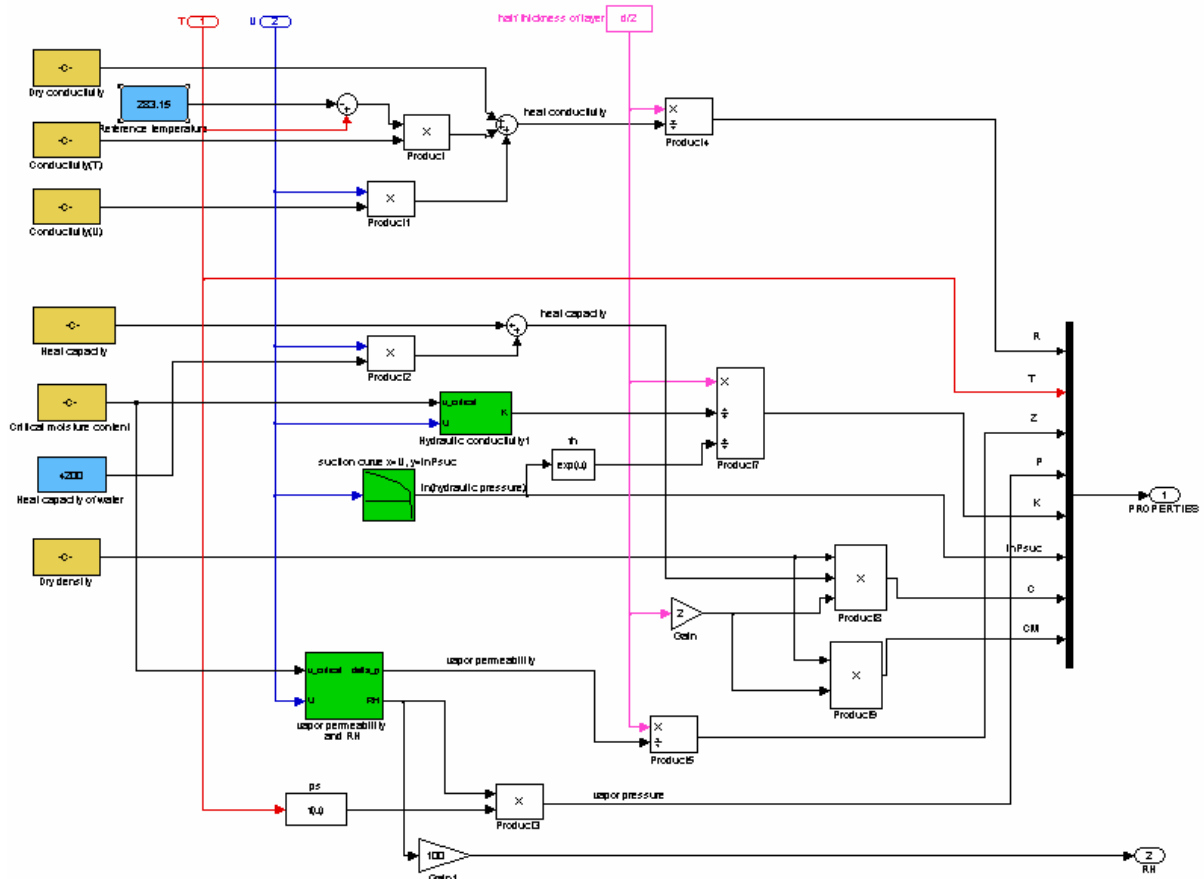


Figure 6: The *hygrothermal material properties* block

There is a possibility of treating sorption isotherms and hysteresis in different ways. The most easy way is just to use an inverse of either a absorption or a desorption isotherm, which converts the moisture content to the relative humidity. This is illustrated in Figure 7 (table **u to rh**). A good approximation in most cases is anyway to use the average of ab- and desorption isotherm.

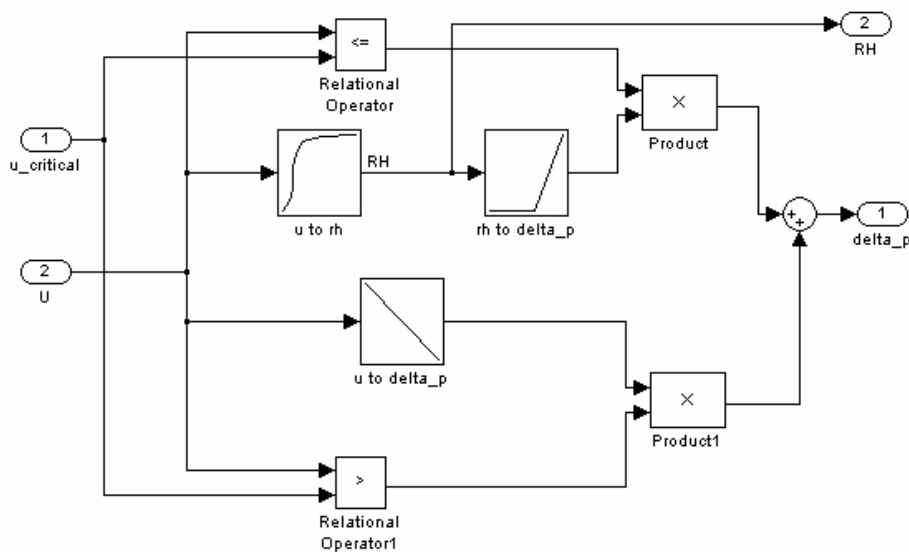


Figure 7: Subsystem calculating vapour permeability and relative humidity. There is no hysteresis in this model, just a table with the inverse of sorption isotherm (**u to rh**).

APPENDIX C: SIMULINK MODEL

For a more accurate describing of the sorption process a hysteresis model is included. The model is shown in Figure 8. The model is defined previously in this Chapter.

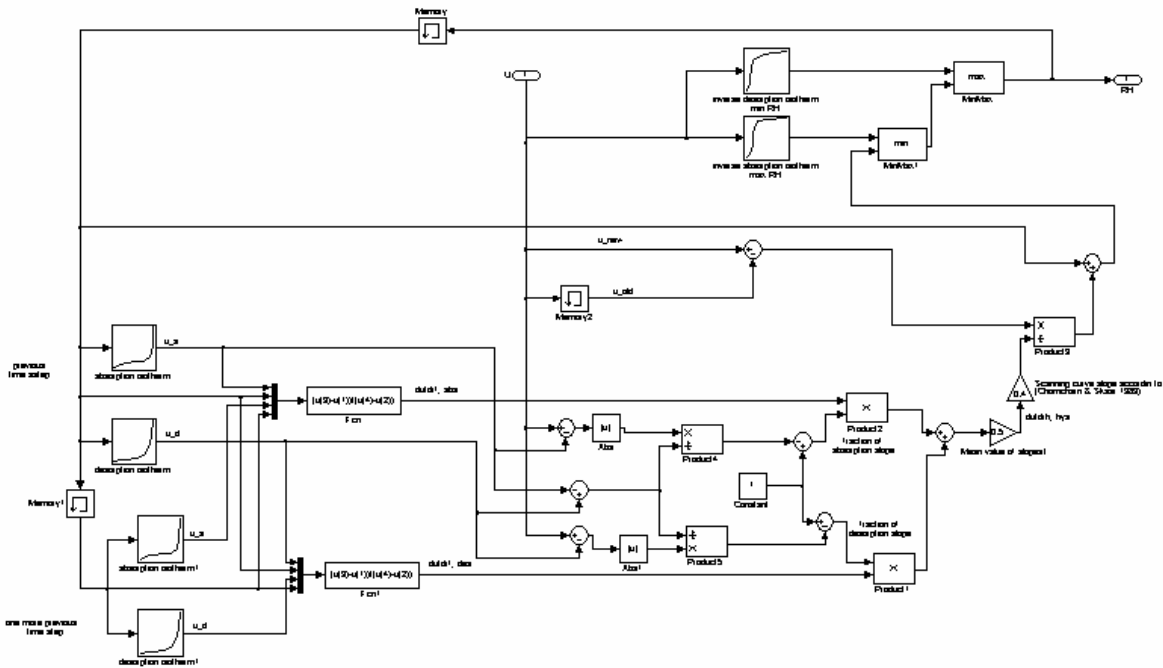


Figure 8: **Hysteresis** model. This subsystem is used in stead of the table u to rh in Figure 7. Input to the block is u and the output is RH

The **heat** and **moisture balances** are very identical. Figure 9 shows moisture balance.

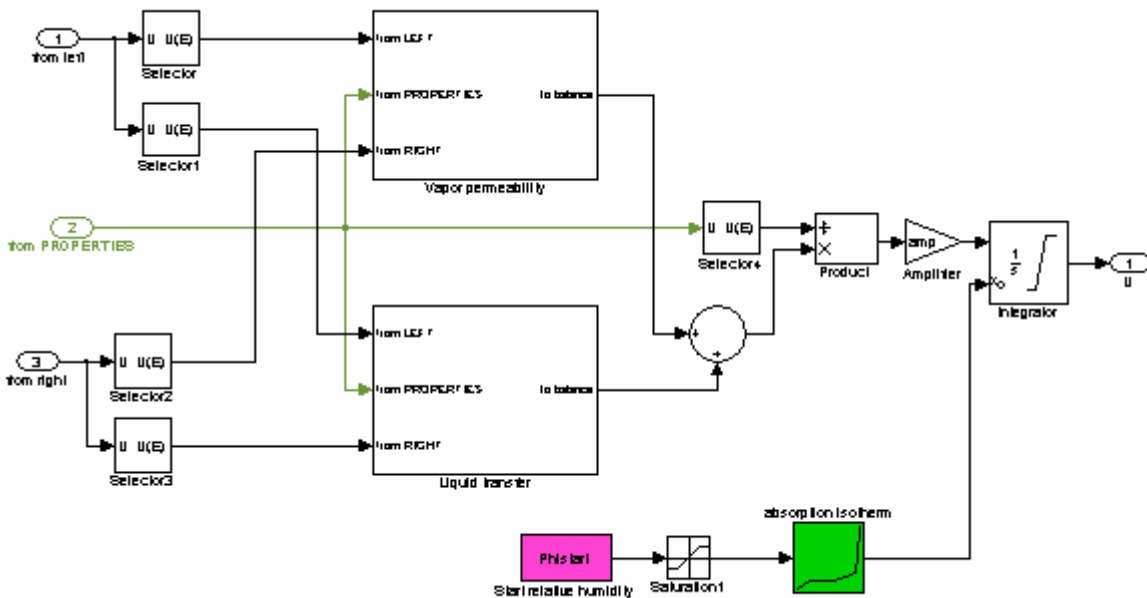


Figure 9: **Moisture balance** subsystem. Initial value for integration of moisture flux is defined by the initial relative humidity and the absorption isotherm. Also the initial moisture content is needed to be defined in the mask because it is used as an initialising value for memory blocks in the **hysteresis** block.

The subsystem *vapour permeability* (Figure 10) consists of the vapour flows in to and out of the node and is describing the 2 first elements in square brackets in the equation 16. On this level all the flows from left and right are described almost identically.

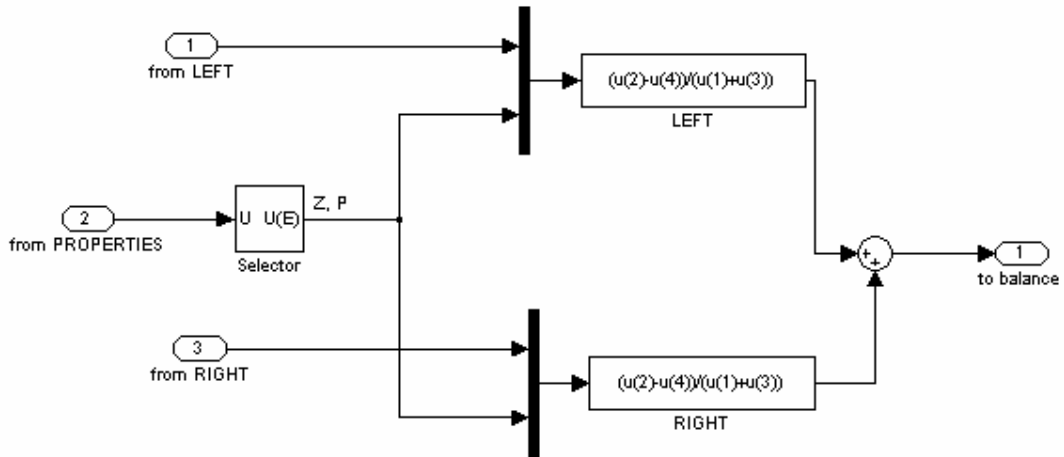


Figure 10 Vapour permeability system in material layer

BC and surface layer block is seen in Figure 11. Input to block is the output from the neighbouring “normal” **material layer** block. Output is the same as for **material layer** block, but there is also an additional output: array from air node. This is used in the case one wants to calculate moisture flux on the surface (see Figure 12). **Flux** block is defined later in this chapter. **Surface material layer** block is almost identical with the **material layer** block. Only the resistances calculated in the **hygrothermal material properties** have to be treated differently, as the they now are valid for the total thickness of the layer, not just for the half of it (see Figure 13).

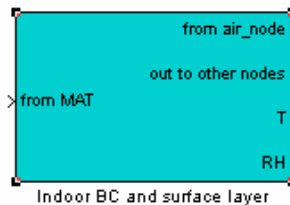


Figure 11: Indoor **BC and surface layer** block. At the moment it is identical with the **outdoor** block, but there is a possibility to define different interactions for both boundaries.

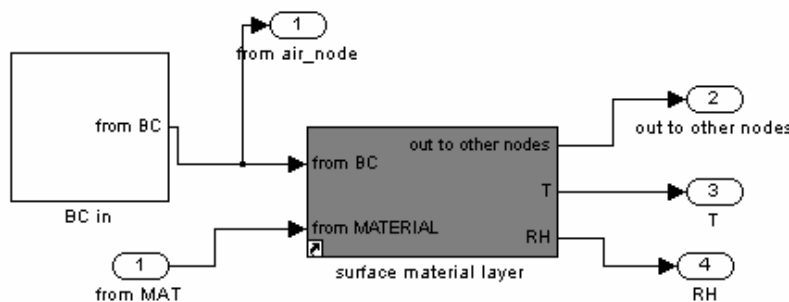


Figure 12: Next level of the **BC and surface layer** block

APPENDIX C: SIMULINK MODEL

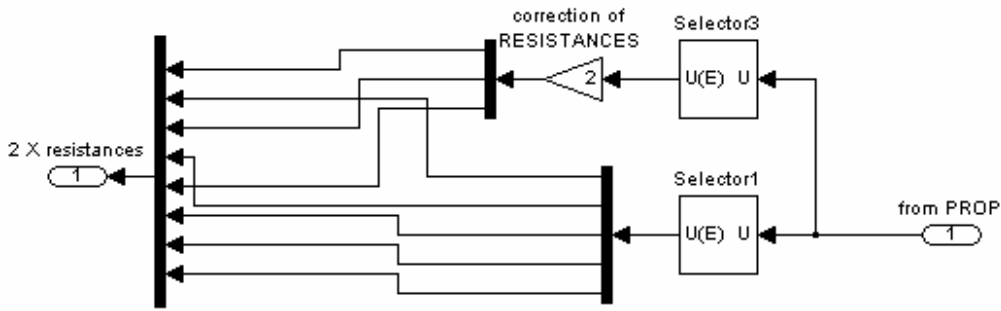


Figure 13: Multiplying resistances by 2 in the **surface material layer** block to make them match the total thickness of the surface layer.

Boundary conditions are defined in **BC in** and **BC out** blocks. These are identical at the moment and is seen in Figure 14. The relative humidity is transferred to water vapour pressure and the temperature in Celcius to Kelvin. User input from the mask defines convective heat and moisture resistances.

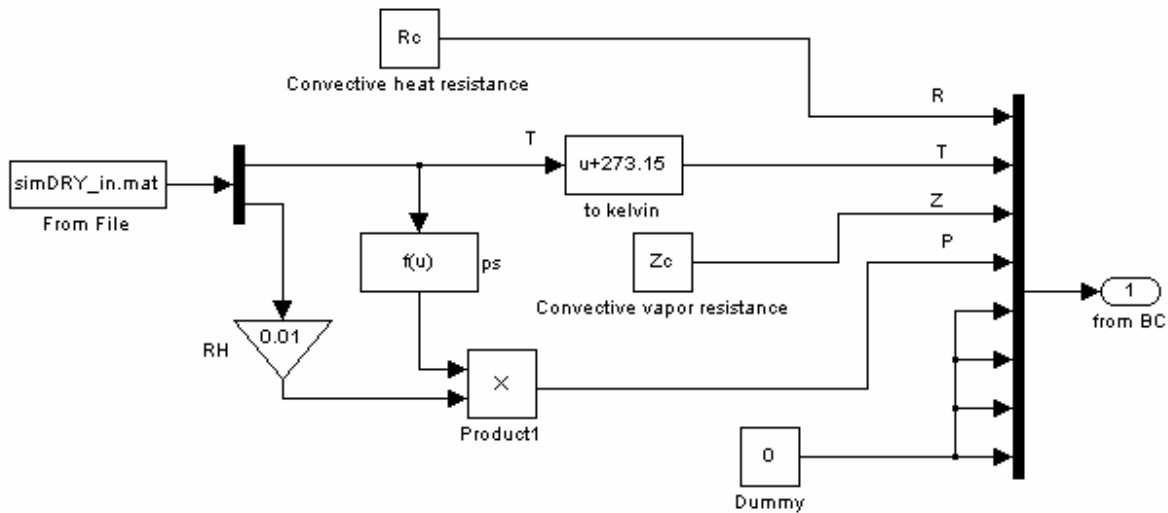


Figure 14: **BC in** block. Input is a file with temperature and relative humidity according to Table 3.

When moisture flux G is used as a boundary condition **BC in** or **BC out** block is replaced with another model, given in Figure 15. **Properties in air** block is given in Figure 16. **Moisture balance** is almost similar with the model in Figure 9 but without liquid moisture flux.

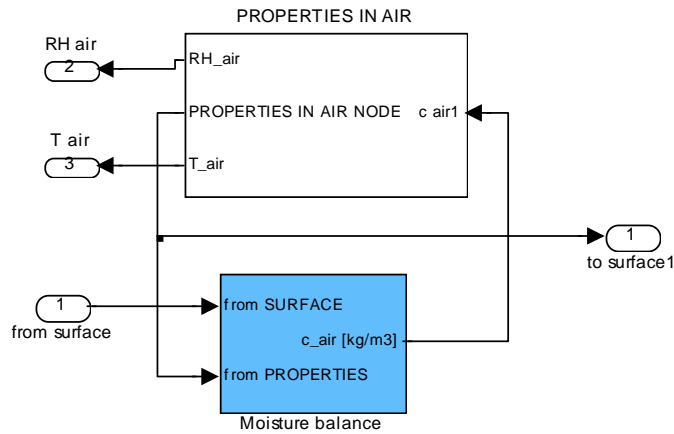


Figure 15: Contents of **BCout** block when *G* is used as a boundary condition for moisture.

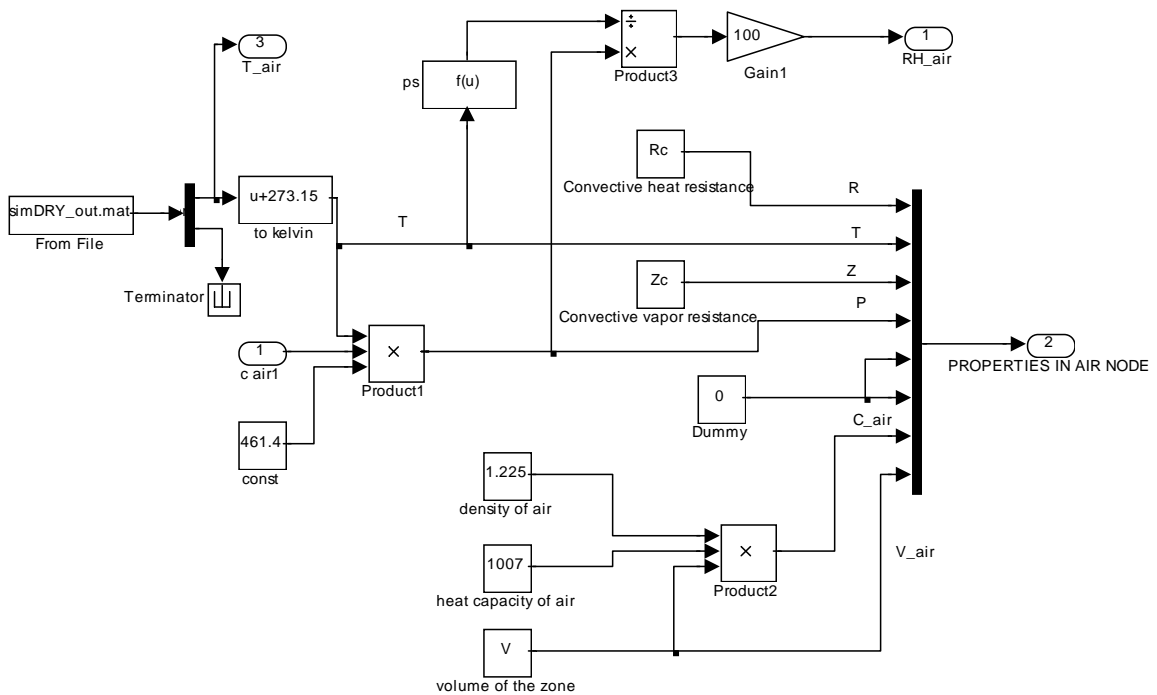


Figure 16: Contents of **Properties in air** block when *G* is used as a boundary condition for moisture.

A **flux** block (Figure 17) is also created to calculate moisture flux in between two nodes. There is no integration in this block, the calculated values in the nodes are just used here to define the flux. **Surface flux** does not include the liquid part. The next level of the **flux** block is simply these operations, see Figure 18.



Figure 17: The **flux** and **surface flux** block. Input is the data arrays from the nodes, one wants to define the flux for. Output is a flux density. The unit of the flux depends on the time defined for integration.

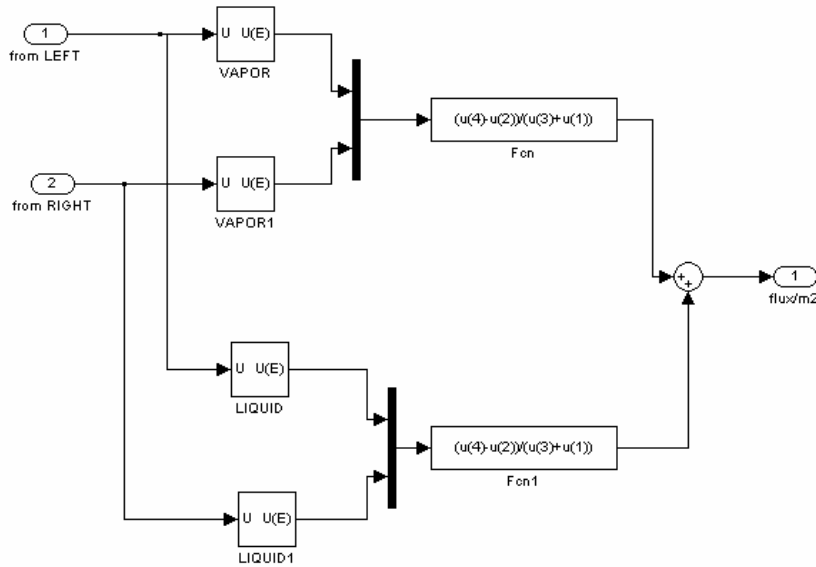


Figure 18: The **flux** block

8. Handling material parameters

The material parameters

In the basic model the material parameters are defined as identical as possible with the parameters in Match. Therefore also all the material data used in the validation process is from the material library in Match. All the material data for some materials is found in a material database – DATABASE.mat. An example of such a material data is presented in the Appendix.

The used functions for heat conductivity and specific heat capacity were given in Chapter 7.

Water vapour permeability

The water vapour permeability is partly defined as a function of the relative humidity (for $u < u_{cr}$) and partly as a function of moisture contents (for $u_{cr} < u < u_{vac}$). The water vapour permeability is zero, when the material has a moisture content at the vacuum moisture content. Figure 19 illustrates the used definitions of the water vapour permeability.

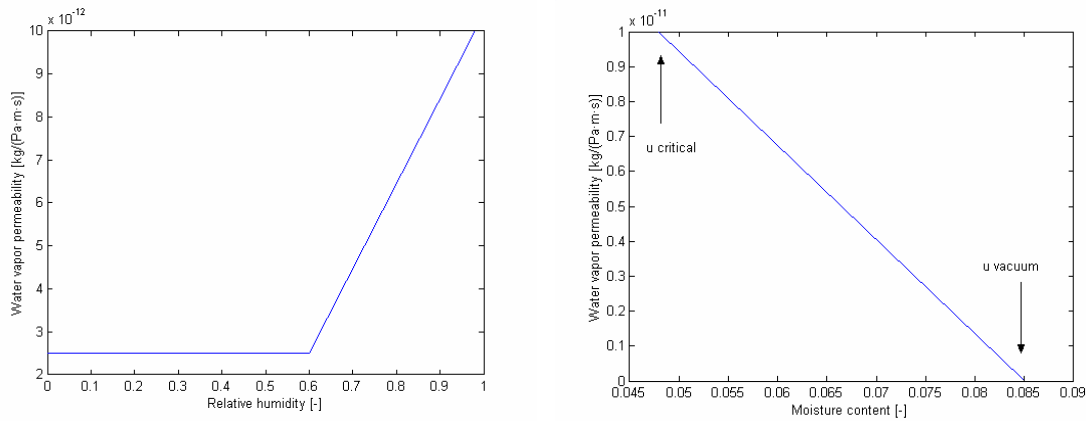


Figure 19: Water vapour permeability. When $u < u_{cr}$ the permeability is a function of relative humidity and for $u_{cr} < u < u_{vac}$ a function of moisture content. The values are valid for concrete.

Hydraulic conductivity

Hydraulic conductivity is dependent on the moisture content of the material. It is assumed that there is no liquid transport, when the moisture content is under the critical moisture content u_{cr} . The hydraulic conductivity is furthermore assumed linear between the critical moisture content and the capillary moisture content and constant up to the vacuum moisture content. This is illustrated in Figure 20.

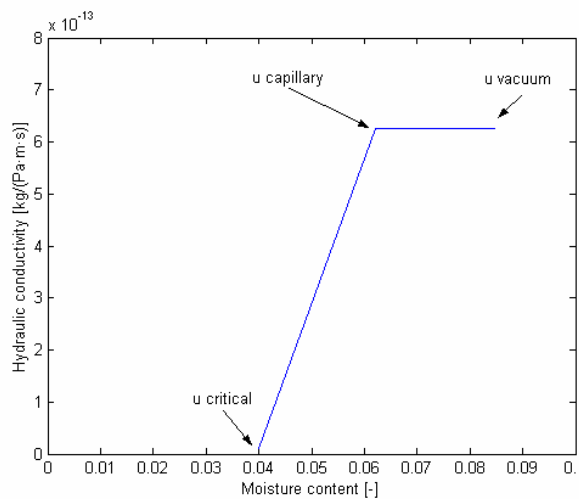


Figure 20: Hydraulic conductivity as a function of moisture content. A principal structure of the values in a look-up table. There is no liquid transport for $u < u_{cr}$. The values are valid for concrete.

Sorption isotherm and hysteresis

The equilibrium moisture content at different relative humidity levels defines a materials ability to store moisture, while the slope of the sorption isotherm defines the moisture storage capacity (see Figure 21, left). In this stage of the modelling, there are 2 possibilities for handling these properties:

1. By using ab- or desorption isotherms or the average of them (just called sorption isotherm)
2. By using a hysteresis model

APPENDIX C: SIMULINK MODEL

For the first case, the inverse of the sorption isotherm is used for calculating the actual relative humidity from the moisture content (see Figure 21, right) in the hygroscopic range.

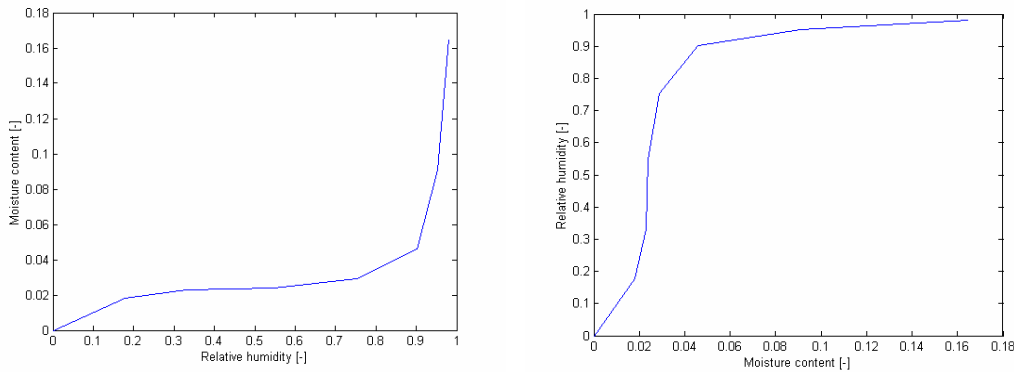


Figure 21: Left: Sorption isotherm. Right: The inverse of the sorption isotherm, which is used for determination of relative humidity from the moisture content. The values are valid for cellular concrete

For the second case, a hysteresis model was developed. The first approach was to make an identical model to Match. This worked well except some strange unstability every now and then. The reason was most probably the on/off regulating strategy, where there were switched in between absorption and desorption isotherm: sometimes the rounding error switched it the wrong way.

To avoid these problems, a linear regulation strategy was developed. The resulting model is still quite close to the Match-algorithm: the slope of the intermediate curve is a weighted version of the slope of the ab- and desorption isotherms, weighted nearest to absorption isotherm when wetting and vice versa. The final slope of the intermediate curve is got by multiplying the slope by 0.4 according to [Chomcharn & Skaar 1983]. The equations are defined in Chapter 8 and the block diagram is shown in Figure 8.

Suction pressure

In the over-hygroscopic range, the moisture storage capacity is described by a suction pressure isotherm. To make the model identical with Match, the suction pressure P_{suc} is transformed to logarithmic suction pressure $\ln P_{suc}$. The logarithmic suction pressure isotherm is used to determine the logarithmic suction pressure from the moisture content. No hysteresis is regarded for suction in the basic model, as the objective of the experimental work is on hygroscopic moisture. In the future, the hysteresis can be easily implemented in the same way as for sorption. As well an example of the suction isotherm – also called retention curve – as the inverse of it is shown in Figure 22.

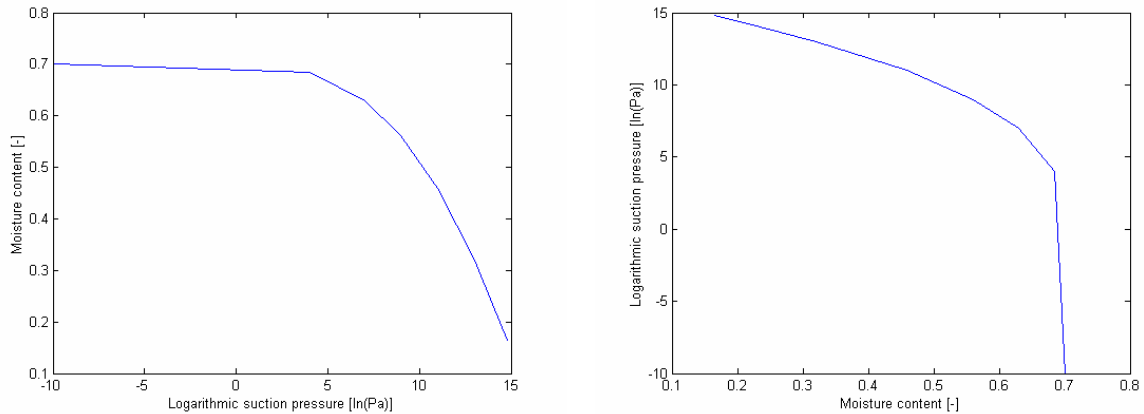


Figure 22: Moisture retention curve(left)and the inverse of it (right), that is used for determining suction pressure.

Material database

The material library is created in the form of **structures**. Structures are multidimensional Matlab arrays with “data containers” called fields. Each field has certain name and can contain any kind of data: text, scalar or array/matrix. Here is an example:

```
data(1).name='insulation'
data(1).dry_density=30
data(1).lambda_dry=0.04
data(1).heat_capacity=1000
data(1).absorption_RH=[0.05 0.015 0.025 ...]
data(1).absorption_U=[0.001 0.002 0.008 ...]
```

Each material from the library is described by the same set of data, but with the different index (data(2)):

```
data(2).name='glass'
data(2).dry_density=2400
...
```

These structures called “data()” are then saved to a file, e.g. DATABASE. In order to access this structure from Simulink, the file is loaded by the block mask initialisation to the local Matlab Workspace. Now there is an access to the structure, which can be used in the model as any other variable. The different materials have been given an index in the block mask by using a pop-up menu and after choosing the material, all the material parameters in this block are valid only for the material chosen (see Figure 2).

Keeping the same structure and especially field names, any user can create his own material library.

9. Validation

The validation is done by comparing the simulation results from Simulink model with results from Match (commercial and “reliable” HM program). As identical input values – material parameters, boundary conditions and initial values – and features as possible are used in both programs.

As boundary conditions, dynamic varying conditions are used to verify the dynamic behaviour of the model. As a0 material is used cellular concrete.

The physical model

The simulated model consists of 6 control volumes (CV) with a thickness of 20 mm each material layer and of 10 mm both surface layers, which makes the total thickness of the construction to 100 mm. On the both surfaces, the boundary conditions are defined by the transmission coefficients for heat and moisture and by the temperature and relative humidity of the ambient air. This set-up is illustrated in Figure 23.

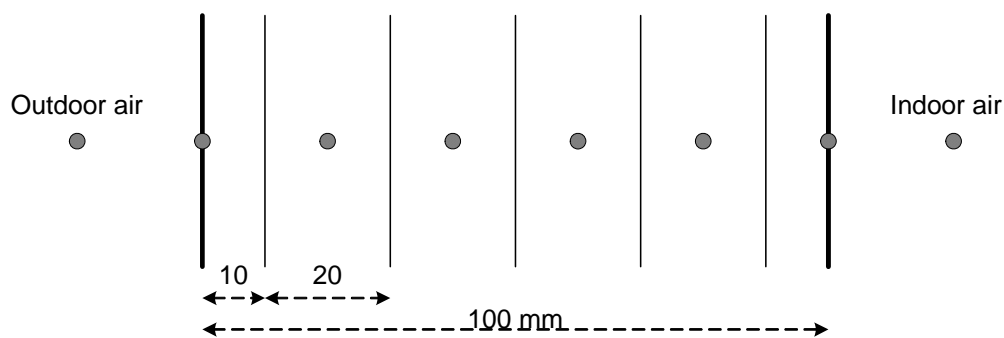


Figure 23: The physical model

The boundary conditions

The transmission coefficients on the boundaries are constant in the validation model, because this is the case in the used model in MATCH and are seen in Table 4. There is no hindrance in the further model development the boundary conditions to be dependent on the ambient conditions. At the moment, variable transmission coefficients are not of the major interest.

Table 4: Boundary conditions

	Temperature	Relative humidity	Convective heat resistance	Convective moisture resistance
Unit	°C	%	m ² ·K/W	Gpa·m ² ·s/kg
Outdoor	From file	From file	0.04	0.016
Indoor	From file (20°C)	From file (50%)	0.13	0.051

Outdoor climate is from the Danish reference year. Outdoor temperature is changed to be only positive values in order to avoid problems with creating weather data to Match. This makes

some relative humidities very low, as the relative humidity is calculated from a dew point temperature. No relative humidity is lower than 10%. Indoor conditions are constant.

The initial conditions are – which means that there is equilibrium at:

	T_{start}	RH_{start}
Glass wool	20 °C	85%
Cellular concrete	20 °C	50 %

In MATCH, it is not possible to define T_{start} . To ensure identical initial conditions, the simulation in MATCH is started with an one year simulation with the initial conditions as the boundary conditions.

Hereby, a sudden change in boundary conditions is simulated and the development of temperature and moisture profiles through the construction can be followed.

The model in Simulink

The validation model with 6 nodes is shown in Figure 24. The resulting state in each node – temperature and relative humidity – is saved after each time step to a file: *temperature.mat* and *humidity.mat*. The arrows in between nodes and boundary conditions define and illustrate the interaction and the relation: The input in each node is the output from the previous (left) and the next (right) neighbour.

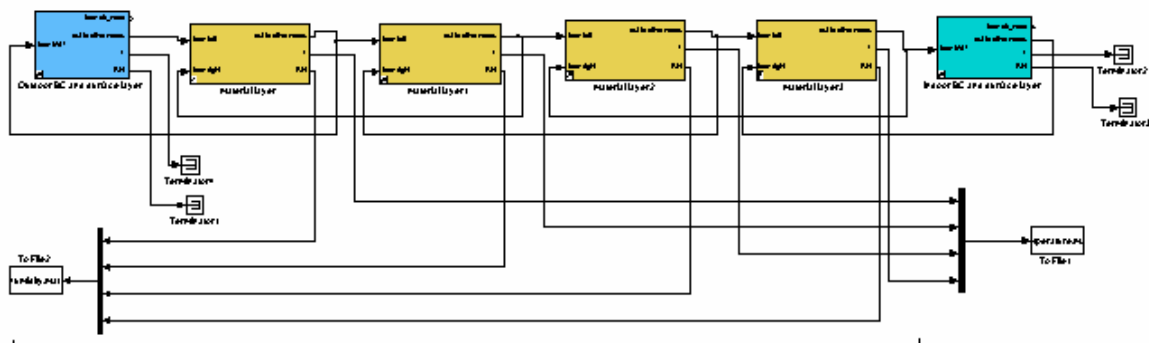


Figure 24: The validation model with 6 nodes.

Results

Following graphs show that there is a good agreement between the Simulink model and Match model, especially when there is no hysteresis. Problems with modelling hysteresis with a steeper slope give the major part of the difference between the Simulink and the Match model.

APPENDIX C: SIMULINK MODEL

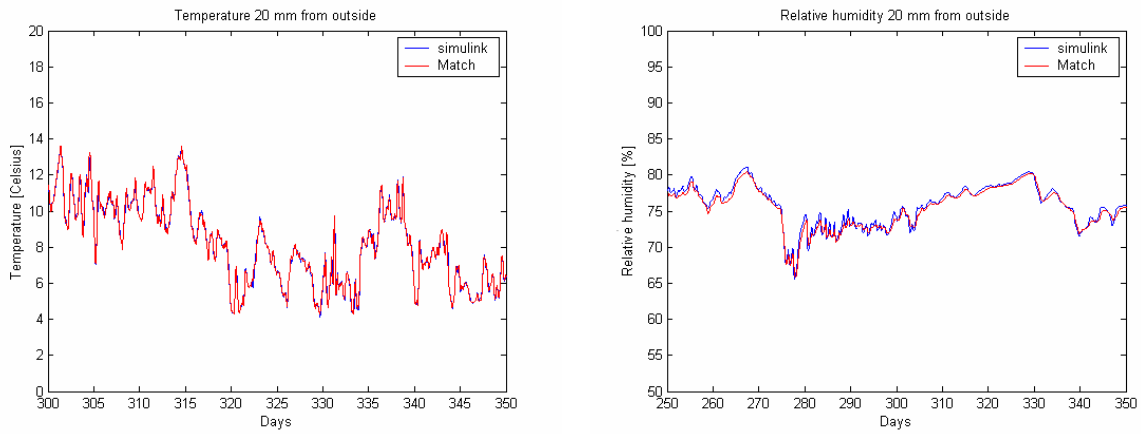


Figure 25: Comparison between Simulink and Match. Temperature (left) and relative humidity (right) 20 mm from outside. Only absorption isotherm is used for both models.

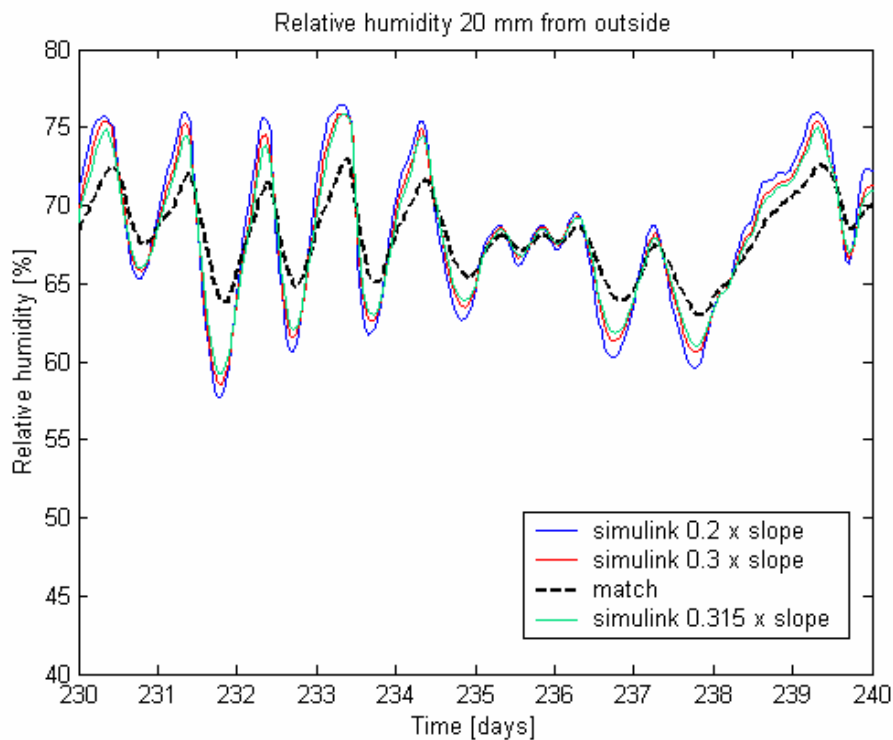


Figure 26: Comparison between Simulink and Match. Effect of hysteresis on relative humidity 20 mm from outside. Different slopes of the intermediate scanning curves are compared.

It has turned out that the model becomes unstable on different values of the slope, depending of the material. The problem is created, when the timestep becomes so short that there is no change in moisture content and thereby neither in relative humidity.

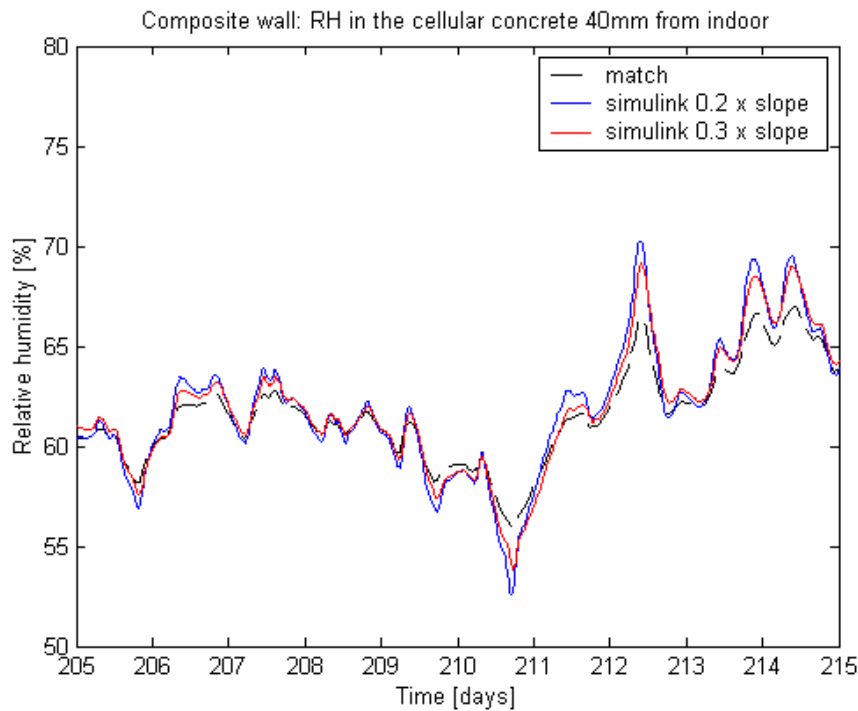


Figure 27: Relative humidity in a composite wall with 50 mm cellular concrete inside and 50 mm glass wool outside. Slope should be steeper.

10. References

- [Chomcharn & Skaar 1983] A. Chomcharn and C. Skaar: *Dynamic sorption and hygroexpansion of wood wafers exposed to sinusoidally varying humidity*. Wood Science and Technology Vol. 17, 259-277. 1983
- [Gudum 2002] C. Gudum: *Moisture transport and convection in building envelopes. Ventilation in light weight outer walls*. Ph.D Thesis. Department of Civil Engineering, Technical University of Denmark 2002
- [Hagentoft 2001] C-E Hagentoft: *Thermal System Analysis Using the Building Physics Toolbox in Simulink*. Proceedings to CIB W40 Meeting, Wellington, New Zealand. 2001
- [Nielsen et al. 2002] T.R. Nielsen, R. Peuhkuri, P. Weitzman and C. Gudum: *Modeling Building Physics in Simulink*, Report SR-02-03, BYG DTU, 2002
- [Rode 1991] C. Rode: *Description of the model MATCH. Theoretical background, equations (T1-DK-91/01)*, IEA Annex 24 Final report, Volume 1: Task 1: Modelling. 1991
- [Report 2002] C. Rode, C. Gudum, P. Weitzmann, R. Peuhkuri, T. R. Nielsen, A. S. Kalagasidis and C-E. Hagentoft: *International Building Physics Toolbox, General report*, R-02:4. Gothenburg: Chalmers University of Technology, Department of Building Physics. 2002. Available on www.ibpt.org

Appendix D

New SIMULINK models

D.1 Non-Fickian model

Non-Fickian model in SIMULINK

The non-Fickian material node has the same structure as the conventional model described in Appendix C. **Heat balance** and **Hygrothermal material properties** blocks are identical with the ones in the conventional model. The **Moisture balance** node is here divided in the two: **MATERIAL Moisture balance** (Figure 5) and **Air node** (Figure 3).

Properties in air (Figure 4) calculates the relative humidity RH and vapour pressure p from the temperature T and vapour concentration of air c_{air} . Figure 6 shows the calculation of sorption coefficient k , which is determined as a 2D-interpolation from the actual relative humidity RH_{air} in air and the relative equilibrium p^*/p .

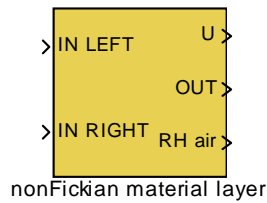


Figure 1: The first level of the non-Fickian model

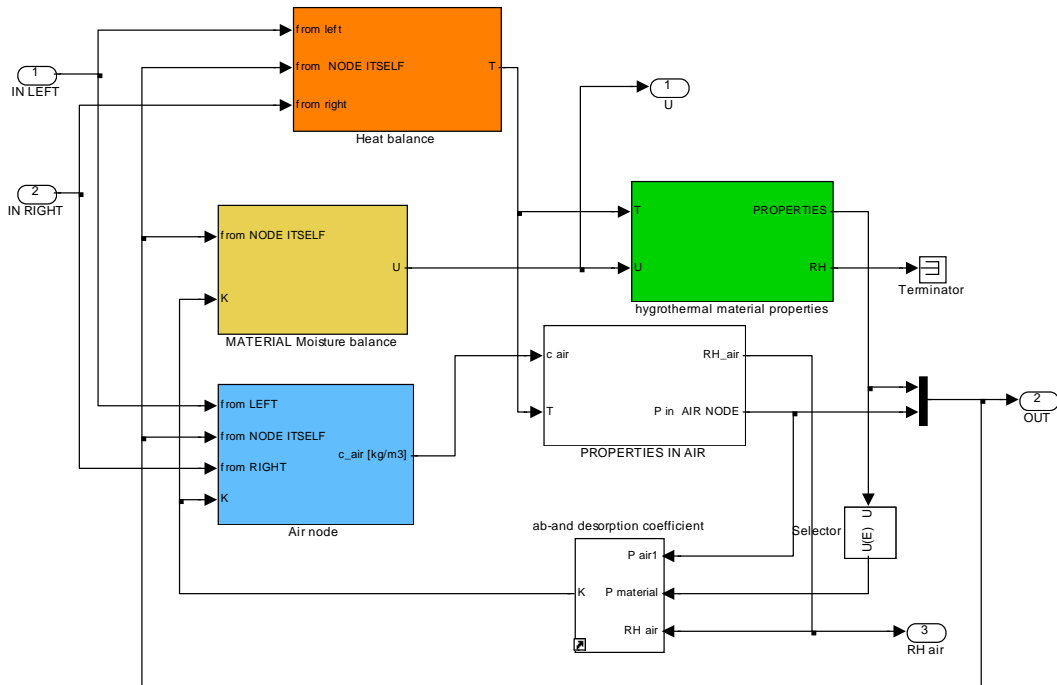


Figure 2: The next level of the non-Fickian model

APPENDIX D.1: NON-FICKIAN MODEL IN SIMULINK

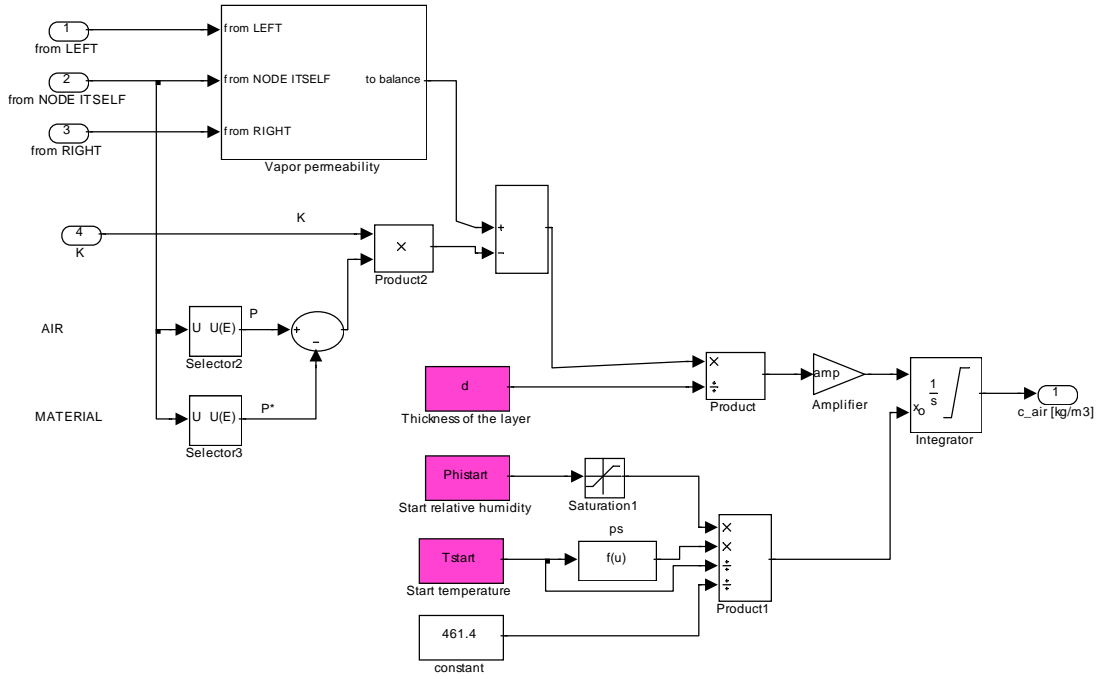


Figure 3: The Air node

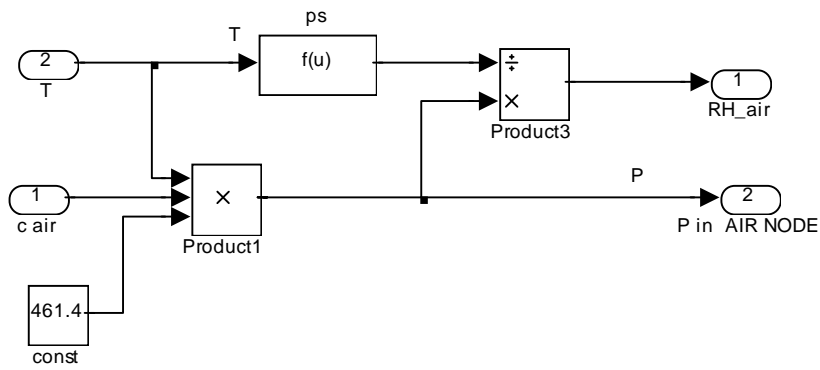


Figure 4: Properties in air

APPENDIX D.1: NON-FICKIAN MODEL IN SIMULINK

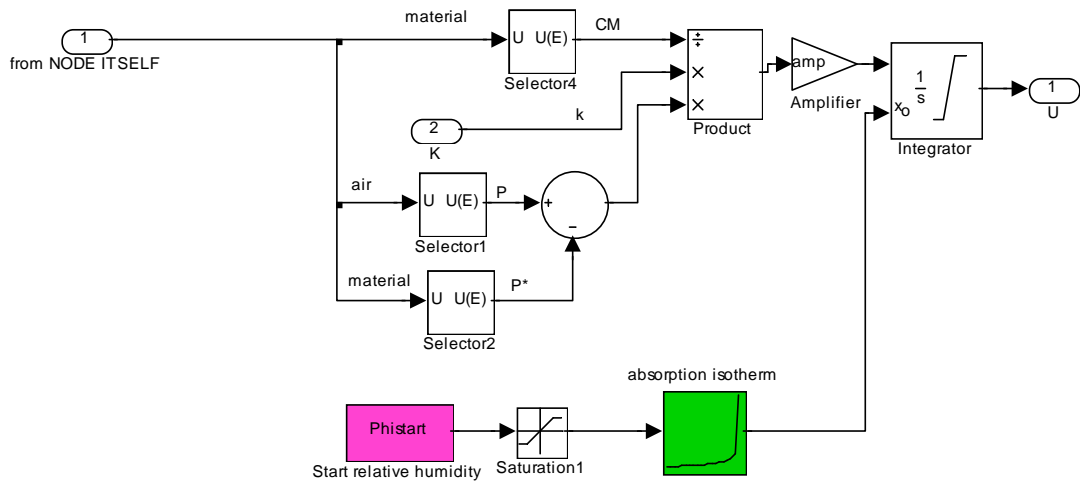


Figure 5: The Material moisture balance

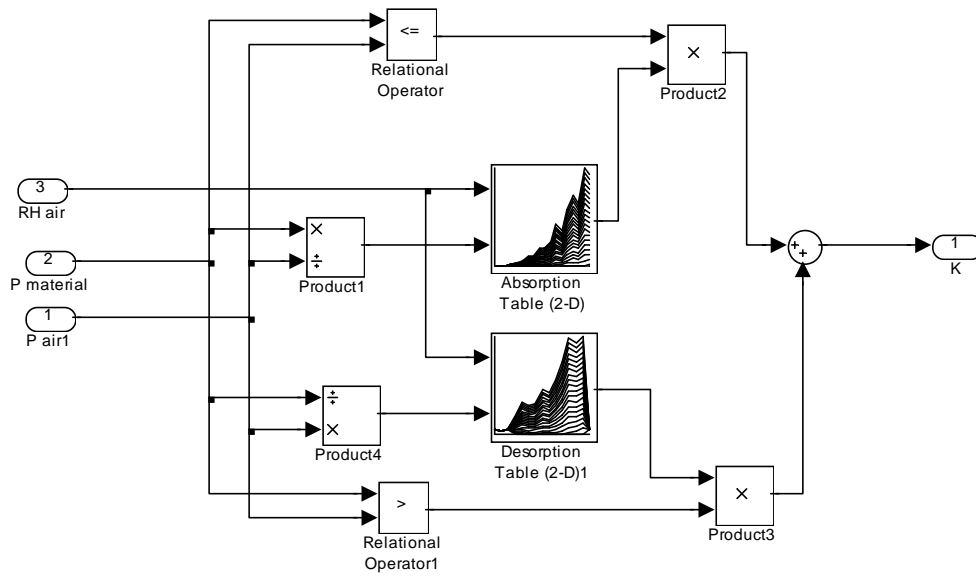


Figure 6: Sorption coefficient

D.2 Model for determination of sorption coefficient

Model for determination of sorption coefficient k

Measurement results, where moisture uptake or moisture release as a result of step changes in relative humidity has been followed as a function of time can be used for determination of the sorption coefficient k with the model shown in Figure 1. Input data is given in matrices as:

Climate in air:

time [s]
 temperature [degrees C]
 relative humidity [%]

Moisture content:

time [s]
 moisture content [-]

The vapour pressure in equilibrium with the absorbed moisture p^* is determined from measured moisture content via sorption isotherm.

Output is a matrix with:

air node relative humidity RH_{air}
 relative equilibrium p^*/p or p/p^*
 sorption coefficient k

Now the sorption coefficient can be determined as a function of RH_{air} and p^*/p or p/p^* .

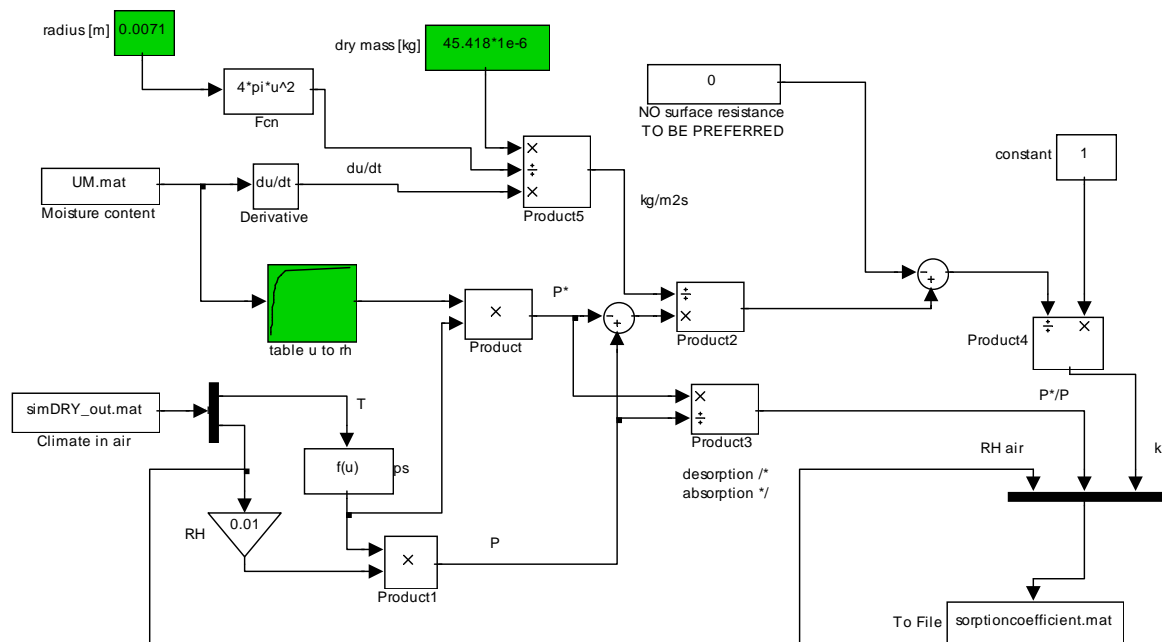


Figure 1: SIMULINK model for determination of the sorption coefficient k . The actual model is used for determining k for absorption steps, where k is a function of p^*/p . For desorption steps k is a function of p/p^* .